

AERO-ASTRONAUTICS REPORT NO. 243

10/10/88  
1300  
1300

OPTIMAL TRAJECTORIES  
FOR THE AEROASSISTED FLIGHT EXPERIMENT,  
PART 4, DATA, TABLES, AND GRAPHS

by

A. MIELE, T. WANG, W. Y. LEE, H. WANG, AND G. D. WU

NAGS-755

(NASA-CR-186164) OPTIMAL TRAJECTORIES FOR  
THE AEROASSISTED FLIGHT EXPERIMENT. PART 4:  
DATA, TABLES, AND GRAPHS (Rice Univ.)  
132 p

N90-21780

CSCL 22A

Unclassified  
G3/13 0252548

RICE UNIVERSITY

1989

AERO-ASTRONAUTICS REPORT NO. 243

OPTIMAL TRAJECTORIES

FOR THE AEROASSISTED FLIGHT EXPERIMENT,  
PART 4, DATA, TABLES, AND GRAPHS

by

A. MIELE, T. WANG, W. Y. LEE, H. WANG, AND G. D. WU

RICE UNIVERSITY

1989

Optimal Trajectories  
for the Aeroassisted Flight Experiment,  
Part 4, Data, Tables, and Graphs<sup>1</sup>

by

A. Miele<sup>2</sup>, T. Wang<sup>3</sup>, W. Y. Lee<sup>4</sup>, H. Wang<sup>5</sup>, and G. D. Wu<sup>6</sup>

---

<sup>1</sup>This work was supported by NASA-Marshall Space Flight Center, Grant No. NAG-8-755, by Jet Propulsion Laboratory, Contract No. 956415, and by Boeing Military Airplane Company.

<sup>2</sup>Foyt Family Professor of Aerospace Sciences and Mathematical Sciences, Aero-Astronautics Group, Rice University, Houston, Texas.

<sup>3</sup>Senior Research Scientist, Aero-Astronautics Group, Rice University, Houston, Texas.

<sup>4</sup>Post-Doctoral Fellow, Aero-Astronautics Group, Rice University, Houston, Texas.

<sup>5</sup>Graduate Student, Aero-Astronautics Group, Rice University, Houston, Texas.

<sup>6</sup>Graduate Student, Aero-Astronautics Group, Rice University, Houston, Texas.

Abstract. This report is the fourth of a series (Refs. 1-4) dealing with the determination of optimal trajectories for the aeroassisted flight experiment (AFE). It is a follow up to Ref. 3 and presents data, tables, and graphs relative to the following transfers: (IA) indirect ascent to a 178 NM perigee via a 197 NM apogee; and (DA) direct ascent to a 178 NM apogee.

For both transfers, two cases are investigated: (i) the bank angle is continuously variable; and (ii) the trajectory is divided into segments along which the bank angle is constant. For case (ii), the following subcases are studied: two segments, three segments, four segments, and five segments; because the time duration of each segment is optimized, the above subcases involve four, six, eight, and ten parameters, respectively.

To sum up, this report presents systematic data on ten optimal trajectories (OT), five for Transfer (IA) and five for Transfer (DA). For comparison purposes and only for transfer (IA), a reference trajectory (RT) is also considered: this is a five-segment trajectory, close to the nominal trajectory given in Ref. 5.

Key Words. Flight mechanics, hypervelocity flight, atmospheric flight, optimal trajectories, aeroassisted flight experiment, aeroassisted orbital transfer, guidance.

## 1. Introduction

This report is the fourth of a series (Refs. 1-4) dealing with the determination of optimal trajectories for the aeroassisted flight experiment (AFE). It is a follow up to Ref. 3 and presents systematic data, tables, and graphs relative to the following transfers: (IA) indirect ascent to a 178 NM perigee via a 197 NM apogee; and (DA) direct ascent to a 178 NM apogee. It is assumed that, during the atmospheric pass, the angle of attack is constant,  $\alpha = 17$  deg; hence, the only control is the angle of bank. The effects due to the oblateness of the Earth are neglected, but those due to the rotation of the Earth are included. The gravitational field is central and is governed by the inverse square law.

Trajectories have been computed in a 3D-space employing the full system of 6 ODEs describing the atmospheric pass. Computations have been done in an Earth-fixed reference frame for the atmospheric part of the trajectory and in an inertial reference frame for the space part of the trajectory. At atmospheric entry and at atmospheric exit, transformation relations have been employed in order to pass from quantities computed in an Earth-fixed system to quantities computed in an inertial system, and viceversa.

The atmospheric entry conditions are given; they correspond to a typical return from GEO, a geosynchronous Earth orbit. The atmospheric exit conditions are adjusted in such a way that the

following requirements are met: (a) the atmospheric velocity depletion is such that, after exiting, the AFE spacecraft first ascends to a specified apogee and then descends to a specified perigee; and (b) the exit orbital plane is identical with the entry orbital plane.

The optimization criterion is the total velocity impulse  $\Delta V$  (total characteristic velocity). For Transfer (IA), propulsive impulses are applied at two points: at the 197 NM apogee in order to raise the height of the perigee; and at the 178 NM perigee in order to circularize the motion. For Transfer (DA), a propulsive impulse is applied at only one point: at the 178 NM apogee in order to circularize the motion.

Optimal trajectories have been computed for the following cases:

(i) Continuous Control. Here, the bank angle is continuously variable. Both the bank angle history  $\mu(t)$  and the flight time  $\tau$  are optimized.

(ii) Discrete Control. Here, the trajectory is divided into segments along which the bank angle is constant. Depending on the number of segments, the following subcases are studied: two segments, three segments, four segments, and five segments. For each segment, the bank angle  $\mu_i$  and the time duration  $\tau_i$  are treated as parameters; hence, the number of parameters being optimized is twice the number of segments.

To sum up, this report presents systematic data on ten optimal trajectories (OT), five for Transfer (IA) and five for

Transfer (DA). For comparison purposes and only for transfer (IA), a reference trajectory (RT) is also considered: this is a five-segment trajectory, close to the nominal trajectory given in Ref. 5.

Notations. The notations used in this report are identical with those of Ref. 3. Therefore, a list of symbols is omitted.

## 2. AFE Data, Tables, and Graphs

As explained in the introduction, this report considers 11 AFE trajectories (one reference trajectory and ten optimal trajectories), more specifically:

Transfer (IA), five-segment reference trajectory;

Transfer (IA), continuous optimal trajectory;

Transfer (IA), two-segment optimal trajectory;

Transfer (IA), three-segment optimal trajectory;

Transfer (IA), four-segment optimal trajectory;

Transfer (IA), five-segment optimal trajectory;

Transfer (DA), continuous optimal trajectory;

Transfer (DA), two-segment optimal trajectory;

Transfer (DA), three-segment optimal trajectory;

Transfer (DA), four-segment optimal trajectory;

Transfer (DA), five-segment optimal trajectory.

For these trajectories, extensive numerical computations were made using the NAS-AS-9000 computer of Rice University. The pertinent information is organized in three parts: data (Section 2.1), summary tables (Section 2.2), and graphs (Section 2.3).

2.1. Data. The data used in the numerical experiments are presented in Tables 1-7.

Table 1 shows the Earth's physical constants. Note that the oblateness of the Earth has been neglected.

Table 2 shows the spacecraft data. Note that the angle of attack is kept constant ( $\alpha = 17$  deg) during the atmospheric pass. Hence, the spacecraft is controlled via the angle of bank.

Table 3 shows the conditions at atmospheric entry in both an inertial system (Table 3A) and an Earth-fixed system (Table 3B).

Table 4 shows the conditions at atmospheric exit in an inertial system.

Table 5 shows the desired apogee conditions,  $h = 197$  NM, in an inertial system.

Table 6 shows the desired perigee conditions,  $h = 178$  NM, in an inertial system.

Table 7 shows the shuttle conditions,  $h = 160$  NM, in an inertial system.

2.2. Summary Tables. Summary results for the numerical experiments are shown in Tables 8-22.

Table 8 shows the characteristic velocity and the flight time for the 11 AFE trajectories. Clearly, the optimal trajectories are characterized by a smaller characteristic velocity and a longer flight time than the reference trajectory.

Table 9 compares the optimal trajectories of Transfer (IA) from the point of view of characteristic velocity, flight time, minimum altitude, peak dynamic pressure, peak heating rate, peak change of the orbital inclination, peak change of the longitude of the ascending node, and peak wedge angle. Clearly, the optimal continuous-control trajectory and the optimal discrete-control trajectories with  $s = 2, 3, 4, 5$  segments coalesce into a single trajectory.

Table 10 compares the optimal trajectories of Transfer (DA) from the point of view of characteristic velocity, flight time, minimum altitude, peak dynamic pressure, peak heating rate, peak change of the orbital inclination, peak change of the longitude of the ascending node, and peak wedge angle. Once more, the optimal continuous-control trajectory and the optimal discrete-control trajectories with  $s = 2, 3, 4, 5$  segments coalesce into a single trajectory.

Table 11 compares the reference trajectory of Transfer (IA), the two-segment optimal trajectory of Transfer (IA), and the two-segment optimal trajectory of Transfer (DA) from the point of view of characteristic velocity, flight time, minimum altitude, peak dynamic pressure, peak heating rate, peak change of the orbital inclination, peak change of the longitude of the ascending node, and peak wedge angle. Clearly, the optimal trajectories are superior to the reference trajectory in terms of all the quantities of interest.

Tables 12-22 contain more detailed information on the 11 AFE trajectories. Each table presents the atmospheric entry conditions; the atmospheric exit conditions; the values of the minimum altitude, peak dynamic pressure, peak heating rate, peak aerodynamic force per unit weight, peak change of the orbital inclination, peak change of the longitude of the ascending node, peak wedge angle; and the components of the characteristic velocity.

More specifically, Table 12 pertains to the reference trajectory for Transfer (IA); Tables 13-17 pertain to the optimal trajectories for Transfer (IA); and Tables 18-22 pertain to the optimal trajectories for Transfer (DA).

2.3. Graphs. The time histories of the reference trajectory and the optimal trajectories are shown in Figs. 1-11. More specifically, Fig. 1 pertains to the reference trajectory for Transfer (IA); Figs. 2-6 pertain to the optimal trajectories for Transfer (IA); and Figs. 7-11 pertain to the optimal trajectories for Transfer (DA). Each figure includes 17 parts, labeled (A) through (Q):

(A) longitude, relative; (B) longitude, inertial; (C) latitude;  
(D) altitude; (E) velocity, relative; (F) velocity, inertial;  
(G) path inclination, relative; (H) path inclination, inertial;  
(I) heading angle, relative; (J) heading angle, inertial; (K)  
bank angle; (L) dynamic pressure; (M) heating rate; (N) aerodynamic  
force per unit weight; (O) orbital inclination; (P) longitude  
of the ascending node; (Q) wedge angle.

References

1. MIELE, A., ZHAO, Z. G., and LEE, W. Y., Optimal Trajectories for the Aeroassisted Flight Experiment, Part 1, Equations of Motion in an Earth-Fixed System, Rice University, Aero-Astronautics Report No. 238, 1989.
2. MIELE, A., ZHAO, Z. G., and LEE, W. Y., Optimal Trajectories for the Aeroassisted Flight Experiment, Part 2, Equations of Motion in an Inertial System, Rice University, Aero-Astronautics Report No. 239, 1989.
3. MIELE, A., WANG, T., LEE, W. Y., and ZHAO, Z. G., Optimal Trajectories for the Aeroassisted Flight Experiment, Part 3, Formulation, Results, and Analysis, Rice University, Aero-Astronautics Report No. 242, 1989.
4. MIELE, A., WANG, T., LEE, W. Y., WANG, H., and WU, G. D., Optimal Trajectories for the Aeroassisted Flight Experiment, Part 4, Data, Tables, and Graphs, Rice University, Aero-Astronautics Report No. 243, 1989.
5. ANONYMOUS, N. N., Aeroassisted Flight Experiment: Preliminary Design Document, NASA Marshall Space Flight Center, 1986.

List of Tables

- Table 1. Earth's physical constants.
- Table 2. Spacecraft data.
- Table 3A. Entry conditions, inertial.
- Table 3B. Entry conditions, relative.
- Table 4. Exit conditions, inertial.
- Table 5. Apogee conditions,  $h = 197$  NM, inertial.
- Table 6. Perigee conditions,  $h = 178$  NM, inertial.
- Table 7. Shuttle conditions,  $h = 160$  NM, inertial.
- Table 8. Characteristic velocity and flight time.
- Table 9. Comparison of optimal trajectories, Transfer (IA).
- Table 10. Comparison of optimal trajectories, Transfer (DA).
- Table 11. Comparison of reference trajectory and optimal trajectories.
- Table 12. Five-segment reference trajectory, Transfer (IA).
- Table 13. Continuous optimal trajectory, Transfer (IA).
- Table 14. Two-segment optimal trajectory, Transfer (IA).
- Table 15. Three-segment optimal trajectory, Transfer (IA).
- Table 16. Four-segment optimal trajectory, Transfer (IA).
- Table 17. Five-segment optimal trajectory, Transfer (IA).
- Table 18. Continuous optimal trajectory, Transfer (DA).
- Table 19. Two-segment optimal trajectory, Transfer (DA).
- Table 20. Three-segment optimal trajectory, Transfer (DA).
- Table 21. Four-segment optimal trajectory, Transfer (DA).
- Table 22. Five-segment optimal trajectory, Transfer (DA).

List of Figures

- Fig. 1. Five-segment reference trajectory, Transfer (IA).  
Fig. 2. Continuous optimal trajectory, Transfer (IA).  
Fig. 3. Two-segment optimal trajectory, Transfer (IA).  
Fig. 4. Three-segment optimal trajectory, Transfer (IA).  
Fig. 5. Four-segment optimal trajectory, Transfer (IA).  
Fig. 6. Five-segment optimal trajectory, Transfer (IA).  
Fig. 7. Continuous optimal trajectory, Transfer (DA).  
Fig. 8. Two-segment optimal trajectory, Transfer (DA).  
Fig. 9. Three-segment optimal trajectory, Transfer (DA).  
Fig. 10. Four-segment optimal trajectory, Transfer (DA).  
Fig. 11. Five-segment optimal trajectory, Transfer (DA).

Remark. Each figure includes the following 17 parts:

- (A) longitude  $\theta$ , relative;
- (B) longitude  $\theta$ , inertial;
- (C) latitude  $\phi$ ;
- (D) altitude  $h$ ;
- (E) velocity  $V$ , relative;
- (F) velocity  $V$ , inertial;
- (G) path inclination  $\gamma$ , relative;
- (H) path inclination  $\gamma$ , inertial;
- (I) heading angle  $\chi$ , relative;
- (J) heading angle  $\chi$ , inertial;
- (K) bank angle  $\mu$ ;
- (L) dynamic pressure DP;
- (M) heating rate HR;
- (N) aerodynamic force per unit weight AF/W;
- (O) orbital inclination  $i$ ;
- (P) longitude of the ascending node  $\Omega$ ;
- (Q) wedge angle  $\eta$ .

Table 1. Earth's physical constants.

Quantity	Symbol	Value	Units
Angular velocity	$\omega$	0.729211595 E-04	rad/sec
Gravitational constant	$\mu_e$	0.39860064 E+15	$m^3/sec^2$
Radius, Earth surface	$r_e$	0.6378164 E+07	m
Thickness of the atmosphere	$h_a$	0.121896 E+06	m
Radius, atmospheric edge	$r_a$	0.6500060 E+07	m

Table 2. Spacecraft data.

Quantity	Symbol	Value	Units
Spacecraft mass at atmospheric entry	m	1678.2918	kg
Reference surface area	S	14.314	$m^2$
Angle of attack	$\alpha$	17.000	deg
Lift coefficient	$C_L$	-0.370696	-
Drag coefficient	$C_D$	1.31452	-

Table 3A. Entry conditions, inertial.

Quantity	Symbol	Value	Units
Longitude	$\theta_0$	-134.51957	deg
Latitude	$\phi_0$	-4.4873862	deg
Altitude	$h_0$	121.896	km
Radius	$r_0$	6500.060	km
Velocity	$v_0$	10.307702	km/sec
Path inclination	$\gamma_0$	-4.4869739	deg
Heading angle	$x_0$	-28.127757	deg
Orbital inclination	$i_0$	28.454568	deg
Longitude of ascending node	$\Omega_0$	-126.19293	deg
Wedge angle	$\eta_0$	0.0	deg

Table 3B. Entry conditions, relative.

Quantity	Symbol	Value	Units
Longitude	$\theta_0$	-134.51957	deg
Latitude	$\phi_0$	-4.4873862	deg
Altitude	$h_0$	121.896	km
Radius	$r_0$	6500.060	km
Velocity	$v_0$	9.8948096	km/sec
Path inclination	$\gamma_0$	-4.6746153	deg
Heading angle	$x_0$	-29.422139	deg

Table 4. Exit conditions, inertial.

Quantity	Symbol	Value	Units
Altitude	$h_1$	121.896	km
Radius	$r_1$	6500.060	km
Orbital inclination	$i_1$	28.454568	deg
Longitude of ascending node	$\Omega_1$	-126.19293	deg
Wedge angle	$\eta_1$	0.0	deg

Table 5. Apogee conditions,  $h = 197$  NM, inertial.

Quantity	Symbol	Value	Units
Altitude	$h_{22}$	364.844	km
Radius	$r_{22}$	6743.008	km
Path inclination	$\gamma_{22}$	0.0	deg
Orbital inclination	$i_{22}$	28.454568	deg
Longitude of ascending node	$\Omega_{22}$	-126.19293	deg
Wedge angle	$\eta_{22}$	0.0	deg

Table 6. Perigee conditions,  $h = 178$  NM, inertial.

Quantity	Symbol	Value	Units
Altitude	$h_{11}$	329.656	km
Radius	$r_{11}$	6707.820	km
Velocity	$v_{11}$	7.70865	km/sec
Path inclination	$\gamma_{11}$	0.0	deg
Orbital inclination	$i_{11}$	28.454568	deg
Longitude of ascending node	$\Omega_{11}$	-126.19293	deg
Wedge angle	$\eta_{11}$	0.0	deg

Table 7. Shuttle conditions,  $h = 160$  NM, inertial.

Quantity	Symbol	Value	Units
Altitude	$h_{33}$	296.320	km
Radius	$r_{33}$	6674.484	km
Velocity	$v_{33}$	7.72788	km/sec
Path inclination	$\gamma_{33}$	0.0	deg
Orbital inclination	$i_{33}$	28.454568	deg
Longitude of ascending node	$\Omega_{33}$	-126.19293	deg
Wedge angle	$\eta_{33}$	0.0	deg

Table 8. Characteristic velocity and flight time.

Trajectory	Control	s	$\Delta V$ (m/sec)	$\tau$ (sec)
IART	Discrete	5	97.97	487.6
IAOT	Continuous	$\infty$	81.86	795.3
IAOT	Discrete	2	81.86	795.7
IAOT	Discrete	3	81.86	795.7
IAOT	Discrete	4	81.86	795.8
IAOT	Discrete	5	81.84	796.2
DAOT	Continuous	$\infty$	72.05	817.6
DAOT	Discrete	2	72.03	819.5
DAOT	Discrete	3	72.03	819.6
DAOT	Discrete	4	72.03	819.6
DAOT	Discrete	5	72.01	819.9

IA = indirect ascent,

DA = direct ascent,

OT = optimal trajectory,

RT = reference trajectory,

s = number of segments.

Table 9. Comparison of optimal trajectories, Transfer (IA).

Quantity	IAOT	IAOT	IAOT	IAOT	IAOT	Units
	s = $\infty$	s = 2	s = 3	s = 4	s = 5	
$\Delta V$	81.86	81.86	81.86	81.86	81.84	m/sec
$\tau$	795.3	795.7	795.7	795.8	796.2	sec
min(h)	77.48	77.53	77.53	77.53	77.52	km
max(DP)	1186.1	1174.1	1173.5	1174.1	1174.0	N/m <sup>2</sup>
max(HR)	148.5	148.0	148.0	148.0	148.0	W/cm <sup>2</sup>
max  $\Delta i$	0.25	0.01	0.01	0.01	0.04	deg
max  $\Delta \Omega$	0.04	0.00	0.00	0.00	0.03	deg
max( $\eta$ )	0.24	0.01	0.01	0.01	0.04	deg

IA = indirect ascent, OT = optimal trajectory, s = number of segments.

Table 10. Comparison of optimal trajectories, Transfer (DA).

Quantity	DAOT	DAOT	DAOT	DAOT	DAOT	Units
	s = $\infty$	s = 2	s = 3	s = 4	s = 5	
$\Delta V$	72.05	72.03	72.03	72.03	72.01	m/sec
$\tau$	817.6	819.5	819.6	819.6	819.9	sec
$\min(h)$	77.46	77.53	77.53	77.53	77.52	km
$\max(DP)$	1189.9	1174.2	1173.3	1174.1	1173.6	N/m <sup>2</sup>
$\max(HR)$	148.7	148.0	148.0	148.0	148.0	W/cm <sup>2</sup>
$\max \Delta i $	0.27	0.01	0.01	0.01	0.02	deg
$\max \Delta\Omega $	0.05	0.00	0.00	0.00	0.01	deg
$\max(\eta)$	0.26	0.01	0.01	0.01	0.02	deg

DA = direct ascent, OT = optimal trajectory, s = number of segments.

Table 11. Comparison of reference trajectory  
and optimal trajectories.

Quantity	IART	IAOT	DAOT	Units
	s = 5	s = 2	s = 2	
$\Delta V$	97.97	81.86	72.03	m/sec
$\tau$	487.6	795.7	819.5	sec
$\min(h)$	74.56	77.53	77.53	km
$\max(DP)$	1628.9	1174.1	1174.2	$N/m^2$
$\max(HR)$	158.0	148.0	148.0	$W/cm^2$
$\max \Delta i $	1.08	0.01	0.01	deg
$\max \Delta\Omega $	0.32	0.00	0.00	deg
$\max(\eta)$	1.08	0.01	0.01	deg

IA = indirect ascent,      DA = direct ascent,  
 OT = optimal trajectory,    RT = reference trajectory,  
 s = number of segments.

Table 12. Five-segment reference trajectory, Transfer (IA).

Time	0.0	487.6	sec
Longitude, relative	-134.52	-103.21	deg
Longitude, inertial	-134.52	-101.17	deg
Latitude	-4.49	12.90	deg
Altitude	121.90	121.90	km
Velocity, relative	9.895	7.462	km/sec
Velocity, inertial	10.308	7.876	km/sec
Path inclination, relative	-4.67	1.36	deg
Path inclination, inertial	-4.49	1.29	deg
Heading angle, relative	-29.42	-27.12	deg
Heading angle, inertial	-28.13	-25.59	deg
Orbital inclination	28.45	28.46	deg
Longitude of ascending node	-126.19	-126.16	deg
Wedge angle	0.00	0.02	deg
Minimum altitude, t=151.0 sec		74.56	km
Peak dynamic pressure, t=141.4 sec		1628.9	N/m <sup>2</sup>
Peak heating rate, t=113.8 sec		158.0	w/cm <sup>2</sup>
Peak aerodynamic force / weight, t=141.4 sec		1.93	
Peak change of orbital inclination, t=137.5 sec		1.08	deg
Peak change of longitude of ascending node, t=214.6 sec		0.32	deg
Peak wedge angle, t=137.5 sec		1.08	deg
Characteristic velocity at 197 NM		87.89	m/sec
Characteristic velocity at 178 NM		10.08	m/sec
Total characteristic velocity		97.97	m/sec

Table 13. Continuous optimal trajectory, Transfer (IA).

Time	0.0	795.3	sec
Longitude, relative	-134.52	-82.81	deg
Longitude, inertial	-134.52	-79.49	deg
Latitude	-4.49	21.53	deg
Altitude	121.90	121.90	km
Velocity, relative	9.895	7.476	km/sec
Velocity, inertial	10.308	7.892	km/sec
Path inclination, relative	-4.67	0.86	deg
Path inclination, inertial	-4.49	0.82	deg
Heading angle, relative	-29.42	-20.16	deg
Heading angle, inertial	-28.13	-19.05	deg
Orbital inclination	28.45	28.44	deg
Longitude of ascending node	-126.19	-126.23	deg
Wedge angle	0.00	0.02	deg
Minimum altitude, t=123.3 sec		77.48	km
Peak dynamic pressure, t=111.3 sec		1186.1	N/m <sup>2</sup>
Peak heating rate, t= 99.4 sec		148.5	W/cm <sup>2</sup>
Peak aerodynamic force / weight, t=111.3 sec		1.41	
Peak change of orbital inclination, t=111.3 sec		0.25	deg
Peak change of longitude of ascending node, t=795.3 sec		0.04	deg
Peak wedge angle, t=111.3 sec		0.24	deg
Characteristic velocity at 197 NM		71.78	m/sec
Characteristic velocity at 178 NM		10.08	m/sec
Total characteristic velocity		81.86	m/sec

Table 14. Two-segment optimal trajectory, Transfer (IA).

Time	0.0	795.7	sec
Longitude, relative	-134.52	-82.78	deg
Longitude, inertial	-134.52	-79.45	deg
Latitude	-4.49	21.54	deg
Altitude	121.90	121.90	km
Velocity, relative	9.895	7.476	km/sec
Velocity, inertial	10.308	7.892	km/sec
Path inclination, relative	-4.67	0.86	deg
Path inclination, inertial	-4.49	0.82	deg
Heading angle, relative	-29.42	-20.16	deg
Heading angle, inertial	-28.13	-19.06	deg
Orbital inclination	28.45	28.45	deg
Longitude of ascending node	-126.19	-126.19	deg
Wedge angle	0.00	0.00	deg
Minimum altitude, t=124.5 sec		77.53	km
Peak dynamic pressure, t=110.5 sec		1174.1	N/m <sup>2</sup>
Peak heating rate, t= 95.5 sec		148.0	W/cm <sup>2</sup>
Peak aerodynamic force / weight, t=110.5 sec		1.39	
Peak change of orbital inclination, t=110.5 sec		0.01	deg
Peak change of longitude of ascending node, t=795.7 sec		0.00	deg
Peak wedge angle, t=131.5 sec		0.01	deg
Characteristic velocity at 197 NM		71.78	m/sec
Characteristic velocity at 178 NM		10.08	m/sec
Total characteristic velocity		81.86	m/sec

Table 15. Three-segment optimal trajectory, Transfer (IA).

Time	0.0	795.7	sec
Longitude, relative	-134.52	-82.77	deg
Longitude, inertial	-134.52	-79.45	deg
Latitude	-4.49	21.54	deg
Altitude	121.90	121.90	km
Velocity, relative	9.895	7.476	km/sec
Velocity, inertial	10.308	7.892	km/sec
Path inclination, relative	-4.67	0.86	deg
Path inclination, inertial	-4.49	0.82	deg
Heading angle, relative	-29.42	-20.16	deg
Heading angle, inertial	-28.13	-19.06	deg
Orbital inclination	28.45	28.45	deg
Longitude of ascending node	-126.19	-126.19	deg
wedge angle	0.00	0.00	deg
Minimum altitude, t=123.8 sec		77.53	km
Peak dynamic pressure, t=112.9 sec		1173.5	N/m <sup>2</sup>
Peak heating rate, t= 96.5 sec		148.0	W/cm <sup>2</sup>
Peak aerodynamic force / weight, t=112.9 sec		1.39	
Peak change of orbital inclination, t=107.4 sec		0.01	deg
Peak change of longitude of ascending node, t=790.8 sec		0.00	deg
Peak wedge angle, t=129.3 sec		0.01	deg
Characteristic velocity at 197 NM		71.78	m/sec
Characteristic velocity at 178 NM		10.08	m/sec
Total characteristic velocity		81.86	m/sec

Table 16. Four-segment optimal trajectory, Transfer (IA).

Time	0.0	795.8	sec
Longitude, relative	-134.52	-82.77	deg
Longitude, inertial	-134.52	-79.44	deg
Latitude	-4.49	21.54	deg
Altitude	121.90	121.90	km
Velocity, relative	9.895	7.476	km/sec
Velocity, inertial	10.308	7.892	km/sec
Path inclination, relative	-4.67	0.86	deg
Path inclination, inertial	-4.49	0.82	deg
Heading angle, relative	-29.42	-20.16	deg
Heading angle, inertial	-28.13	-19.05	deg
Orbital inclination	28.45	28.45	deg
Longitude of ascending node	-126.19	-126.19	deg
Wedge angle	0.00	0.00	deg
Minimum altitude, t=125.8 sec		77.53	km
Peak dynamic pressure, t=111.2 sec		1174.1	N/m <sup>2</sup>
Peak heating rate, t= 95.6 sec		148.0	W/cm <sup>2</sup>
Peak aerodynamic force / weight, t=111.2 sec		1.39	
Peak change of orbital inclination, t= 96.5 sec		0.01	deg
Peak change of longitude of ascending node, t=795.8 sec		0.00	deg
Peak wedge angle, t=125.8 sec		0.01	deg
Characteristic velocity at 197 NM		71.78	m/sec
Characteristic velocity at 178 NM		10.08	m/sec
Total characteristic velocity		81.86	m/sec

Table 17. Five-segment optimal trajectory, Transfer (IA).

Time	0.0	796.2	sec
Longitude, relative	-134.52	-82.75	deg
Longitude, inertial	-134.52	-79.42	deg
Latitude	-4.49	21.55	deg
Altitude	121.90	121.90	km
Velocity, relative	9.895	7.476	km/sec
Velocity, inertial	10.308	7.892	km/sec
Path inclination, relative	-4.67	0.86	deg
Path inclination, inertial	-4.49	0.82	deg
Heading angle, relative	-29.42	-20.14	deg
Heading angle, inertial	-28.13	-19.04	deg
Orbital inclination	28.45	28.45	deg
Longitude of ascending node	-126.19	-126.22	deg
Wedge angle	0.00	0.01	deg
Minimum altitude, t=123.5 sec		77.52	km
Peak dynamic pressure, t=112.7 sec		1174.0	N/m <sup>2</sup>
Peak heating rate, t= 96.5 sec		148.0	W/cm <sup>2</sup>
Peak aerodynamic force / weight, t=112.7 sec		1.39	
Peak change of orbital inclination, t=329.1 sec		0.04	deg
Peak change of longitude of ascending node, t=796.2 sec		0.03	deg
Peak wedge angle, t=318.1 sec		0.04	deg
Characteristic velocity at 197 NM		71.76	m/sec
Characteristic velocity at 178 NM		10.08	m/sec
Total characteristic velocity		81.84	m/sec

Table 18. Continuous optimal trajectory, Transfer (DA).

Time	0.0	817.6	sec
Longitude, relative	-134.52	-81.35	deg
Longitude, inertial	-134.52	-77.94	deg
Latitude	-4.49	22.02	deg
Altitude	121.90	121.90	km
Velocity, relative	9.895	7.466	km/sec
Velocity, inertial	10.308	7.881	km/sec
Path inclination, relative	-4.67	0.81	deg
Path inclination, inertial	-4.49	0.77	deg
Heading angle, relative	-29.42	-19.56	deg
Heading angle, inertial	-28.13	-18.49	deg
Orbital inclination	28.45	28.45	deg
Longitude of ascending node	-126.19	-126.21	deg
Wedge angle	0.00	0.01	deg
Minimum altitude, t=122.6 sec		77.46	km
Peak dynamic pressure, t=110.4 sec		1189.9	N/m <sup>2</sup>
Peak heating rate, t= 98.1 sec		148.7	w/cm <sup>2</sup>
Peak aerodynamic force / weight, t=110.4 sec		1.41	
Peak change of orbital inclination, t=114.5 sec		0.27	deg
Peak change of longitude of ascending node, t=269.8 sec		0.05	deg
Peak wedge angle, t=118.6 sec		0.26	deg
Characteristic velocity at 178 NM		72.05	m/sec
Total characteristic velocity		72.05	m/sec

Table 19. Two-segment optimal trajectory, Transfer (DA).

Time	0.0	819.5	sec
Longitude, relative	-134.52	-81.21	deg
Longitude, inertial	-134.52	-77.79	deg
Latitude	-4.49	22.06	deg
Altitude	121.90	121.90	km
Velocity, relative	9.895	7.466	km/sec
Velocity, inertial	10.308	7.881	km/sec
Path inclination, relative	-4.67	0.81	deg
Path inclination, inertial	-4.49	0.76	deg
Heading angle, relative	-29.42	-19.51	deg
Heading angle, inertial	-28.13	-18.44	deg
Orbital inclination	28.45	28.46	deg
Longitude of ascending node	-126.19	-126.19	deg
Wedge angle	0.00	0.00	deg
Minimum altitude, t=125.4 sec		77.53	km
Peak dynamic pressure, t=111.0 sec		1174.2	N/m <sup>2</sup>
Peak heating rate, t= 95.5 sec		148.0	W/cm <sup>2</sup>
Peak aerodynamic force / weight, t=111.0 sec		1.39	
Peak change of orbital inclination, t=111.0 sec		0.01	deg
Peak change of longitude of ascending node, t=819.5 sec		0.00	deg
Peak wedge angle, t=132.7 sec		0.01	deg
Characteristic velocity at 178 NM		72.03	m/sec
Total characteristic velocity		72.03	m/sec

Table 20. Three-segment optimal trajectory, Transfer (DA).

Time	0.0	819.6	sec
Longitude, relative	-134.52	-81.20	deg
Longitude, inertial	-134.52	-77.78	deg
Latitude	-4.49	22.06	deg
Altitude	121.90	121.90	km
Velocity, relative	9.895	7.466	km/sec
Velocity, inertial	10.308	7.881	km/sec
Path inclination, relative	-4.67	0.81	deg
Path inclination, inertial	-4.49	0.76	deg
Heading angle, relative	-29.42	-19.50	deg
Heading angle, inertial	-28.13	-18.44	deg
Orbital inclination	28.45	28.45	deg
Longitude of ascending node	-126.19	-126.19	deg
Wedge angle	0.00	0.00	deg
Minimum altitude, t=124.5 sec		77.53	km
Peak dynamic pressure, t=113.3 sec		1173.3	N/m <sup>2</sup>
Peak heating rate, t= 96.5 sec		148.0	W/cm <sup>2</sup>
Peak aerodynamic force / weight, t=113.3 sec		1.39	
Peak change of orbital inclination, t=107.7 sec		0.01	deg
Peak change of longitude of ascending node, t=814.4 sec		0.00	deg
Peak wedge angle, t=135.7 sec		0.01	deg
Characteristic velocity at 178 NM		72.03	m/sec
Total characteristic velocity		72.03	m/sec

Table 21. Four-segment optimal trajectory, Transfer (DA).

Time	0.0	819.6	sec
Longitude, relative	-134.52	-81.20	deg
Longitude, inertial	-134.52	-77.78	deg
Latitude	-4.49	22.06	deg
Altitude	121.90	121.90	km
Velocity, relative	9.895	7.466	km/sec
Velocity, inertial	10.308	7.881	km/sec
Path inclination, relative	-4.67	0.81	deg
Path inclination, inertial	-4.49	0.76	deg
Heading angle, relative	-29.42	-19.50	deg
Heading angle, inertial	-28.13	-18.44	deg
Orbital inclination	28.45	28.45	deg
Longitude of ascending node	-126.19	-126.19	deg
Wedge angle	0.00	0.00	deg
Minimum altitude, t=126.5 sec		77.53	km
Peak dynamic pressure, t=111.5 sec		1174.1	N/m <sup>2</sup>
Peak heating rate, t= 95.6 sec		148.0	W/cm <sup>2</sup>
Peak aerodynamic force / weight, t=111.5 sec		1.39	
Peak change of orbital inclination, t=111.5 sec		0.01	deg
Peak change of longitude of ascending node, t=819.6 sec		0.00	deg
Peak wedge angle, t=134.0 sec		0.01	deg
Characteristic velocity at 178 NM		72.03	m/sec
Total characteristic velocity		72.03	m/sec

Table 22. Five-segment optimal trajectory, Transfer (DA).

Time	0.0	819.9	sec
Longitude, relative	-134.52	-81.19	deg
Longitude, inertial	-134.52	-77.76	deg
Latitude	-4.49	22.07	deg
Altitude	121.90	121.90	km
Velocity, relative	9.895	7.466	km/sec
Velocity, inertial	10.308	7.881	km/sec
Path inclination, relative	-4.67	0.81	deg
Path inclination, inertial	-4.49	0.76	deg
Heading angle, relative	-29.42	-19.49	deg
Heading angle, inertial	-28.13	-18.43	deg
Orbital inclination	28.45	28.46	deg
Longitude of ascending node	-126.19	-126.20	deg
Wedge angle	0.00	0.00	deg
Minimum altitude, t=124.3 sec		77.52	km
Peak dynamic pressure, t=113.2 sec		1173.6	N/m <sup>2</sup>
Peak heating rate, t= 96.5 sec		148.0	W/cm <sup>2</sup>
Peak aerodynamic force / weight, t=113.2 sec		1.39	
Peak change of orbital inclination, t=375.0 sec		0.02	deg
Peak change of longitude of ascending node, t=819.9 sec		0.01	deg
Peak wedge angle, t=341.3 sec		0.02	deg
Characteristic velocity at 178 NM		72.01	m/sec
Total characteristic velocity		72.01	m/sec

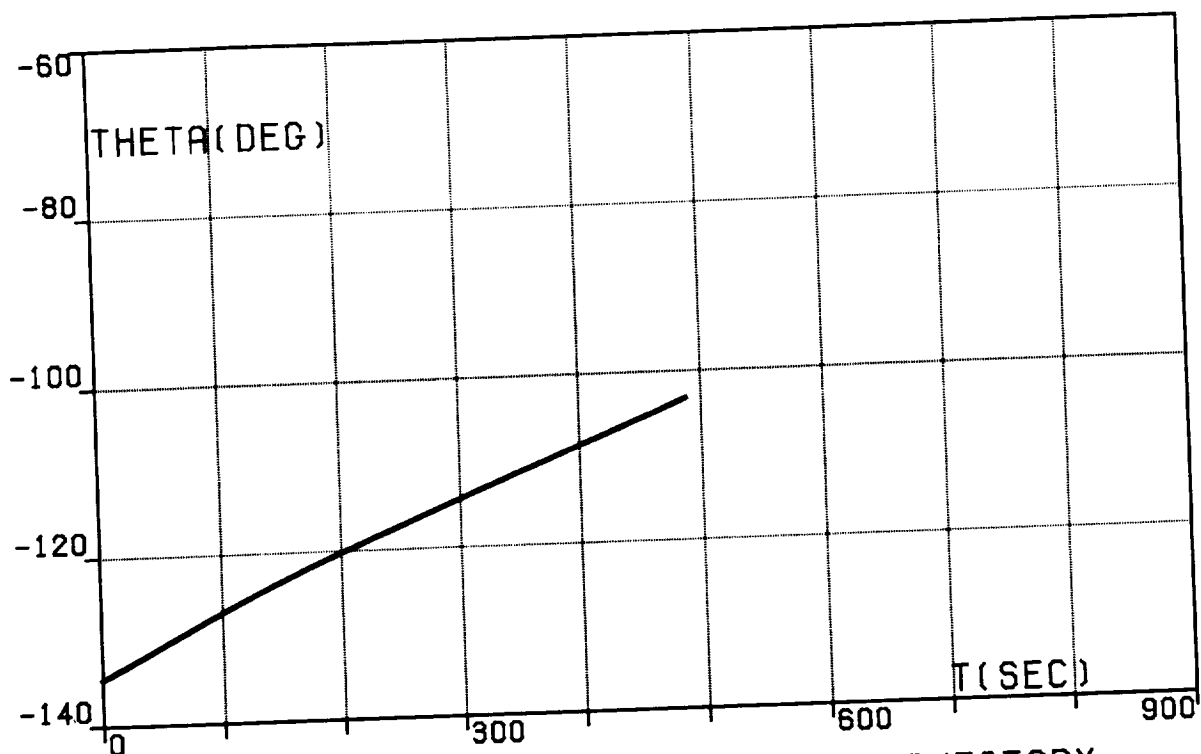


FIG.1A. FIVE-SEGMENT REFERENCE TRAJECTORY,  
TRANSFER (IA), LONGITUDE, RELATIVE.

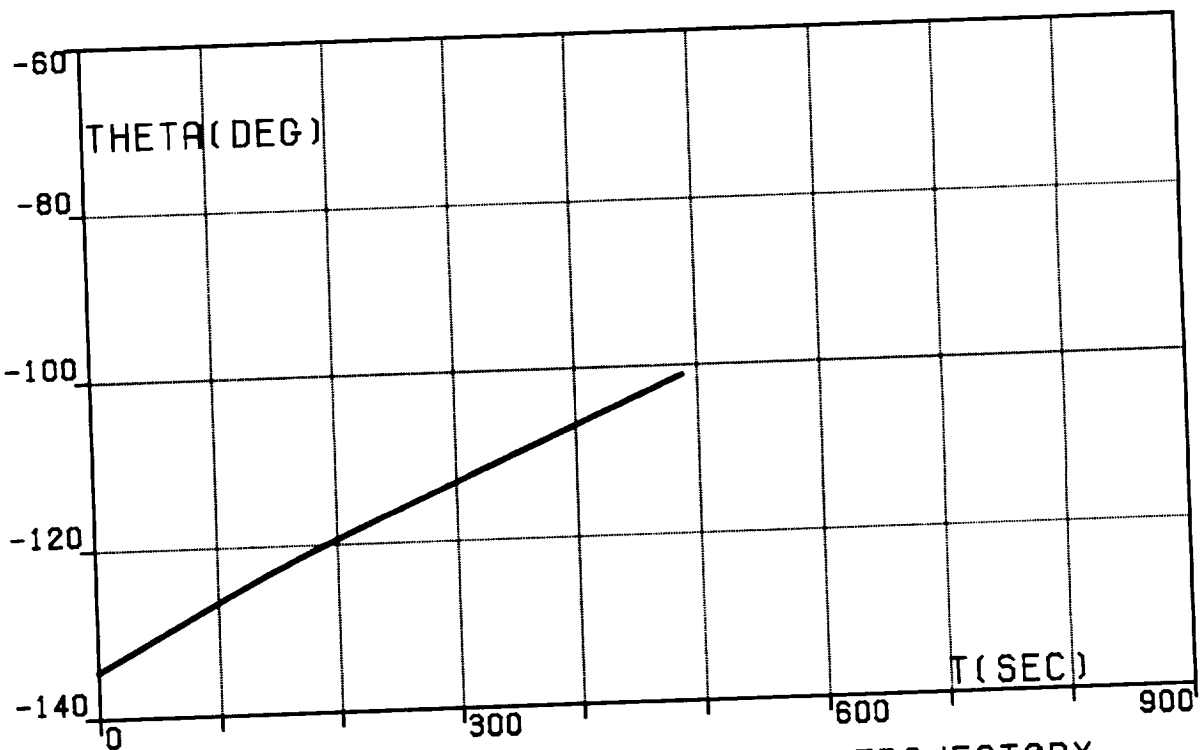


FIG.1B. FIVE-SEGMENT REFERENCE TRAJECTORY,  
TRANSFER (IA), LONGITUDE, INERTIAL.

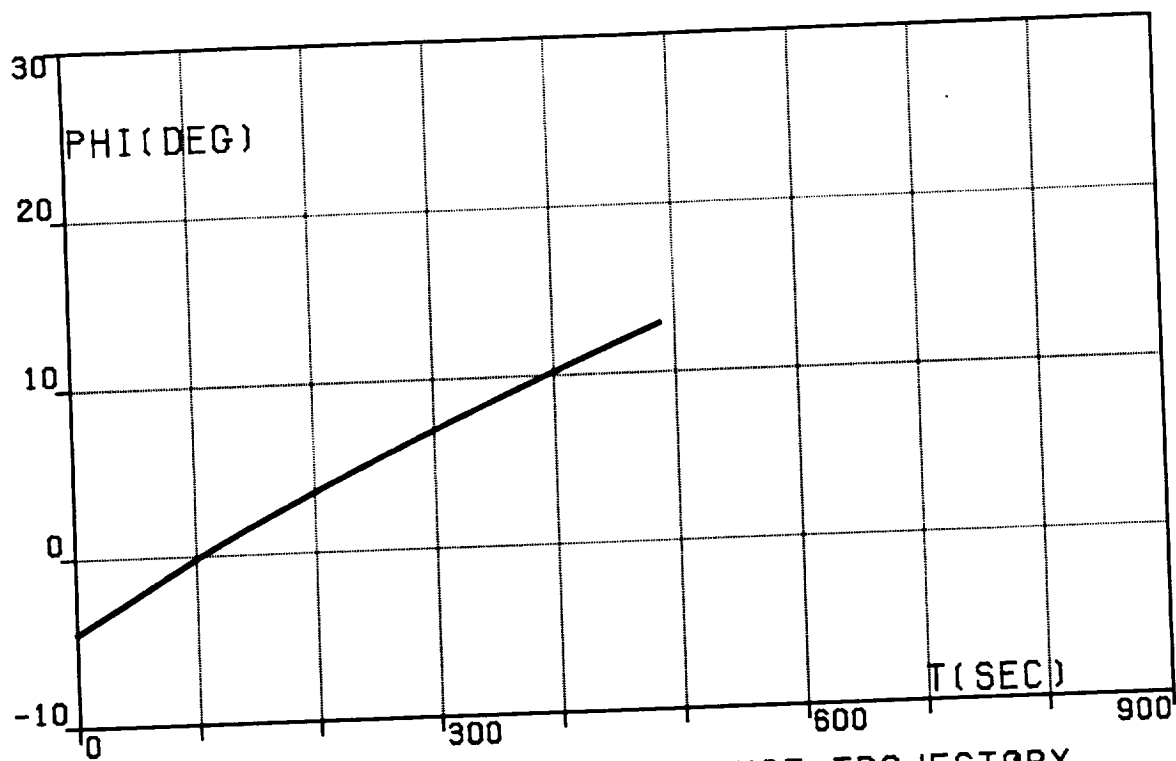


FIG.1C. FIVE-SEGMENT REFERENCE TRAJECTORY,  
TRANSFER (IA), LATITUDE.

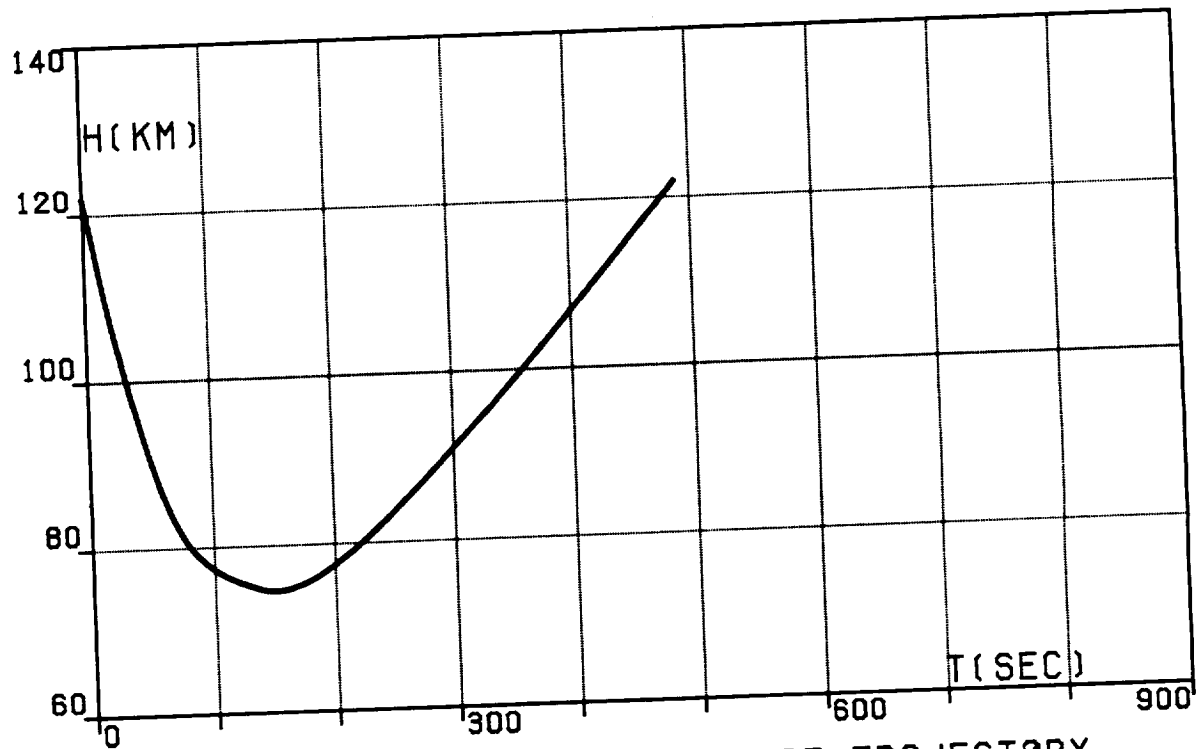


FIG.1D. FIVE-SEGMENT REFERENCE TRAJECTORY,  
TRANSFER (IA), ALTITUDE.

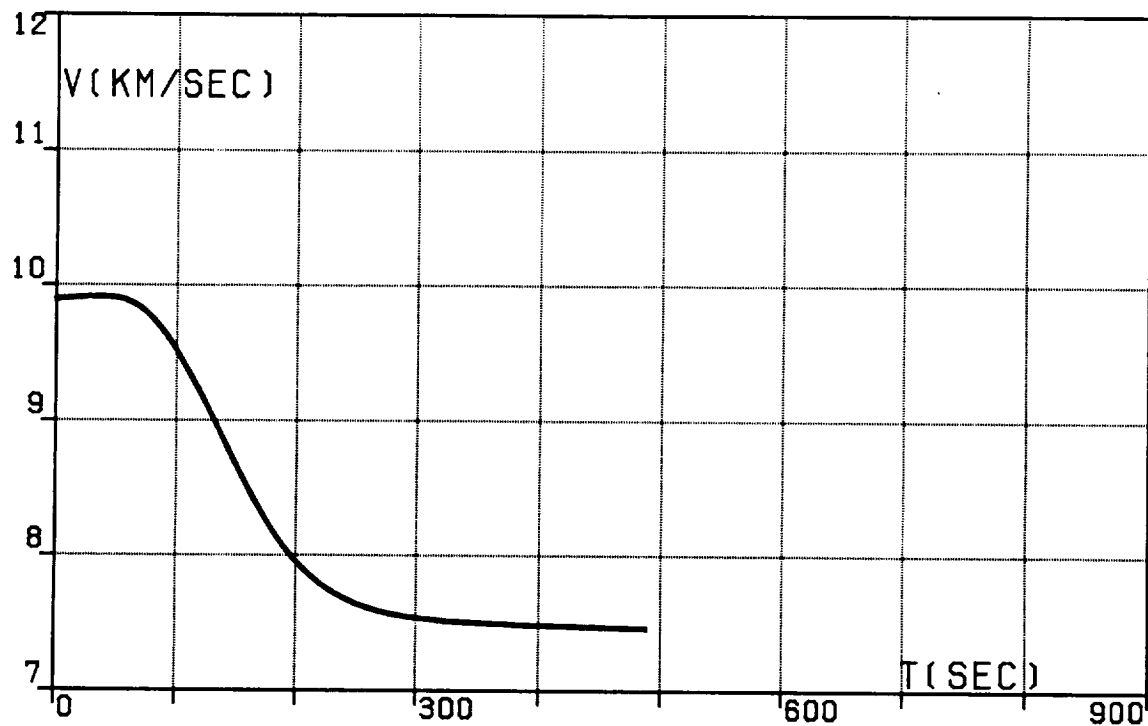


FIG.1E. FIVE-SEGMENT REFERENCE TRAJECTORY,  
TRANSFER (IA), VELOCITY, RELATIVE.

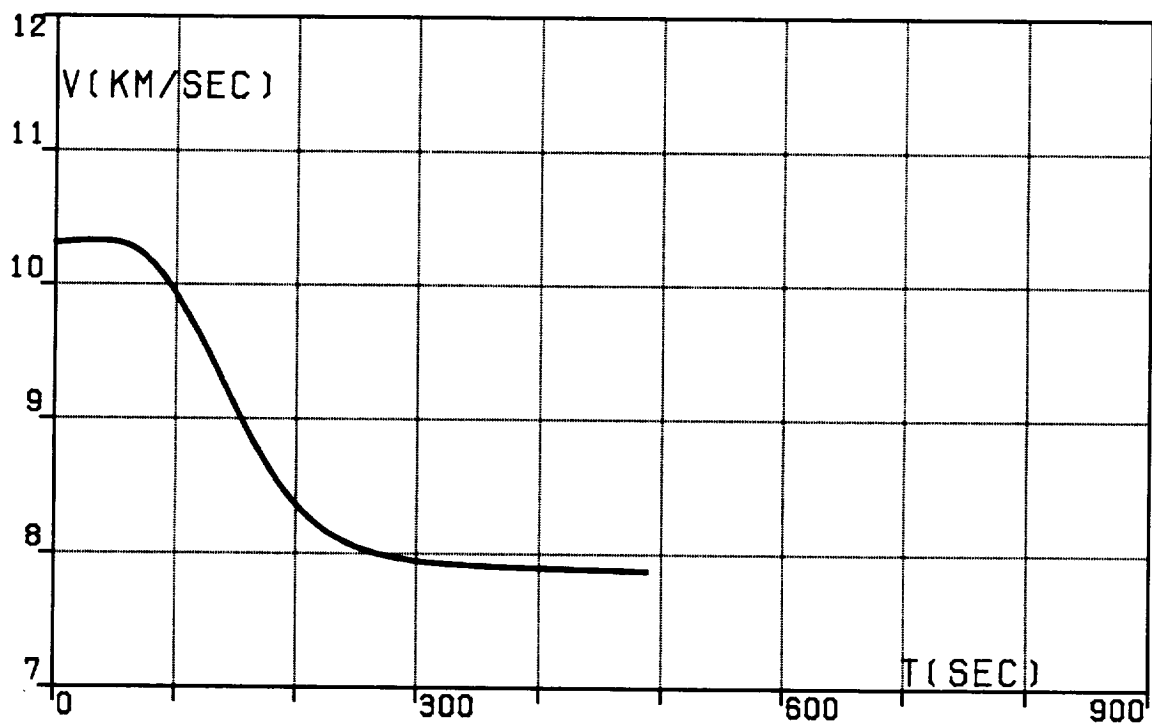


FIG.1F. FIVE-SEGMENT REFERENCE TRAJECTORY,  
TRANSFER (IA), VELOCITY, INERTIAL.

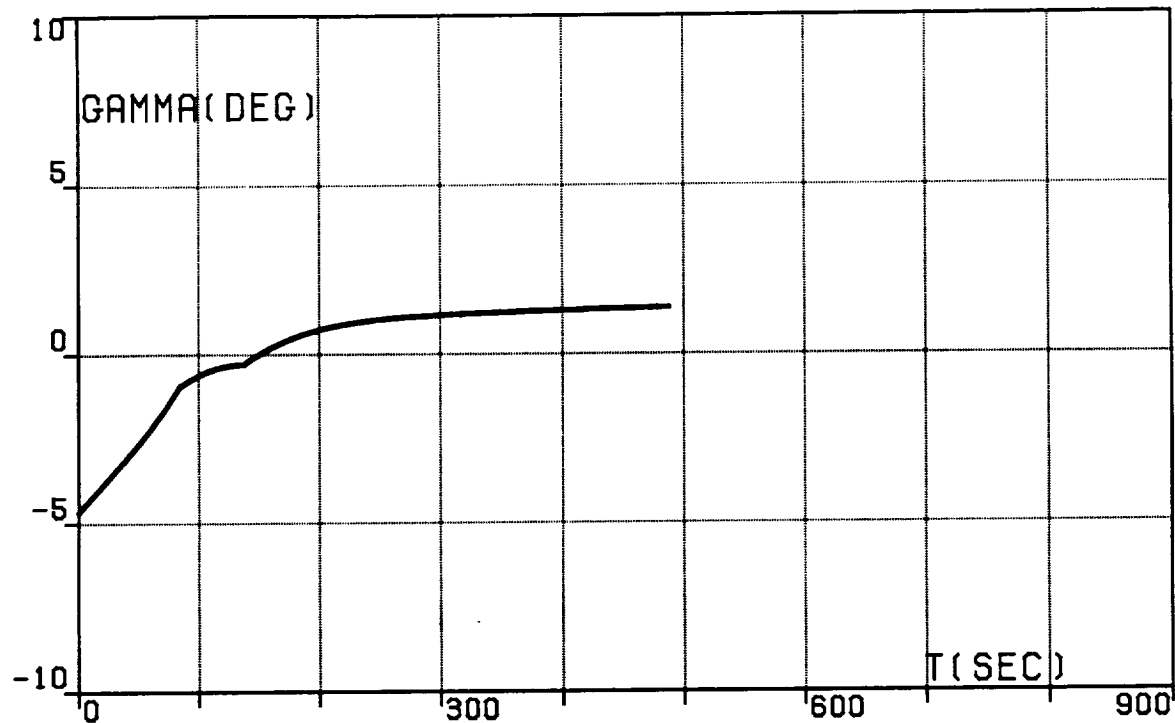


FIG.1G. FIVE-SEGMENT REFERENCE TRAJECTORY.  
TRANSFER (IA).  
PATH INCLINATION, RELATIVE.

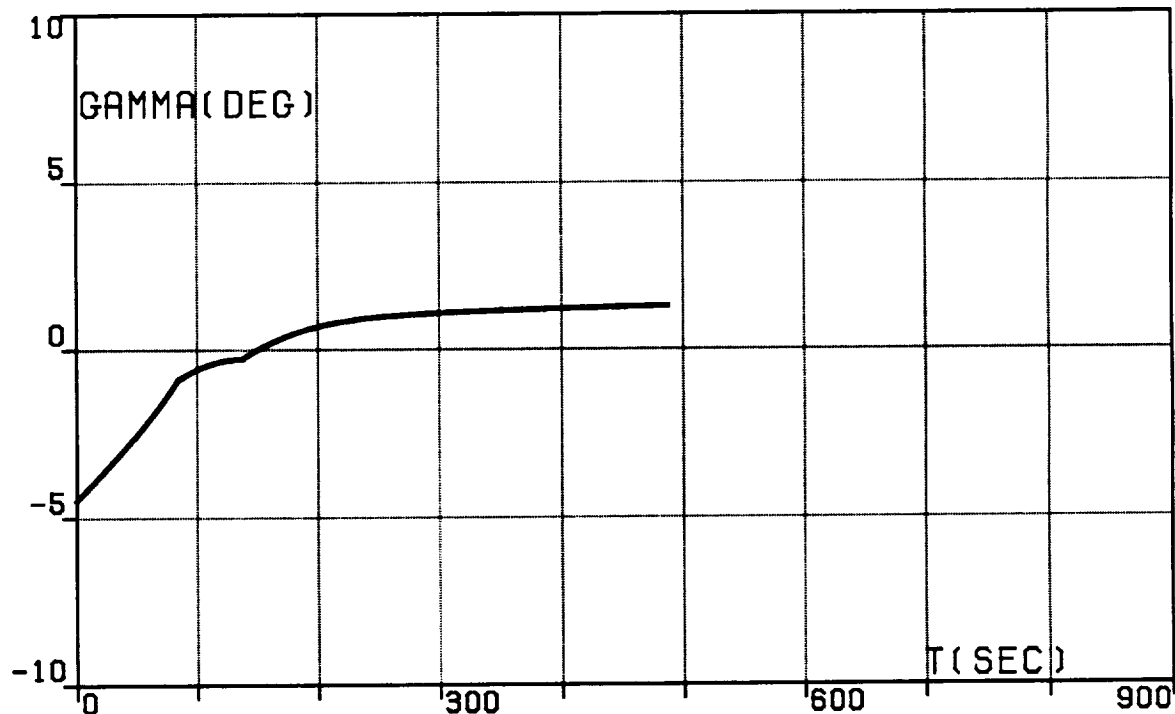


FIG.1H. FIVE-SEGMENT REFERENCE TRAJECTORY.  
TRANSFER (IA).  
PATH INCLINATION, INERTIAL.

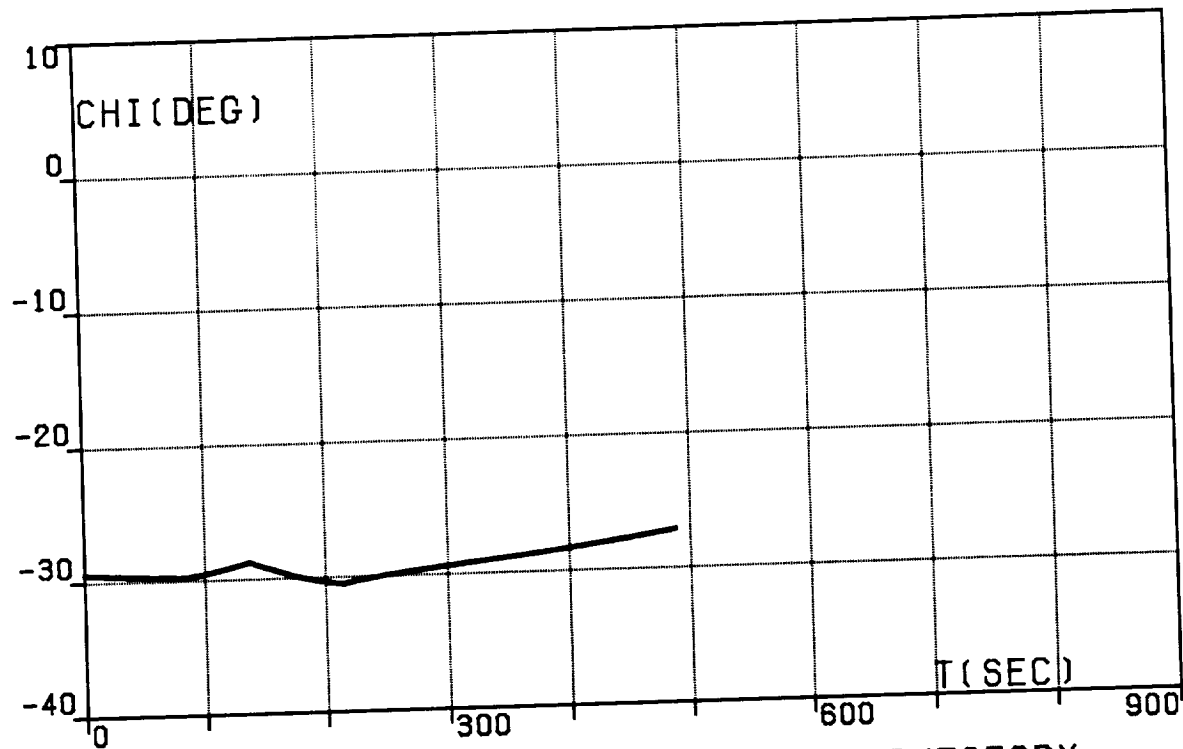


FIG.1I. FIVE-SEGMENT REFERENCE TRAJECTORY,  
TRANSFER (IA), HEADING ANGLE, RELATIVE.

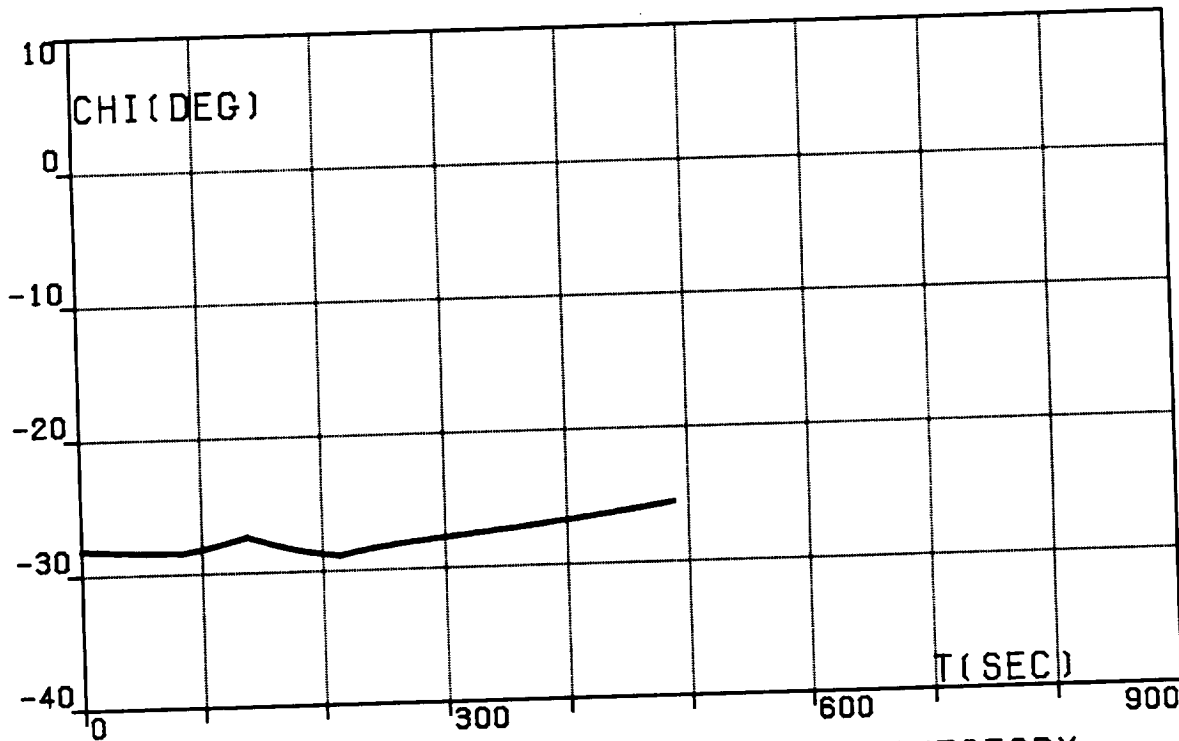


FIG.1J. FIVE-SEGMENT REFERENCE TRAJECTORY,  
TRANSFER (IA), HEADING ANGLE, INERTIAL.

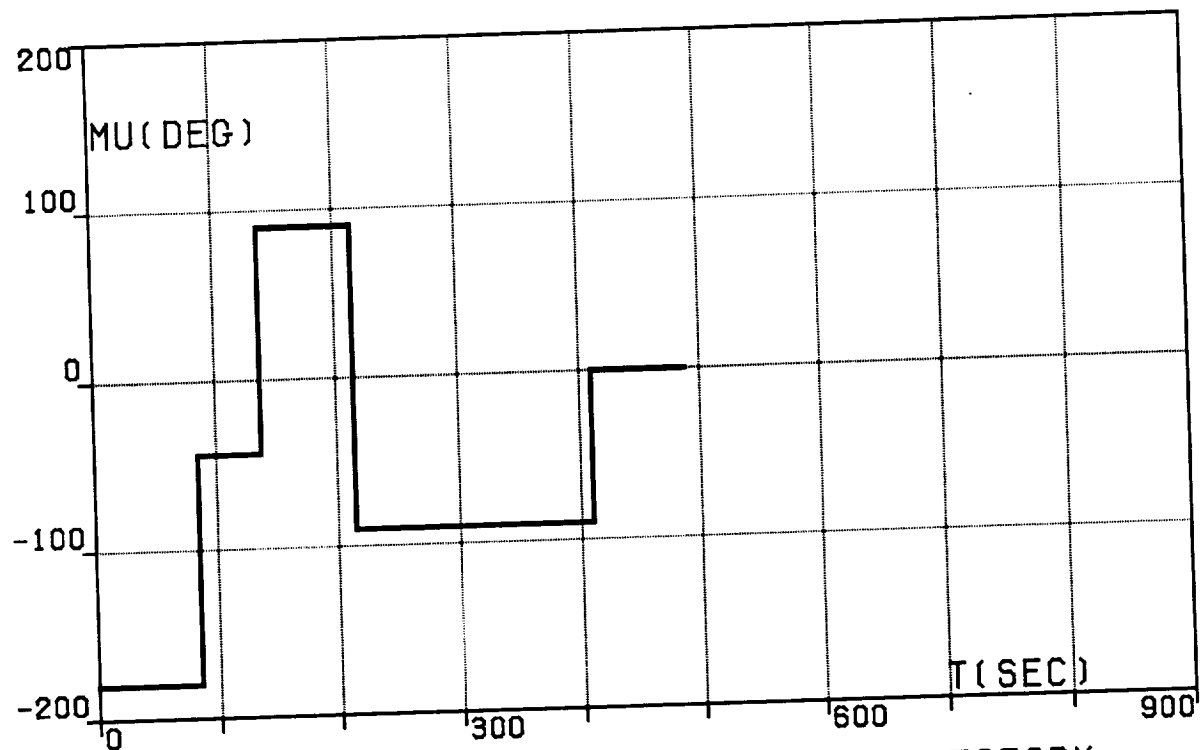


FIG.1K. FIVE-SEGMENT REFERENCE TRAJECTORY,  
TRANSFER (IA), BANK ANGLE.

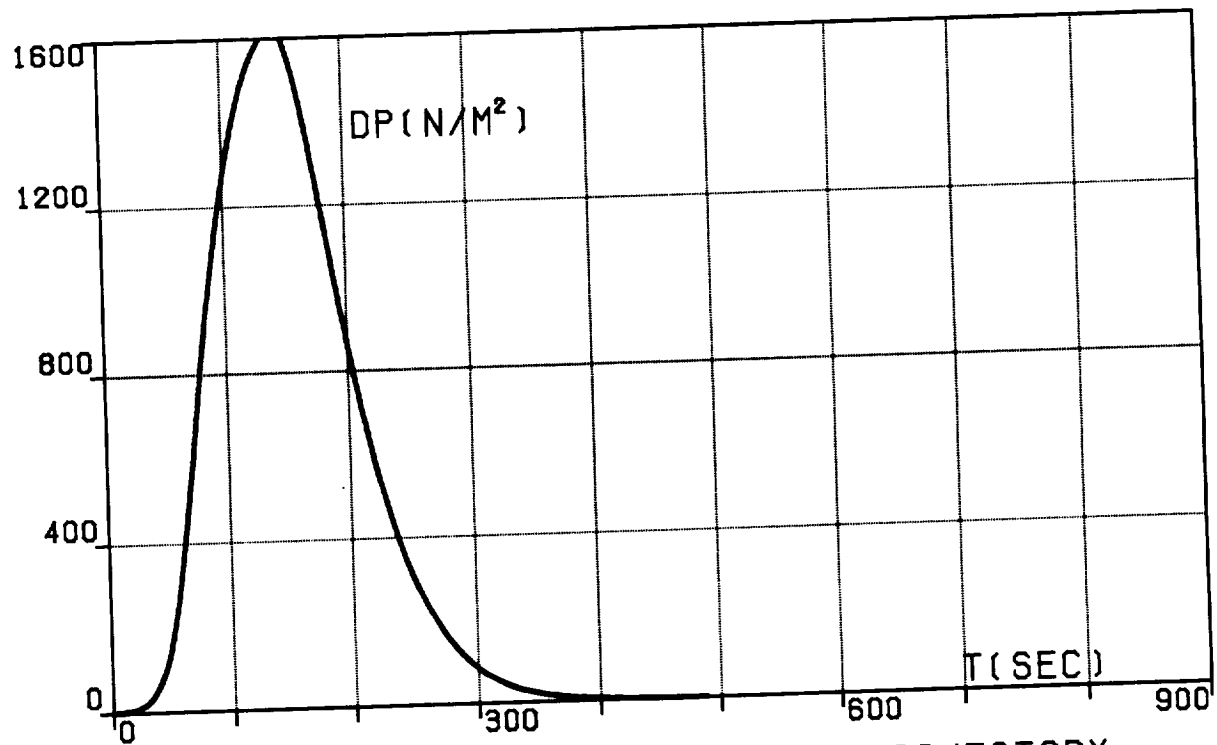


FIG.1L. FIVE-SEGMENT REFERENCE TRAJECTORY,  
TRANSFER (IA), DYNAMIC PRESSURE.

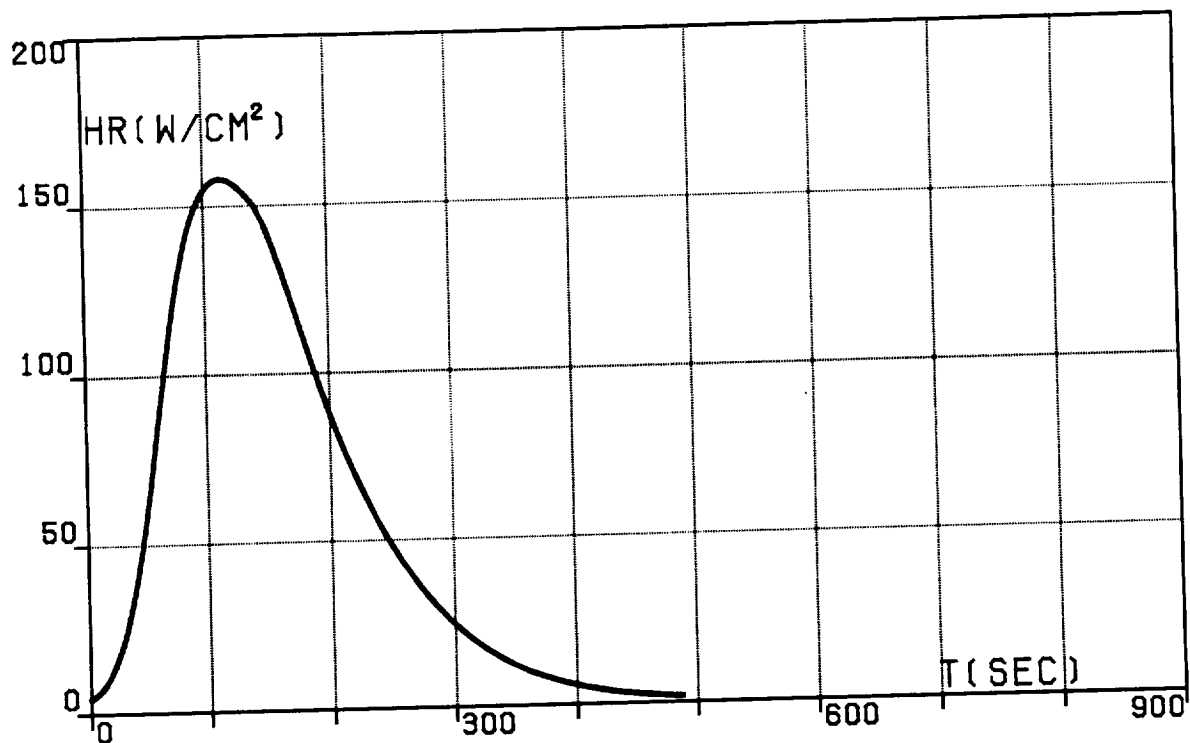


FIG.1M. FIVE-SEGMENT REFERENCE TRAJECTORY,  
TRANSFER (IA), HEATING RATE.

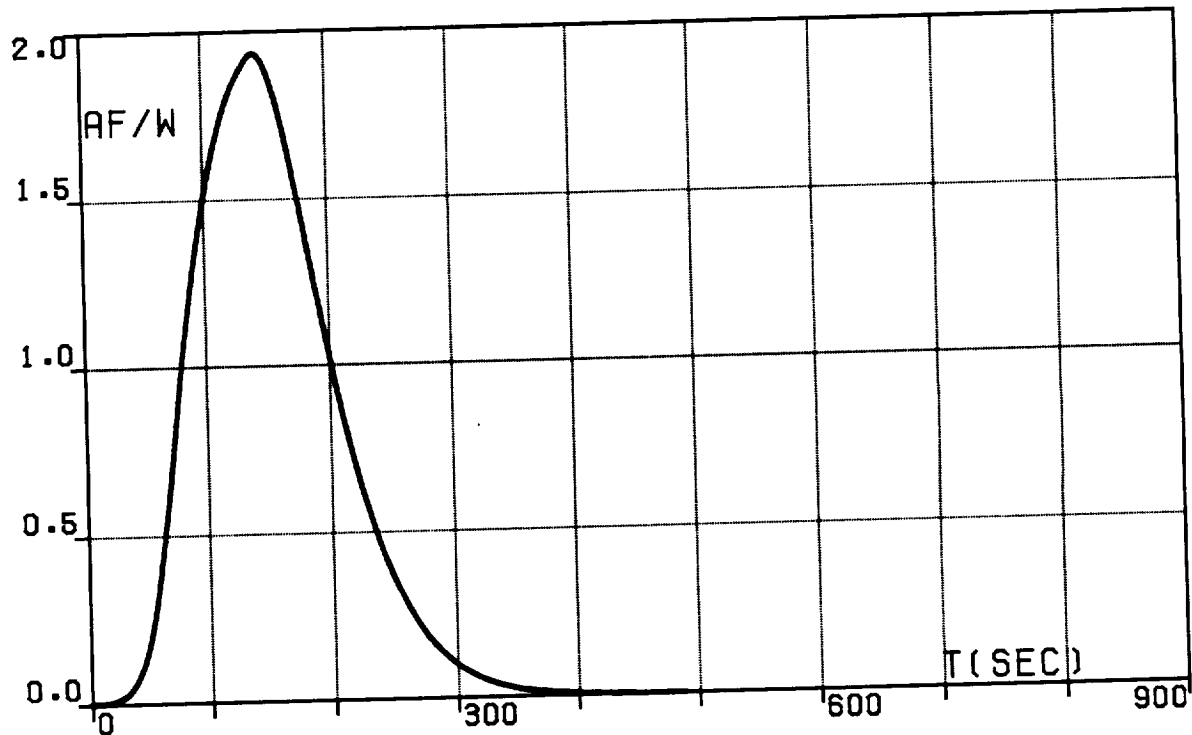


FIG.1N. FIVE-SEGMENT REFERENCE TRAJECTORY,  
TRANSFER (IA),  
AERODYNAMIC FORCE PER UNIT WEIGHT.

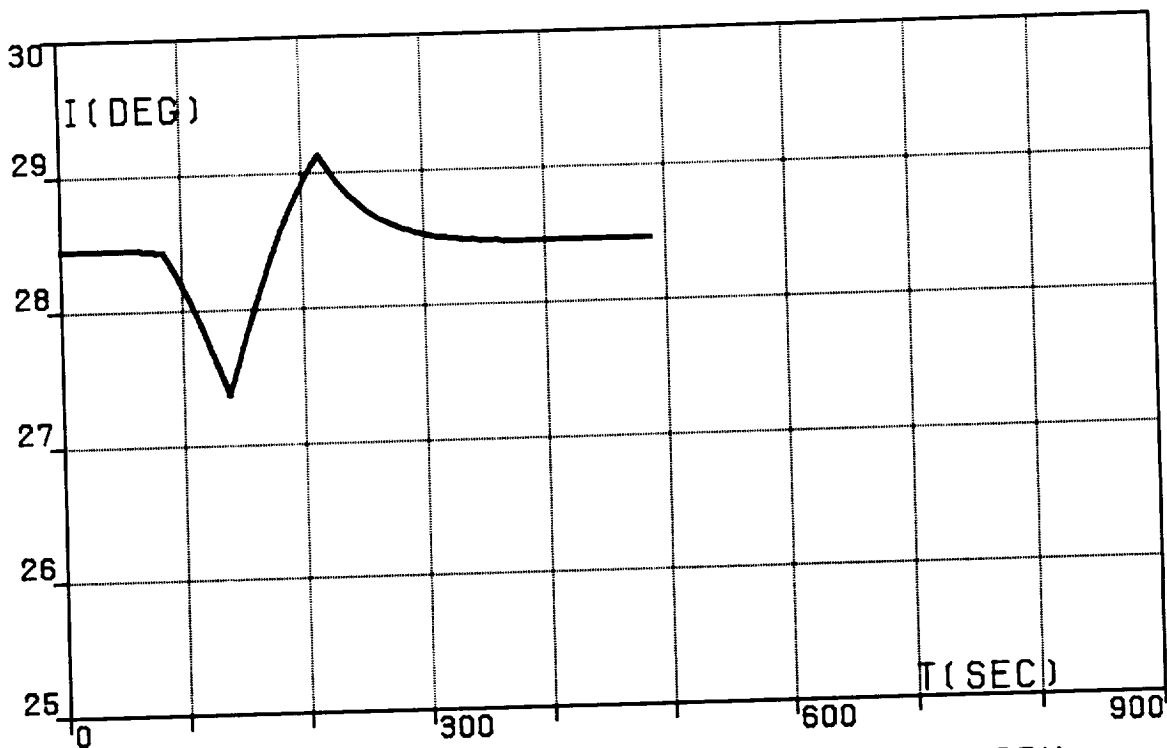


FIG.10. FIVE-SEGMENT REFERENCE TRAJECTORY,  
TRANSFER (IA), ORBITAL INCLINATION.

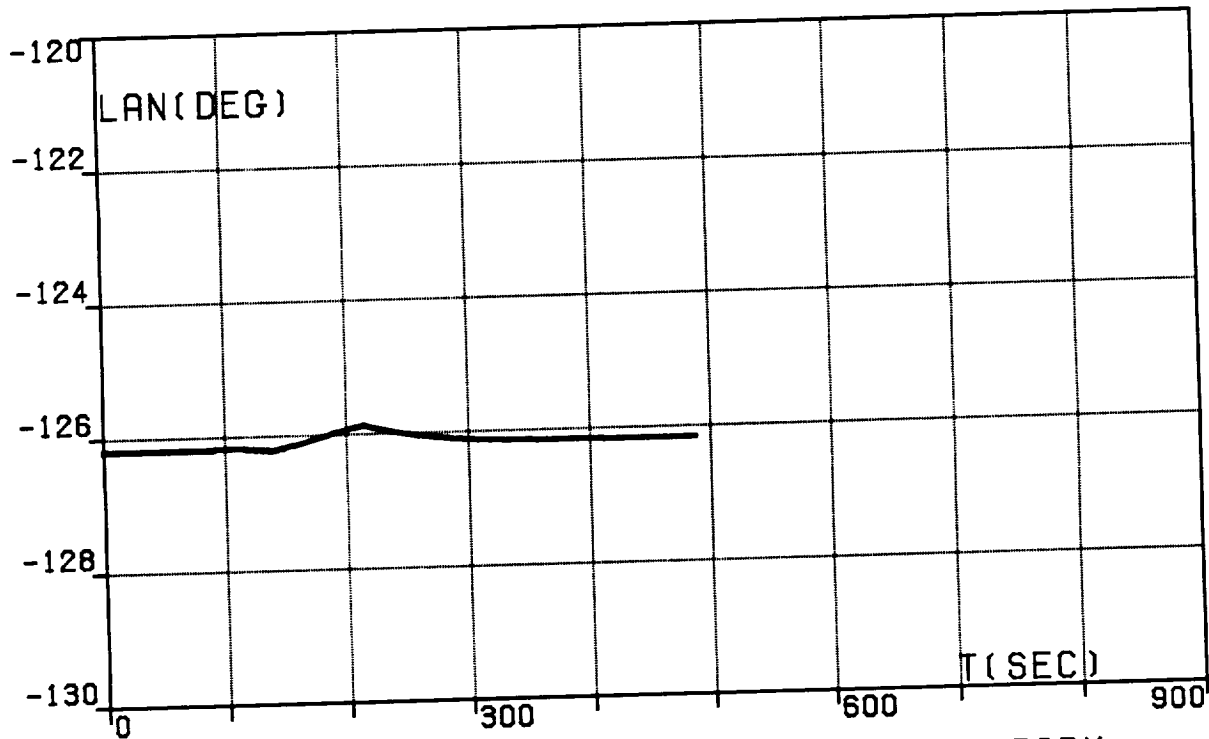


FIG.1P. FIVE-SEGMENT REFERENCE TRAJECTORY,  
TRANSFER (IA),  
LONGITUDE OF THE ASCENDING NODE.

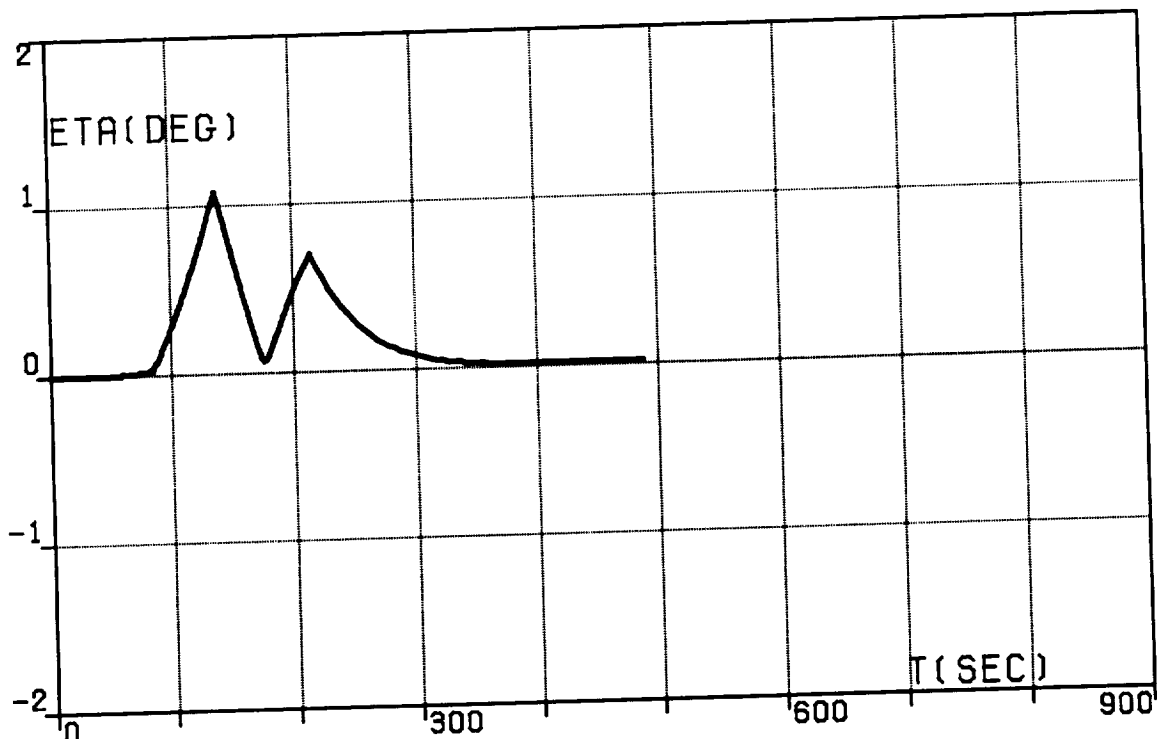


FIG.1Q. FIVE-SEGMENT REFERENCE TRAJECTORY,  
TRANSFER (IA), WEDGE ANGLE.

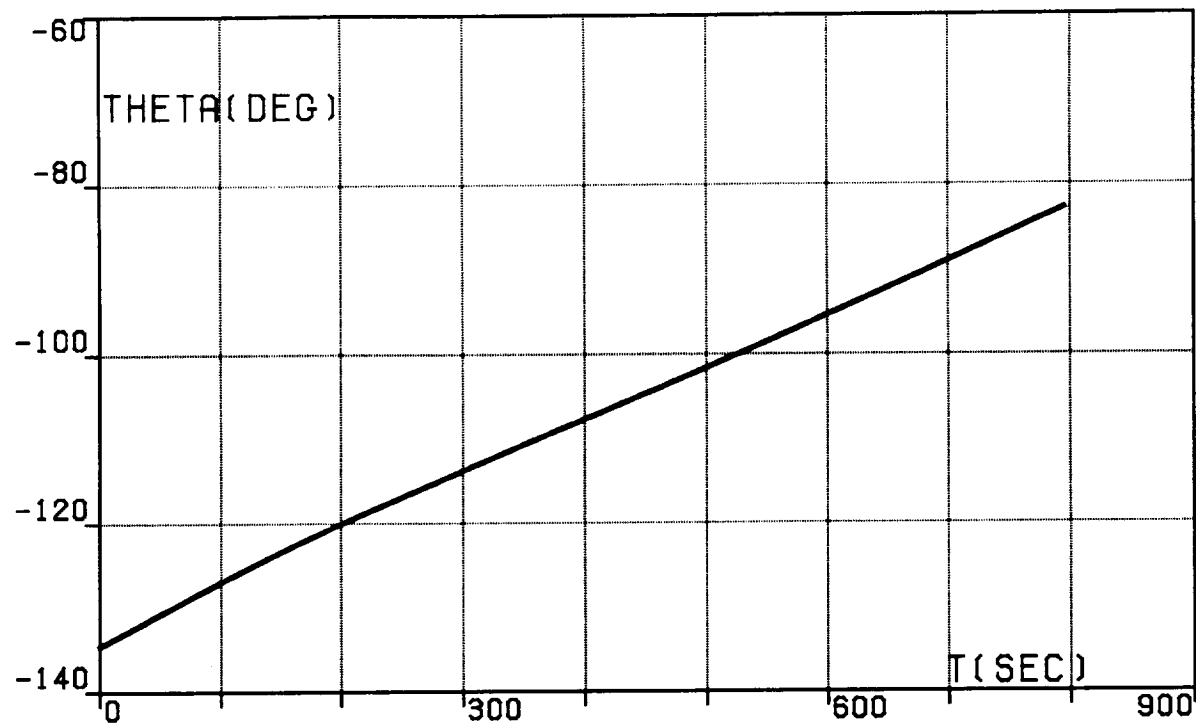


FIG.2A. CONTINUOUS OPTIMAL TRAJECTORY,  
TRANSFER (IA), LONGITUDE, RELATIVE.

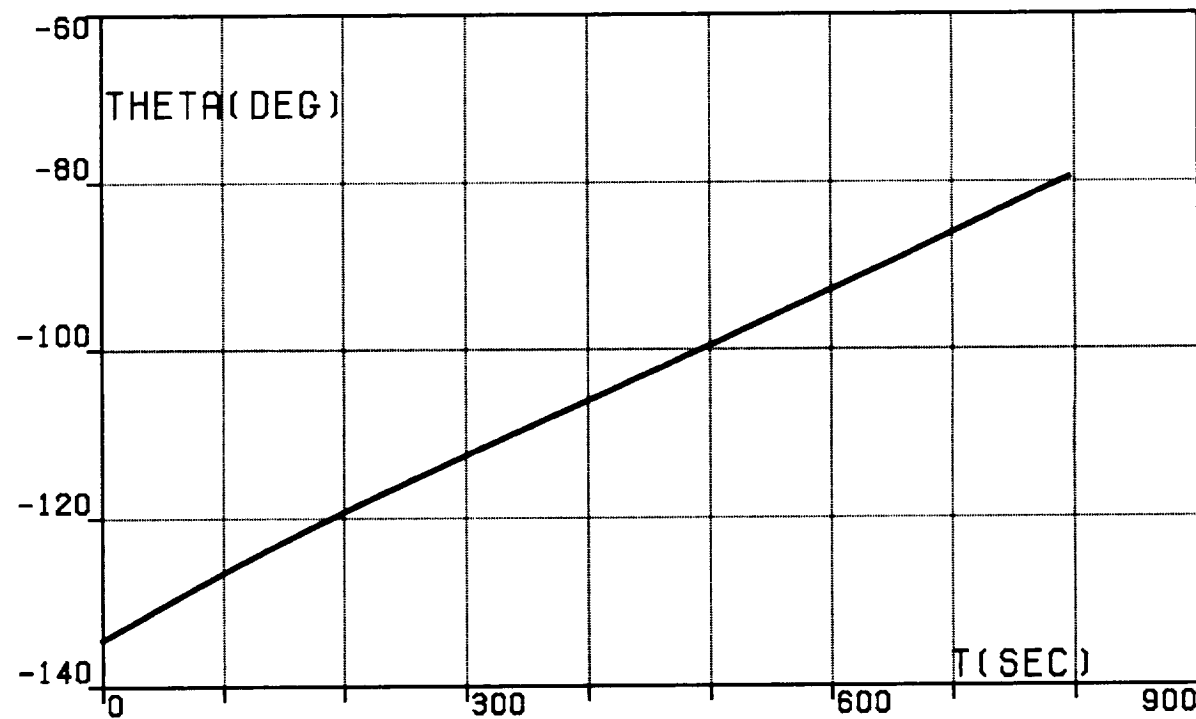


FIG.2B. CONTINUOUS OPTIMAL TRAJECTORY,  
TRANSFER (IA), LONGITUDE, INERTIAL.

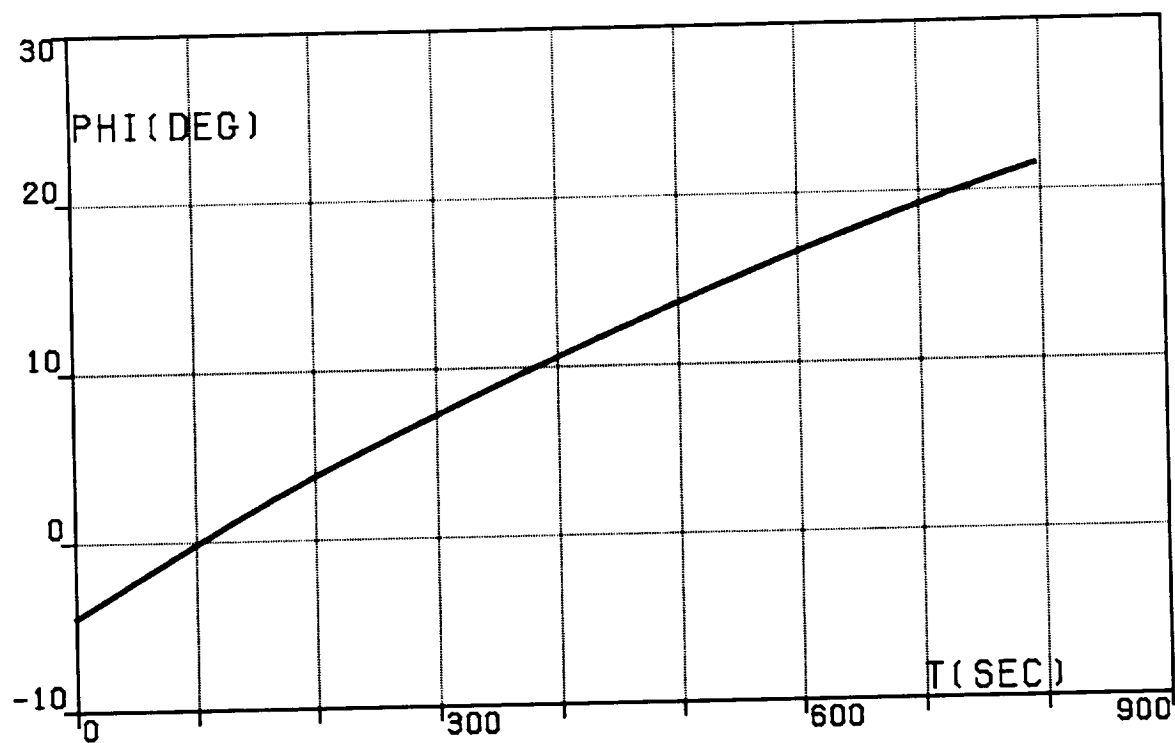


FIG.2C. CONTINUOUS OPTIMAL TRAJECTORY,  
TRANSFER (IA), LATITUDE.

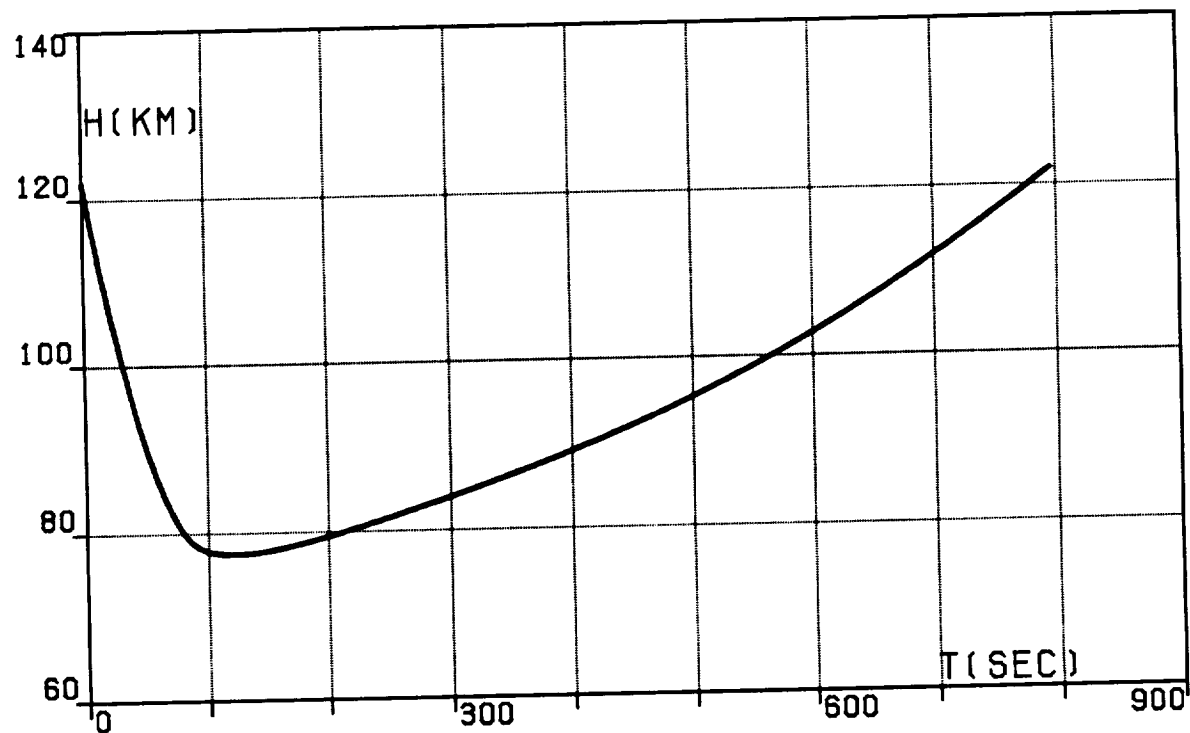


FIG.2D. CONTINUOUS OPTIMAL TRAJECTORY,  
TRANSFER (IA), ALTITUDE.

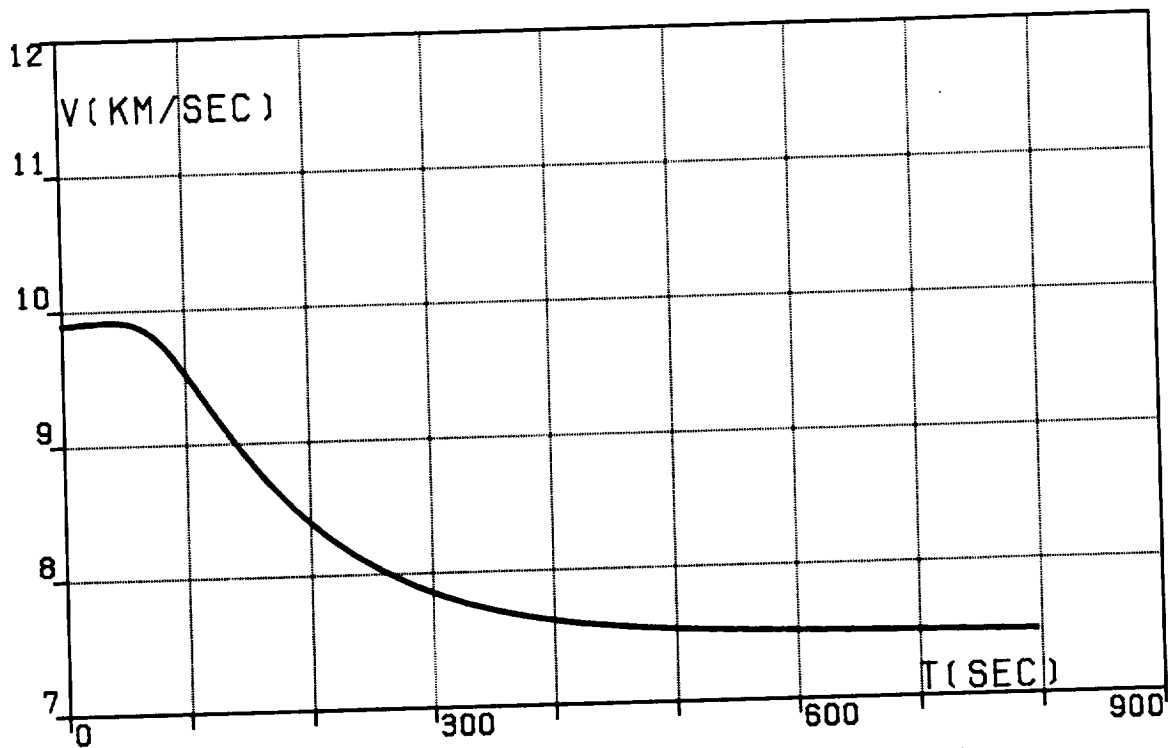


FIG.2E. CONTINUOUS OPTIMAL TRAJECTORY,  
TRANSFER (IA), VELOCITY, RELATIVE.

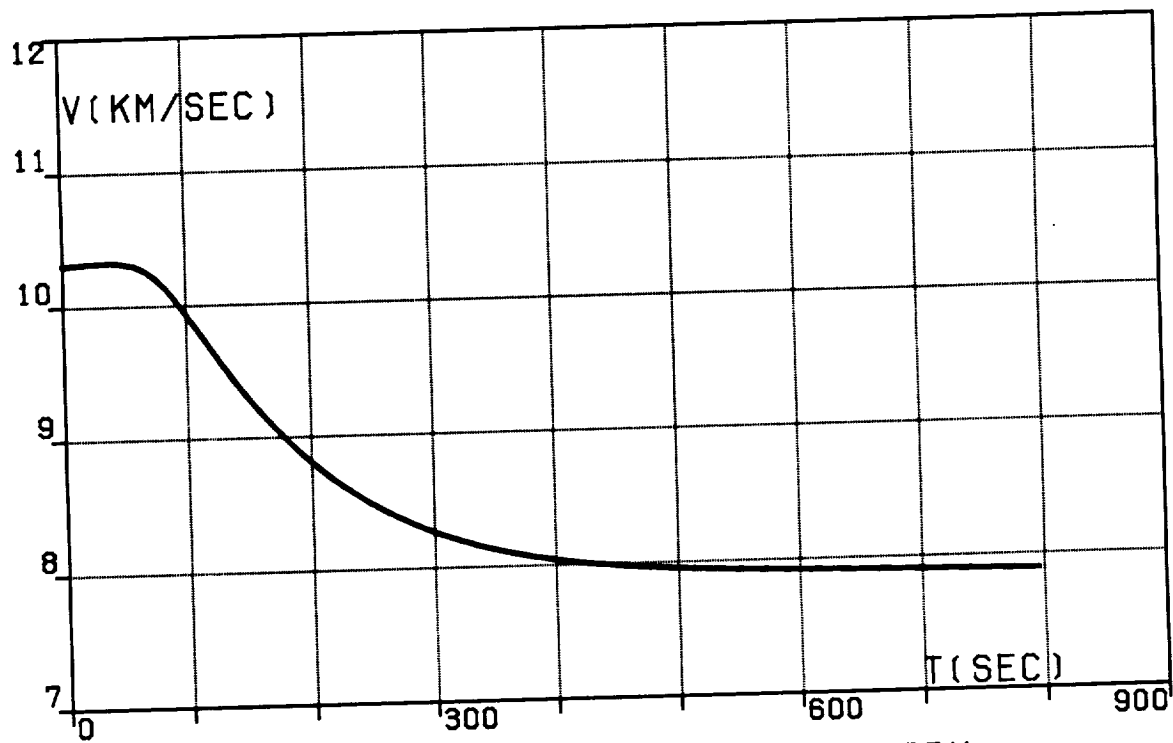


FIG.2F. CONTINUOUS OPTIMAL TRAJECTORY,  
TRANSFER (IA), VELOCITY, INERTIAL.

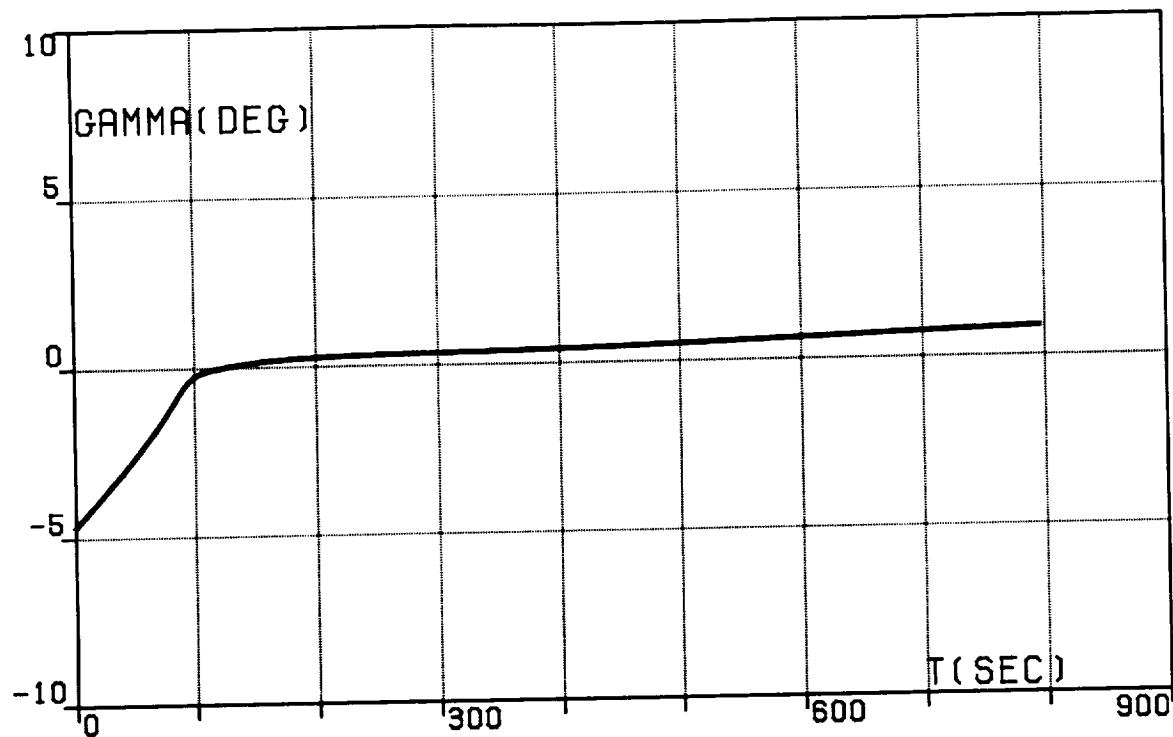


FIG.2G. CONTINUOUS OPTIMAL TRAJECTORY,  
TRANSFER (IA),  
PATH INCLINATION, RELATIVE.

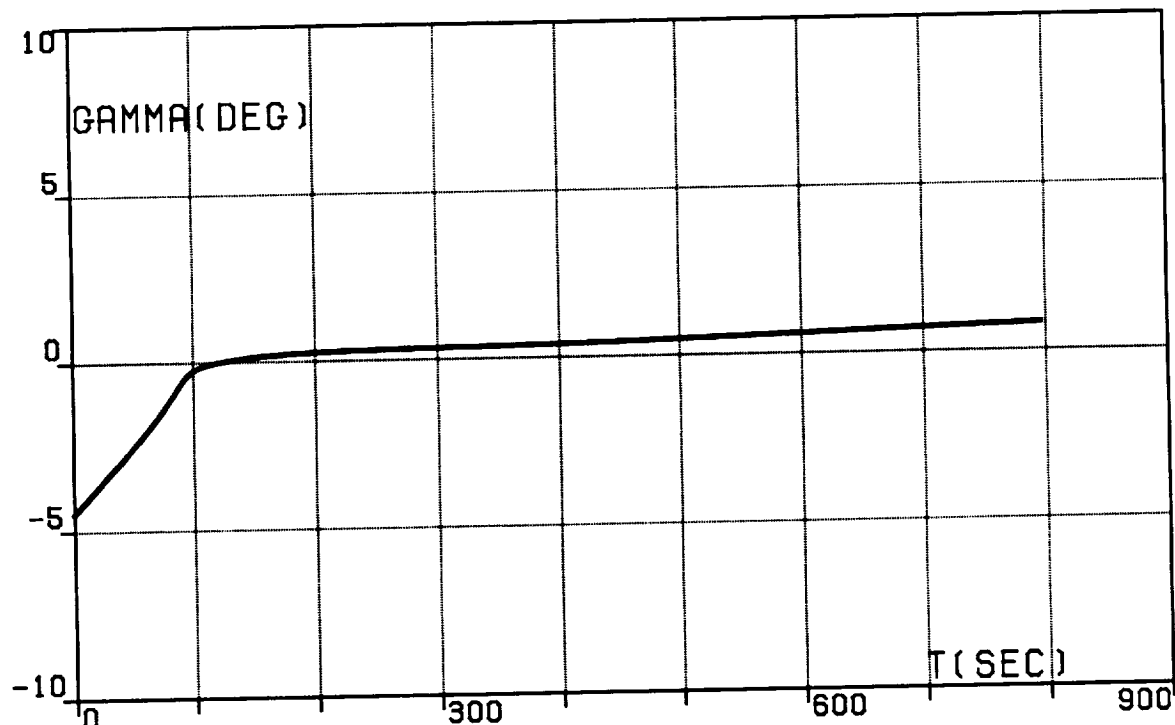


FIG.2H. CONTINUOUS OPTIMAL TRAJECTORY,  
TRANSFER (IA),  
PATH INCLINATION, INERTIAL.

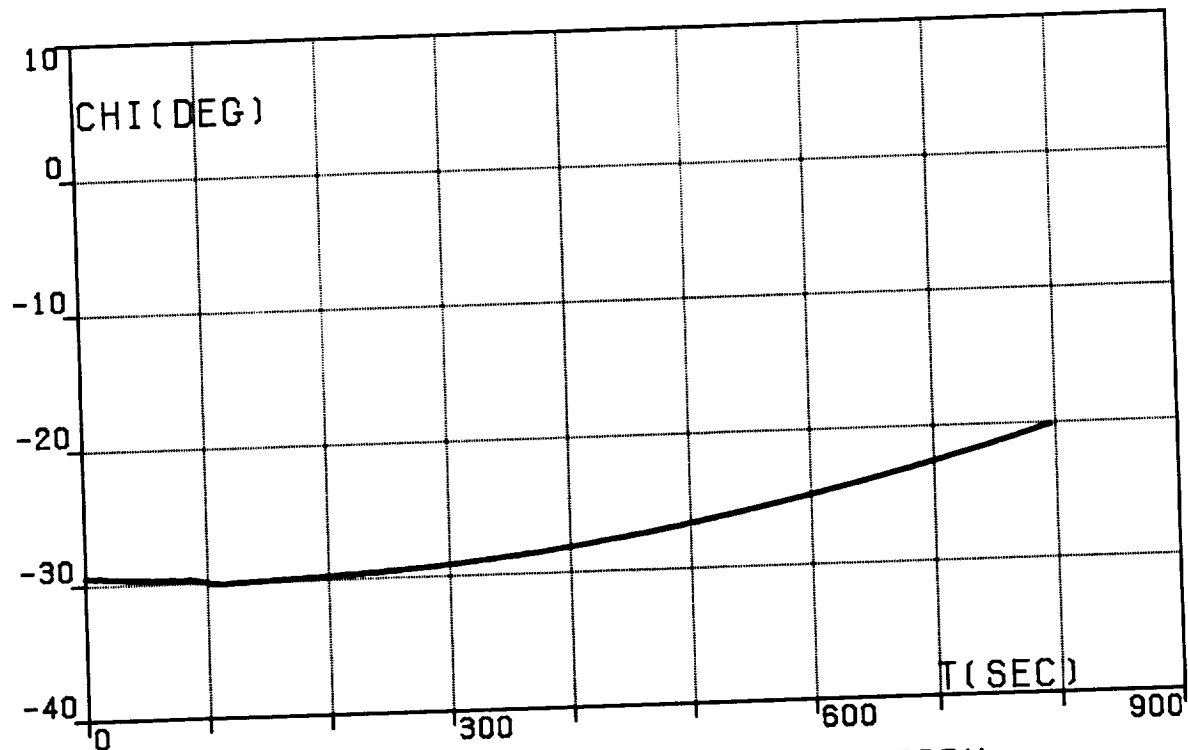


FIG.2I. CONTINUOUS OPTIMAL TRAJECTORY.  
TRANSFER (IA), HEADING ANGLE, RELATIVE.

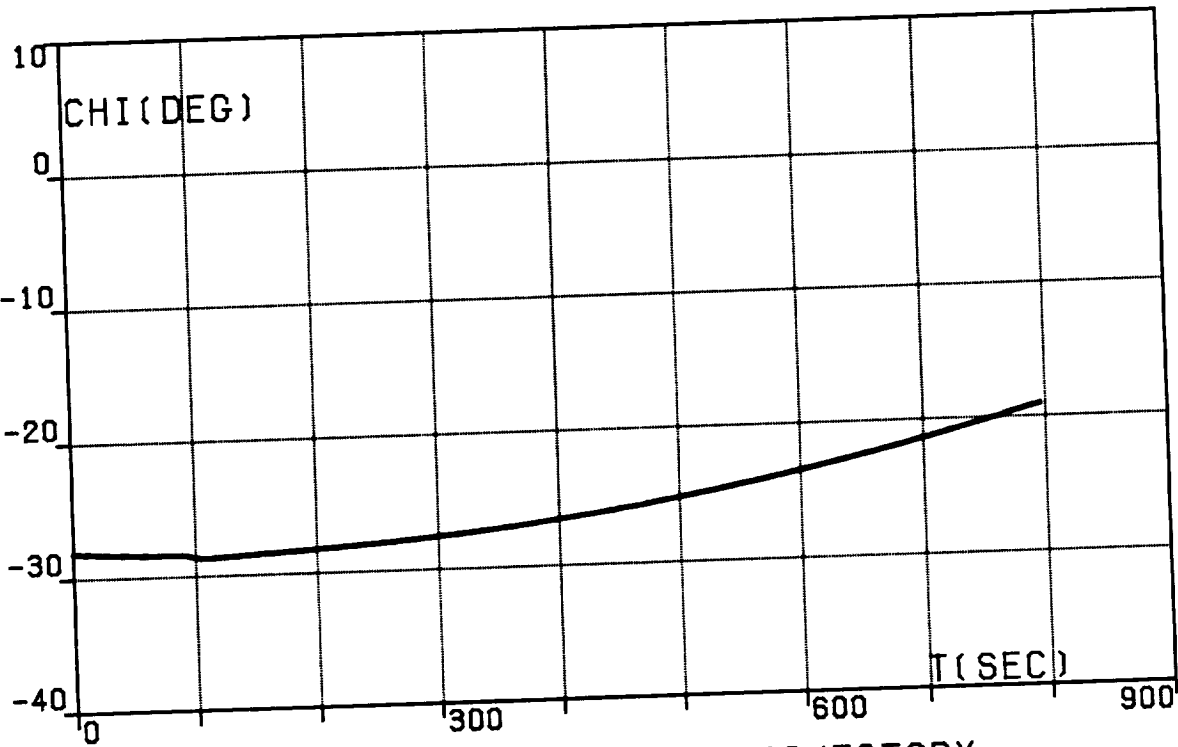


FIG.2J. CONTINUOUS OPTIMAL TRAJECTORY,  
TRANSFER (IA), HEADING ANGLE, INERTIAL.

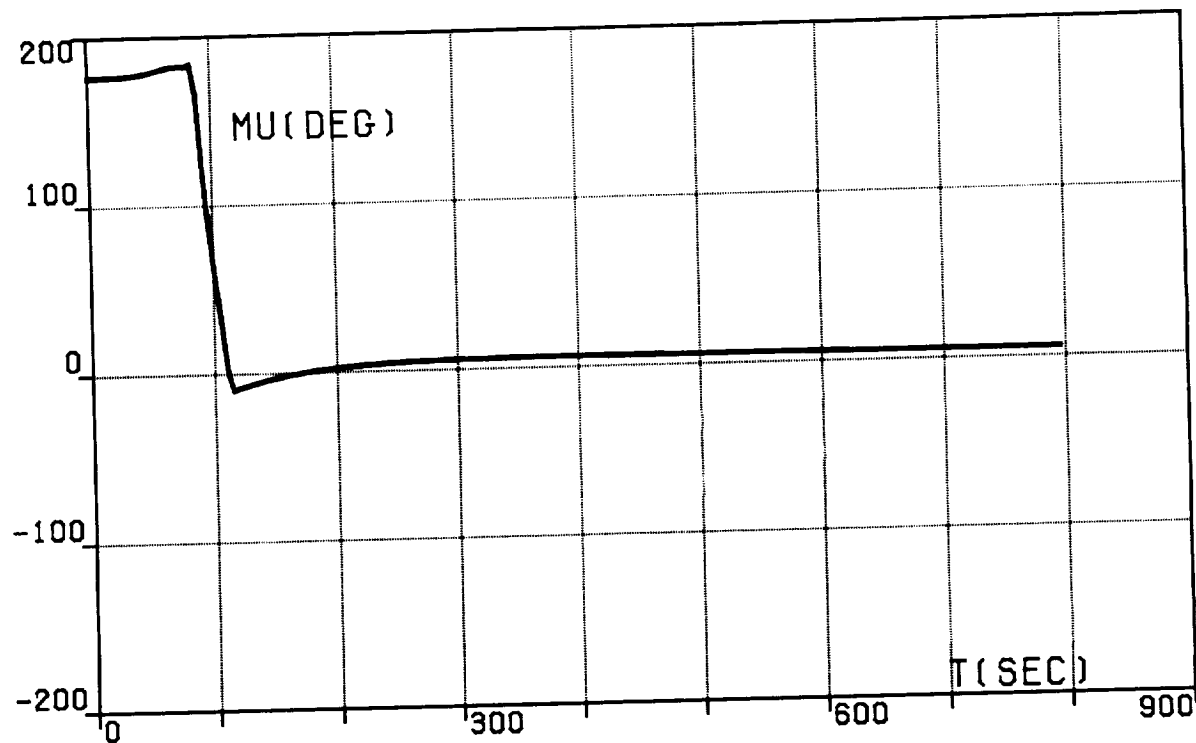


FIG.2K. CONTINUOUS OPTIMAL TRAJECTORY,  
TRANSFER (IA), BANK ANGLE.

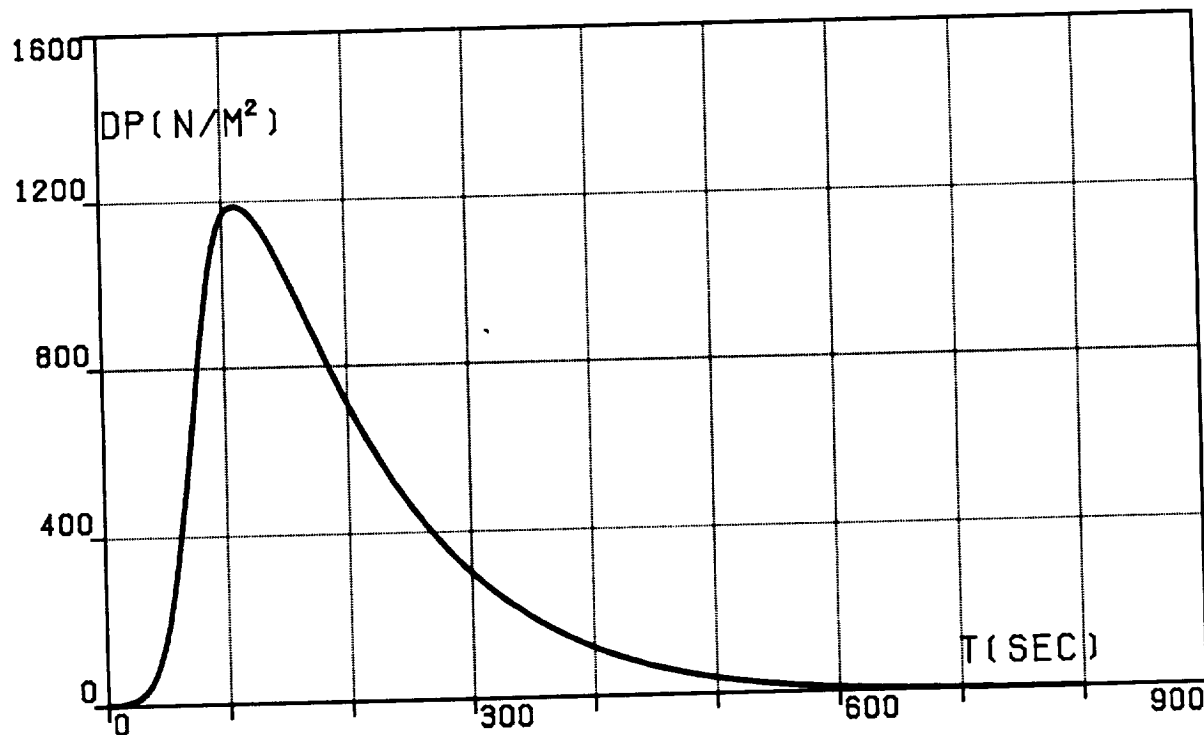


FIG.2L. CONTINUOUS OPTIMAL TRAJECTORY,  
TRANSFER (IA), DYNAMIC PRESSURE.

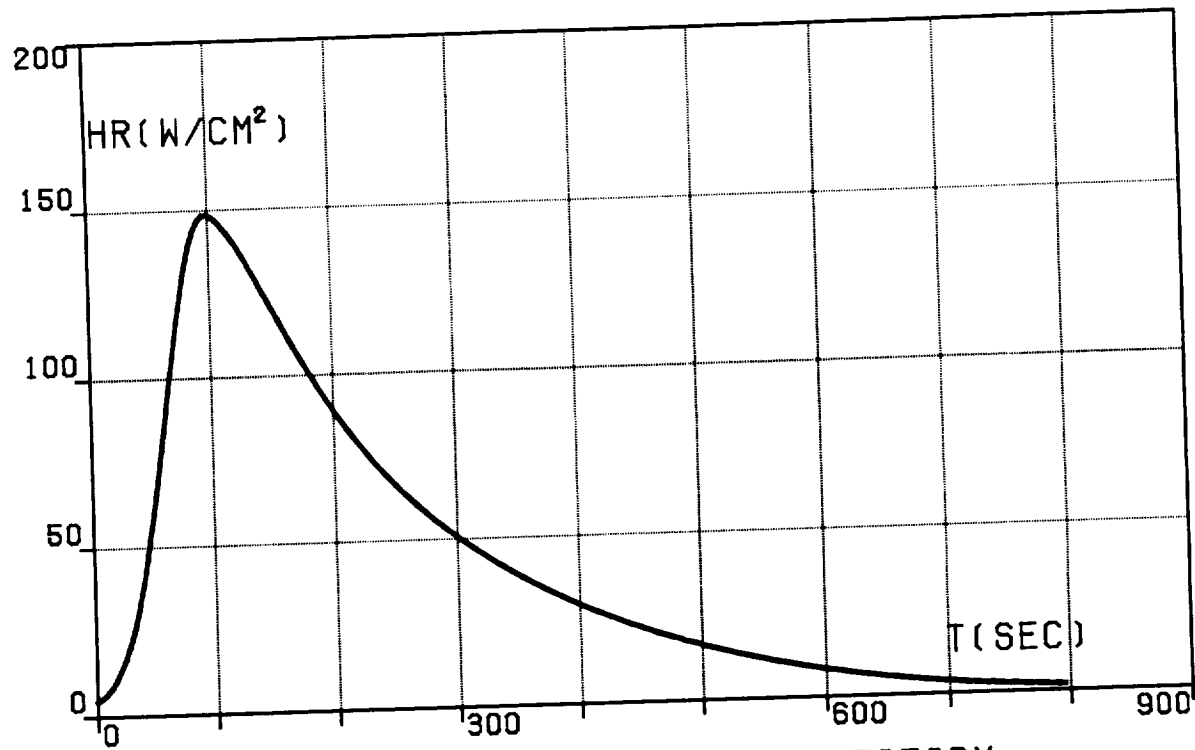


FIG.2M. CONTINUOUS OPTIMAL TRAJECTORY,  
TRANSFER (IA). HEATING RATE.

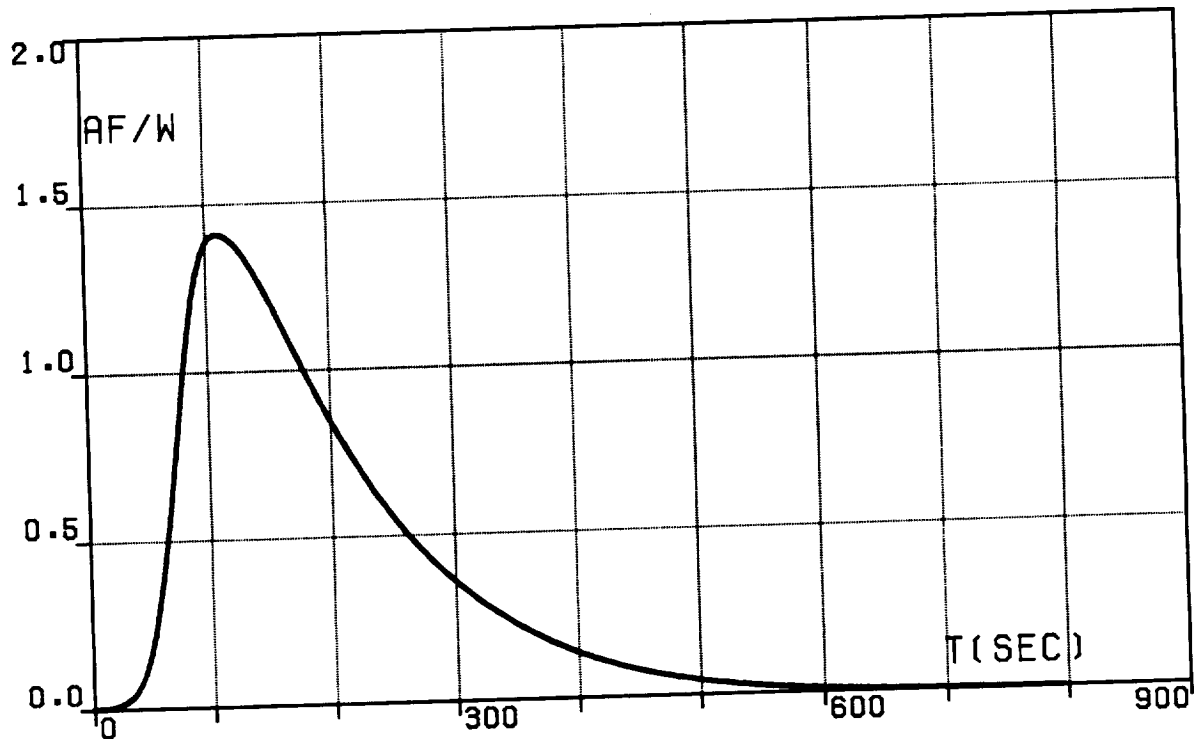


FIG.2N. CONTINUOUS OPTIMAL TRAJECTORY,  
TRANSFER (IA).  
AERODYNAMIC FORCE PER UNIT WEIGHT.

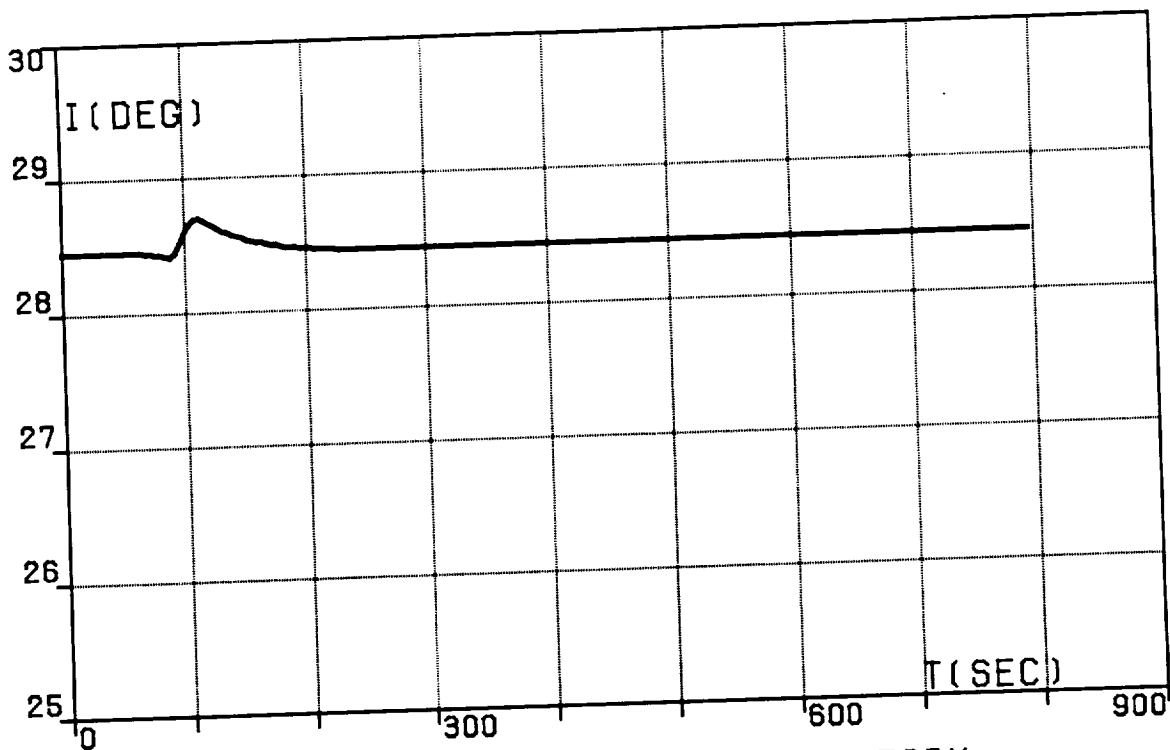


FIG.20. CONTINUOUS OPTIMAL TRAJECTORY,  
TRANSFER (IA), ORBITAL INCLINATION.

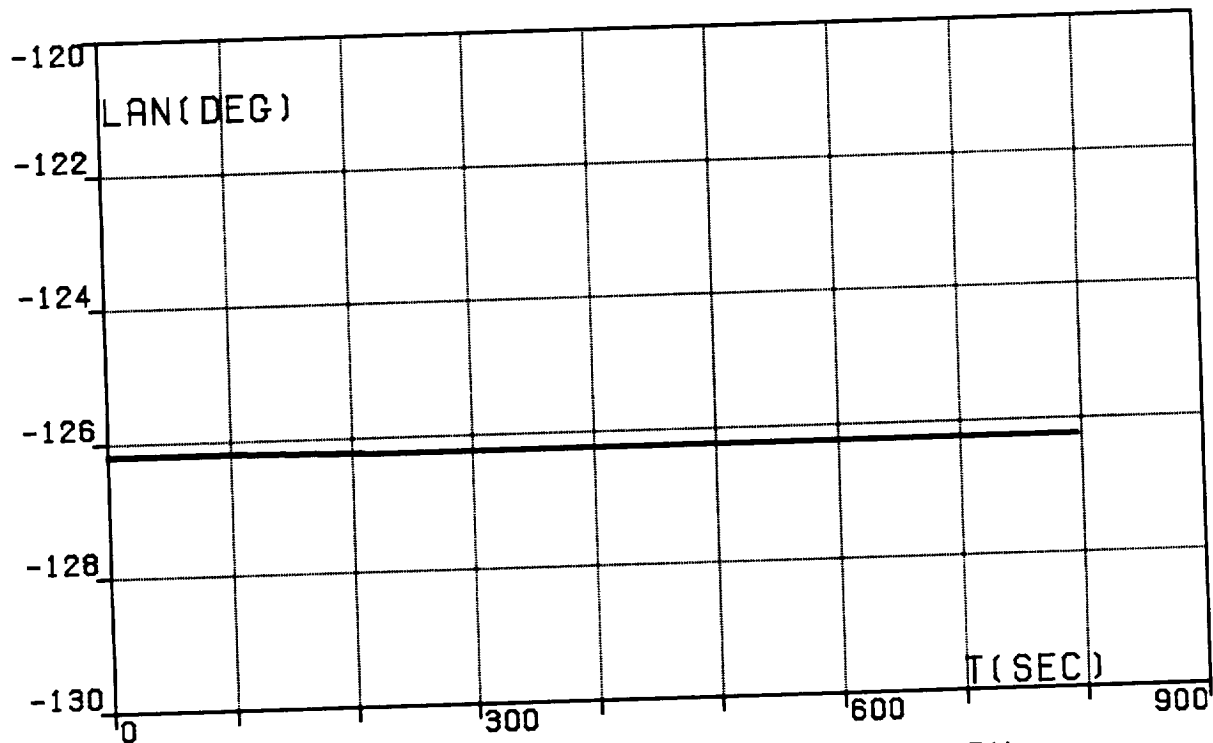


FIG.2P. CONTINUOUS OPTIMAL TRAJECTORY,  
TRANSFER (IA),  
LONGITUDE OF THE ASCENDING NODE.

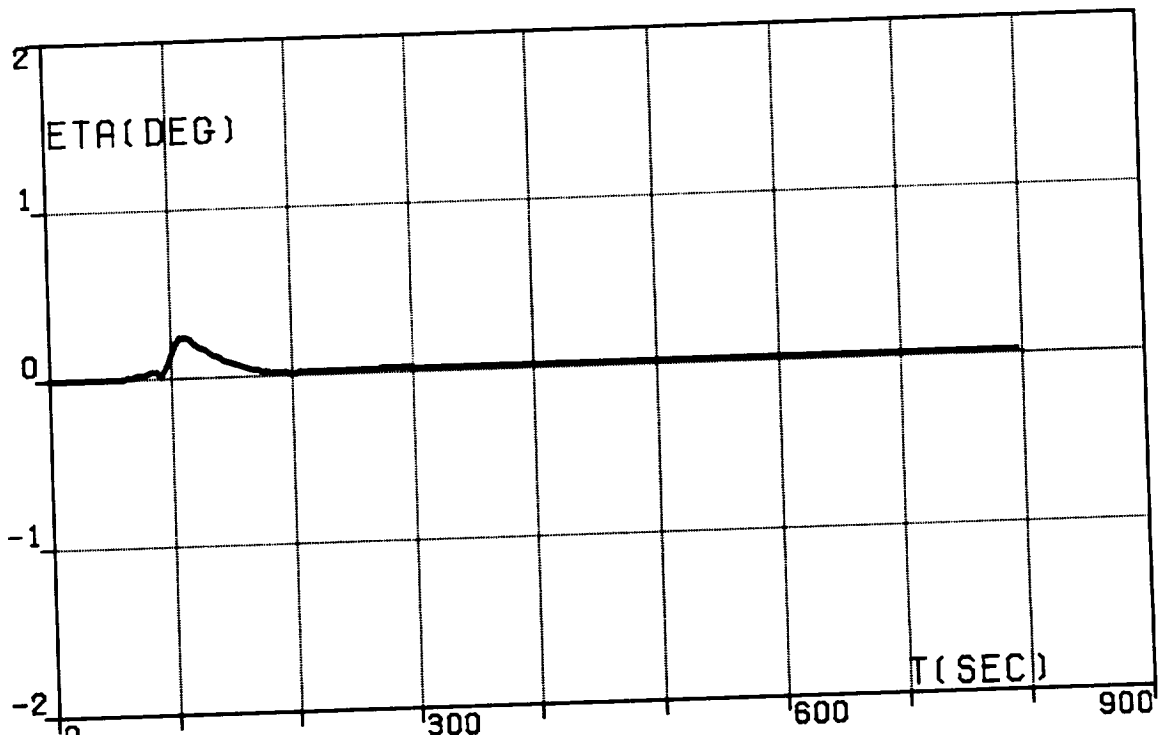


FIG. 2Q. CONTINUOUS OPTIMAL TRAJECTORY.  
TRANSFER (IA), WEDGE ANGLE.

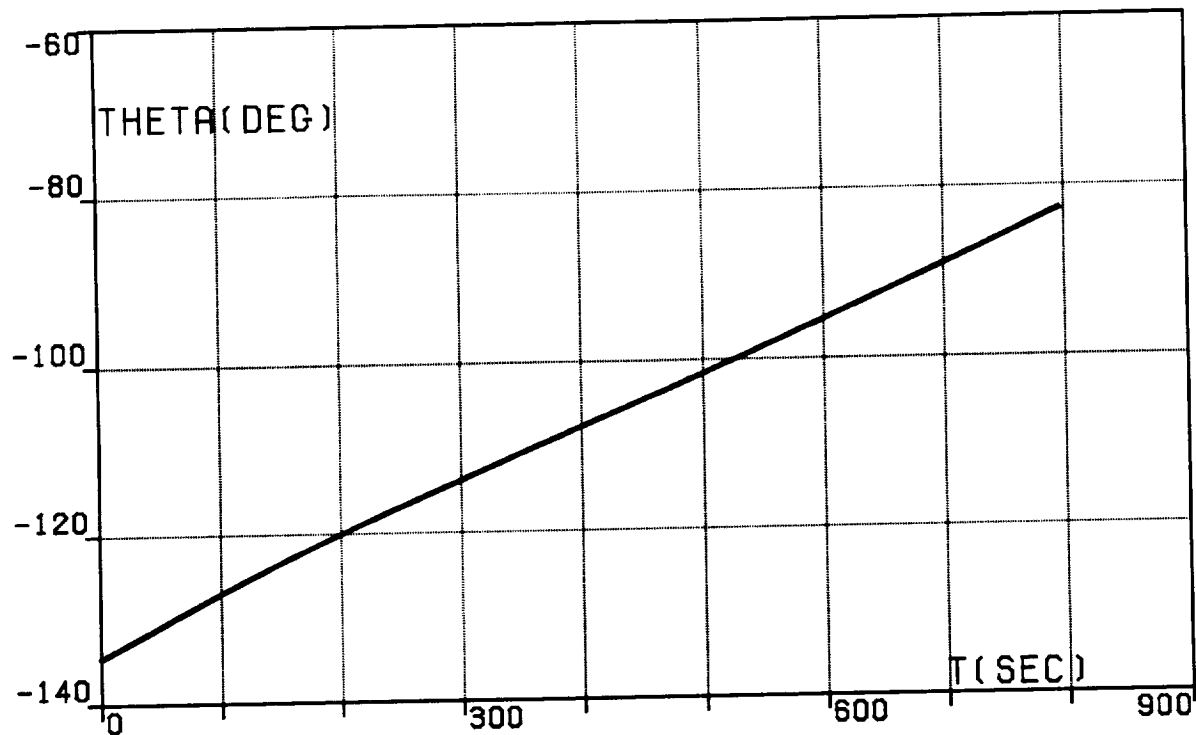


FIG.3A. TWO-SEGMENT OPTIMAL TRAJECTORY,  
TRANSFER (IA), LONGITUDE, RELATIVE.

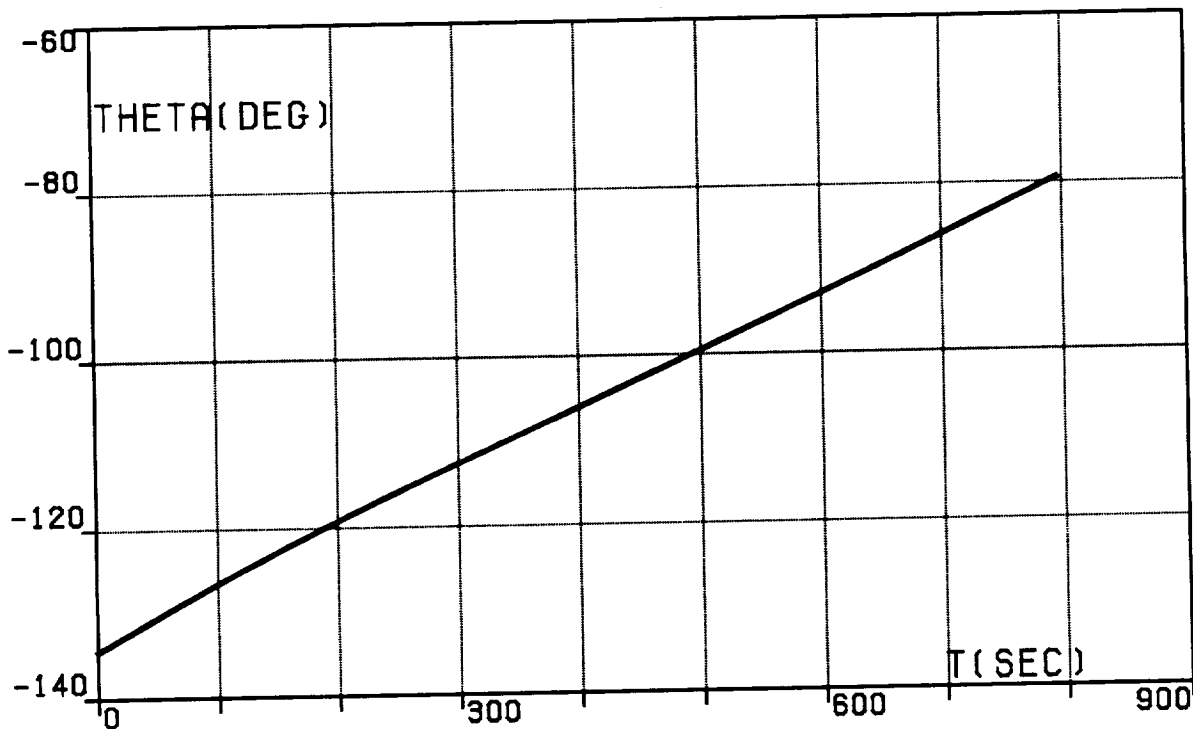


FIG.3B. TWO-SEGMENT OPTIMAL TRAJECTORY,  
TRANSFER (IA), LONGITUDE, INERTIAL.

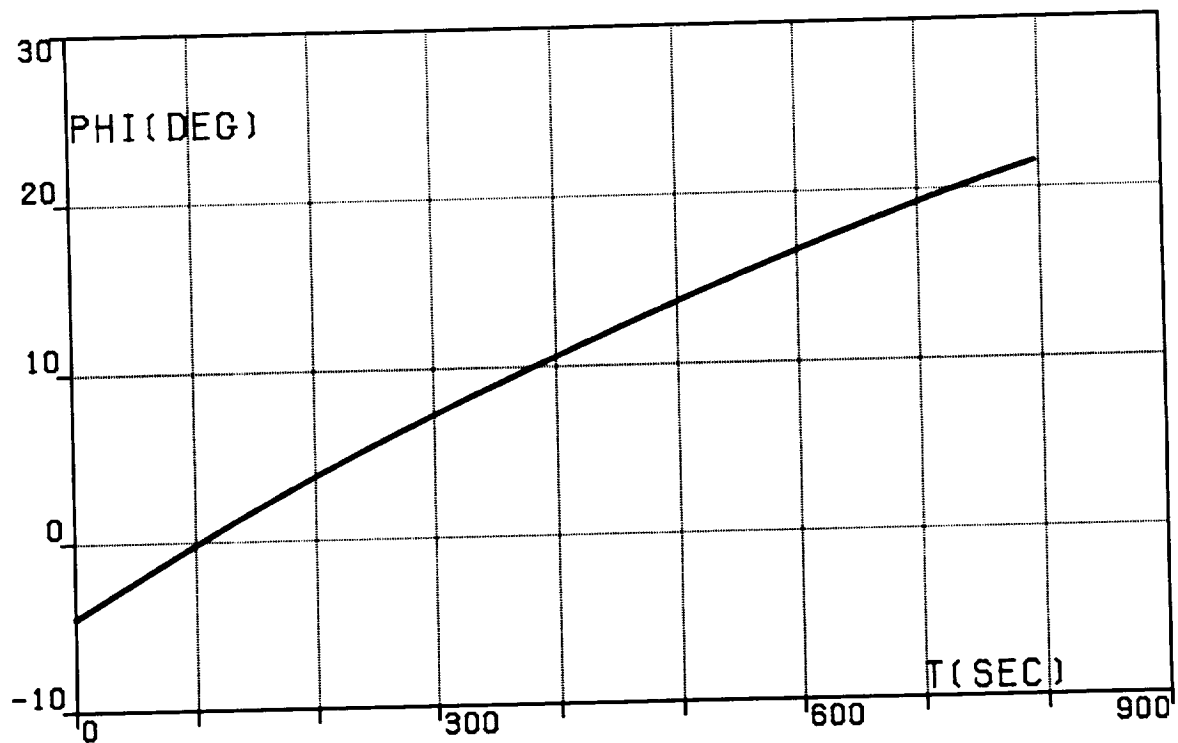


FIG.3C. TWO-SEGMENT OPTIMAL TRAJECTORY.  
TRANSFER (IA), LATITUDE.

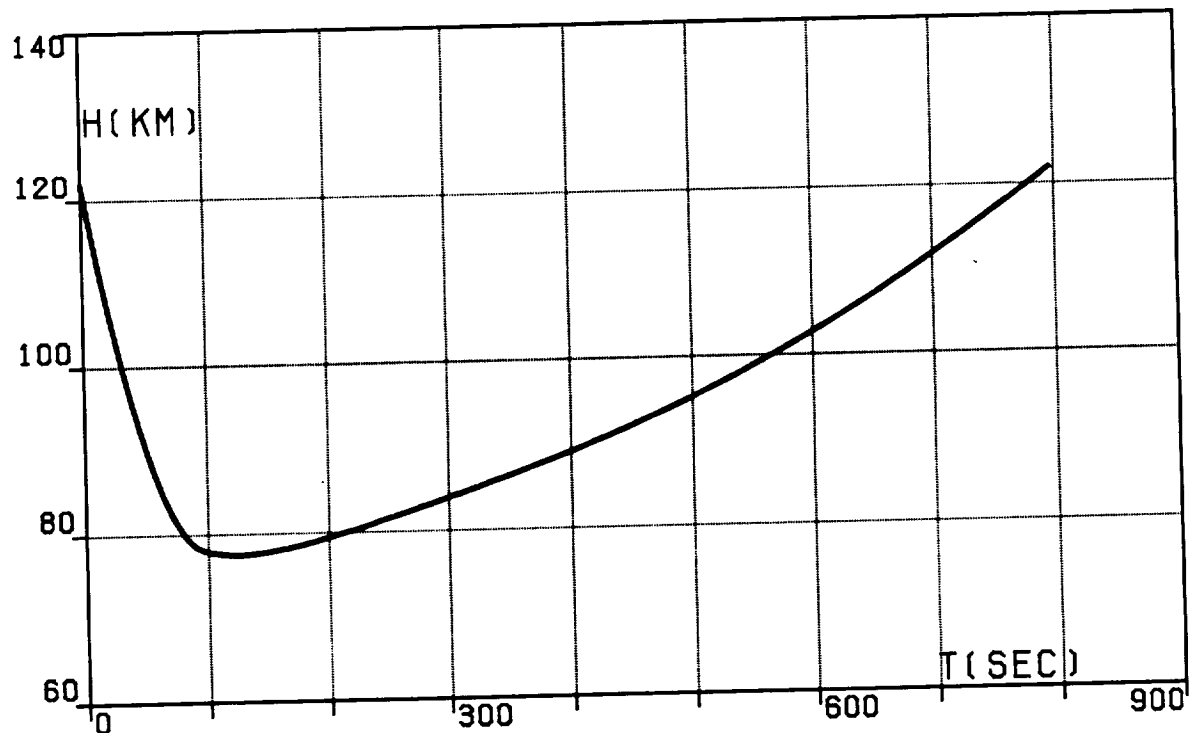


FIG.3D. TWO-SEGMENT OPTIMAL TRAJECTORY.  
TRANSFER (IA), ALTITUDE.

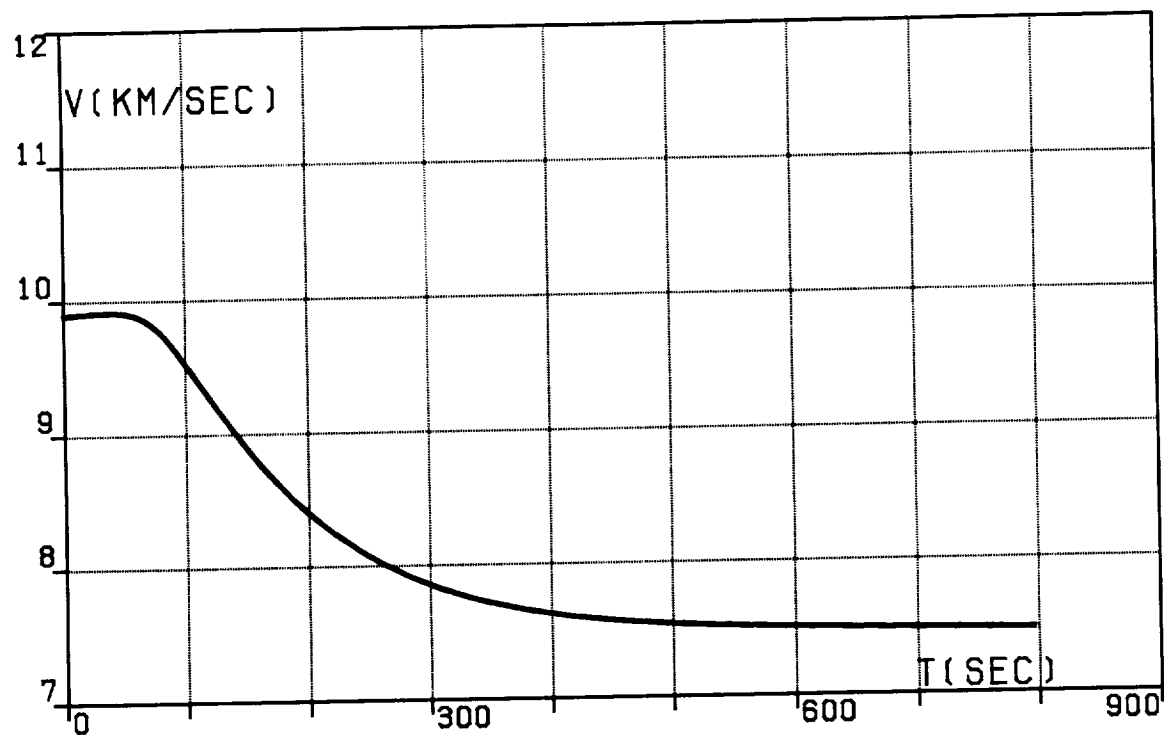


FIG. 3E. TWO-SEGMENT OPTIMAL TRAJECTORY,  
TRANSFER (IA), VELOCITY, RELATIVE.

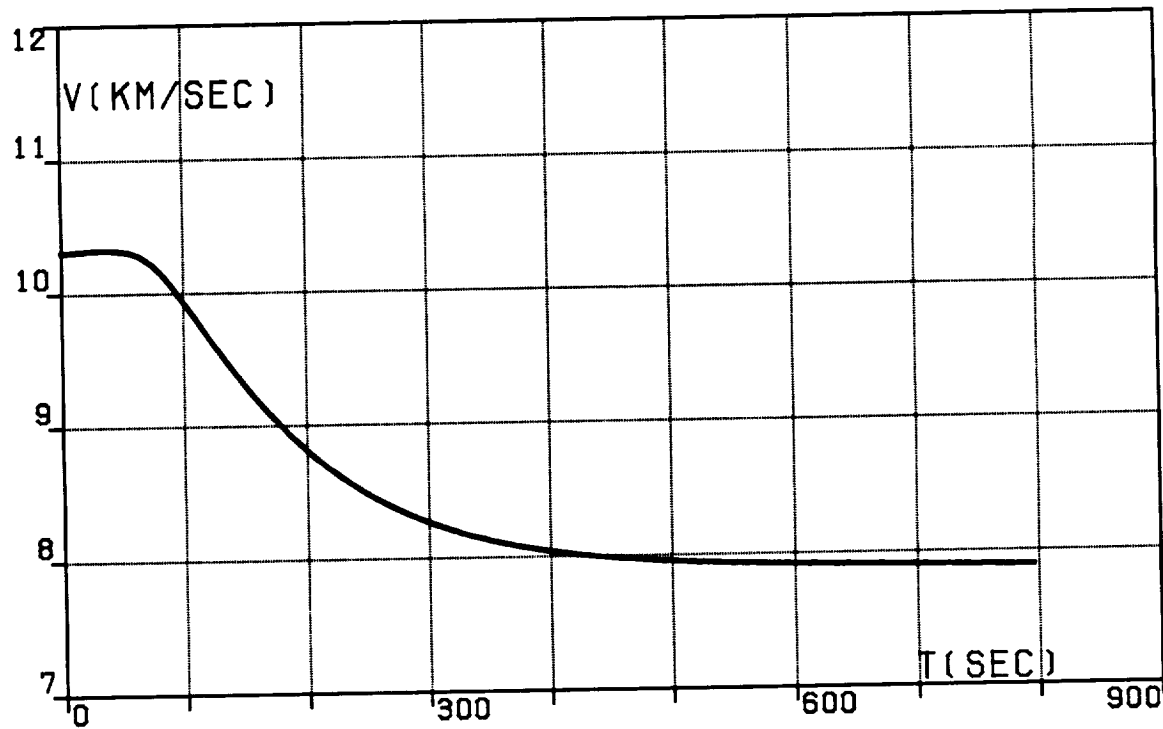


FIG. 3F. TWO-SEGMENT OPTIMAL TRAJECTORY,  
TRANSFER (IA), VELOCITY, INERTIAL.

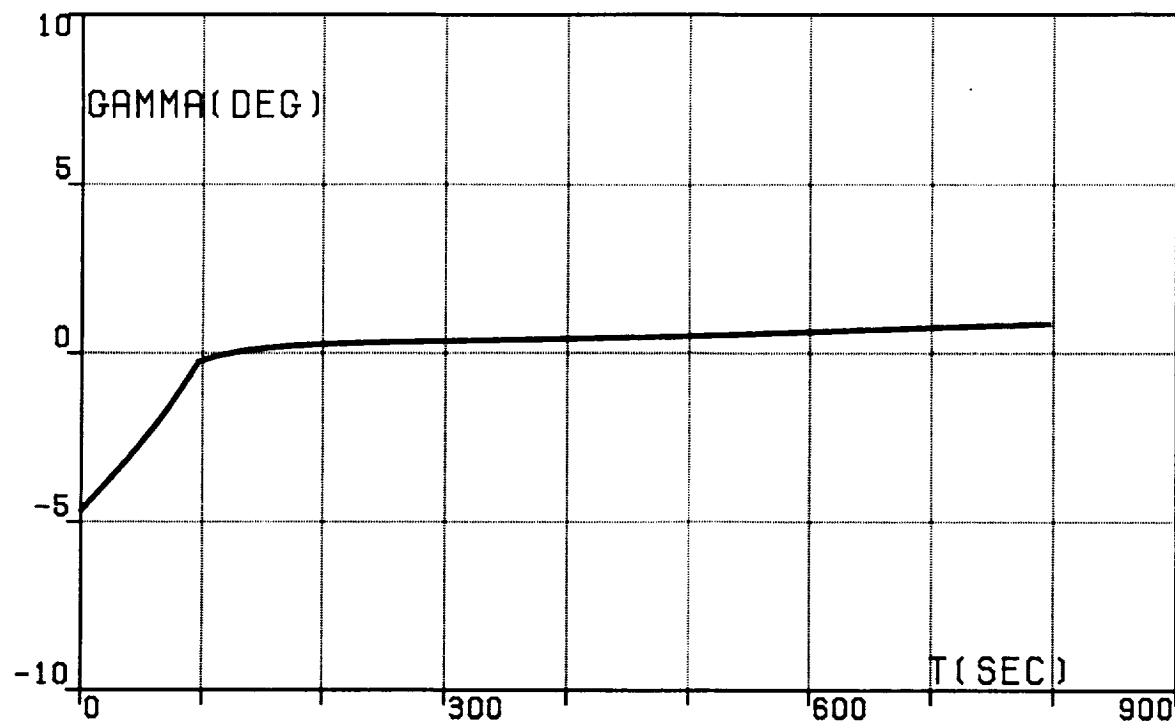


FIG.3G. TWO-SEGMENT OPTIMAL TRAJECTORY,  
TRANSFER (IA),  
PATH INCLINATION, RELATIVE.

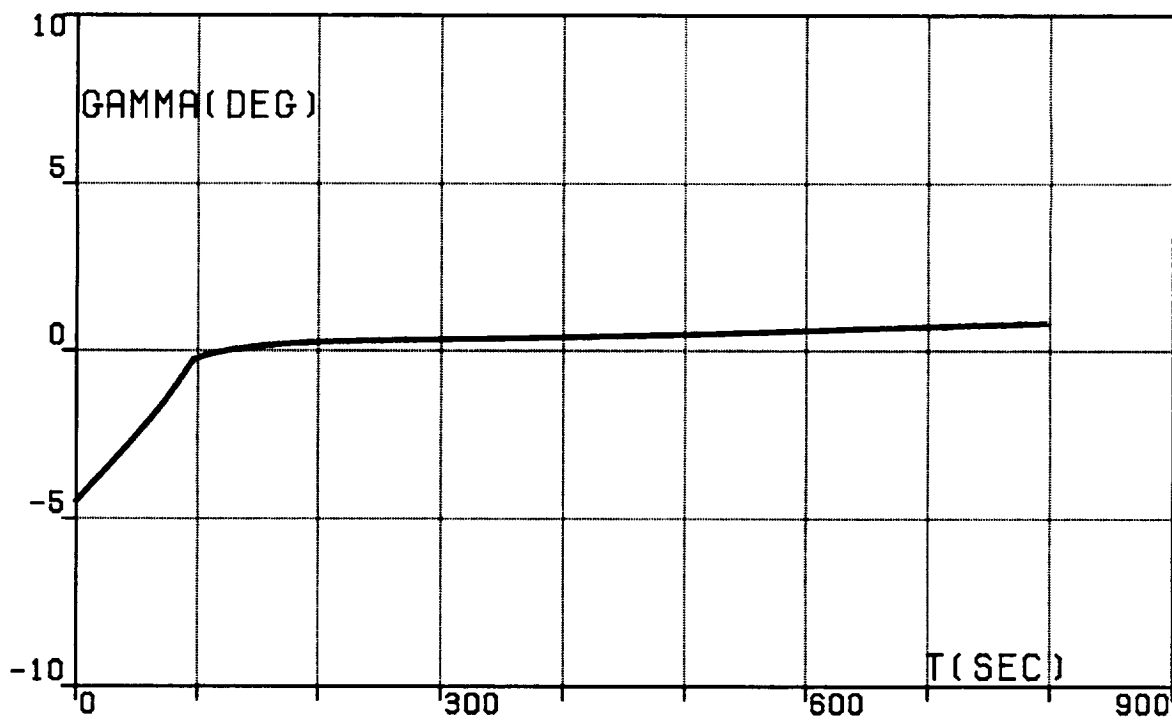


FIG.3H. TWO-SEGMENT OPTIMAL TRAJECTORY,  
TRANSFER (IA),  
PATH INCLINATION, INERTIAL.

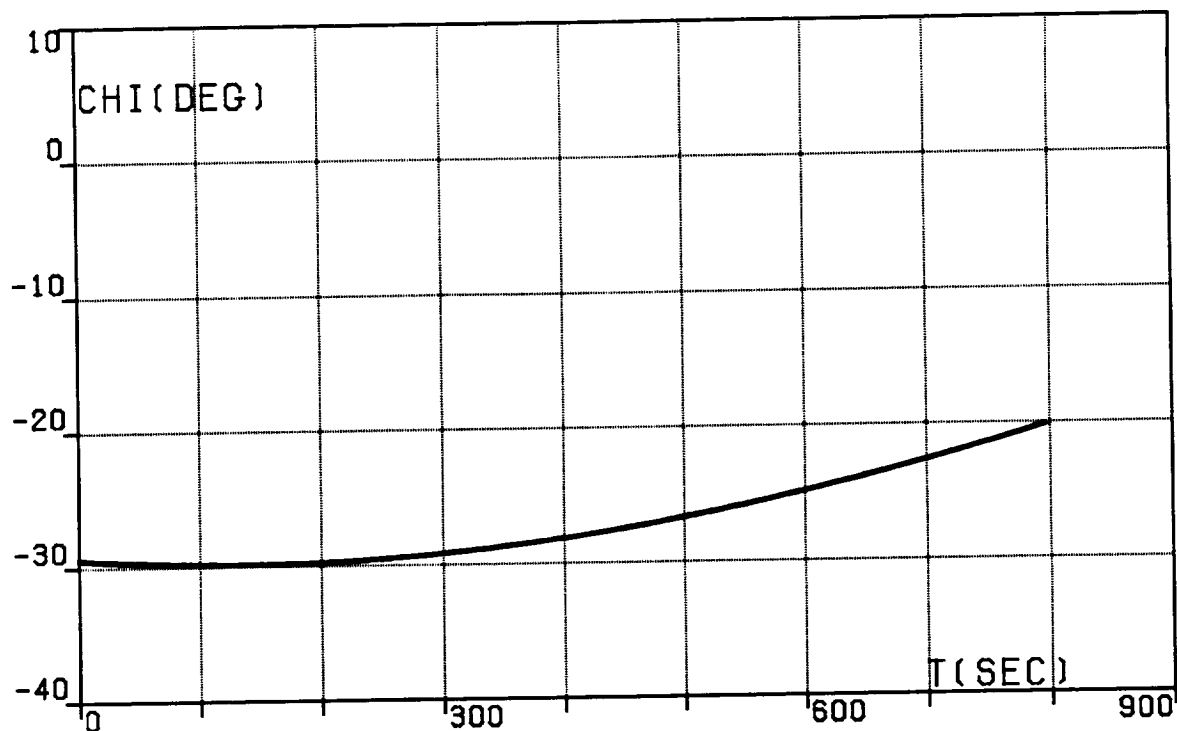


FIG.3I. TWO-SEGMENT OPTIMAL TRAJECTORY,  
TRANSFER (IA), HEADING ANGLE, RELATIVE.

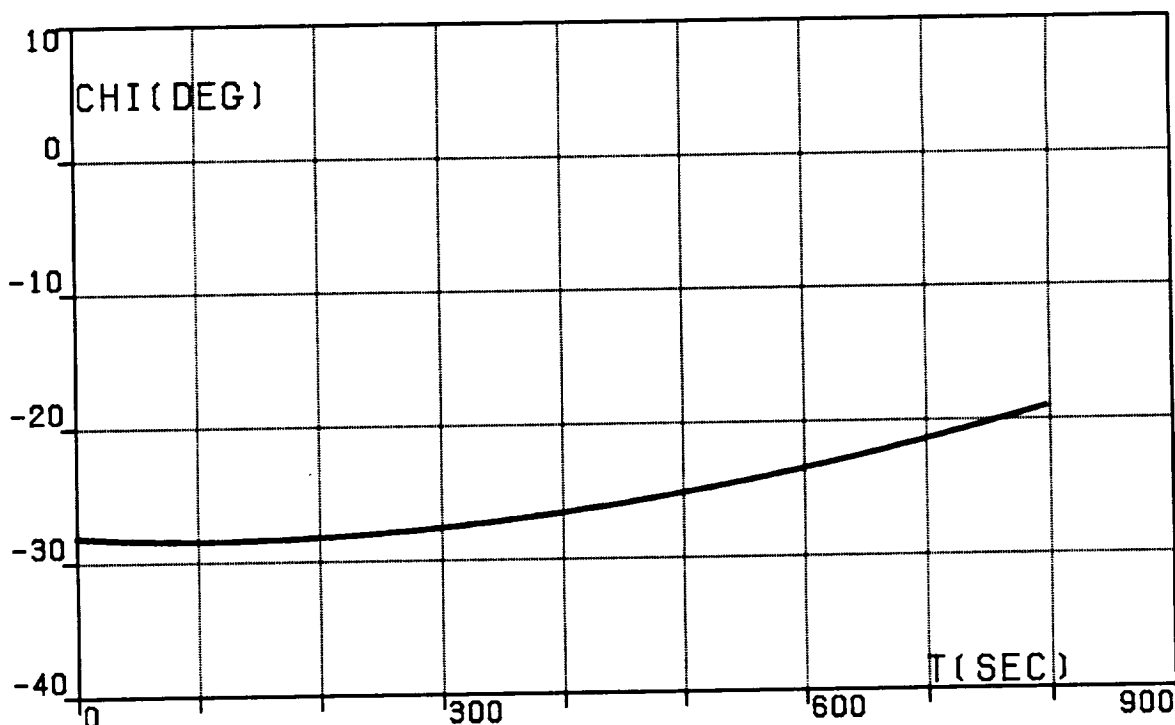


FIG.3J. TWO-SEGMENT OPTIMAL TRAJECTORY,  
TRANSFER (IA), HEADING ANGLE, INERTIAL.

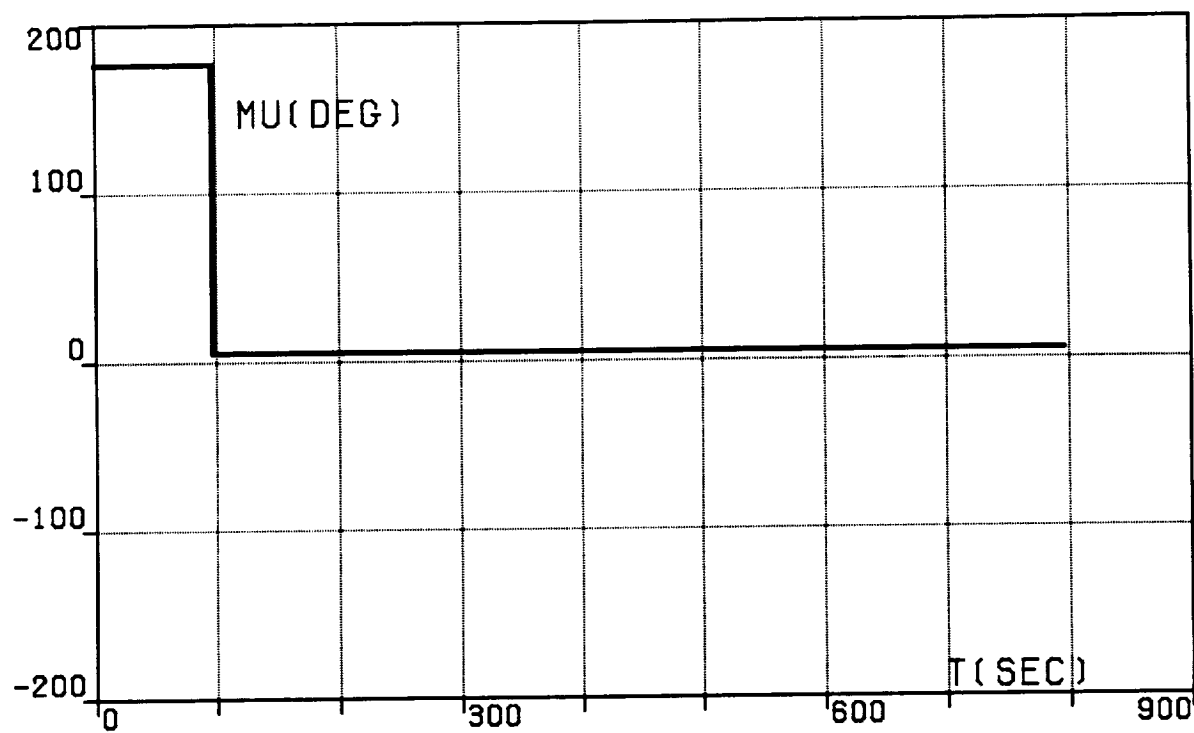


FIG.3K. TWO-SEGMENT OPTIMAL TRAJECTORY,  
TRANSFER (IA), BANK ANGLE.

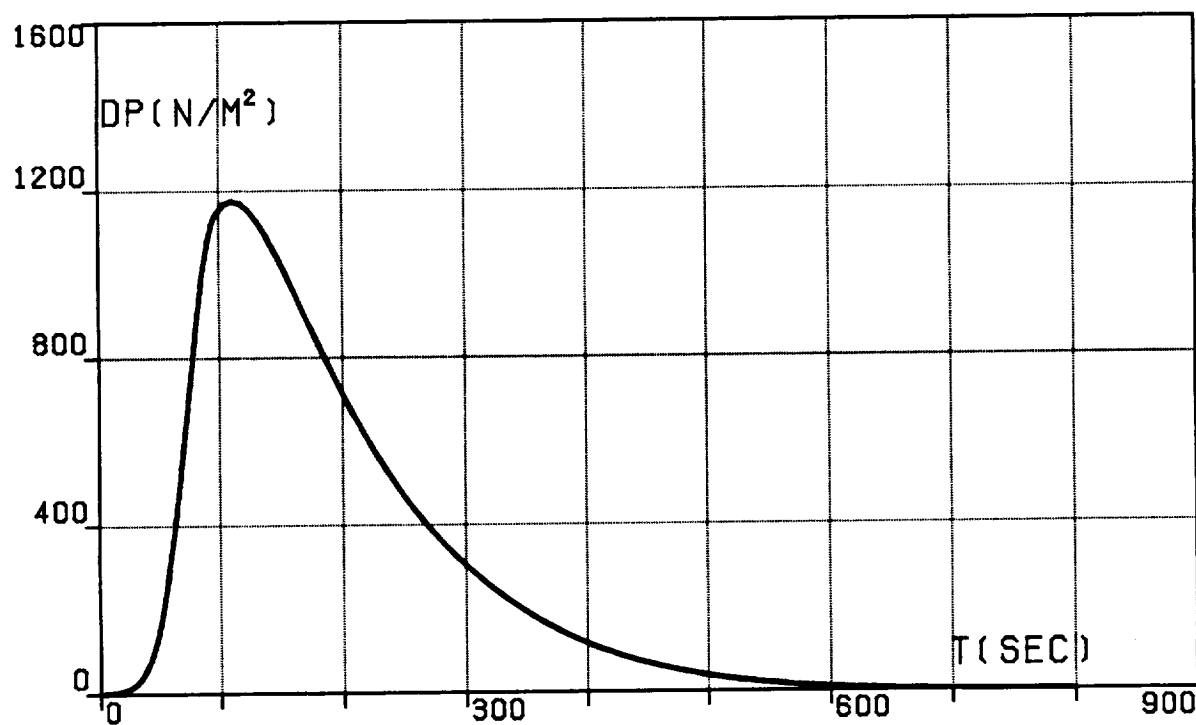


FIG.3L. TWO-SEGMENT OPTIMAL TRAJECTORY,  
TRANSFER (IA), DYNAMIC PRESSURE.

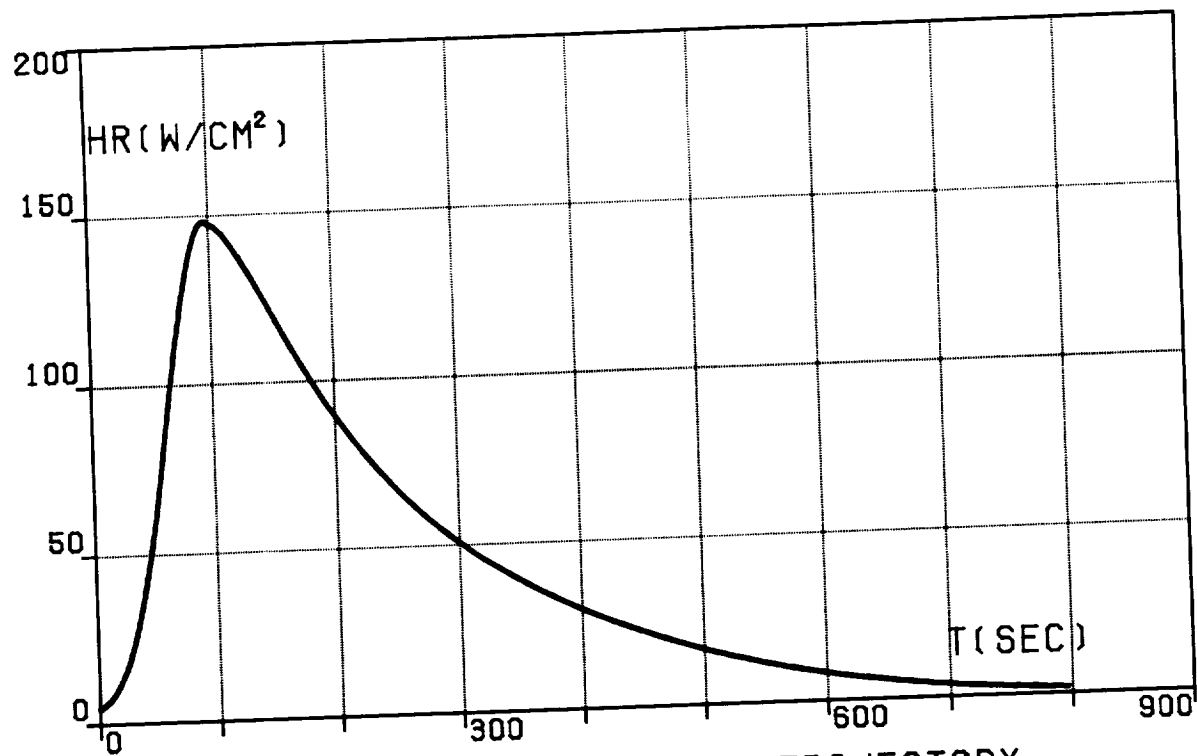


FIG.3M. TWO-SEGMENT OPTIMAL TRAJECTORY.  
TRANSFER (IA). HEATING RATE.

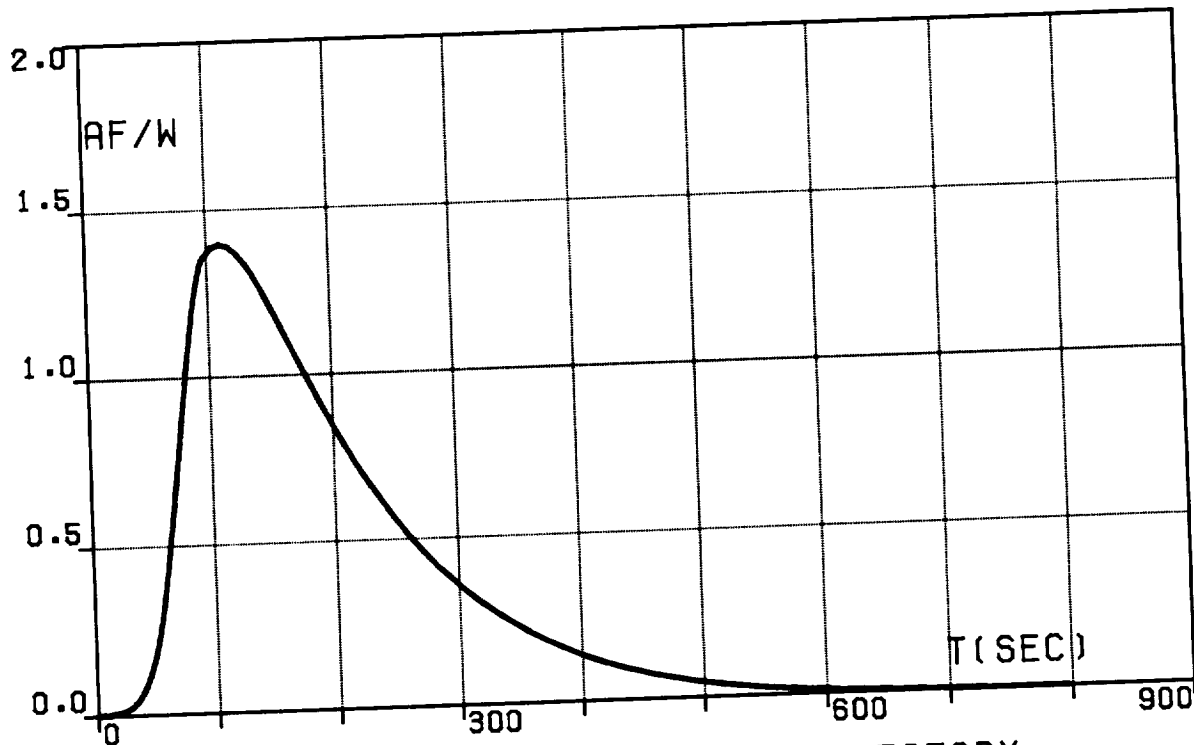


FIG.3N. TWO-SEGMENT OPTIMAL TRAJECTORY.  
TRANSFER (IA).  
AERODYNAMIC FORCE PER UNIT WEIGHT.

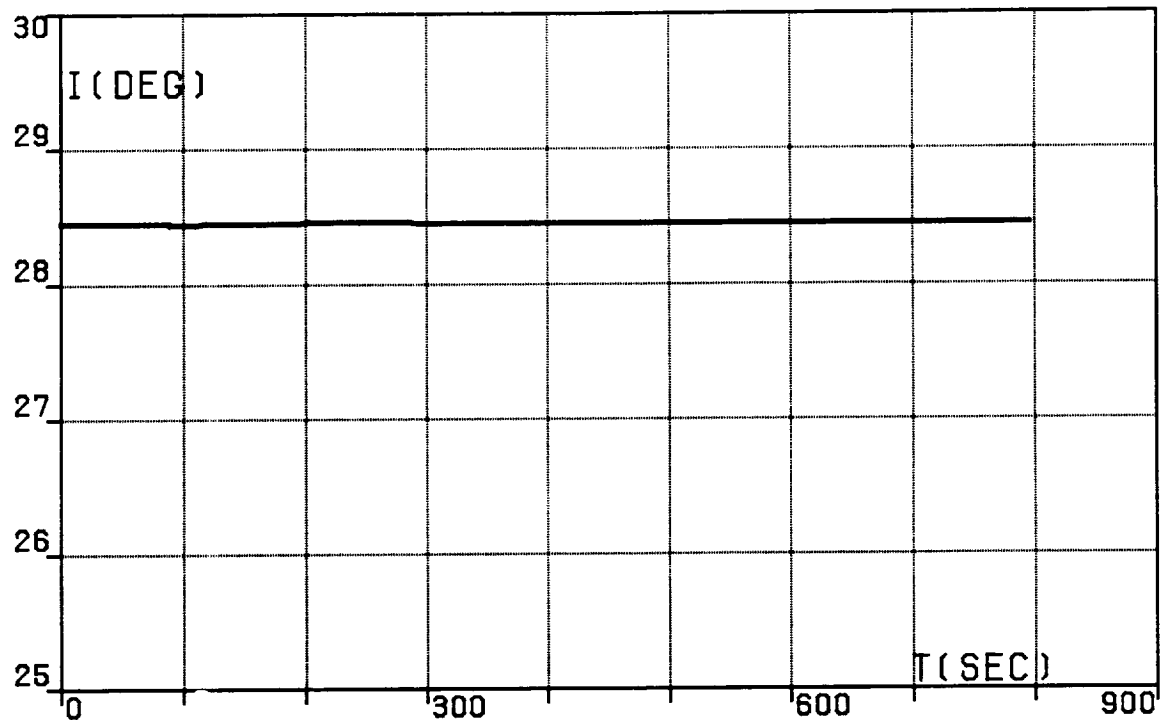


FIG.30. TWO-SEGMENT OPTIMAL TRAJECTORY,  
TRANSFER (IA), ORBITAL INCLINATION.

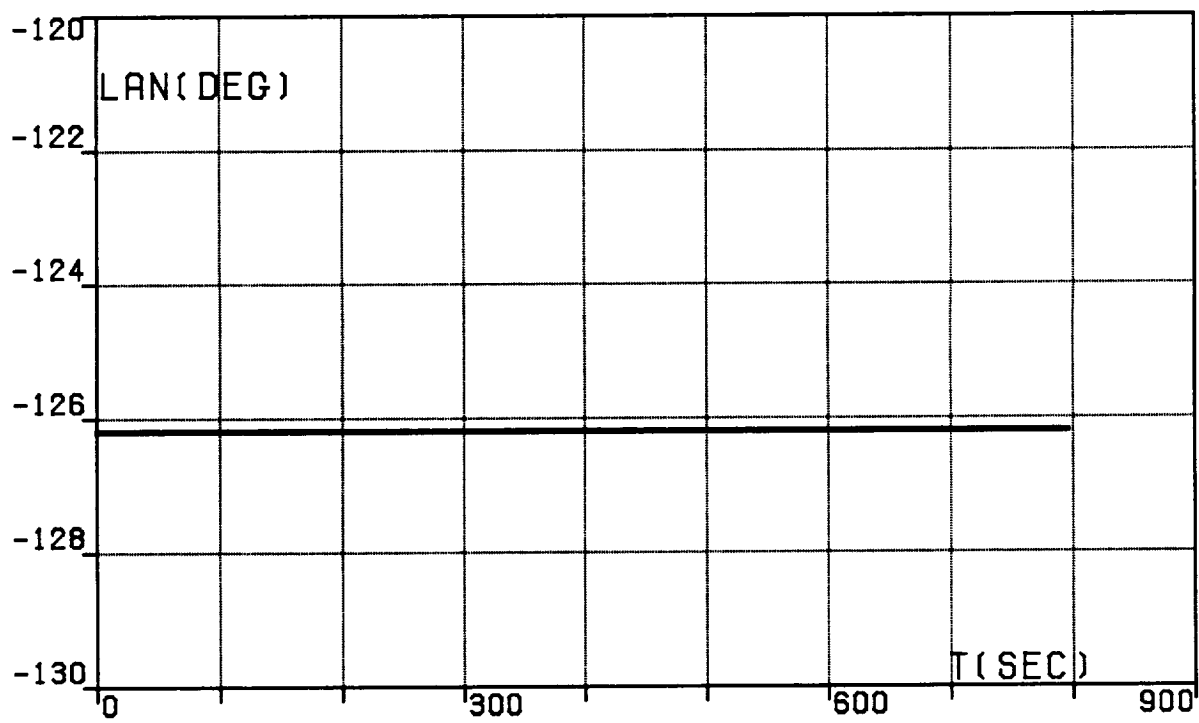


FIG.3P. TWO-SEGMENT OPTIMAL TRAJECTORY,  
TRANSFER (IA),  
LONGITUDE OF THE ASCENDING NODE.

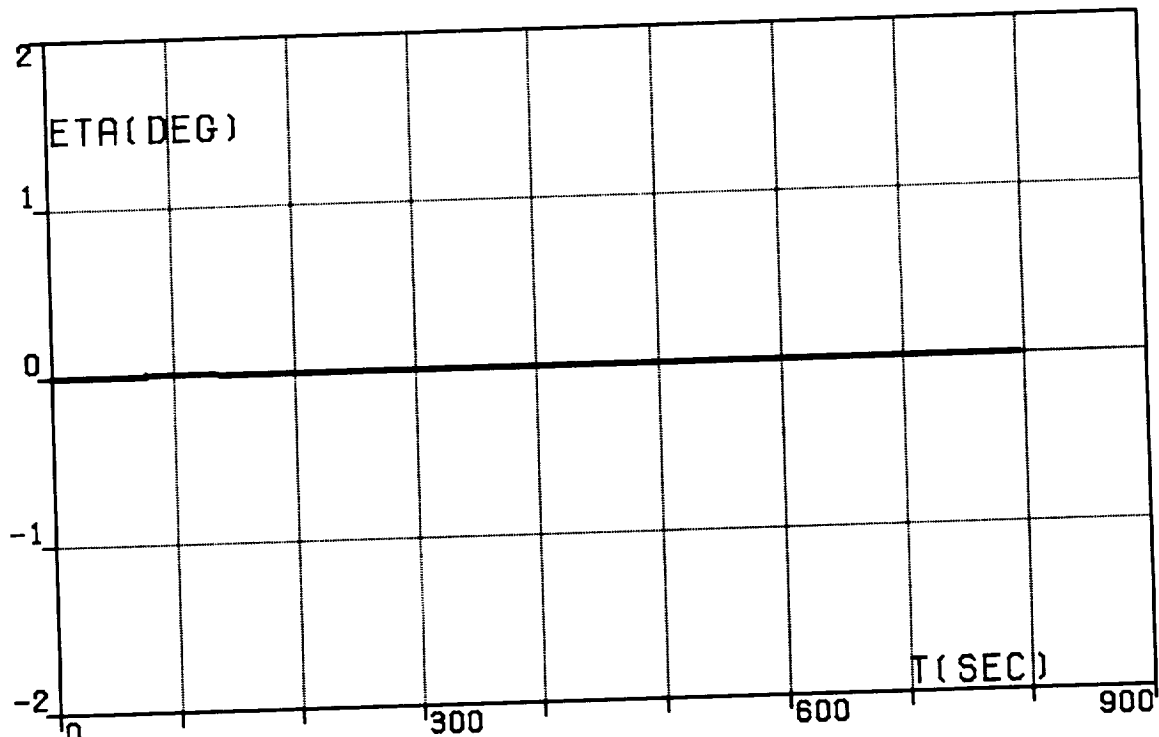


FIG.3Q. TWO-SEGMENT OPTIMAL TRAJECTORY.  
TRANSFER (IA). WEDGE ANGLE.

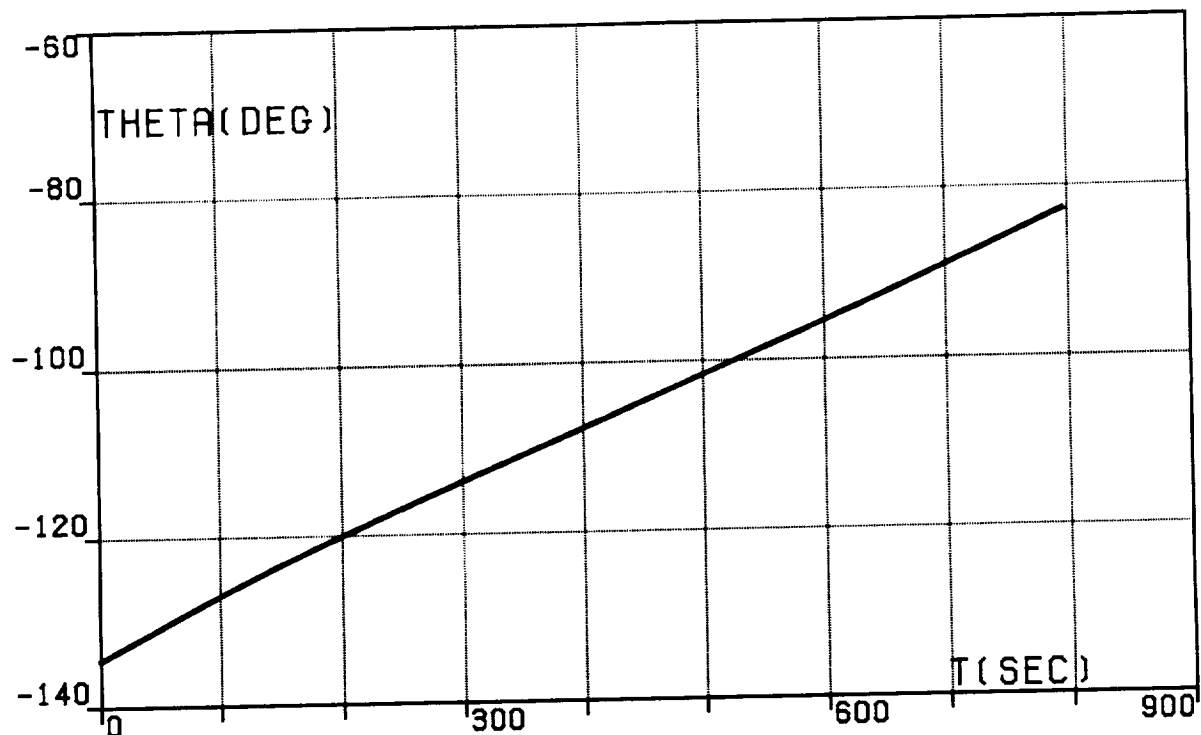


FIG.4A. THREE-SEGMENT OPTIMAL TRAJECTORY,  
TRANSFER (IA), LONGITUDE, RELATIVE.

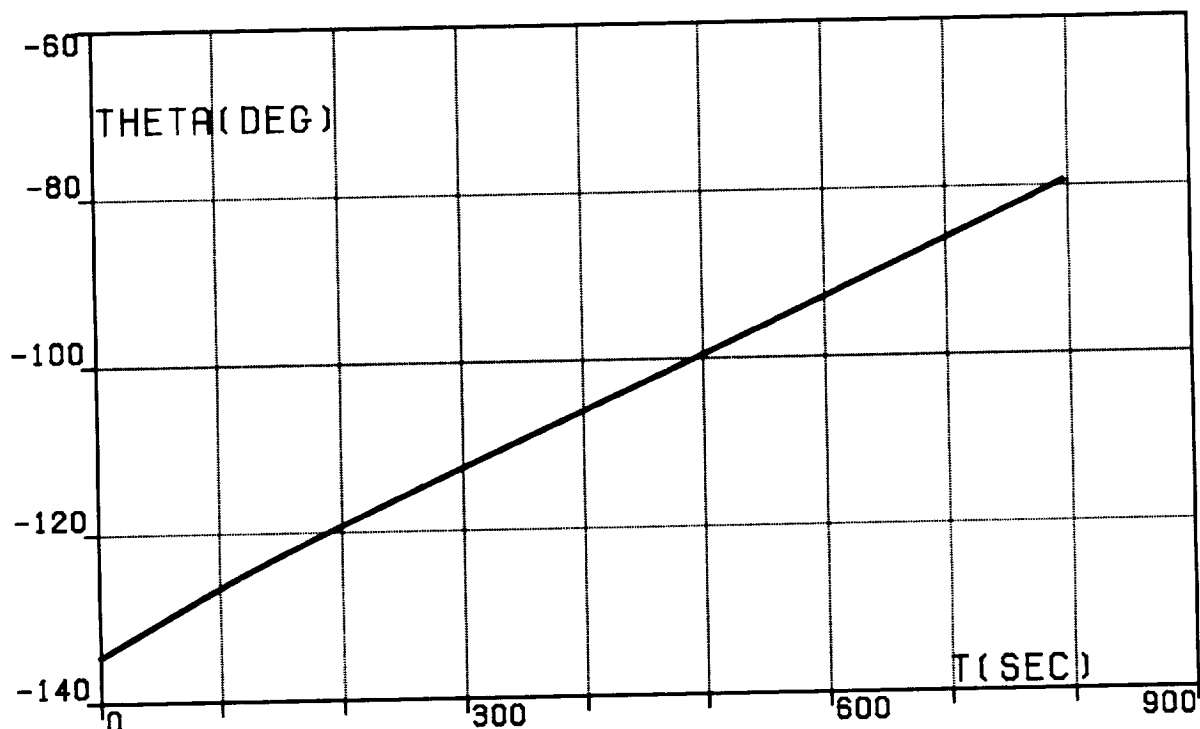


FIG.4B. THREE-SEGMENT OPTIMAL TRAJECTORY,  
TRANSFER (IA), LONGITUDE, INERTIAL.

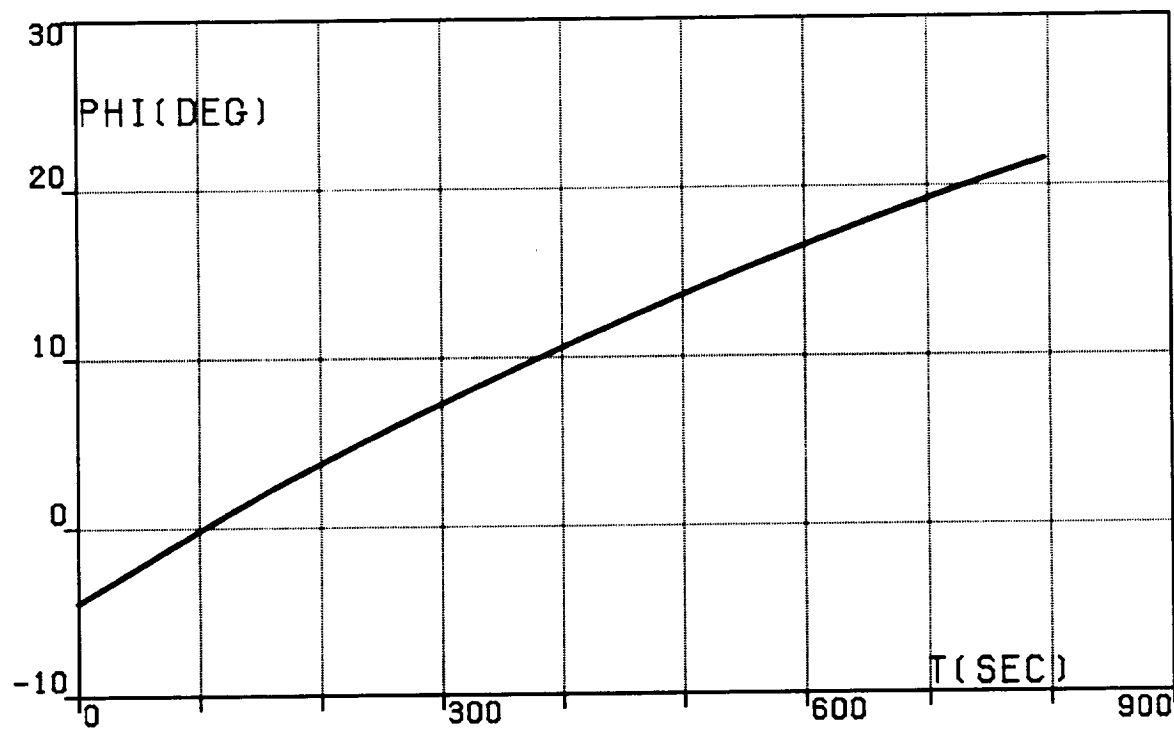


FIG.4C. THREE-SEGMENT OPTIMAL TRAJECTORY,  
TRANSFER (IA), LATITUDE.

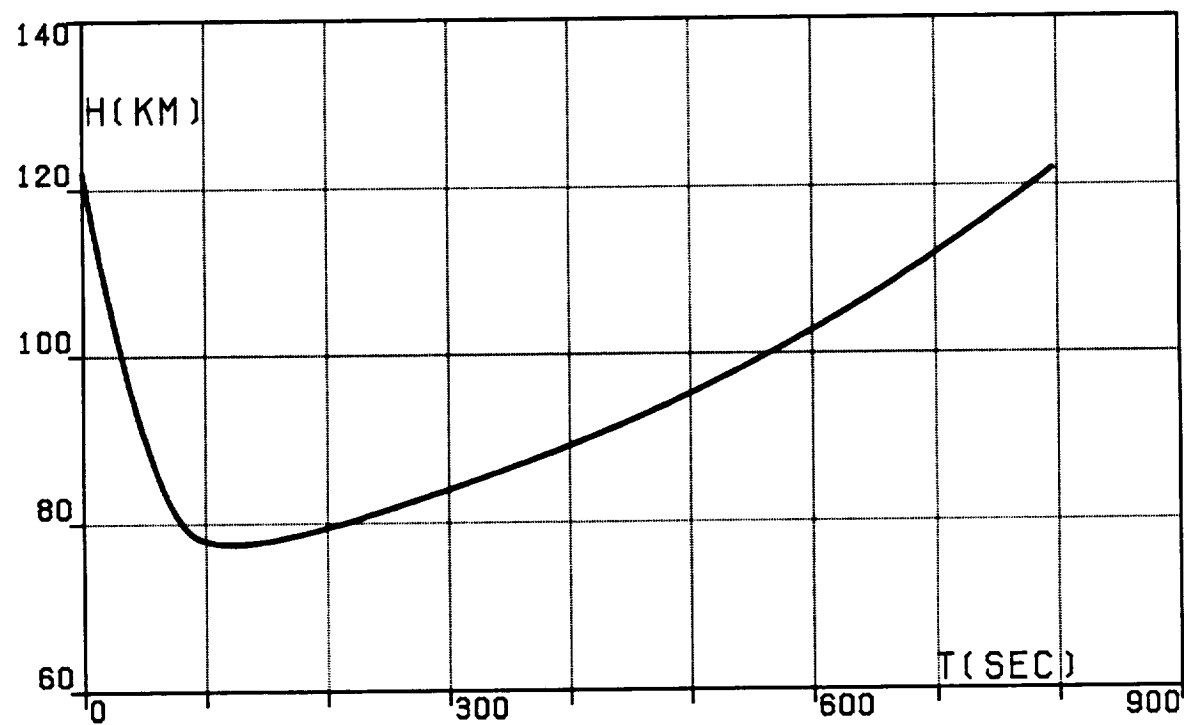


FIG.4D. THREE-SEGMENT OPTIMAL TRAJECTORY,  
TRANSFER (IA), ALTITUDE.

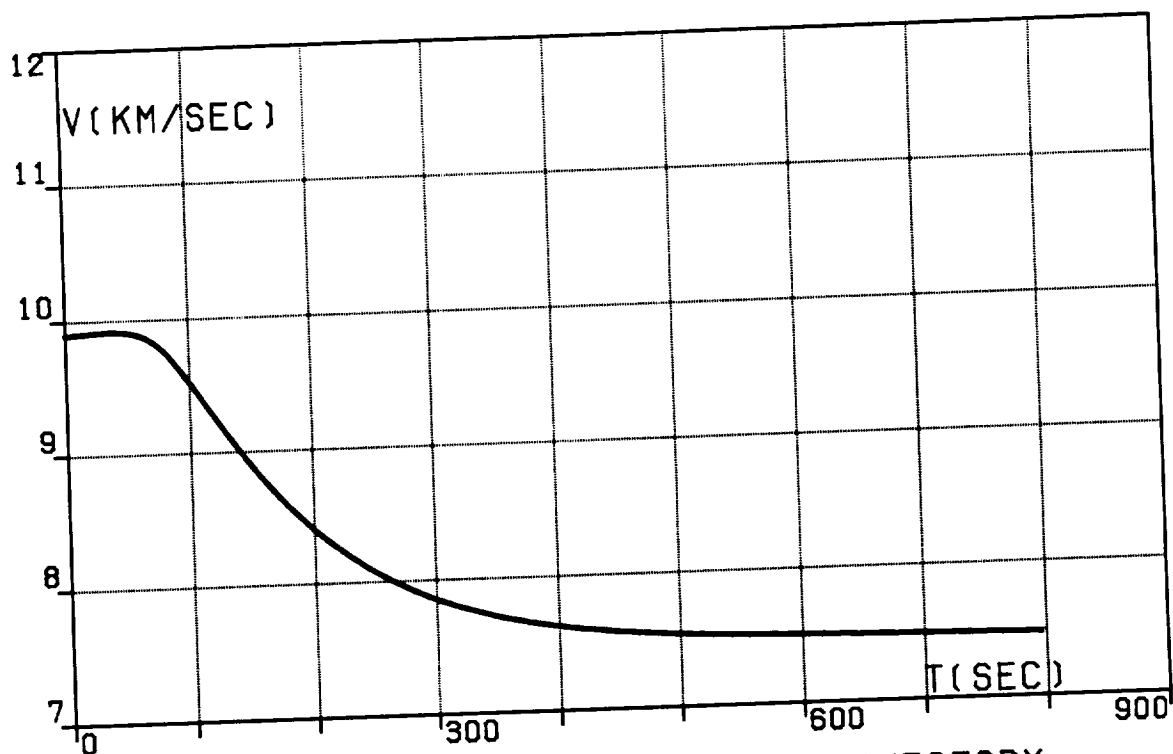


FIG.4E. THREE-SEGMENT OPTIMAL TRAJECTORY,  
TRANSFER (IA), VELOCITY, RELATIVE.

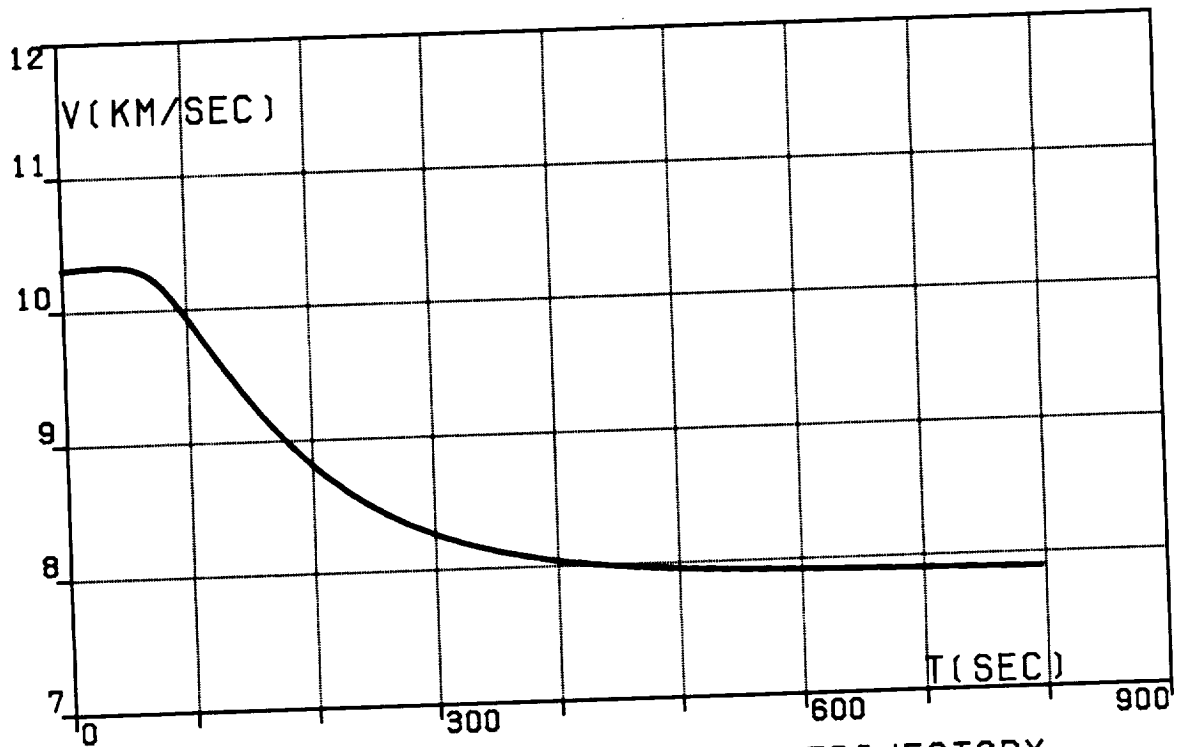


FIG.4F. THREE-SEGMENT OPTIMAL TRAJECTORY,  
TRANSFER (IA), VELOCITY, INERTIAL.

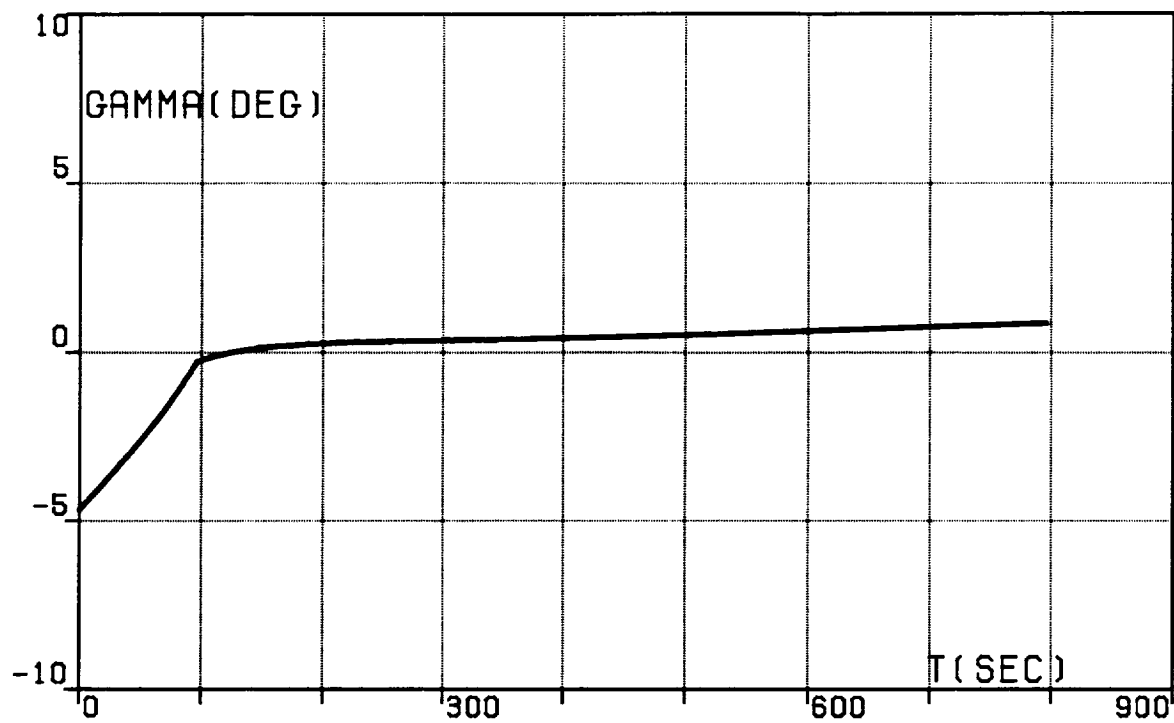


FIG.4G. THREE-SEGMENT OPTIMAL TRAJECTORY,  
TRANSFER (IA),  
PATH INCLINATION, RELATIVE.

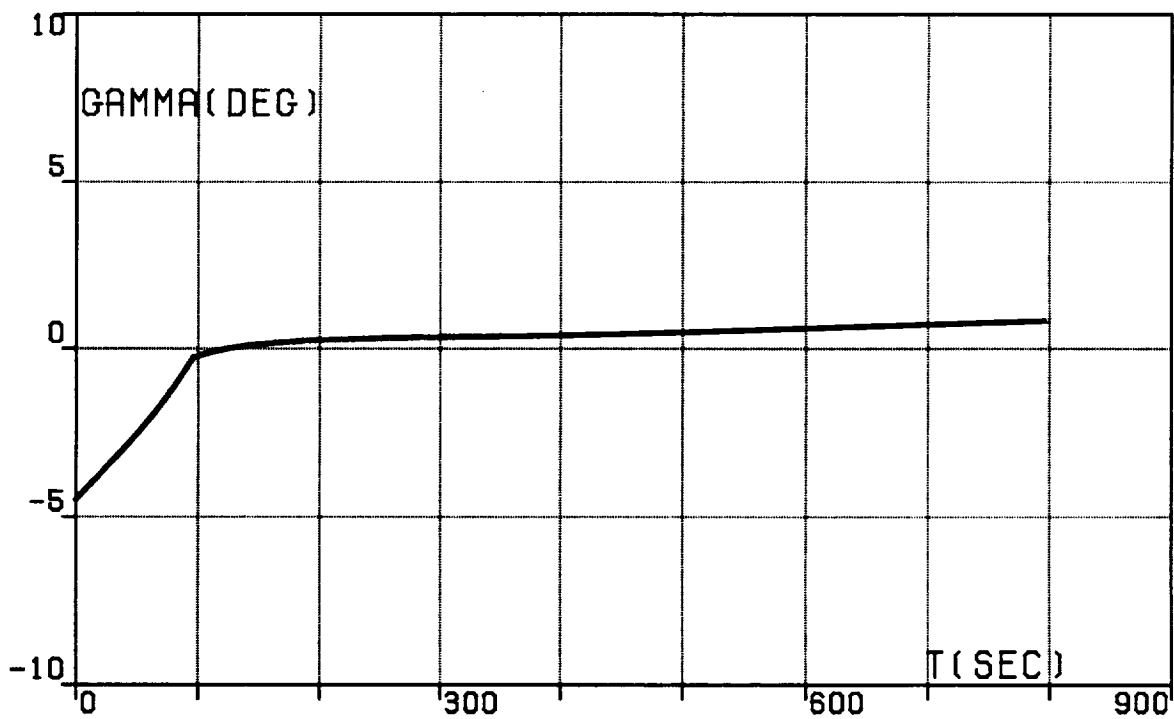


FIG.4H. THREE-SEGMENT OPTIMAL TRAJECTORY,  
TRANSFER (IA),  
PATH INCLINATION, INERTIAL.

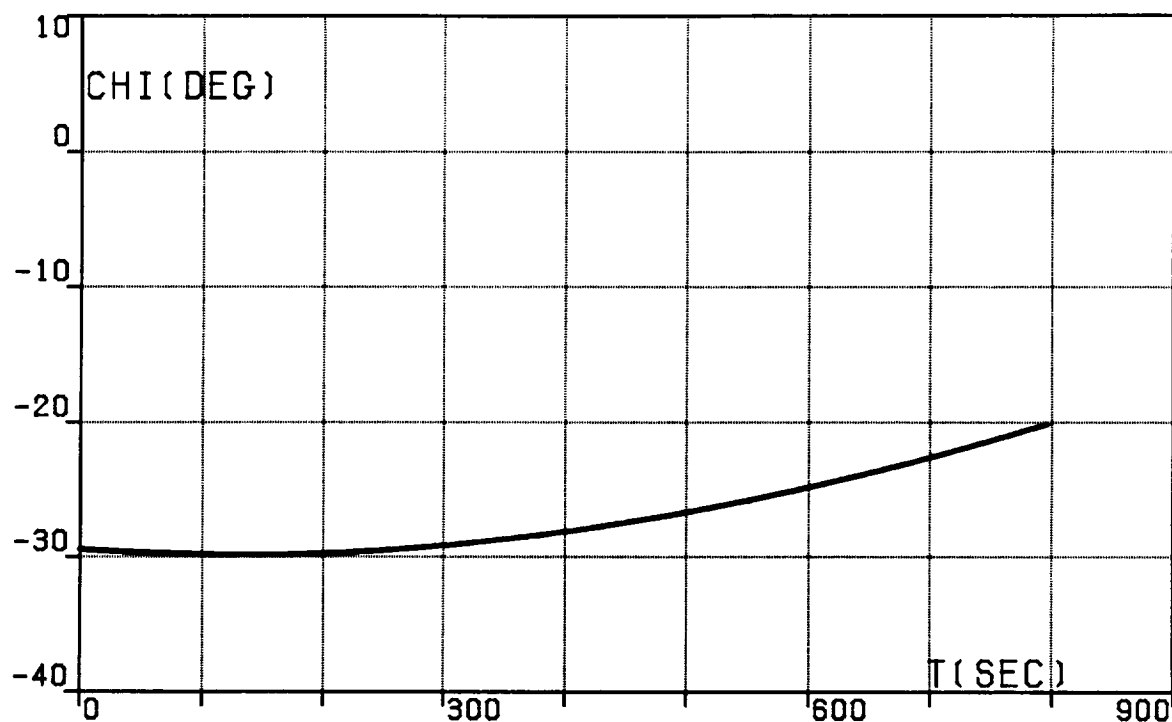


FIG.4I. THREE-SEGMENT OPTIMAL TRAJECTORY,  
TRANSFER (IA), HEADING ANGLE, RELATIVE.

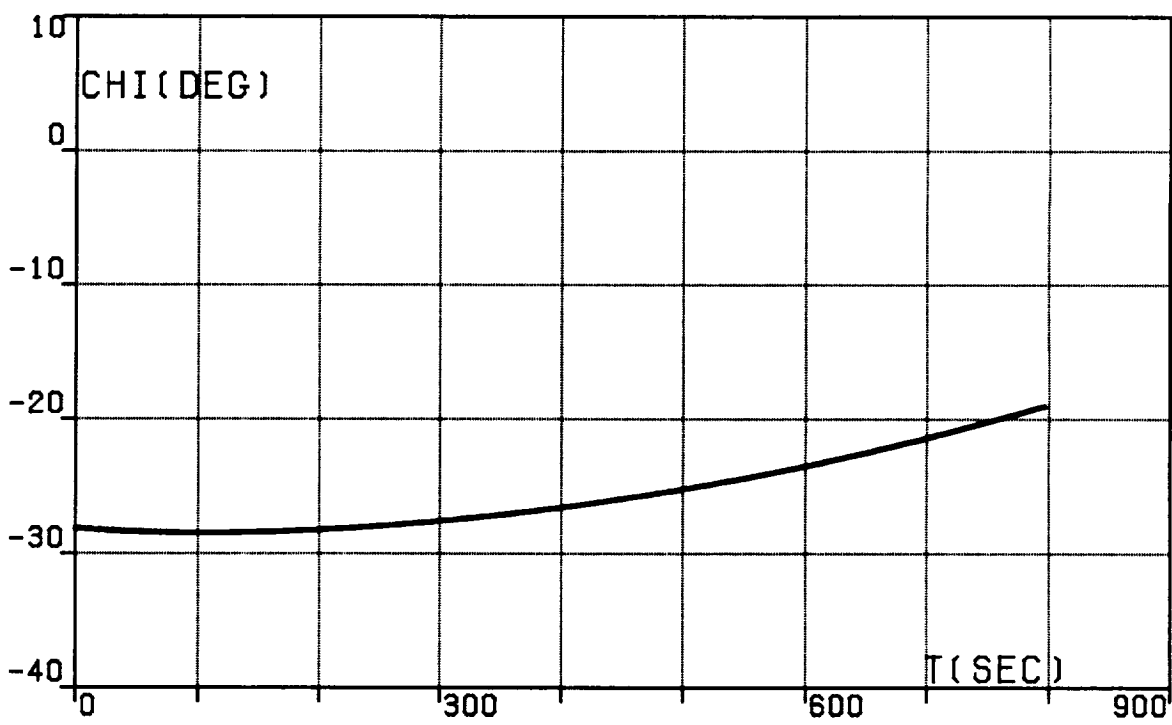


FIG.4J. THREE-SEGMENT OPTIMAL TRAJECTORY,  
TRANSFER (IA), HEADING ANGLE, INERTIAL.

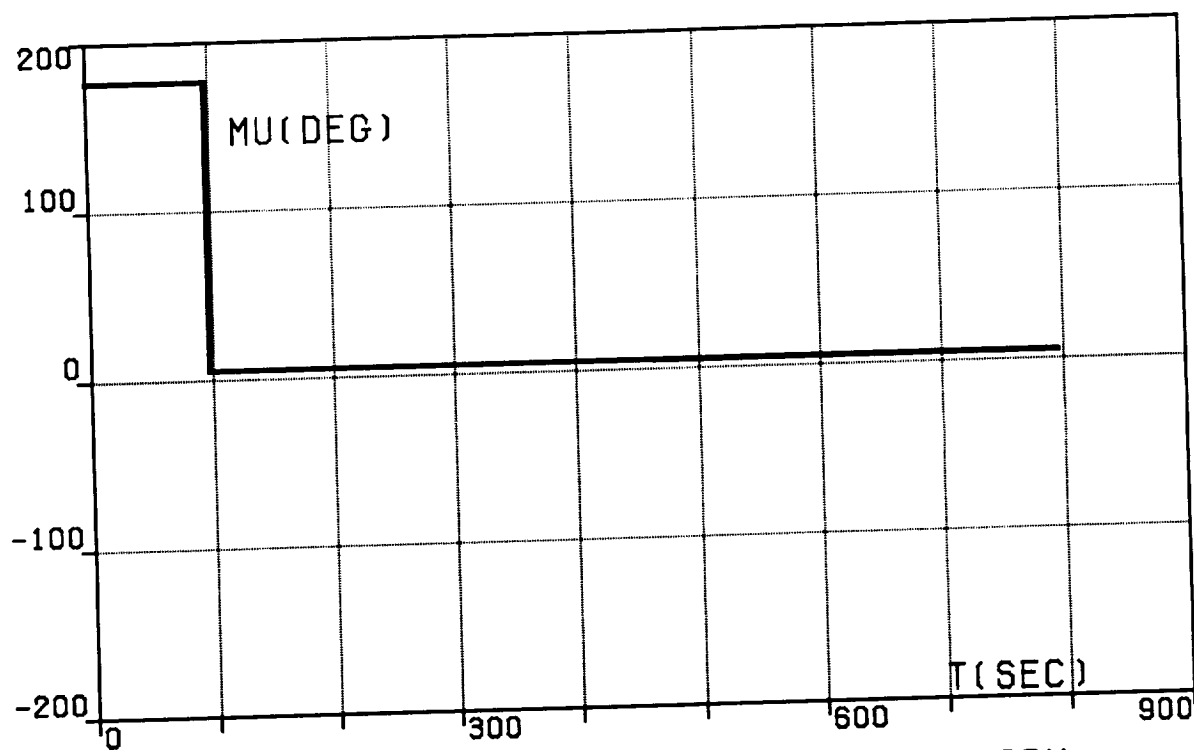


FIG.4K. THREE-SEGMENT OPTIMAL TRAJECTORY,  
TRANSFER (IA), BANK ANGLE.

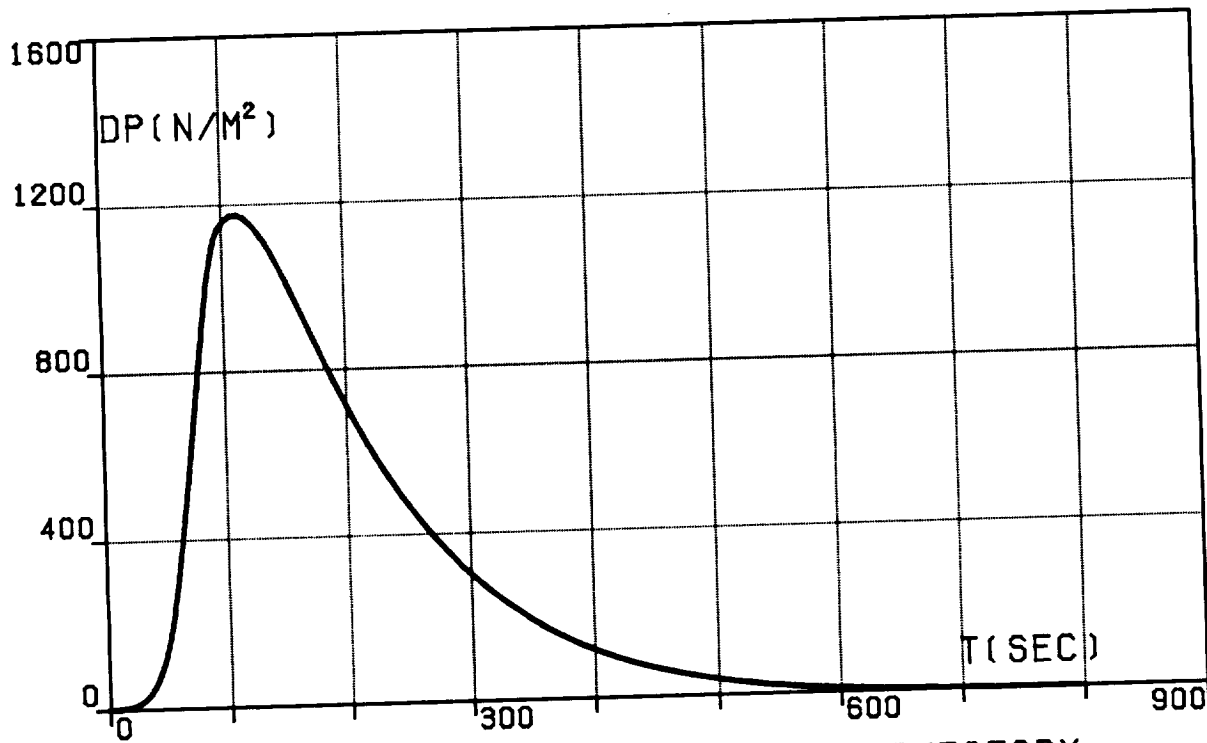


FIG.4L. THREE-SEGMENT OPTIMAL TRAJECTORY,  
TRANSFER (IA), DYNAMIC PRESSURE.

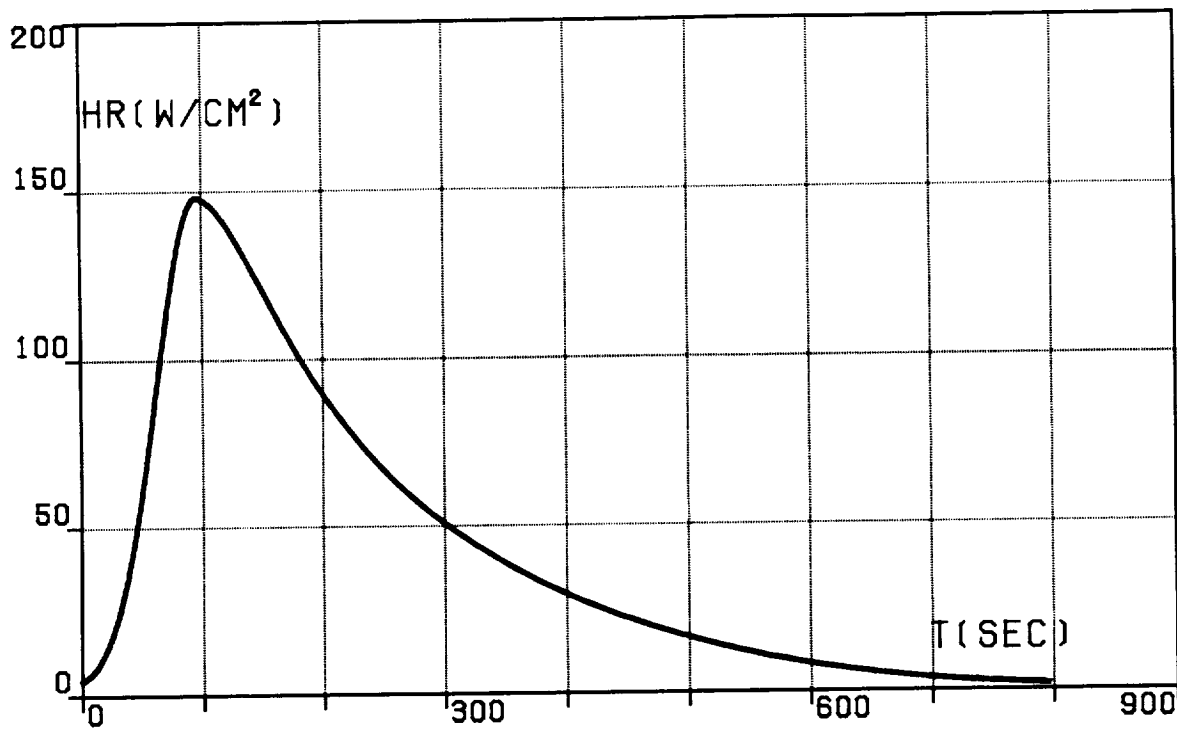


FIG.4M. THREE-SEGMENT OPTIMAL TRAJECTORY,  
TRANSFER (IA), HEATING RATE.

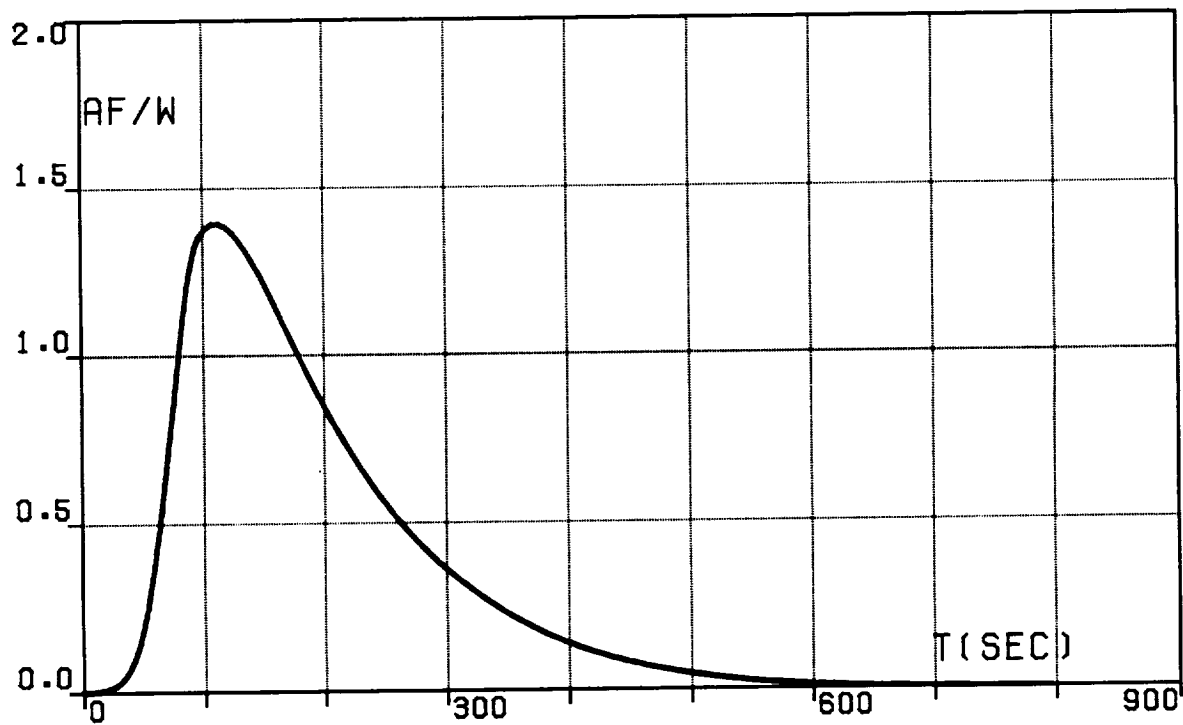


FIG.4N. THREE-SEGMENT OPTIMAL TRAJECTORY,  
TRANSFER (IA),  
AERODYNAMIC FORCE PER UNIT WEIGHT.

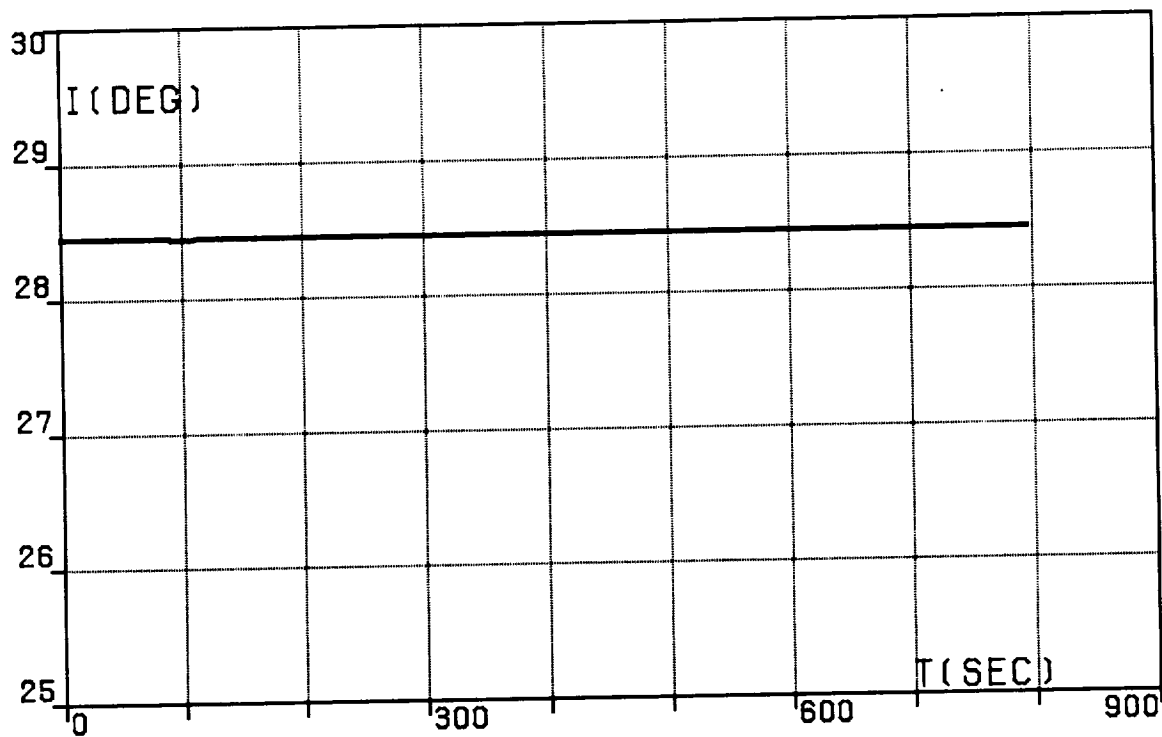


FIG.40. THREE-SEGMENT OPTIMAL TRAJECTORY,  
TRANSFER (IA). ORBITAL INCLINATION.

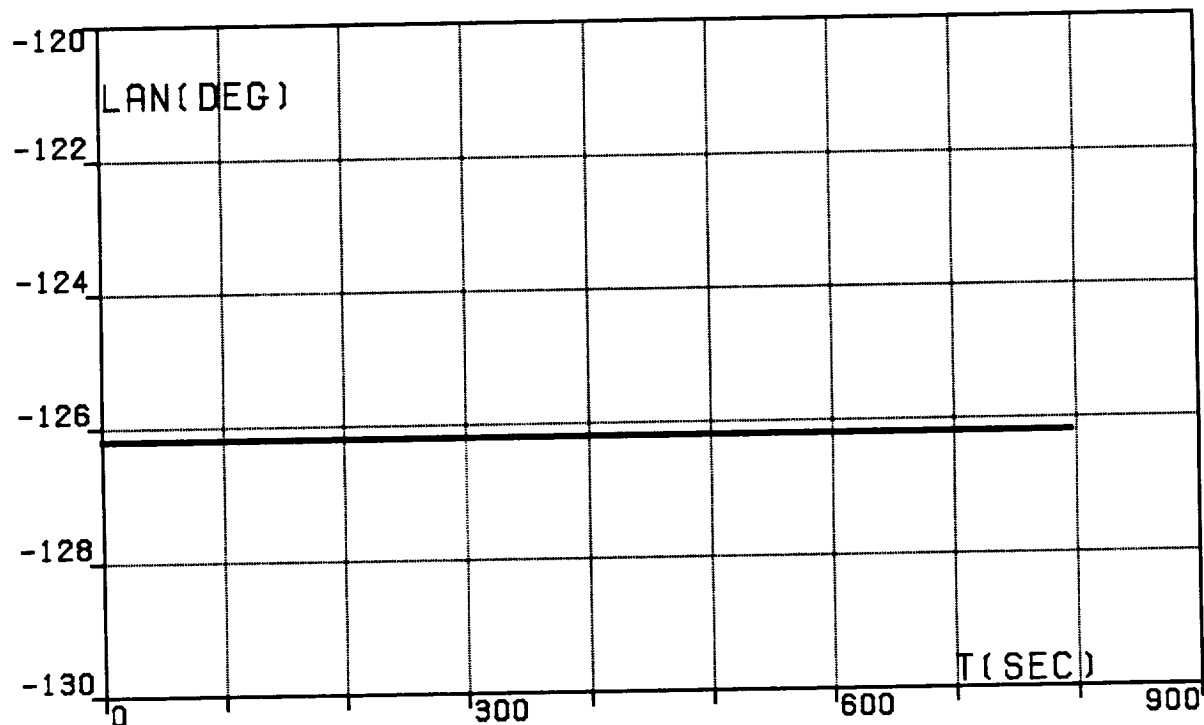


FIG.4P. THREE-SEGMENT OPTIMAL TRAJECTORY,  
TRANSFER (IA),  
LONGITUDE OF THE ASCENDING NODE.

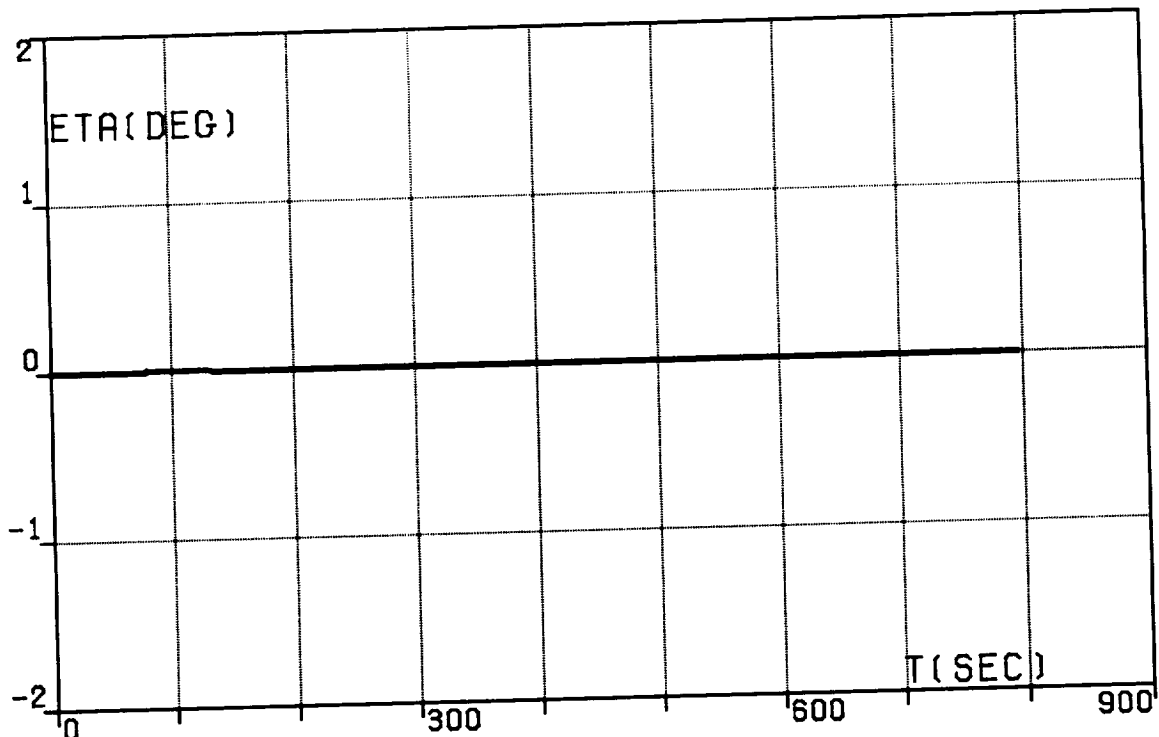


FIG. 4Q. THREE-SEGMENT OPTIMAL TRAJECTORY,  
TRANSFER (IA), WEDGE ANGLE.

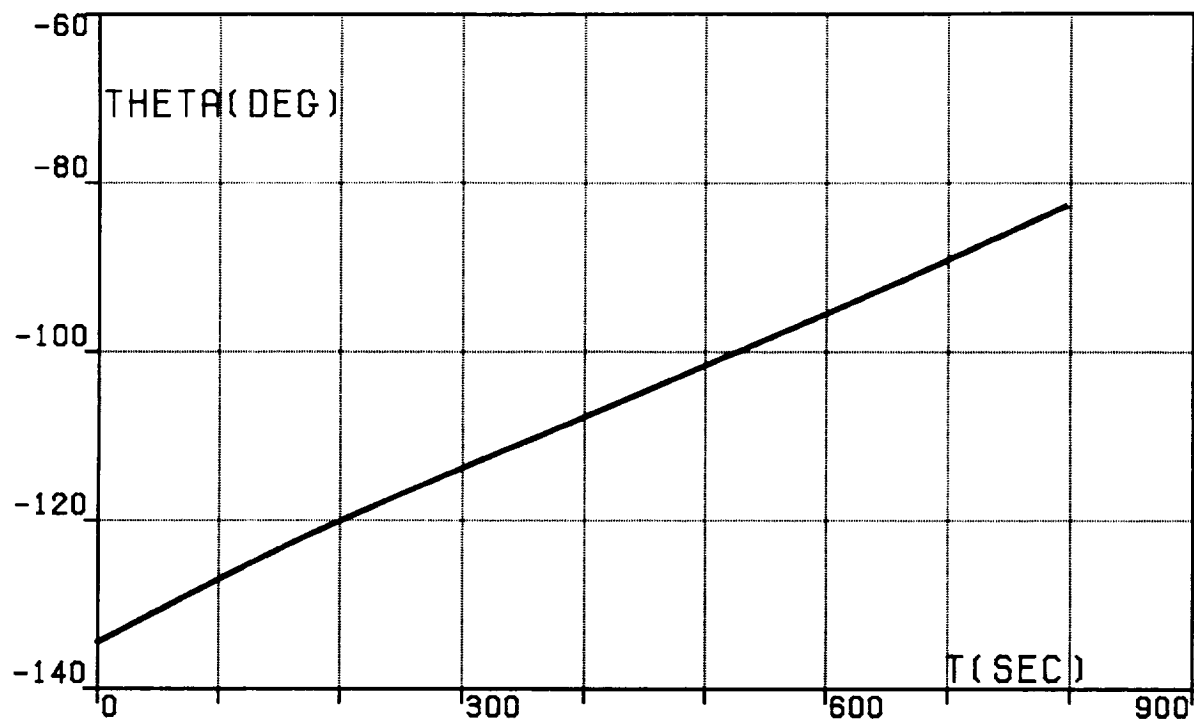


FIG.5A. FOUR-SEGMENT OPTIMAL TRAJECTORY,  
TRANSFER (IA), LONGITUDE, RELATIVE.

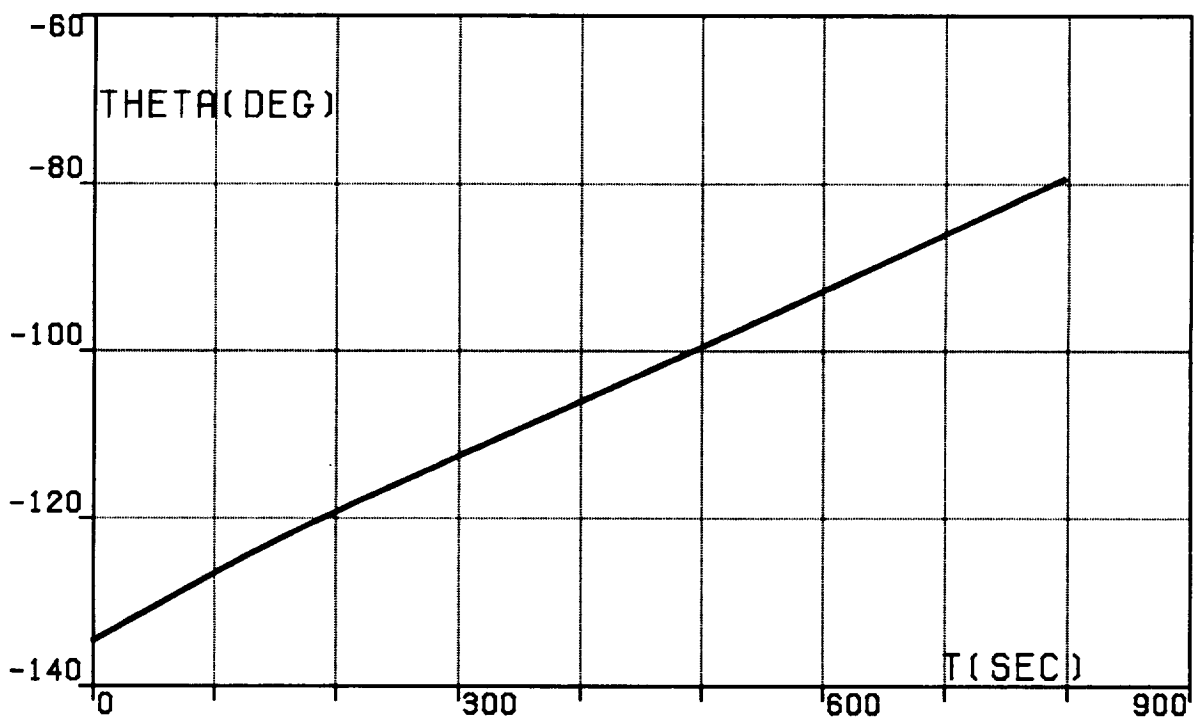


FIG.5B. FOUR-SEGMENT OPTIMAL TRAJECTORY,  
TRANSFER (IA), LONGITUDE, INERTIAL.

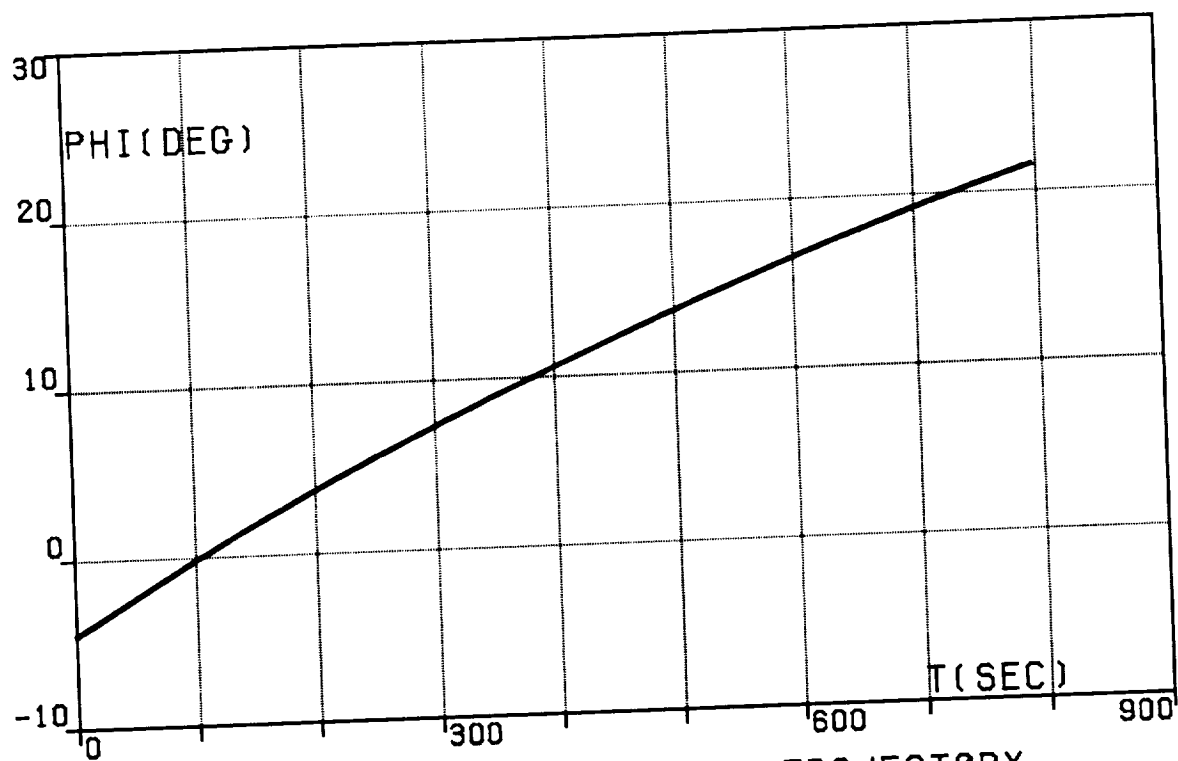


FIG.5C. FOUR-SEGMENT OPTIMAL TRAJECTORY,  
TRANSFER (IA). LATITUDE.

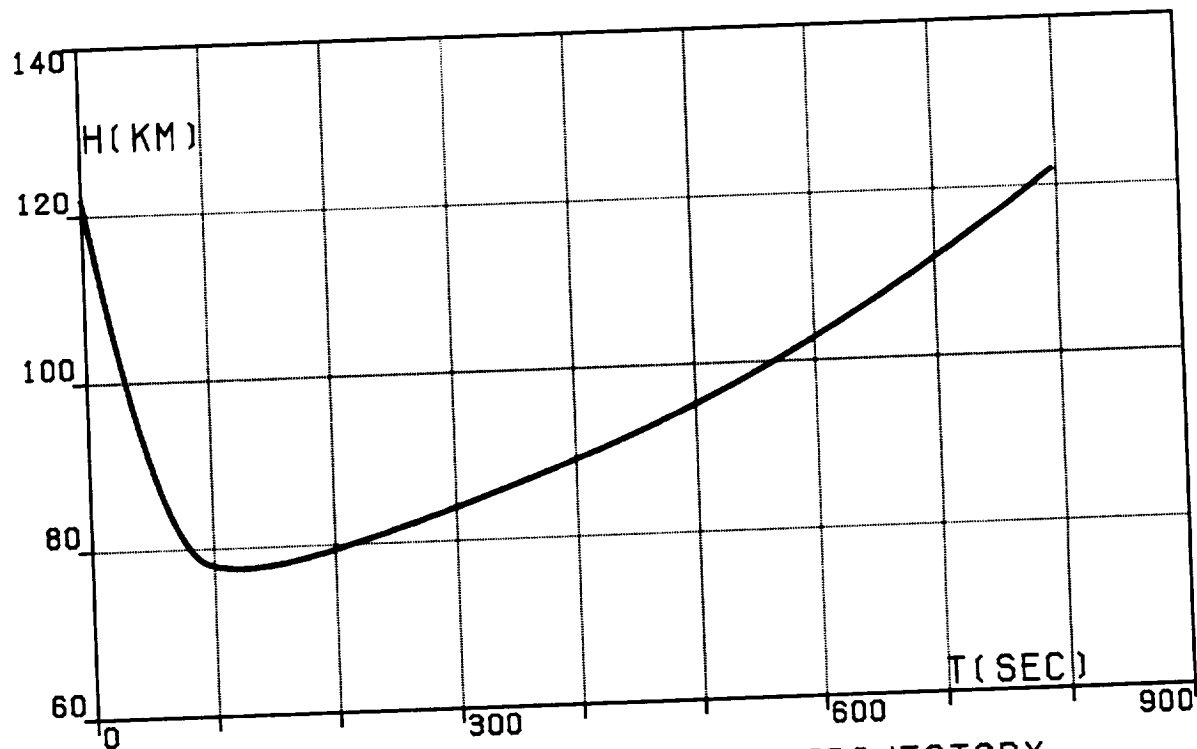


FIG.5D. FOUR-SEGMENT OPTIMAL TRAJECTORY,  
TRANSFER (IA). ALTITUDE.

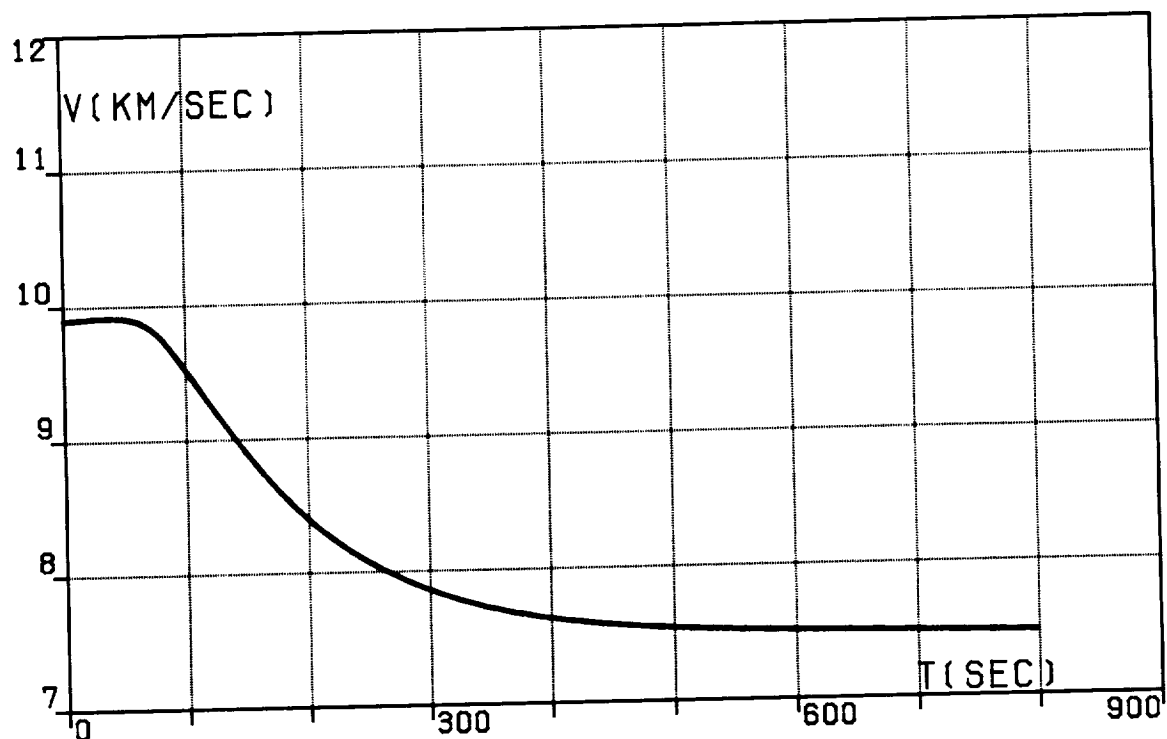


FIG.5E. FOUR-SEGMENT OPTIMAL TRAJECTORY,  
TRANSFER (IA), VELOCITY, RELATIVE.

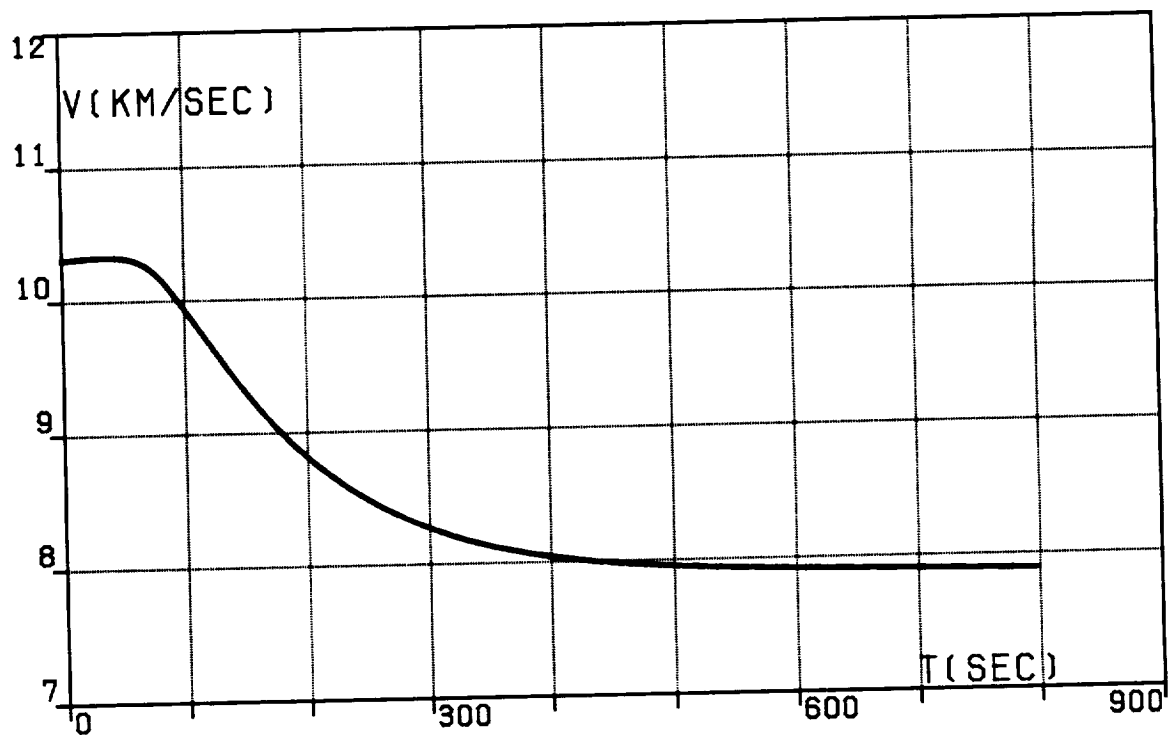


FIG.5F. FOUR-SEGMENT OPTIMAL TRAJECTORY,  
TRANSFER (IA), VELOCITY, INERTIAL.

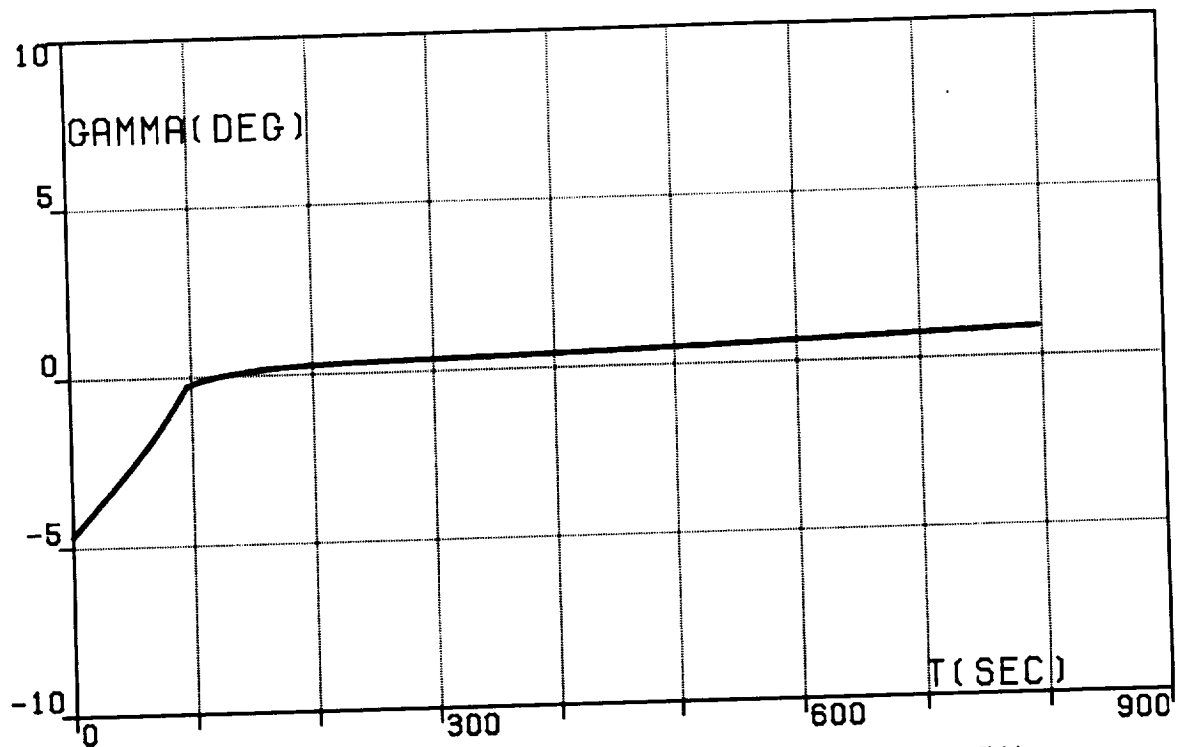


FIG.5G. FOUR-SEGMENT OPTIMAL TRAJECTORY,  
TRANSFER (IA).  
PATH INCLINATION, RELATIVE.

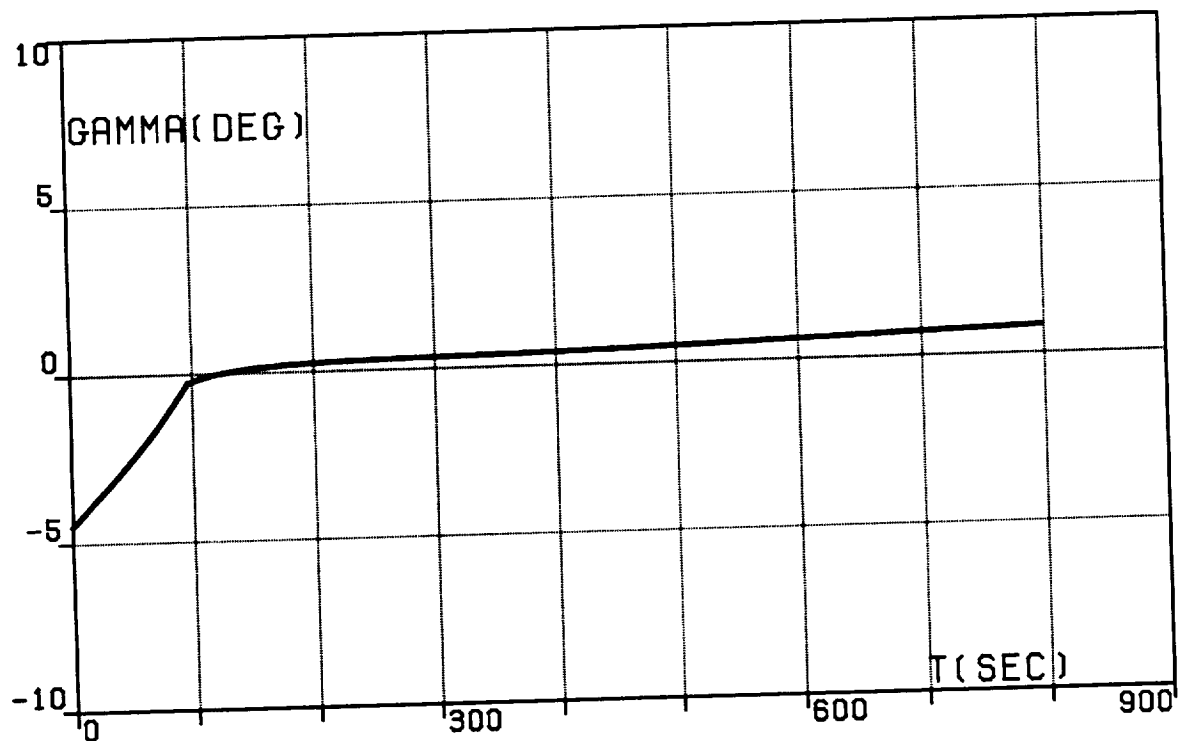


FIG.5H. FOUR-SEGMENT OPTIMAL TRAJECTORY,  
TRANSFER (IA).  
PATH INCLINATION, INERTIAL.

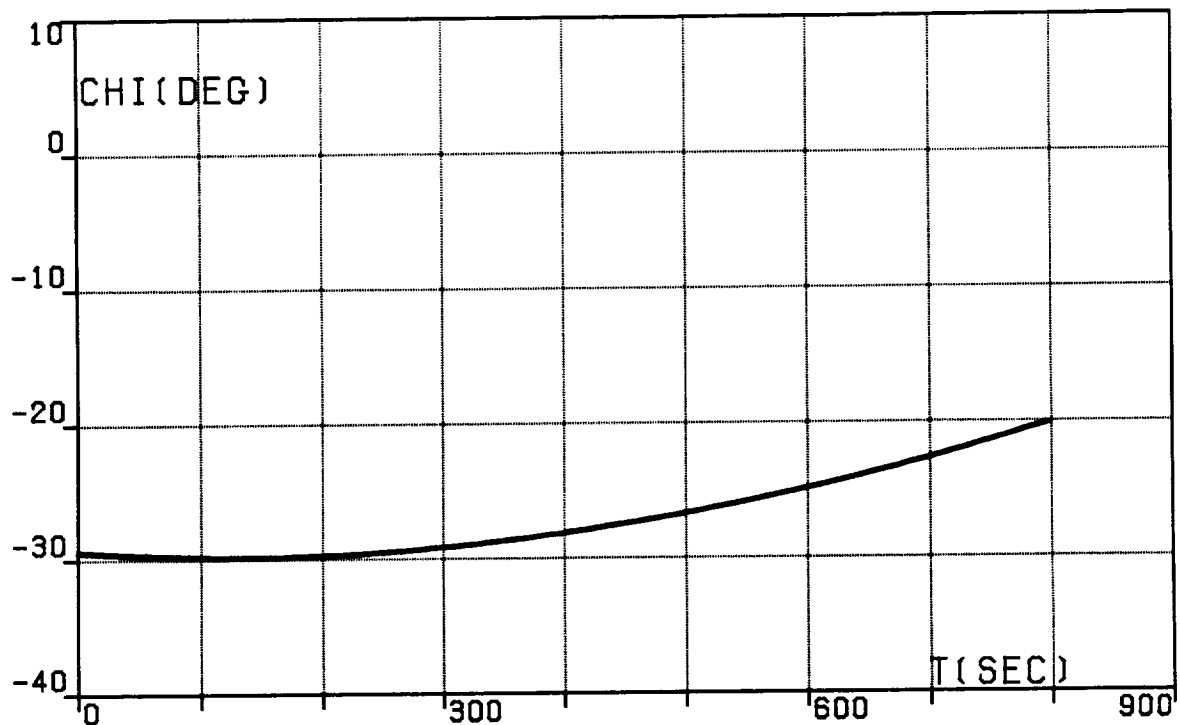


FIG.5I. FOUR-SEGMENT OPTIMAL TRAJECTORY,  
TRANSFER (IA), HEADING ANGLE, RELATIVE.

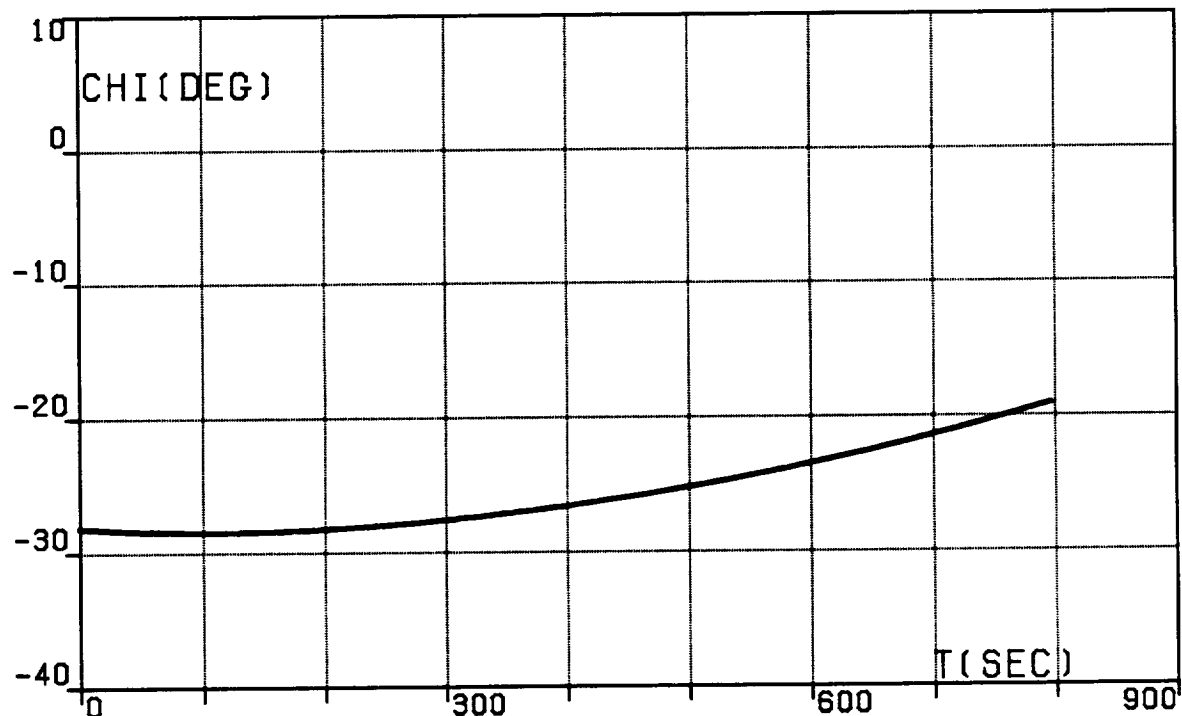


FIG.5J. FOUR-SEGMENT OPTIMAL TRAJECTORY,  
TRANSFER (IA), HEADING ANGLE, INERTIAL.

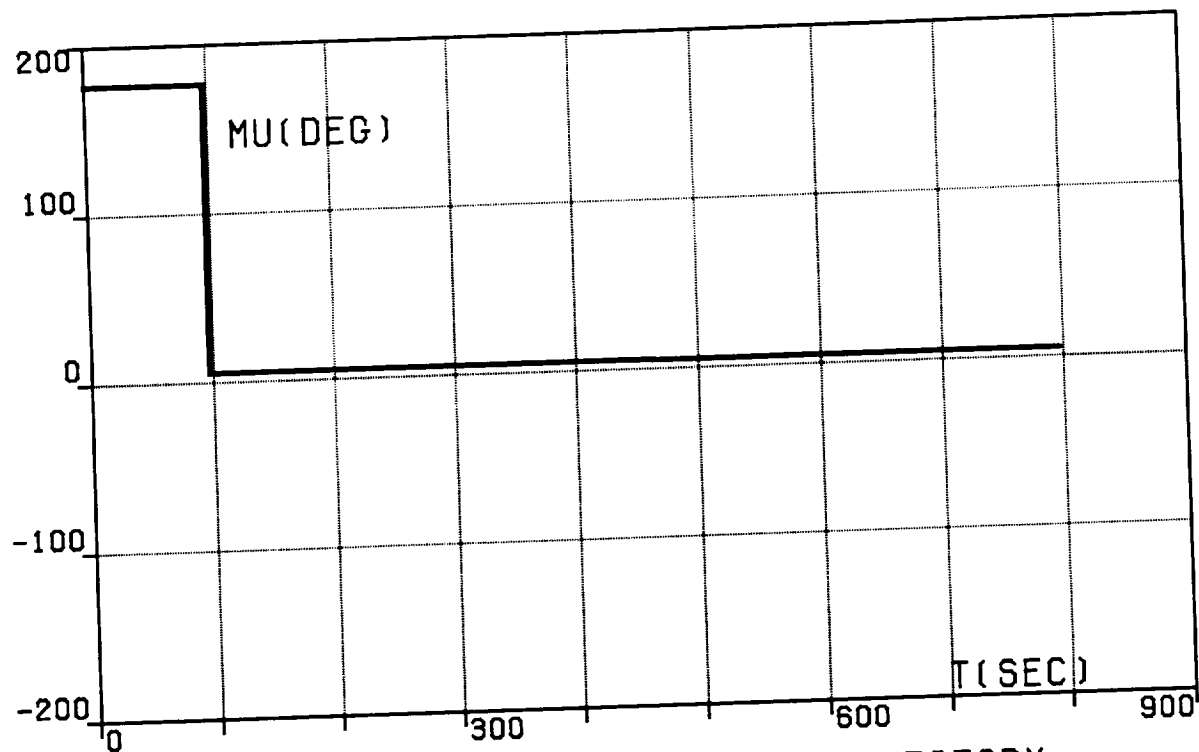


FIG.5K. FOUR-SEGMENT OPTIMAL TRAJECTORY,  
TRANSFER (IA), BANK ANGLE.

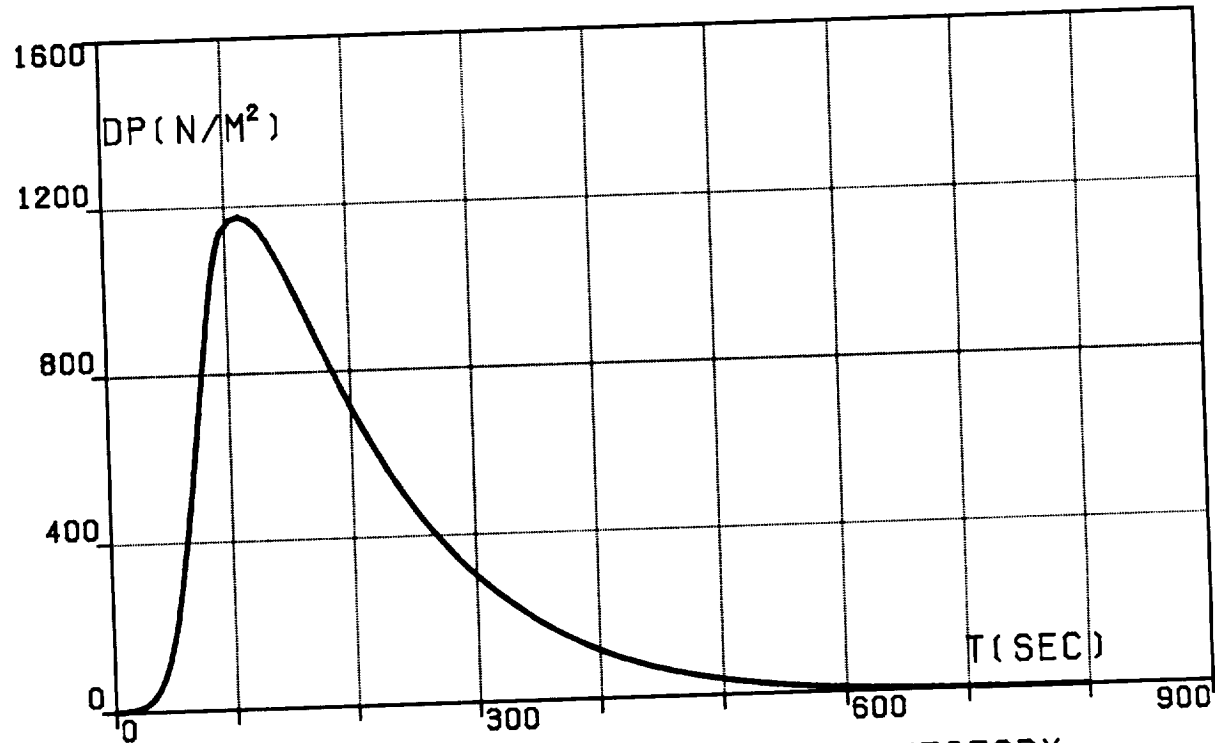


FIG.5L. FOUR-SEGMENT OPTIMAL TRAJECTORY,  
TRANSFER (IA), DYNAMIC PRESSURE.

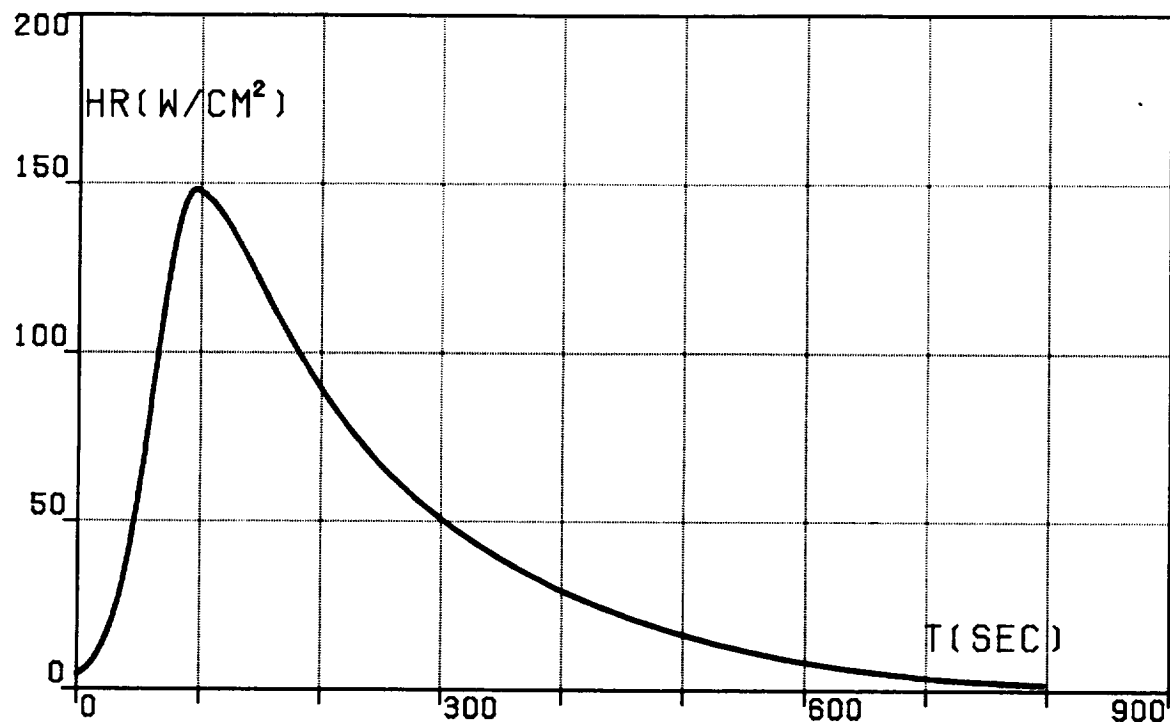


FIG.5M. FOUR-SEGMENT OPTIMAL TRAJECTORY,  
TRANSFER (IA), HEATING RATE.

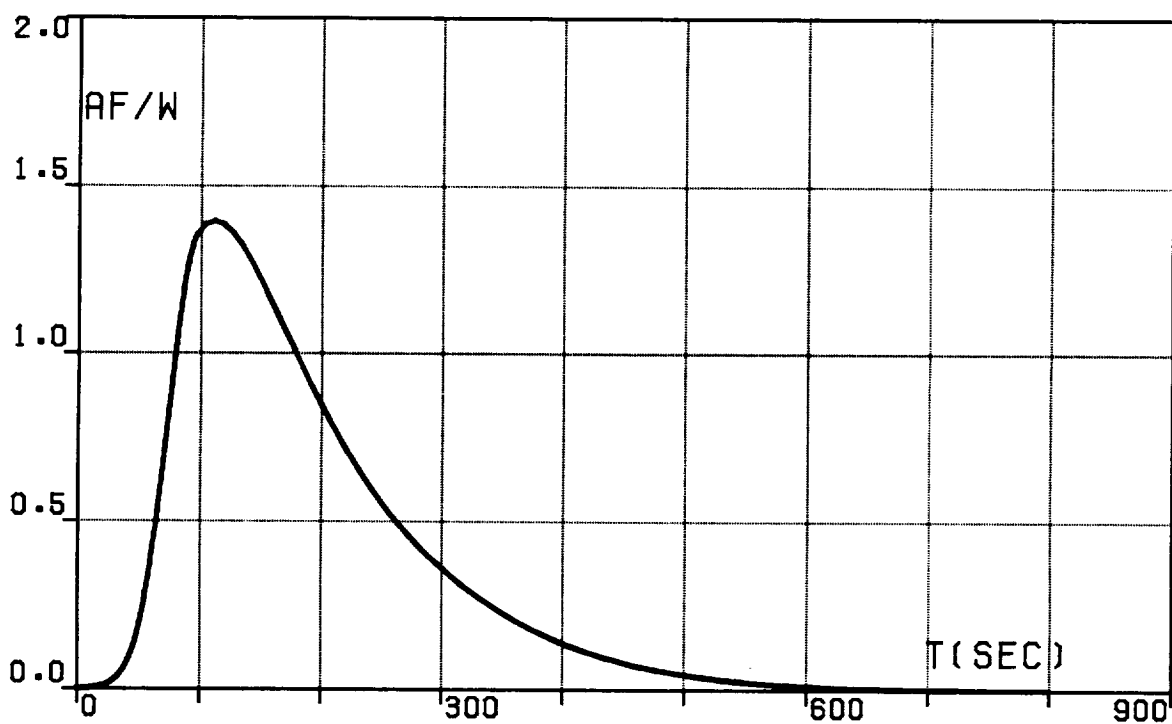


FIG.5N. FOUR-SEGMENT OPTIMAL TRAJECTORY,  
TRANSFER (IA),  
AERODYNAMIC FORCE PER UNIT WEIGHT.

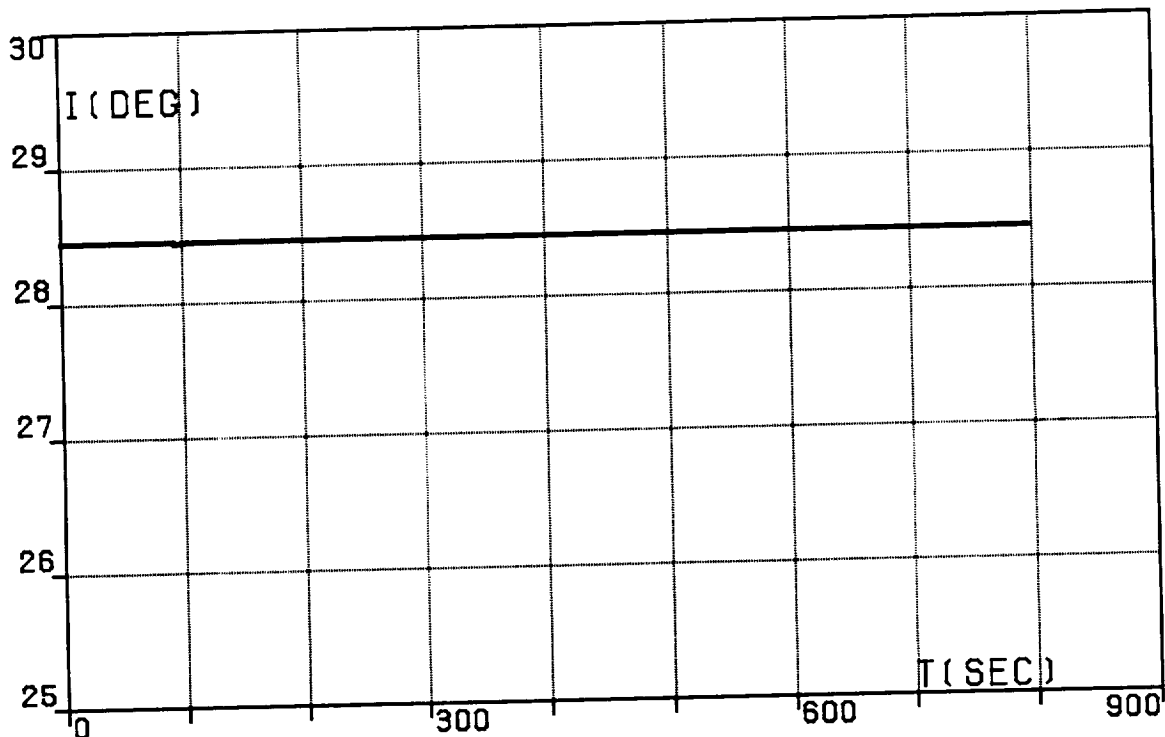


FIG.50. FOUR-SEGMENT OPTIMAL TRAJECTORY,  
TRANSFER (IA), ORBITAL INCLINATION.

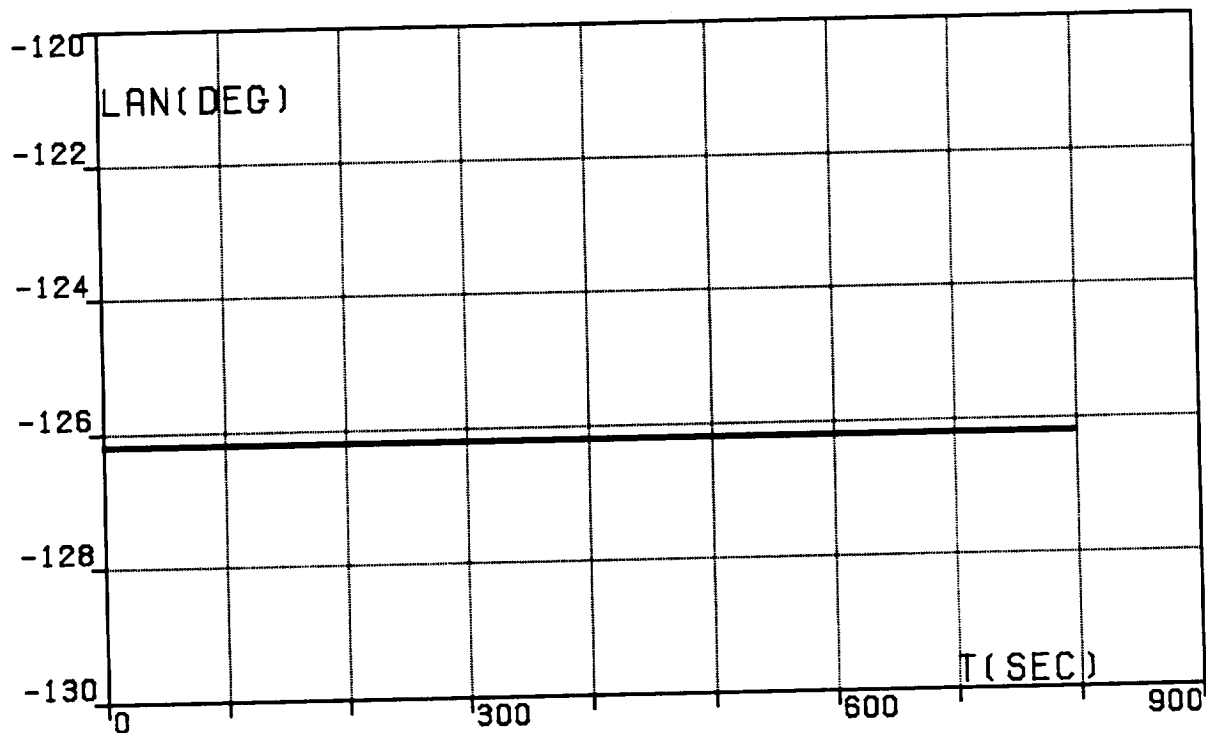


FIG.5P. FOUR-SEGMENT OPTIMAL TRAJECTORY,  
TRANSFER (IA),  
LONGITUDE OF THE ASCENDING NODE.

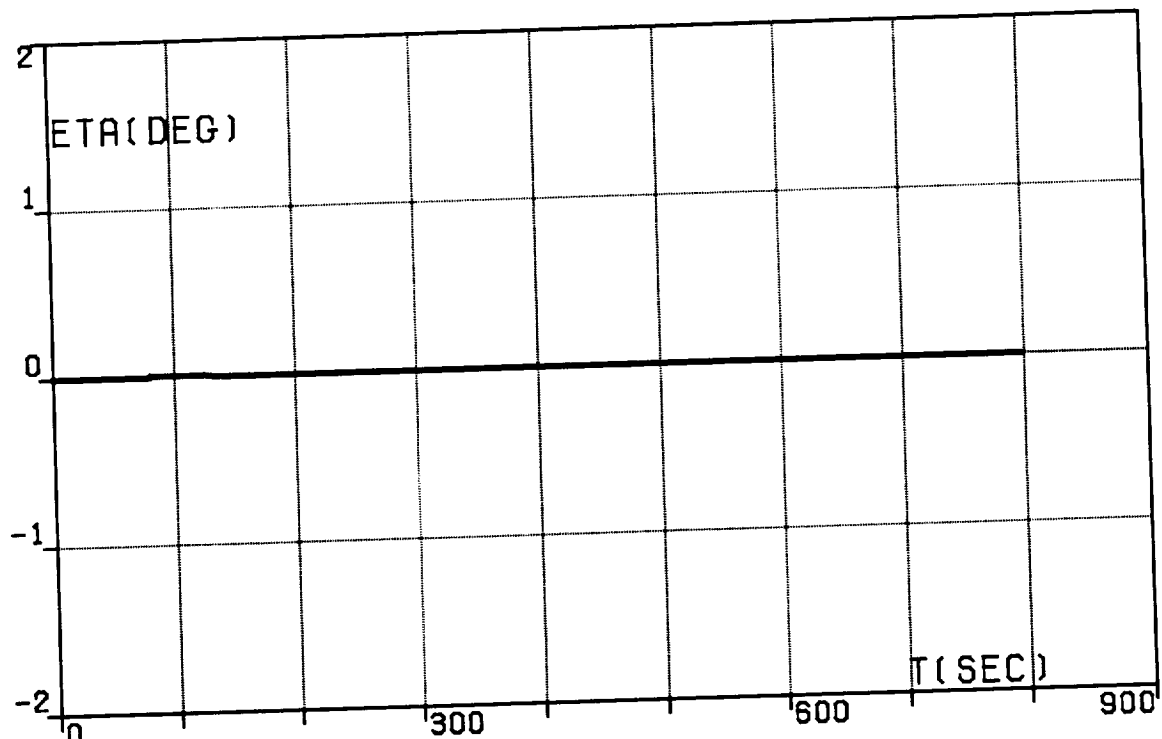


FIG.5Q. FOUR-SEGMENT OPTIMAL TRAJECTORY,  
TRANSFER (IA), WEDGE ANGLE.

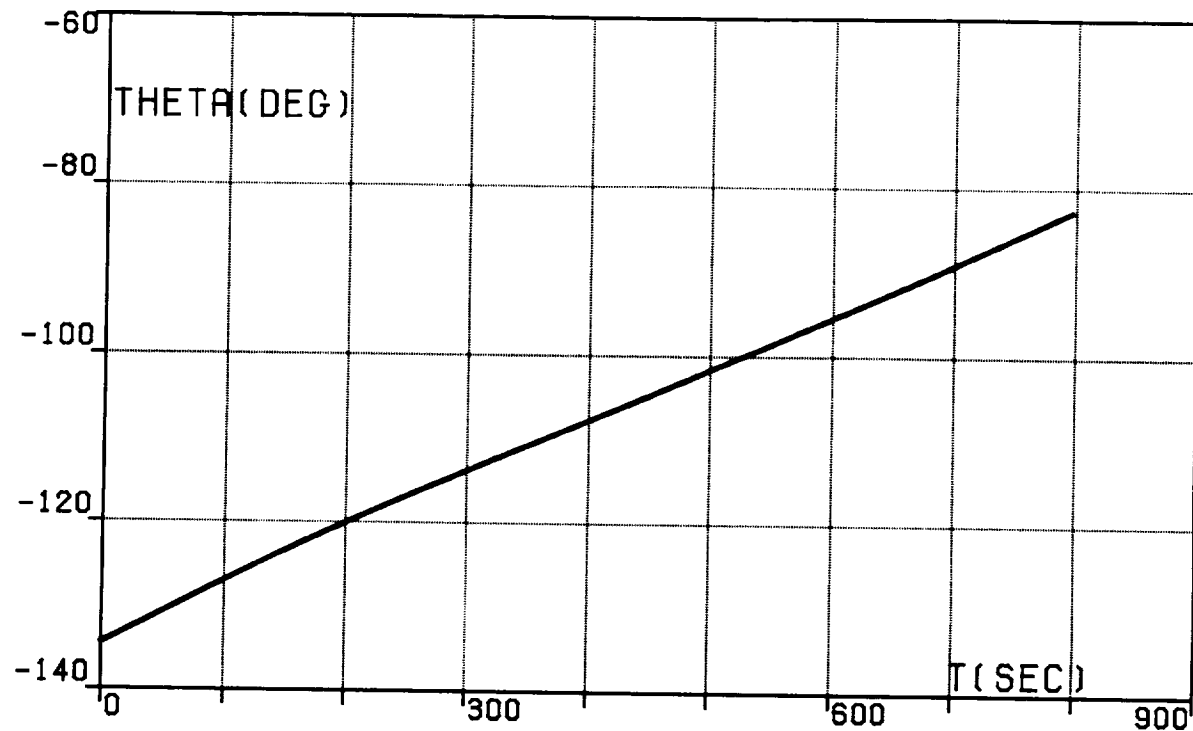


FIG.6A. FIVE-SEGMENT OPTIMAL TRAJECTORY,  
TRANSFER (IA), LONGITUDE, RELATIVE.

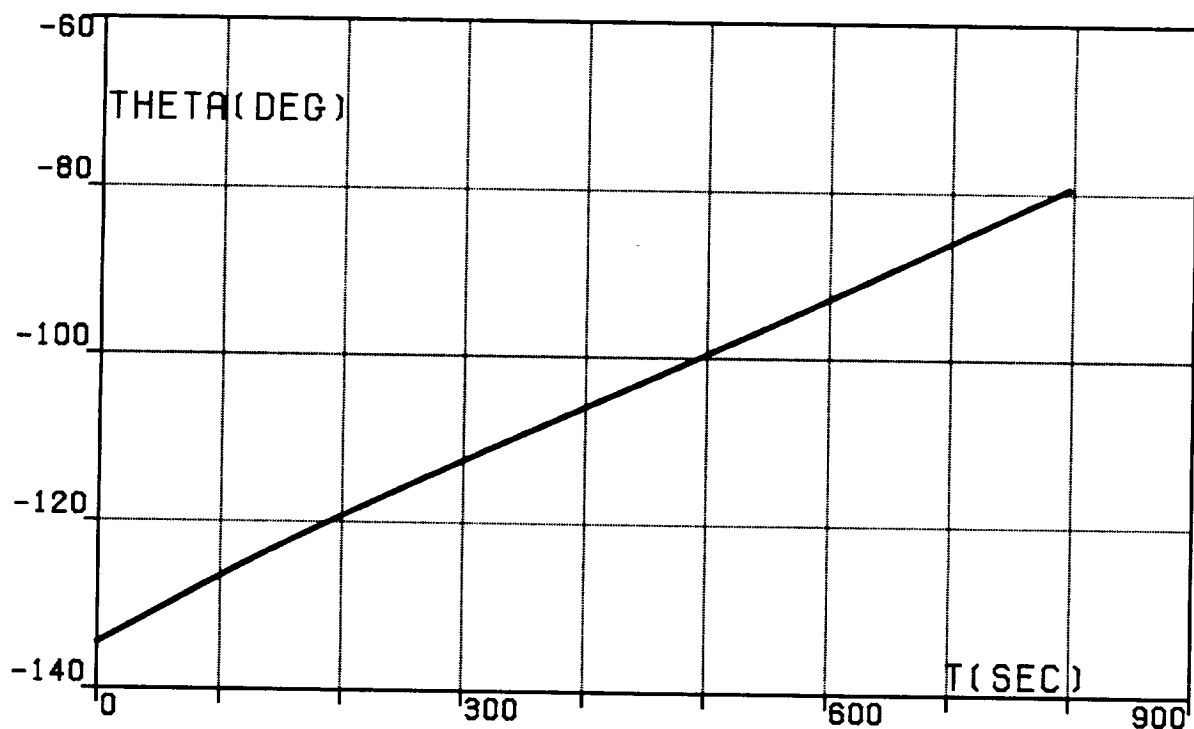


FIG.6B. FIVE-SEGMENT OPTIMAL TRAJECTORY,  
TRANSFER (IA), LONGITUDE, INERTIAL.

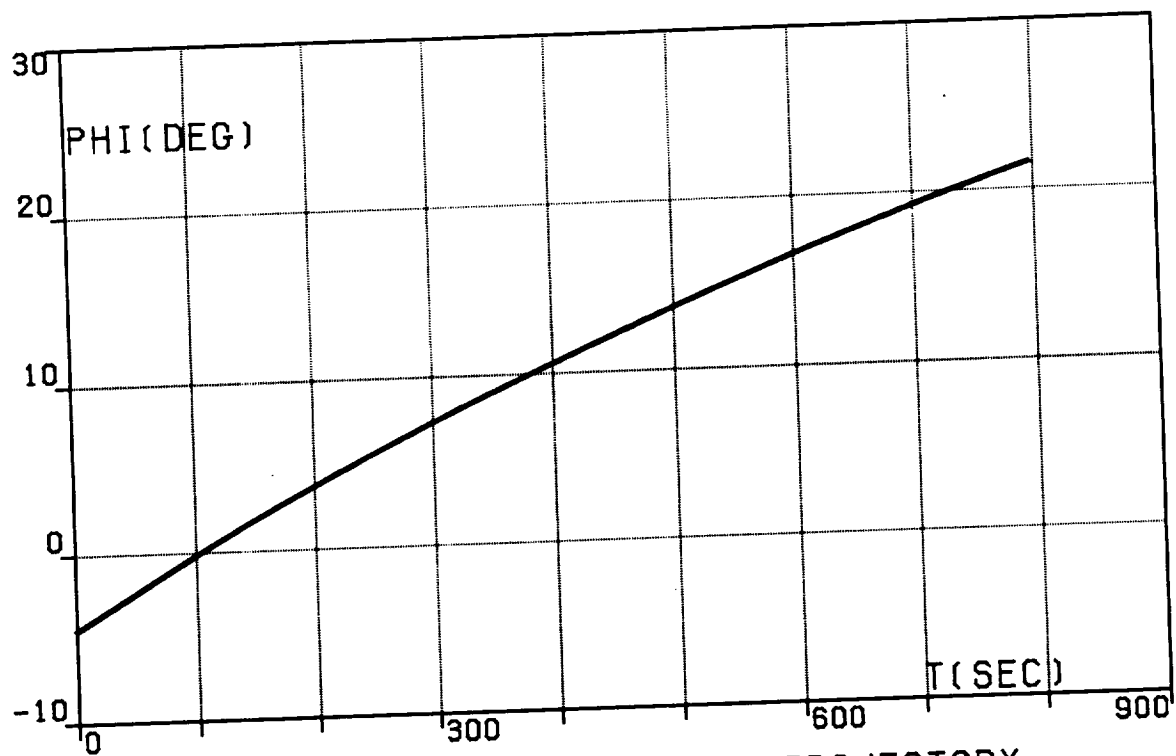


FIG.6C. FIVE-SEGMENT OPTIMAL TRAJECTORY,  
TRANSFER (IA), LATITUDE.

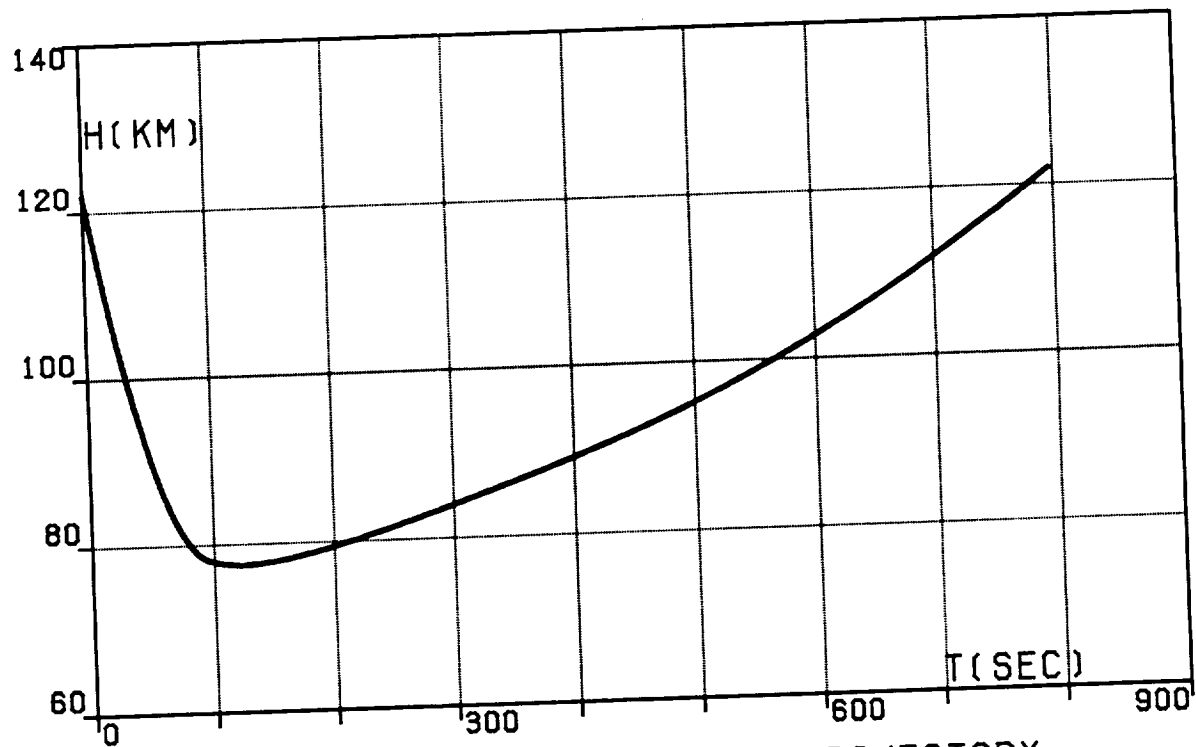


FIG.6D. FIVE-SEGMENT OPTIMAL TRAJECTORY,  
TRANSFER (IA), ALTITUDE.

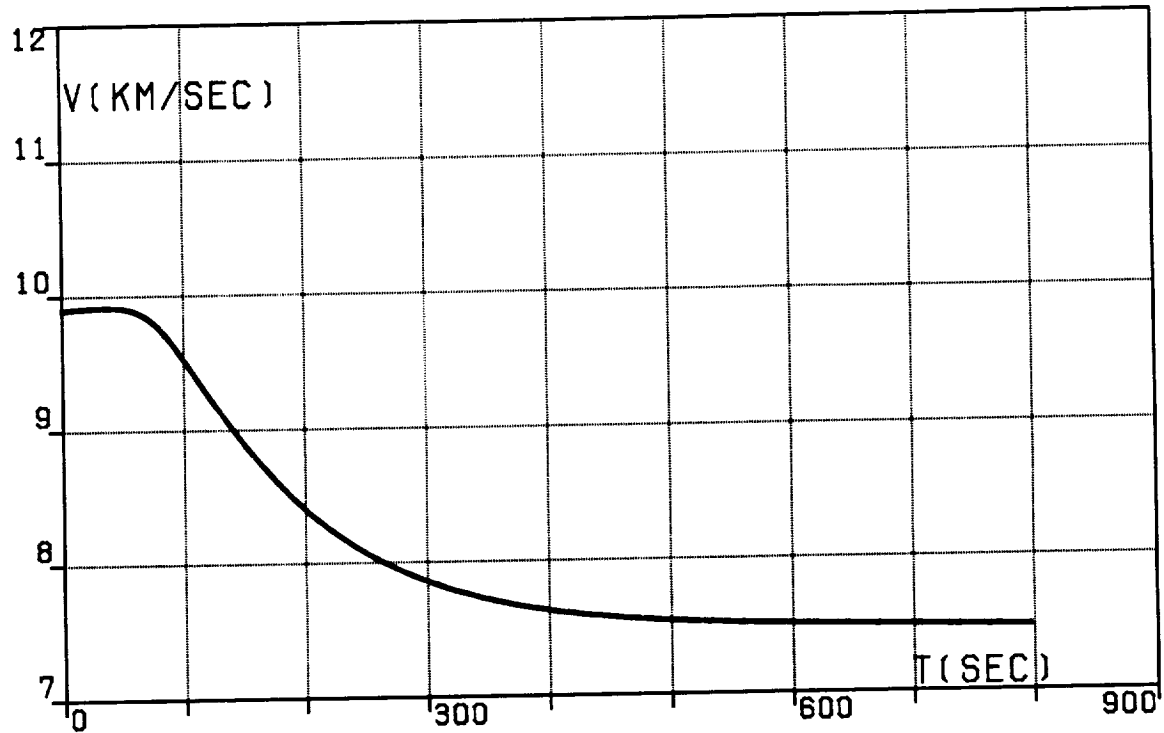


FIG.6E. FIVE-SEGMENT OPTIMAL TRAJECTORY,  
TRANSFER (IA), VELOCITY, RELATIVE.

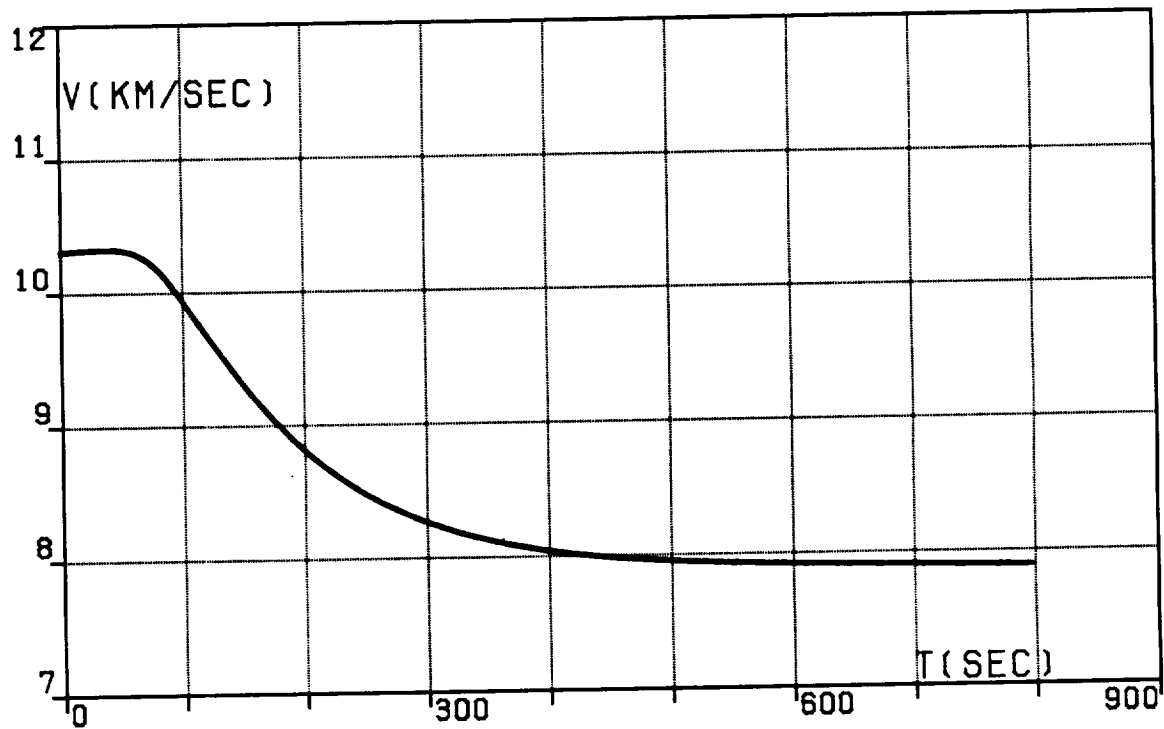


FIG.6F. FIVE-SEGMENT OPTIMAL TRAJECTORY,  
TRANSFER (IA), VELOCITY, INERTIAL.

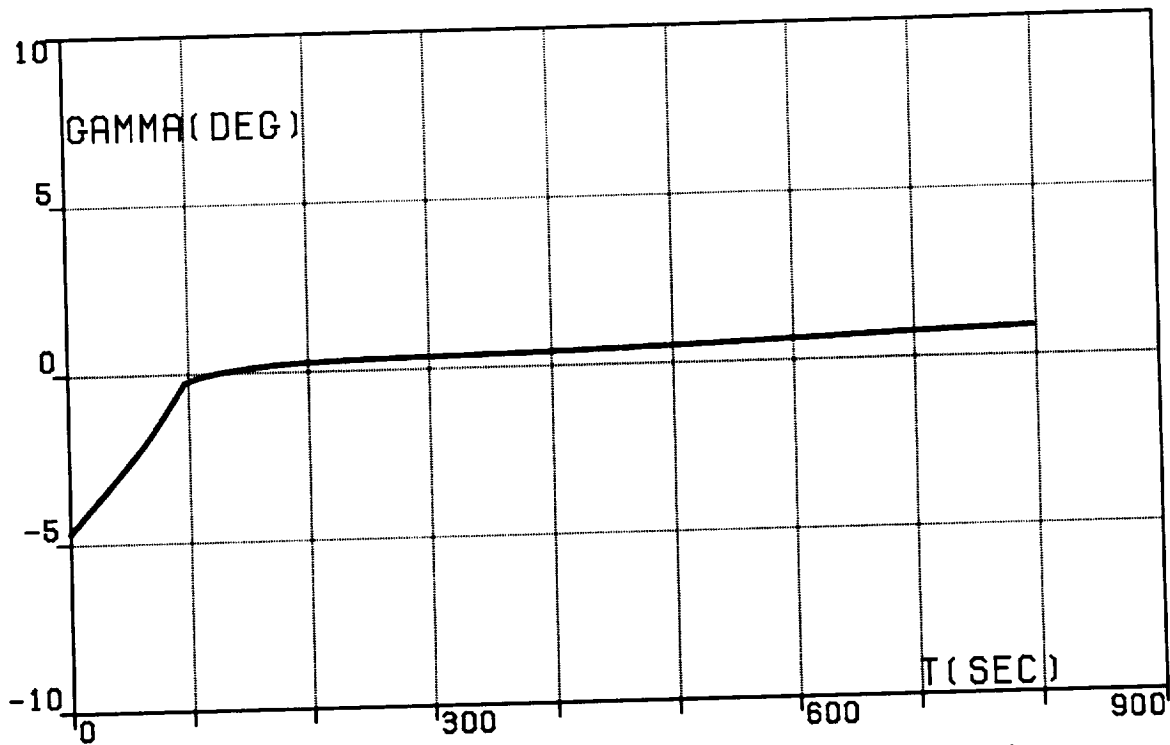


FIG.6G. FIVE-SEGMENT OPTIMAL TRAJECTORY,  
TRANSFER (IA),  
PATH INCLINATION, RELATIVE.

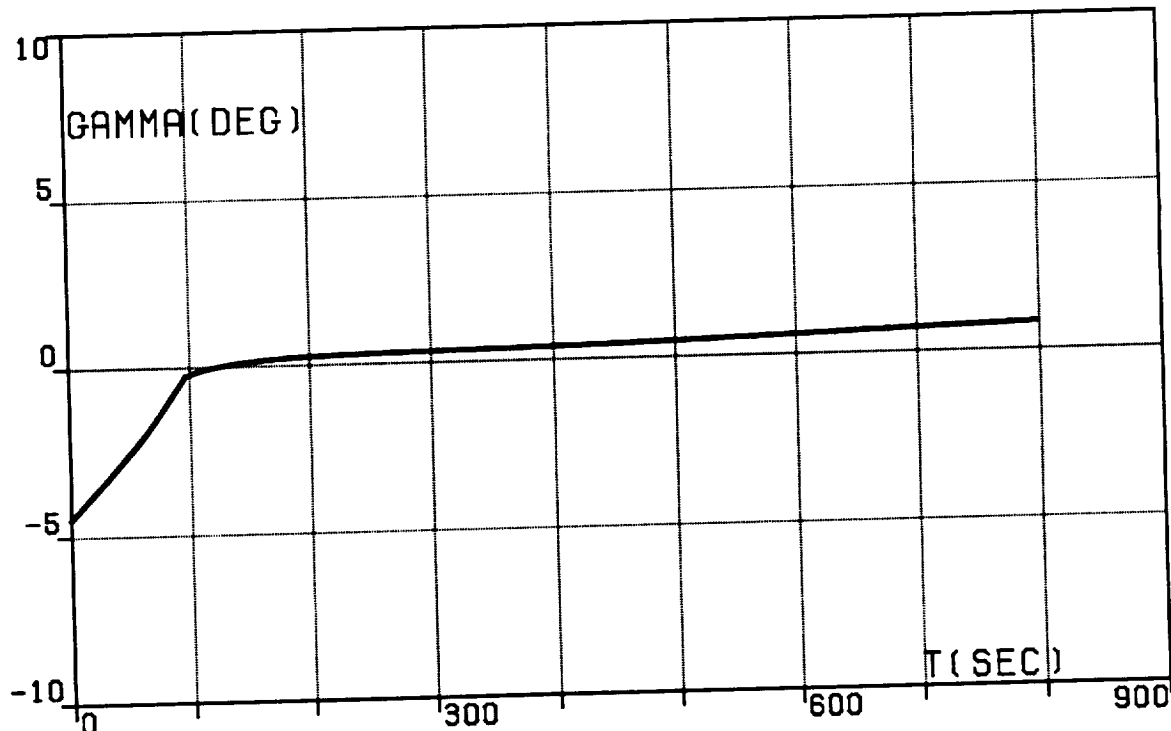


FIG.6H. FIVE-SEGMENT OPTIMAL TRAJECTORY,  
TRANSFER (IA),  
PATH INCLINATION, INERTIAL.

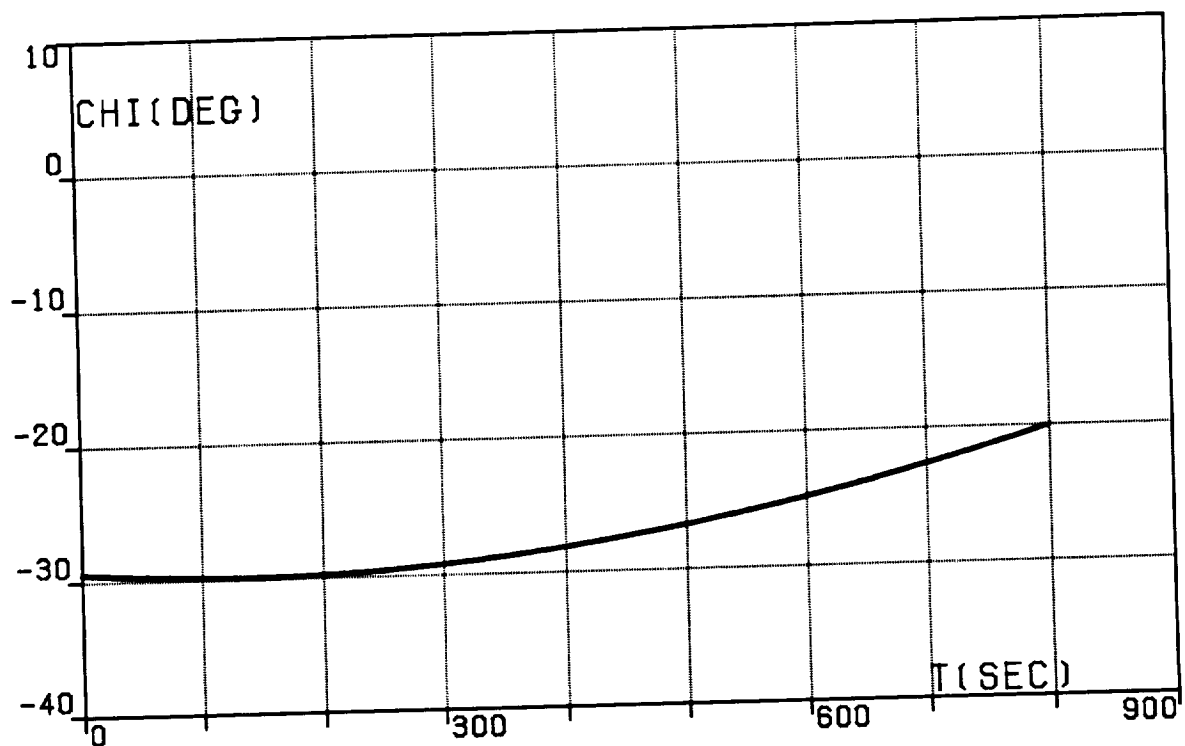


FIG.6I. FIVE-SEGMENT OPTIMAL TRAJECTORY,  
TRANSFER (IA), HEADING ANGLE, RELATIVE.

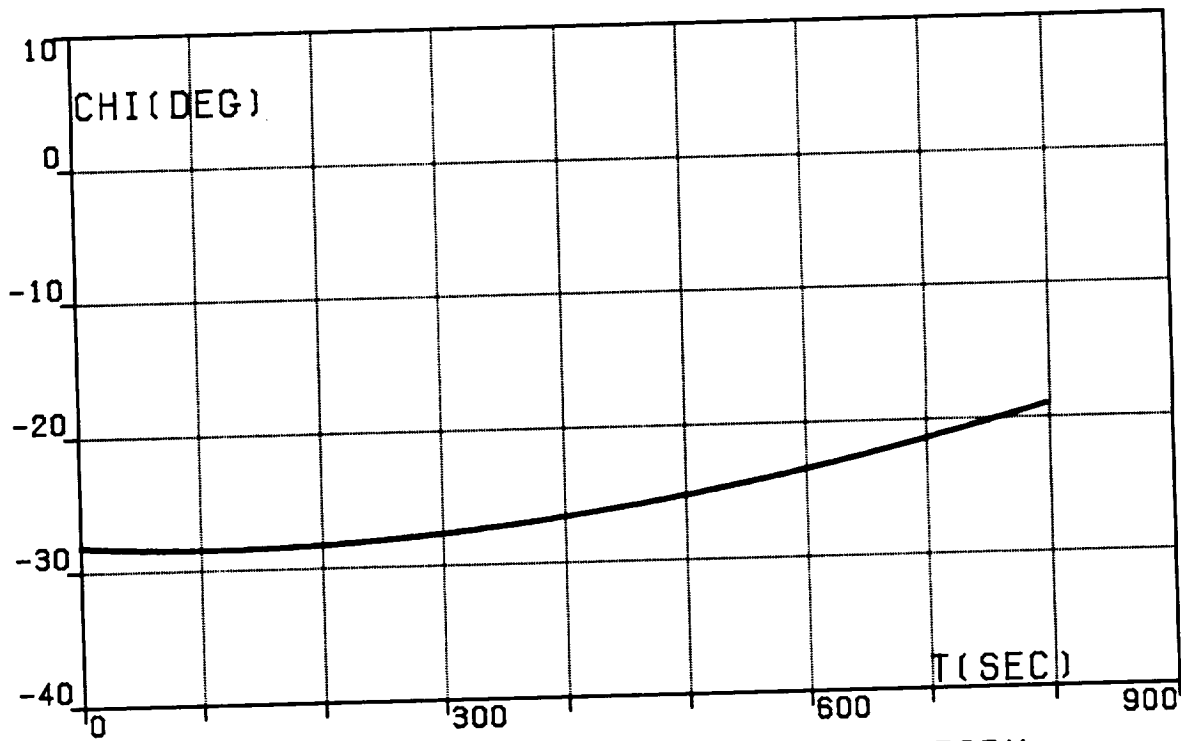


FIG.6J. FIVE-SEGMENT OPTIMAL TRAJECTORY,  
TRANSFER (IA), HEADING ANGLE, INERTIAL.

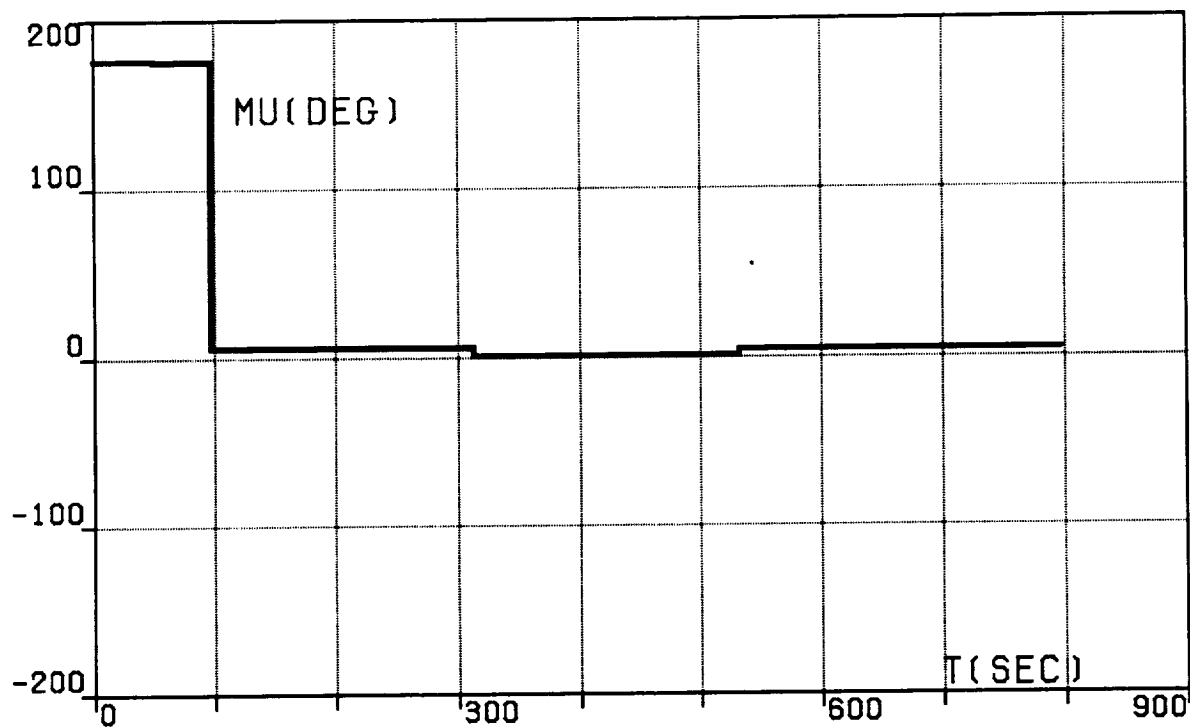


FIG.6K. FIVE-SEGMENT OPTIMAL TRAJECTORY,  
TRANSFER (IA), BANK ANGLE.

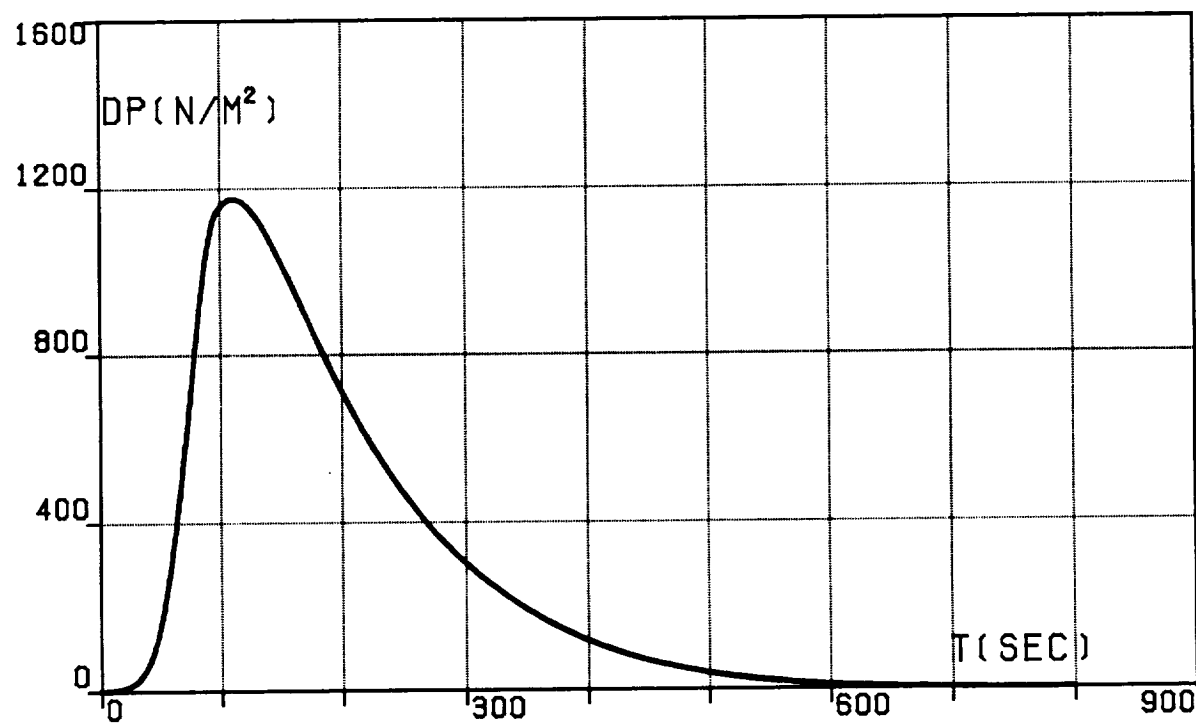


FIG.6L. FIVE-SEGMENT OPTIMAL TRAJECTORY,  
TRANSFER (IA), DYNAMIC PRESSURE.

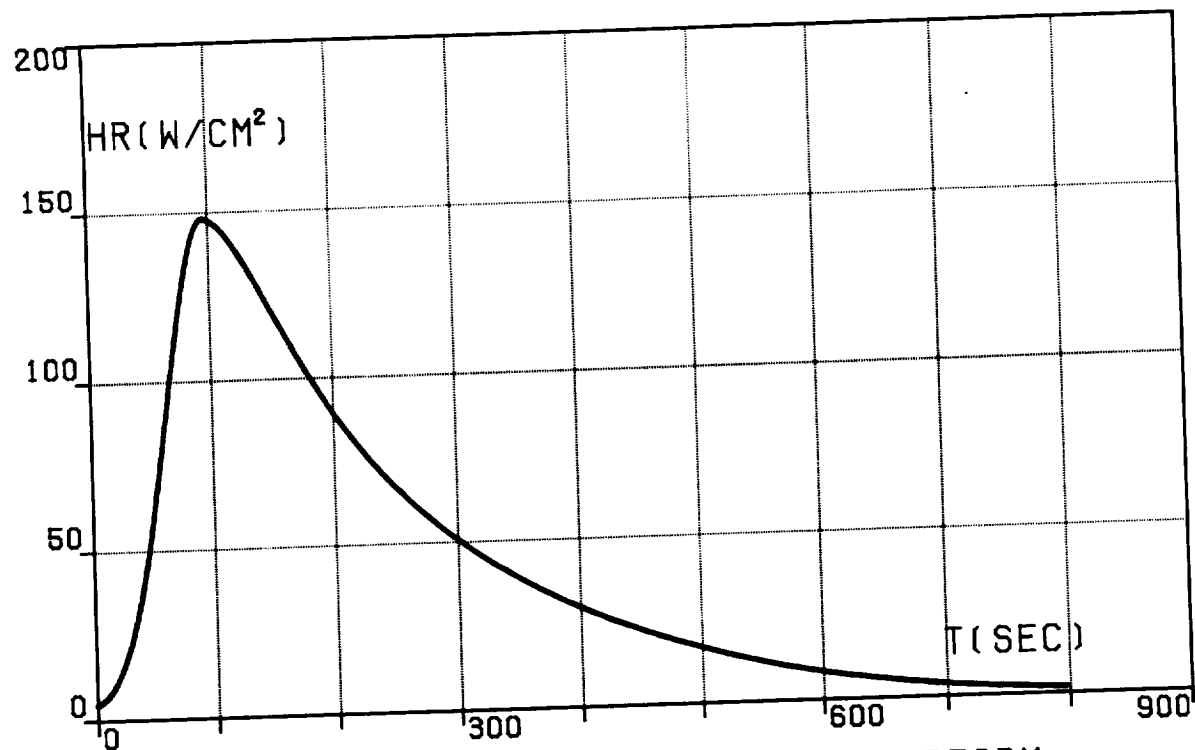


FIG.6M. FIVE-SEGMENT OPTIMAL TRAJECTORY,  
TRANSFER (IA), HEATING RATE.

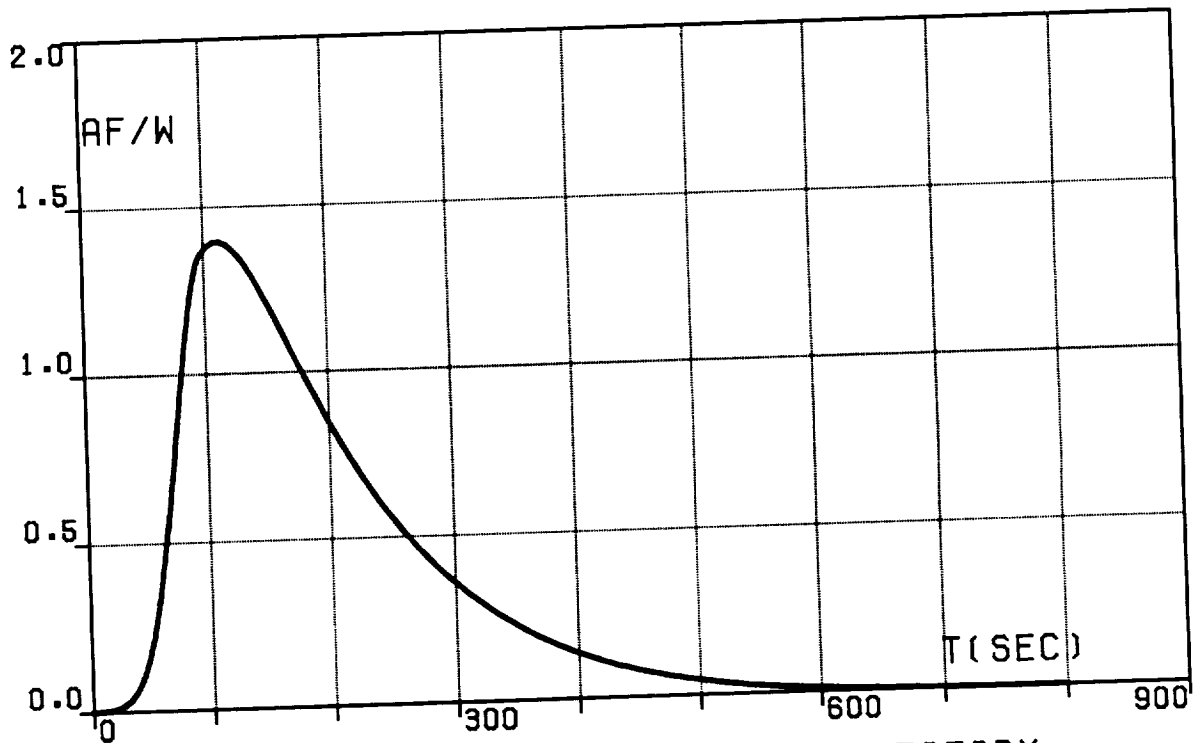


FIG.6N. FIVE-SEGMENT OPTIMAL TRAJECTORY,  
TRANSFER (IA),  
AERODYNAMIC FORCE PER UNIT WEIGHT.

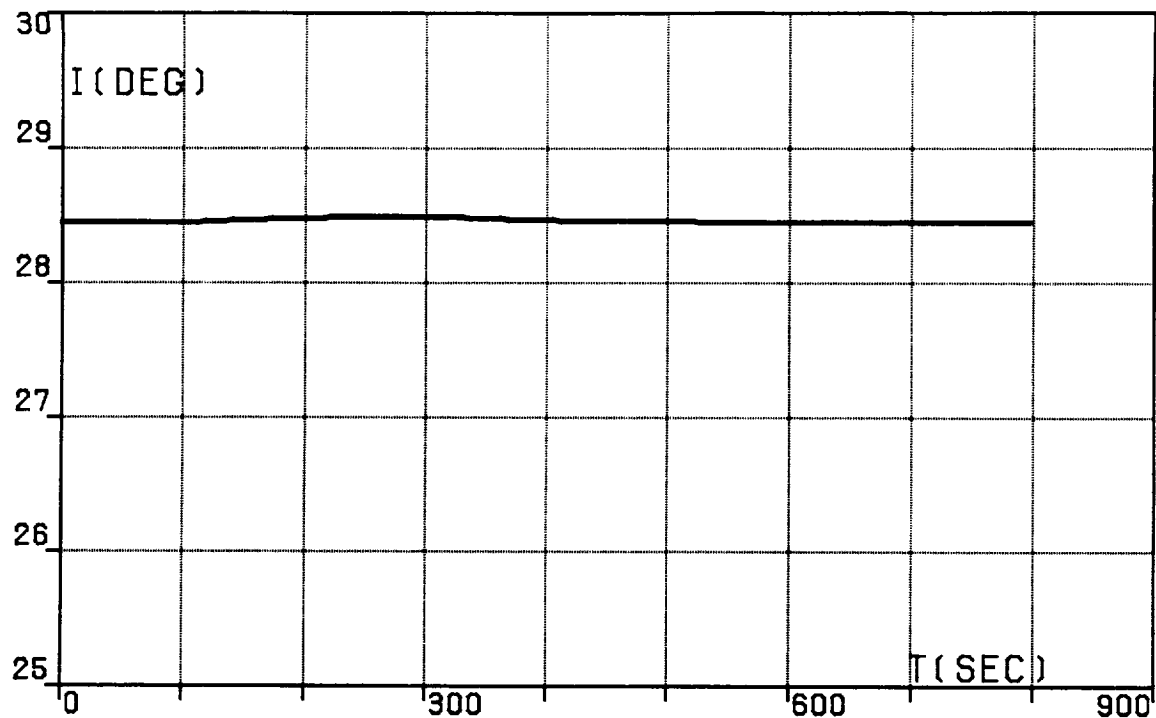


FIG.60. FIVE-SEGMENT OPTIMAL TRAJECTORY,  
TRANSFER (IA), ORBITAL INCLINATION.

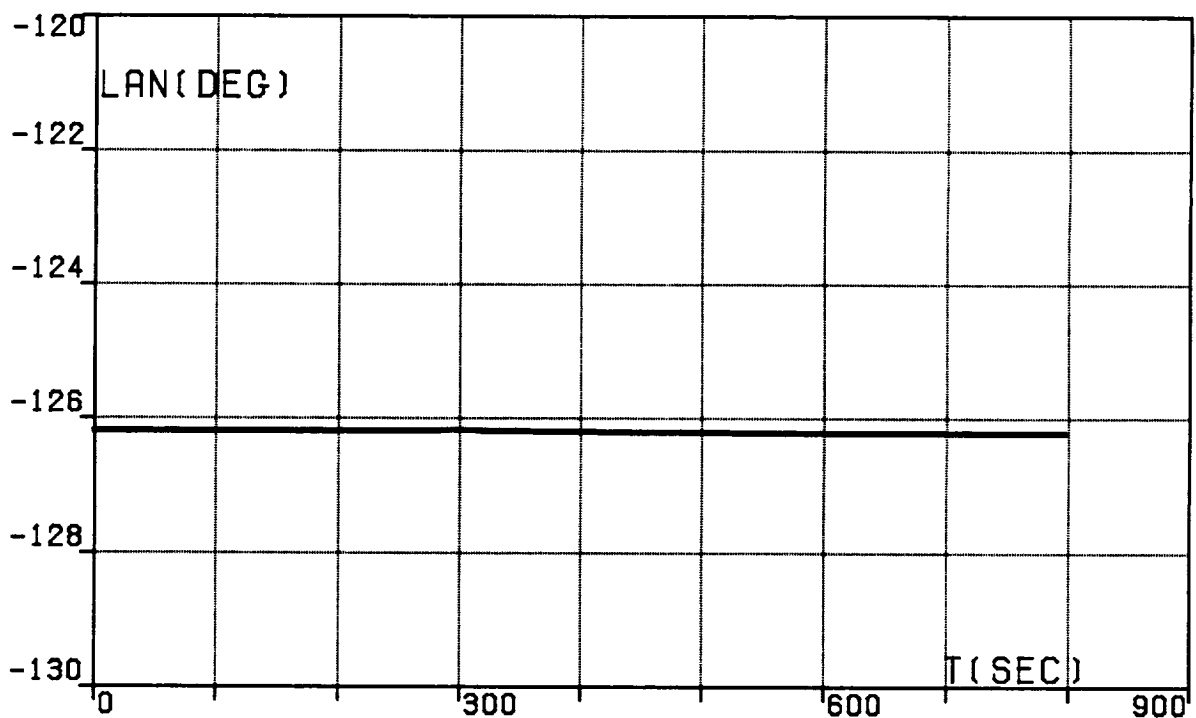


FIG.6P. FIVE-SEGMENT OPTIMAL TRAJECTORY,  
TRANSFER (IA),  
LONGITUDE OF THE ASCENDING NODE.

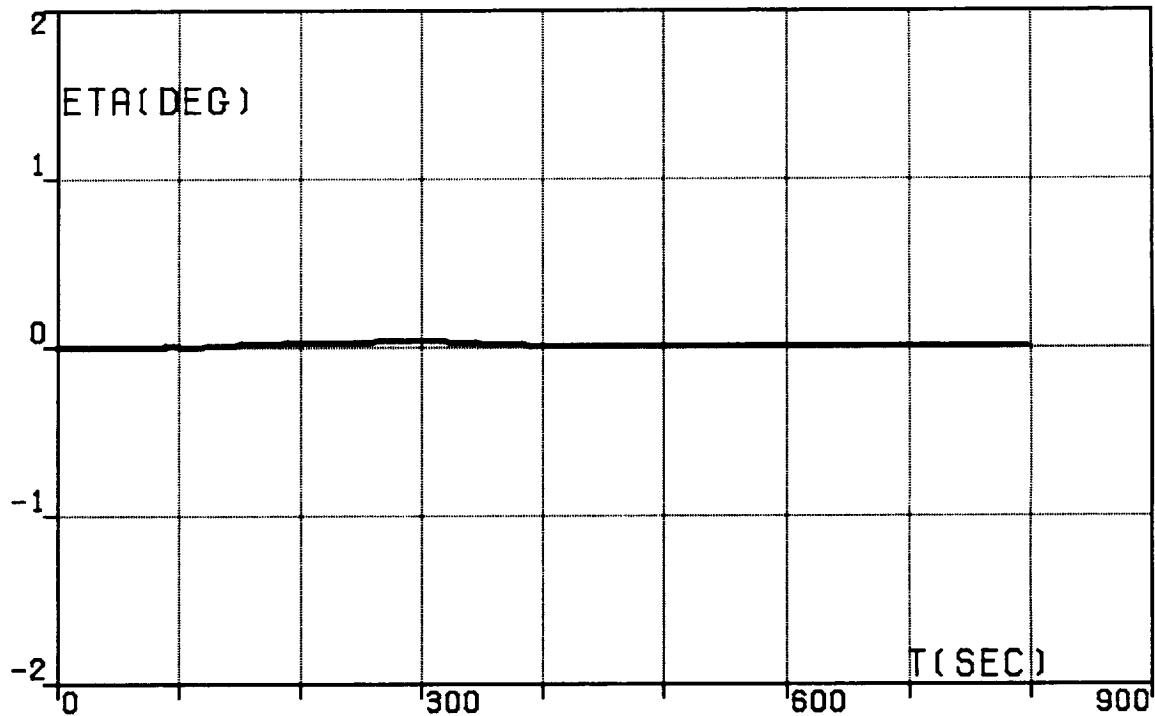


FIG. 6Q. FIVE-SEGMENT OPTIMAL TRAJECTORY,  
TRANSFER (IA), WEDGE ANGLE.

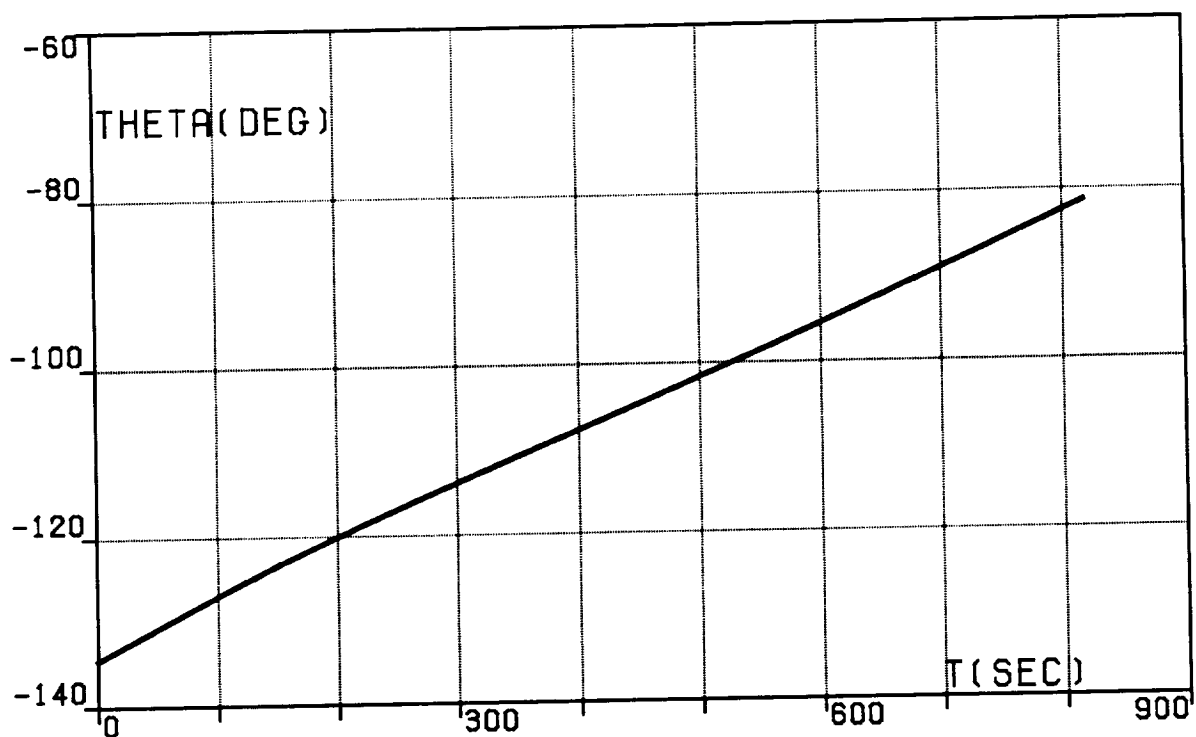


FIG.7A. CONTINUOUS OPTIMAL TRAJECTORY,  
TRANSFER (DA), LONGITUDE, RELATIVE.

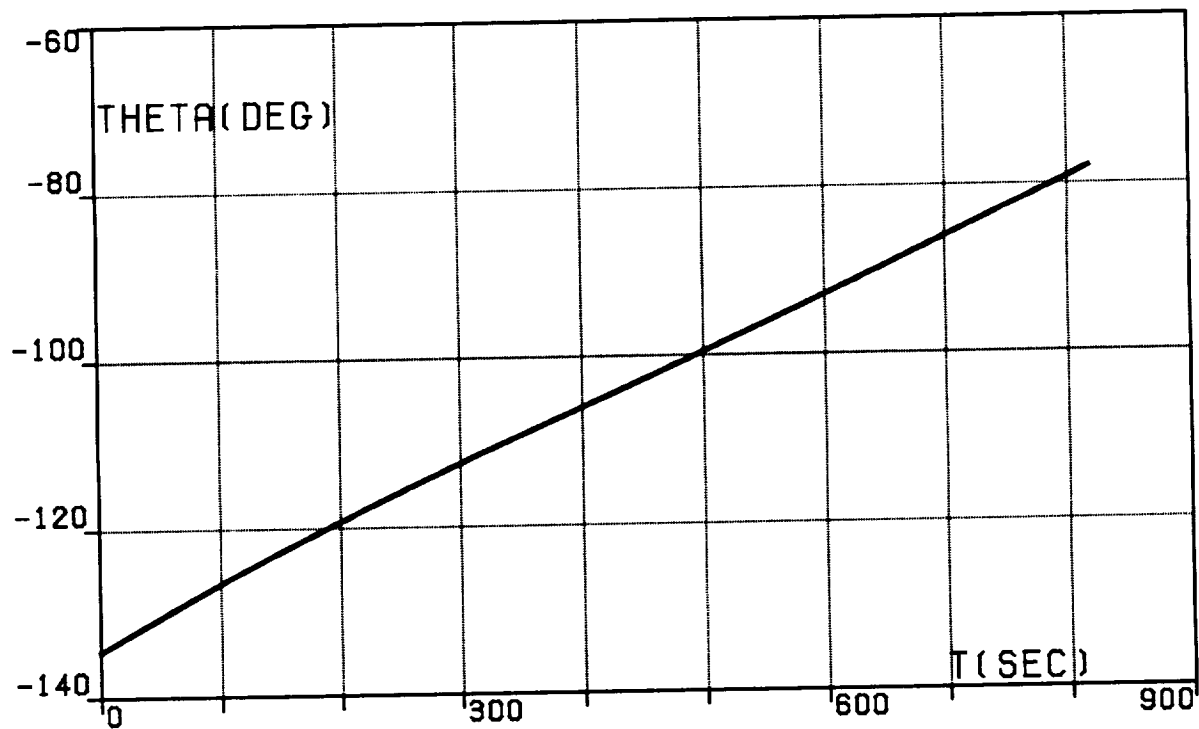


FIG.7B. CONTINUOUS OPTIMAL TRAJECTORY,  
TRANSFER (DA), LONGITUDE, INERTIAL.

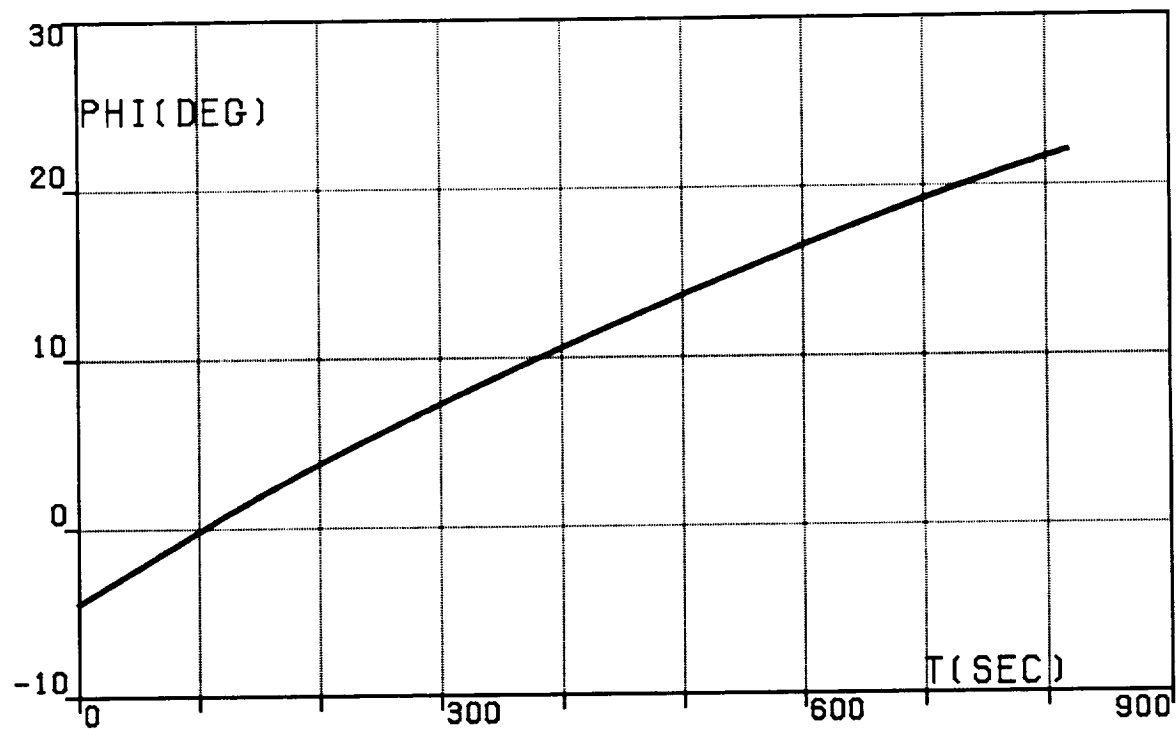


FIG. 7C. CONTINUOUS OPTIMAL TRAJECTORY,  
TRANSFER (DA), LATITUDE.

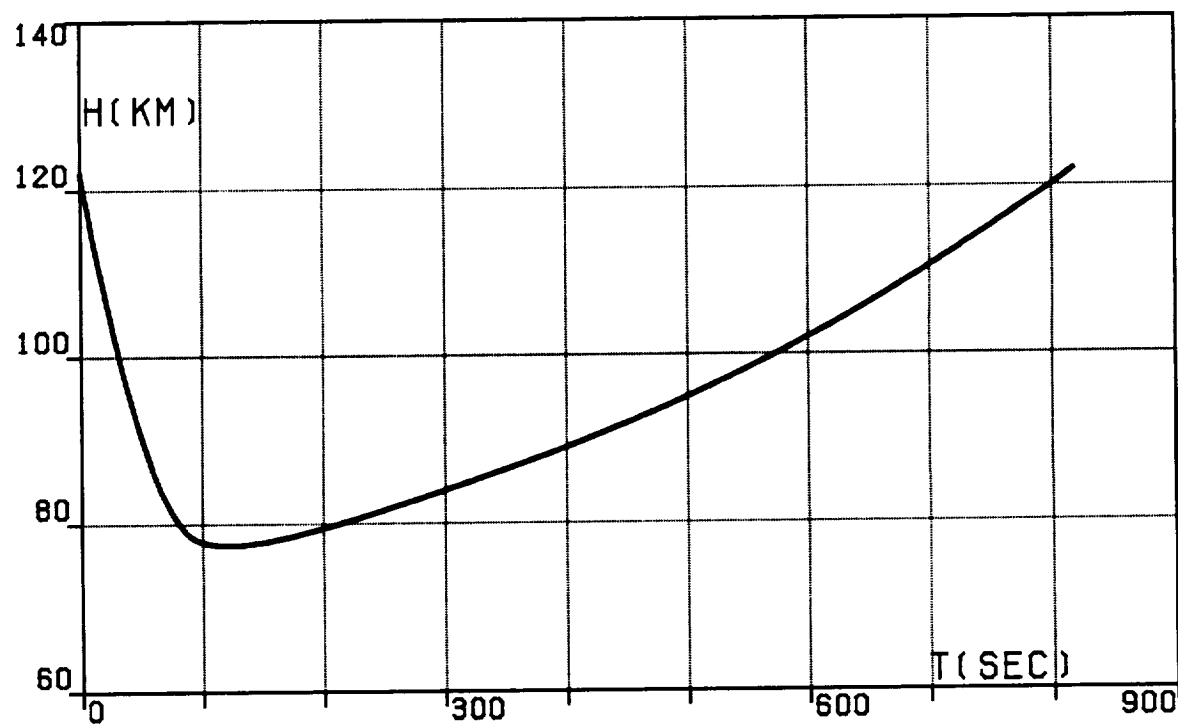


FIG. 7D. CONTINUOUS OPTIMAL TRAJECTORY,  
TRANSFER (DA), ALTITUDE.

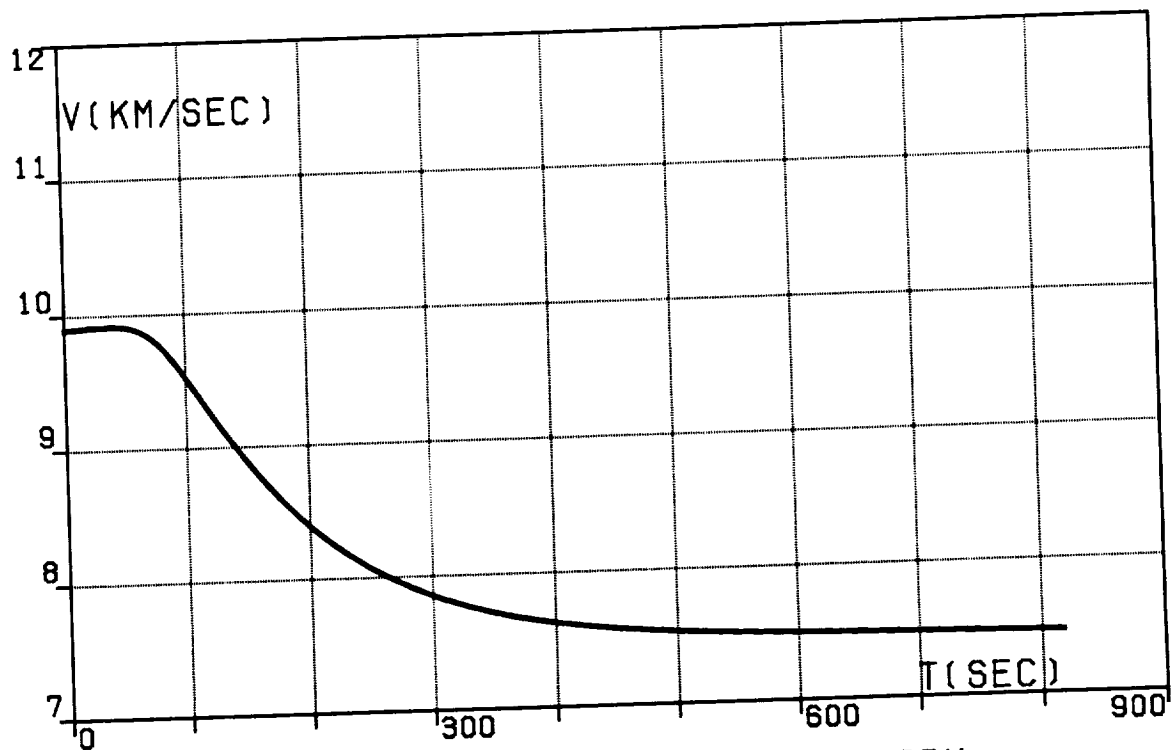


FIG.7E. CONTINUOUS OPTIMAL TRAJECTORY,  
TRANSFER (DA), VELOCITY, RELATIVE.

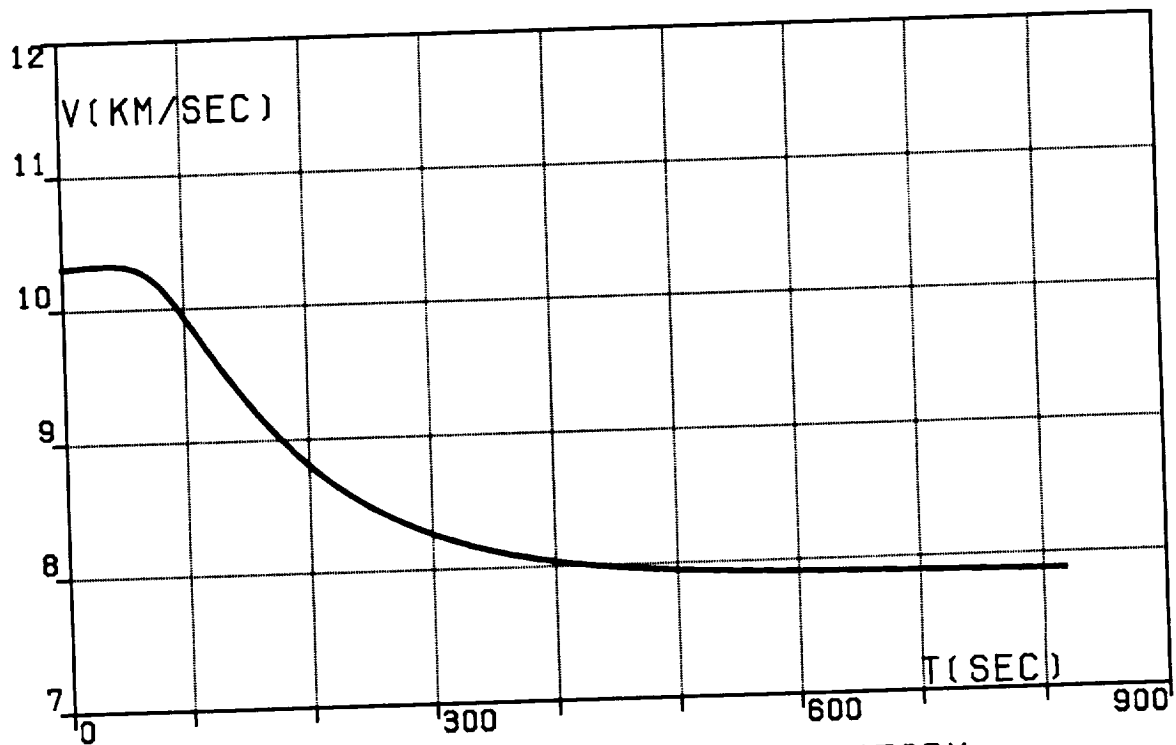


FIG.7F. CONTINUOUS OPTIMAL TRAJECTORY,  
TRANSFER (DA), VELOCITY, INERTIAL.

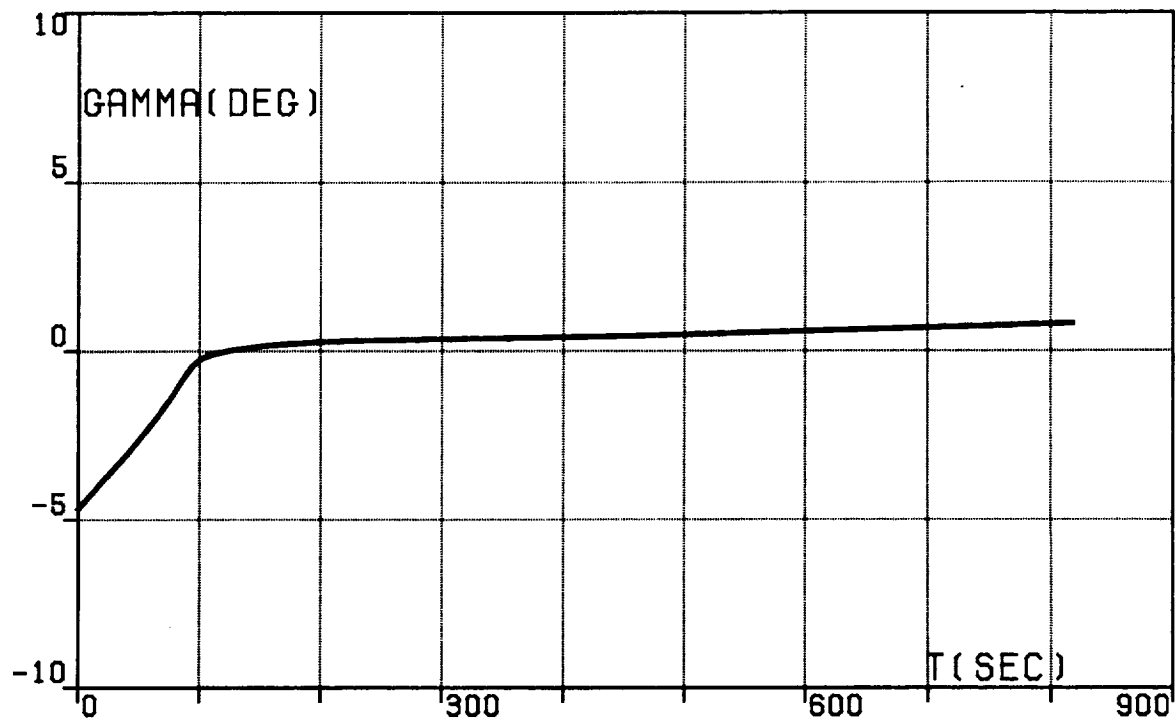


FIG.7G. CONTINUOUS OPTIMAL TRAJECTORY,  
TRANSFER (DA),  
PATH INCLINATION, RELATIVE.

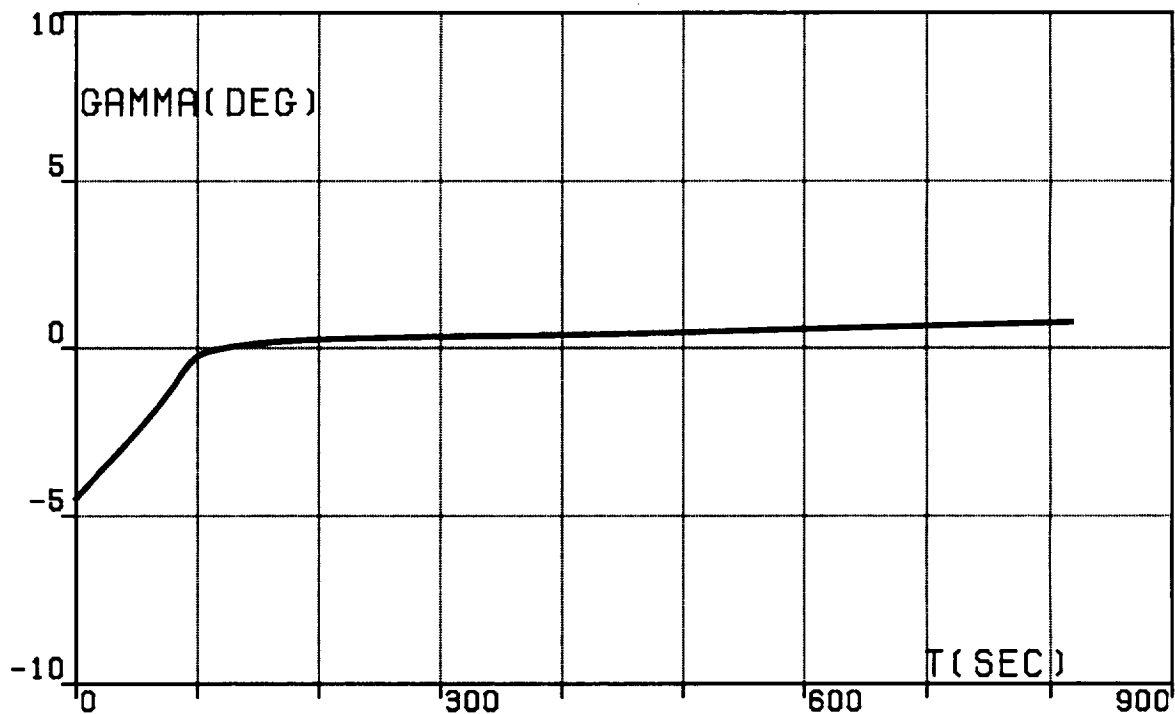


FIG.7H. CONTINUOUS OPTIMAL TRAJECTORY,  
TRANSFER (DA),  
PATH INCLINATION, INERTIAL.

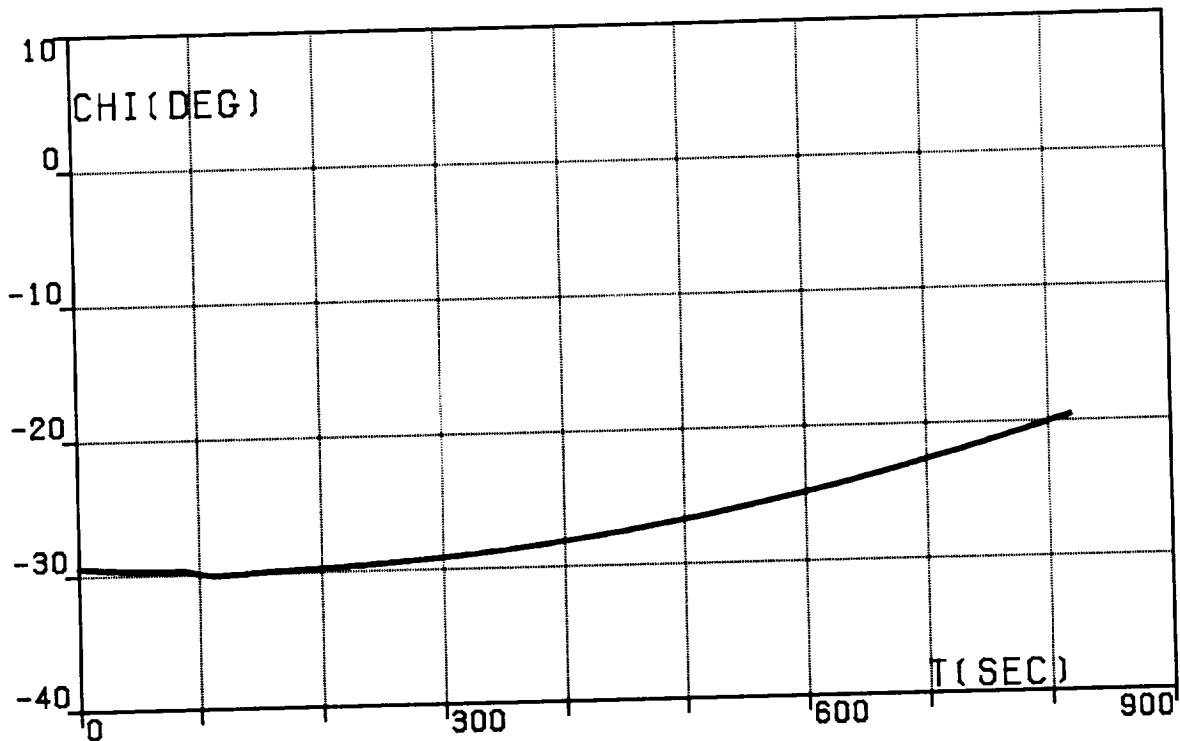


FIG.7I. CONTINUOUS OPTIMAL TRAJECTORY,  
TRANSFER (DA), HEADING ANGLE, RELATIVE.

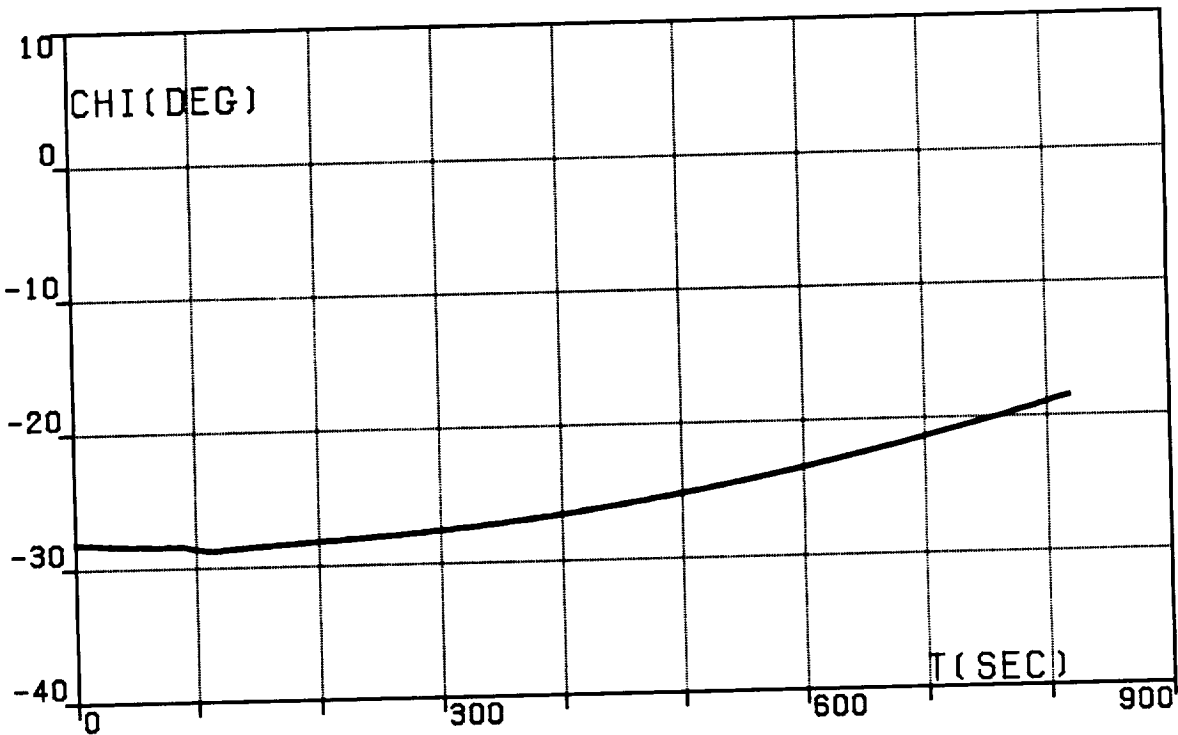


FIG.7J. CONTINUOUS OPTIMAL TRAJECTORY,  
TRANSFER (DA), HEADING ANGLE, INERTIAL.

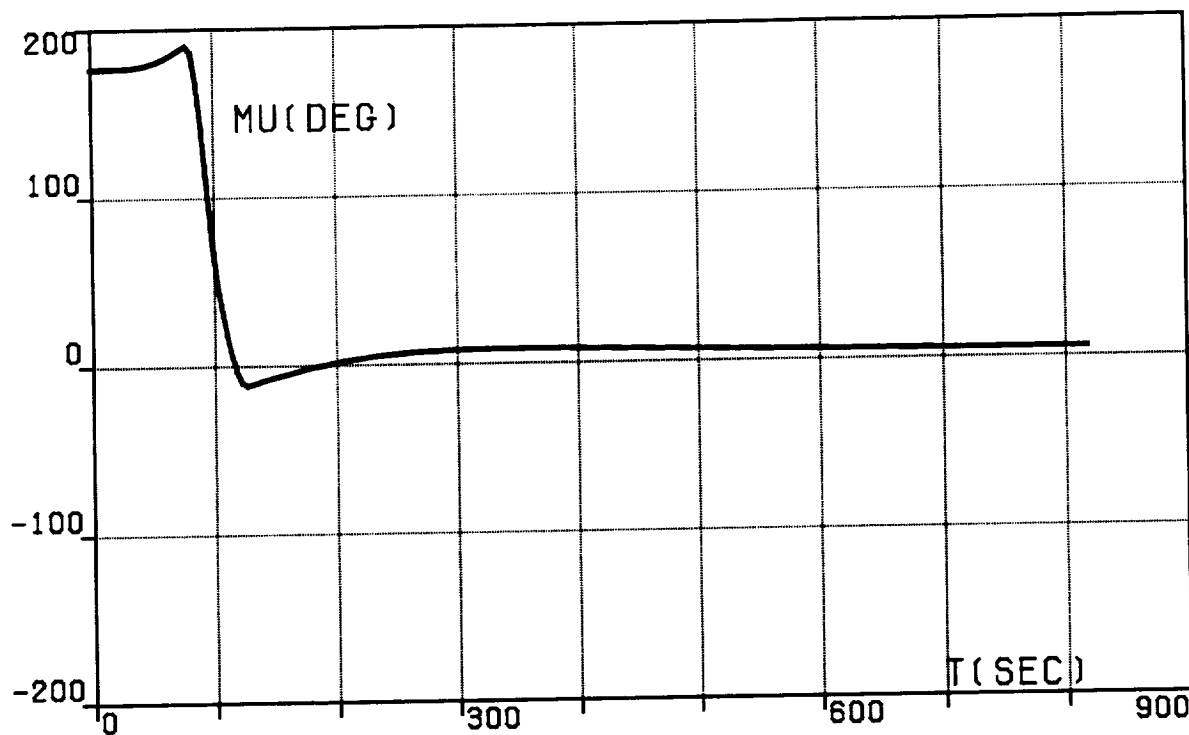


FIG.7K. CONTINUOUS OPTIMAL TRAJECTORY,  
TRANSFER (DA), BANK ANGLE.

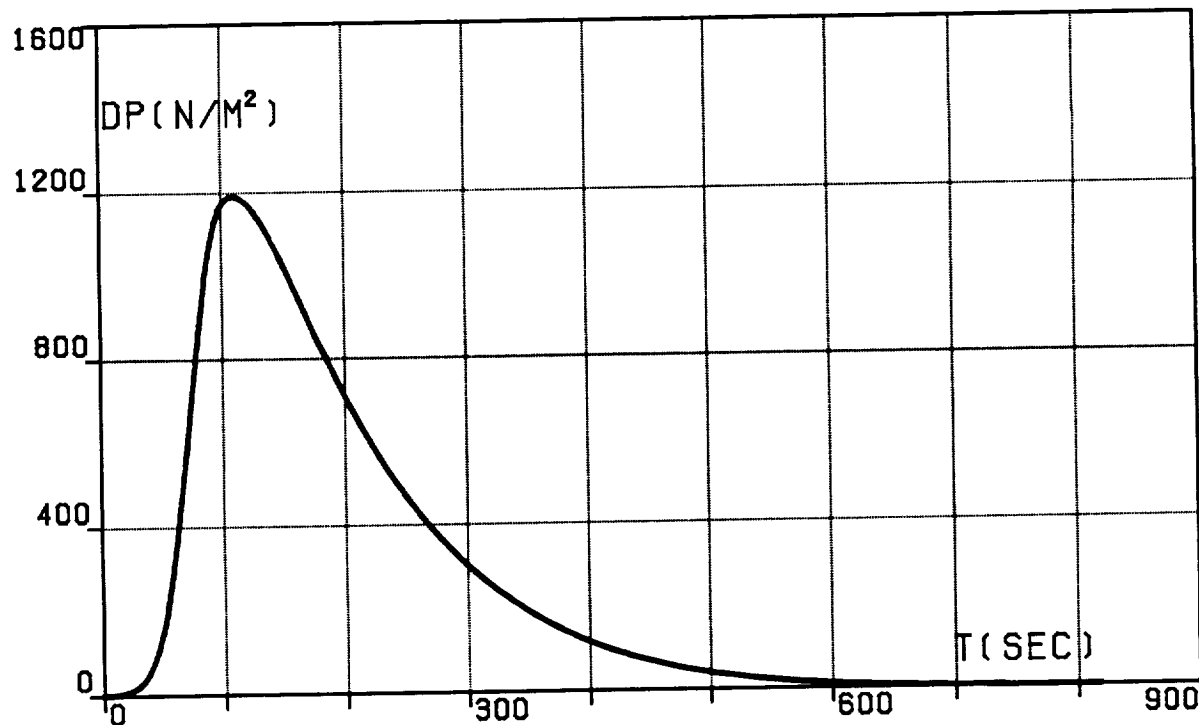


FIG.7L. CONTINUOUS OPTIMAL TRAJECTORY,  
TRANSFER (DA), DYNAMIC PRESSURE.

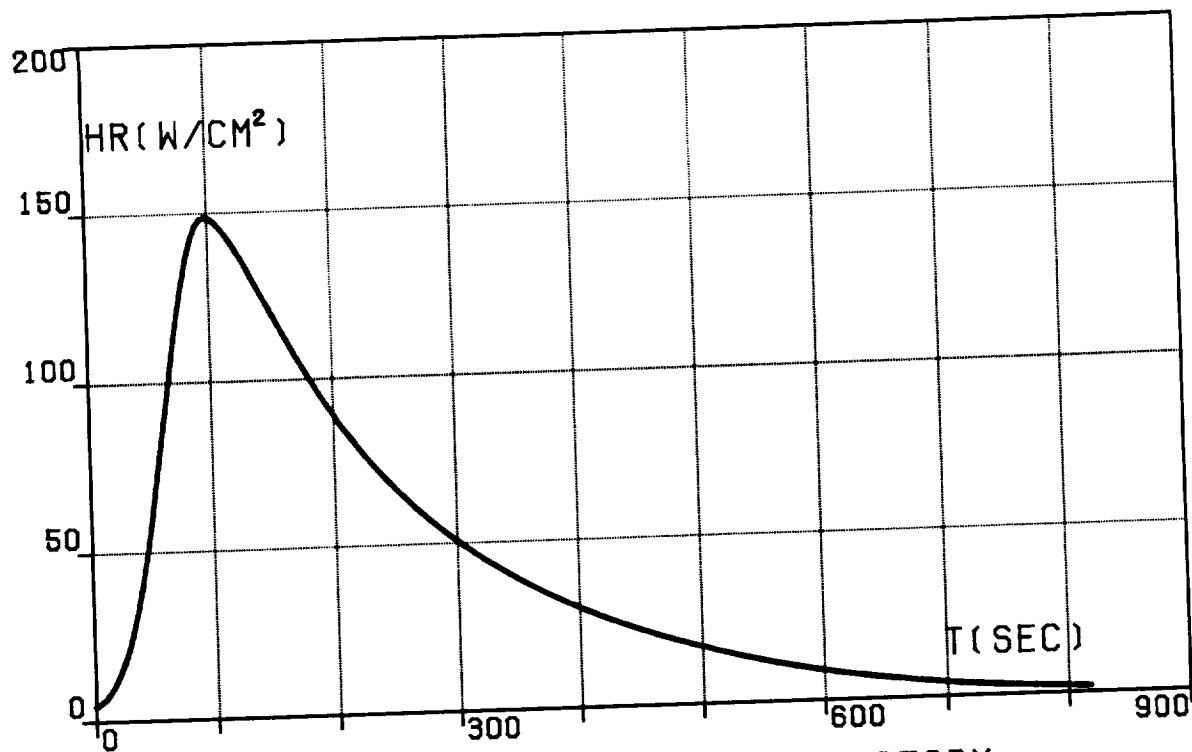


FIG.7M. CONTINUOUS OPTIMAL TRAJECTORY.  
TRANSFER (DA), HEATING RATE.

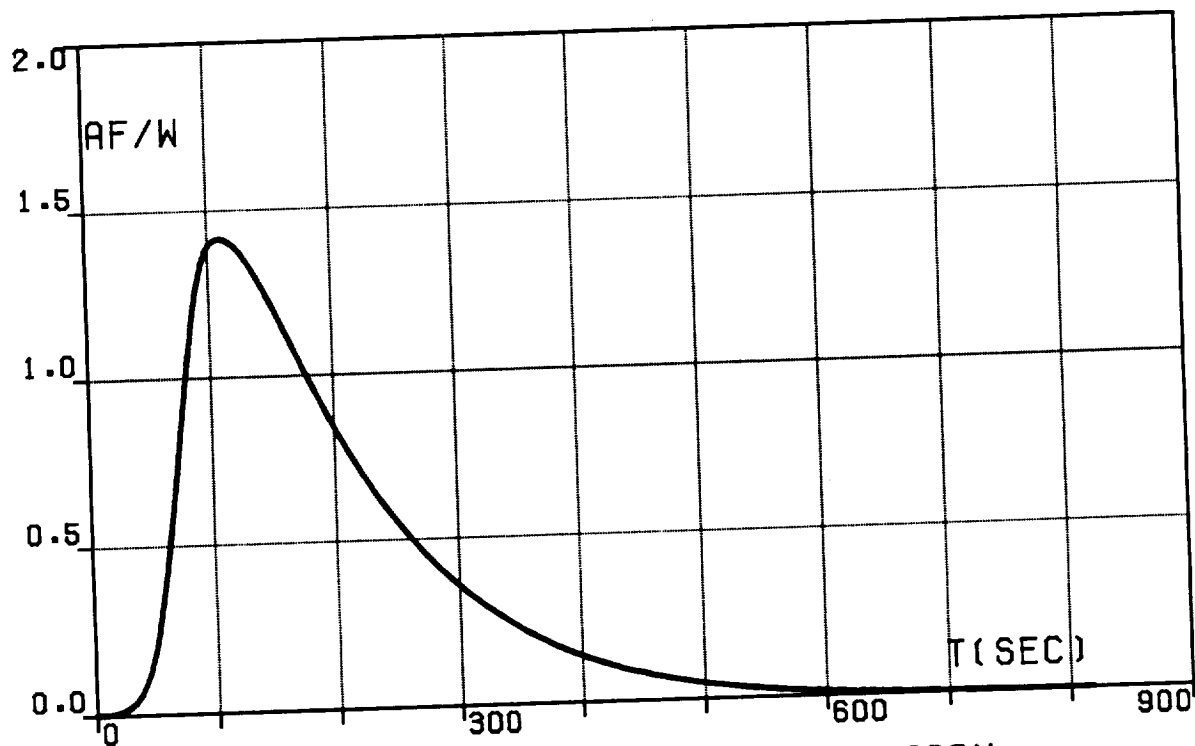


FIG.7N. CONTINUOUS OPTIMAL TRAJECTORY.  
TRANSFER (DA),  
AERODYNAMIC FORCE PER UNIT WEIGHT.

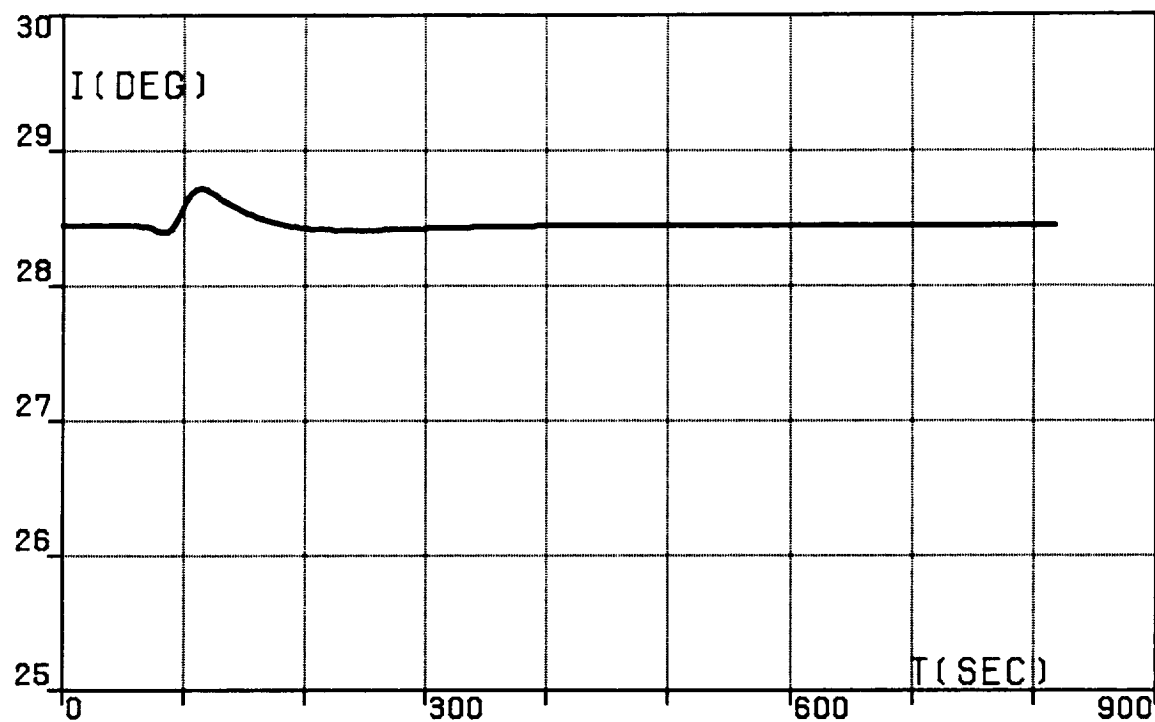


FIG.7O. CONTINUOUS OPTIMAL TRAJECTORY,  
TRANSFER (DA), ORBITAL INCLINATION.

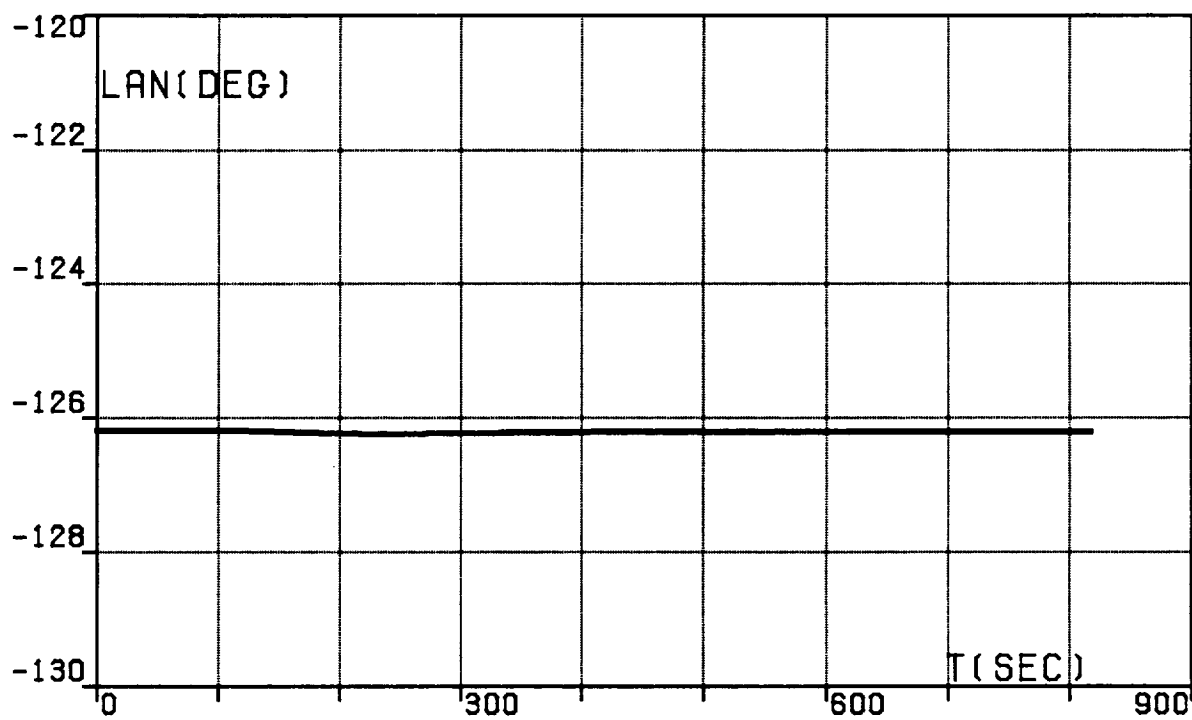


FIG.7P. CONTINUOUS OPTIMAL TRAJECTORY,  
TRANSFER (DA),  
LONGITUDE OF THE ASCENDING NODE.

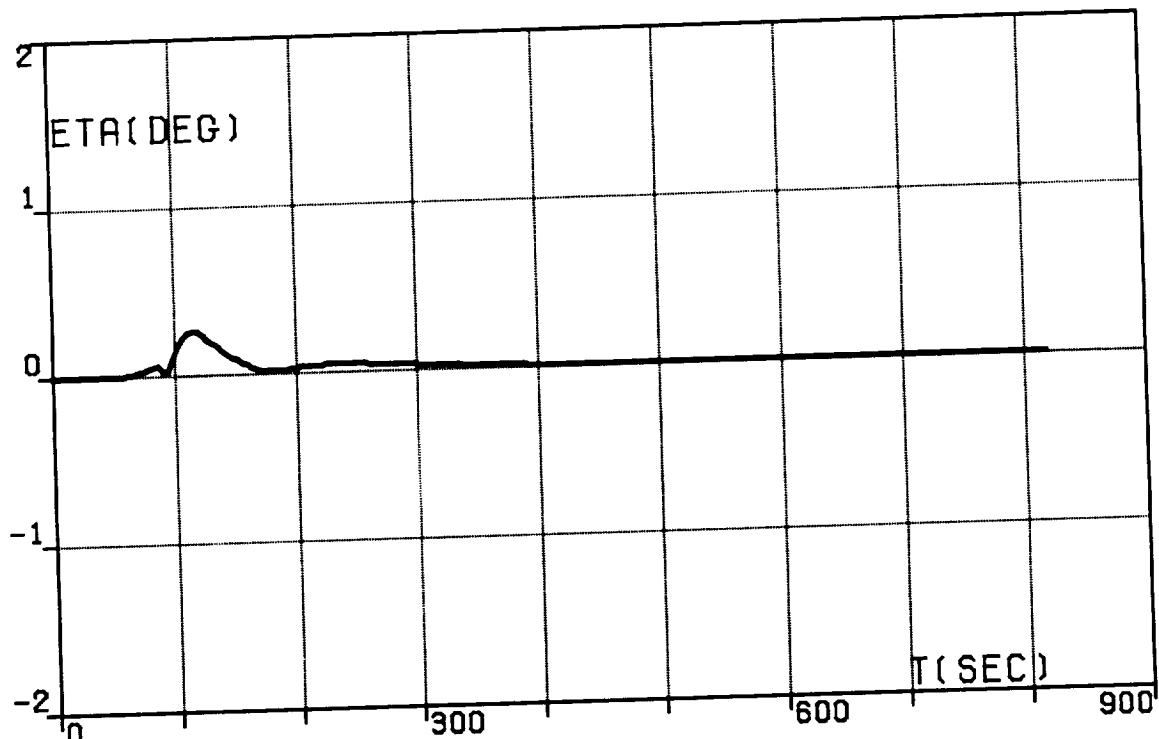


FIG. 7Q. CONTINUOUS OPTIMAL TRAJECTORY,  
TRANSFER (DA), WEDGE ANGLE.

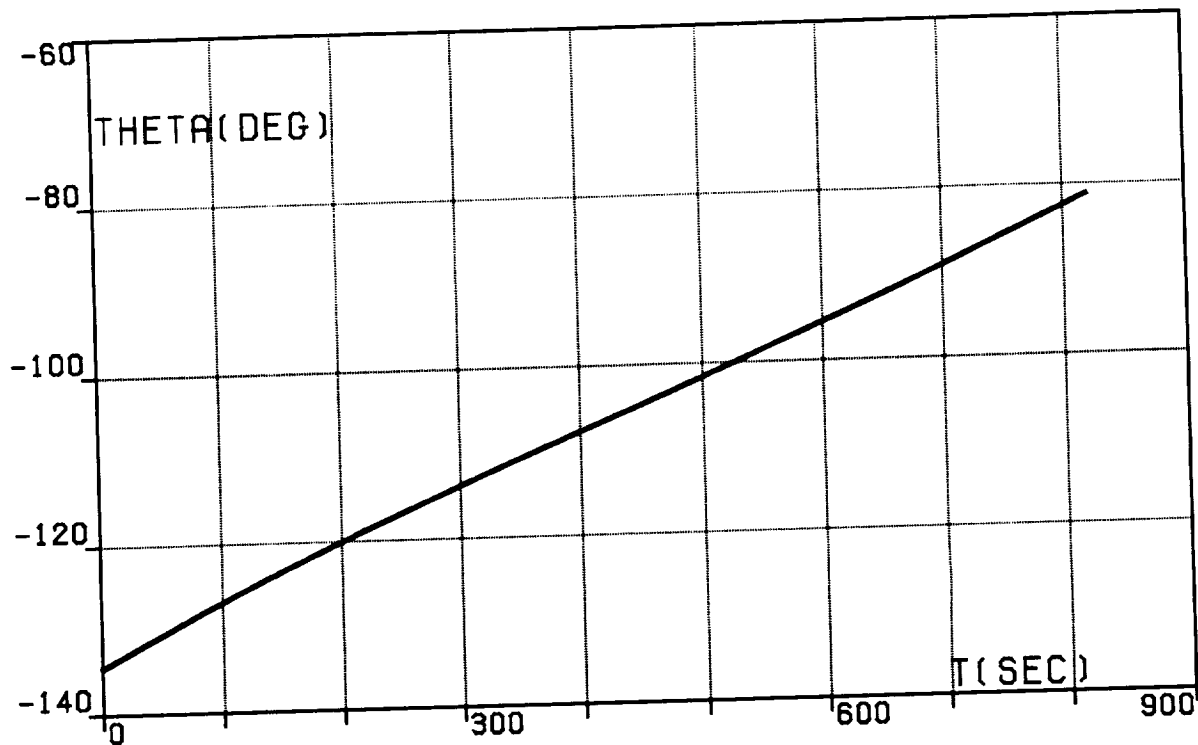


FIG.8A. TWO-SEGMENT OPTIMAL TRAJECTORY,  
TRANSFER (DA), LONGITUDE, RELATIVE.

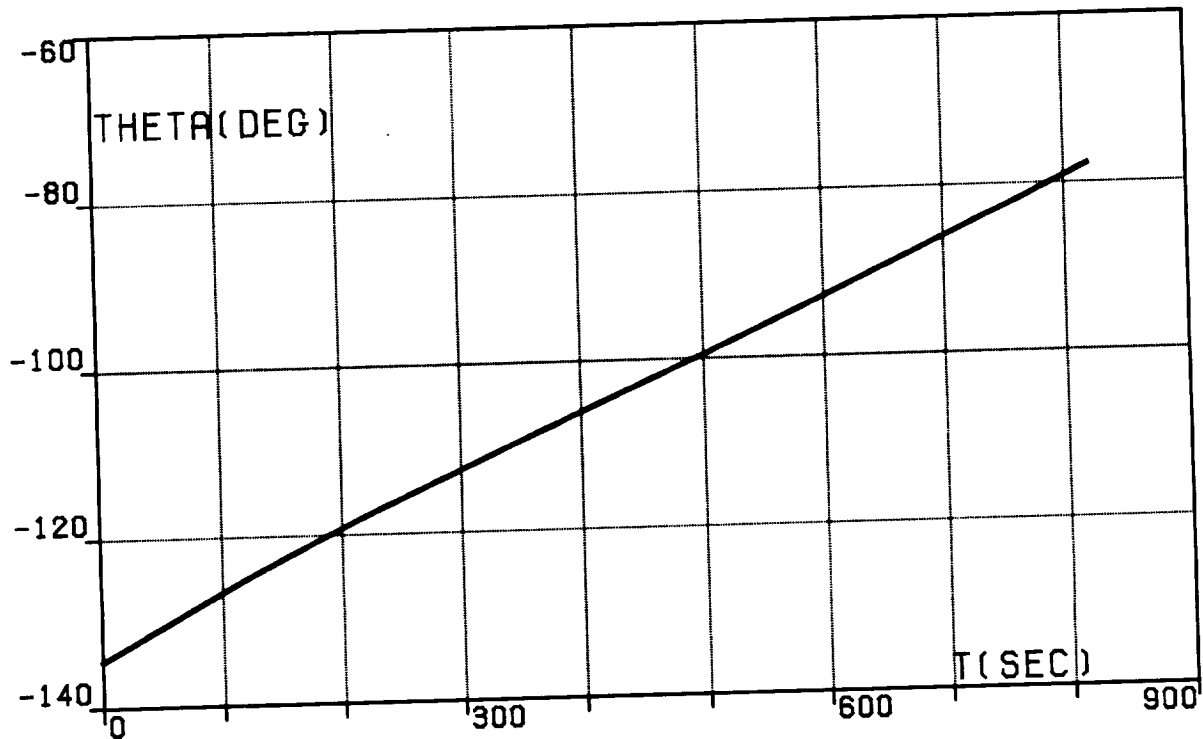


FIG.8B. TWO-SEGMENT OPTIMAL TRAJECTORY,  
TRANSFER (DA), LONGITUDE, INERTIAL.

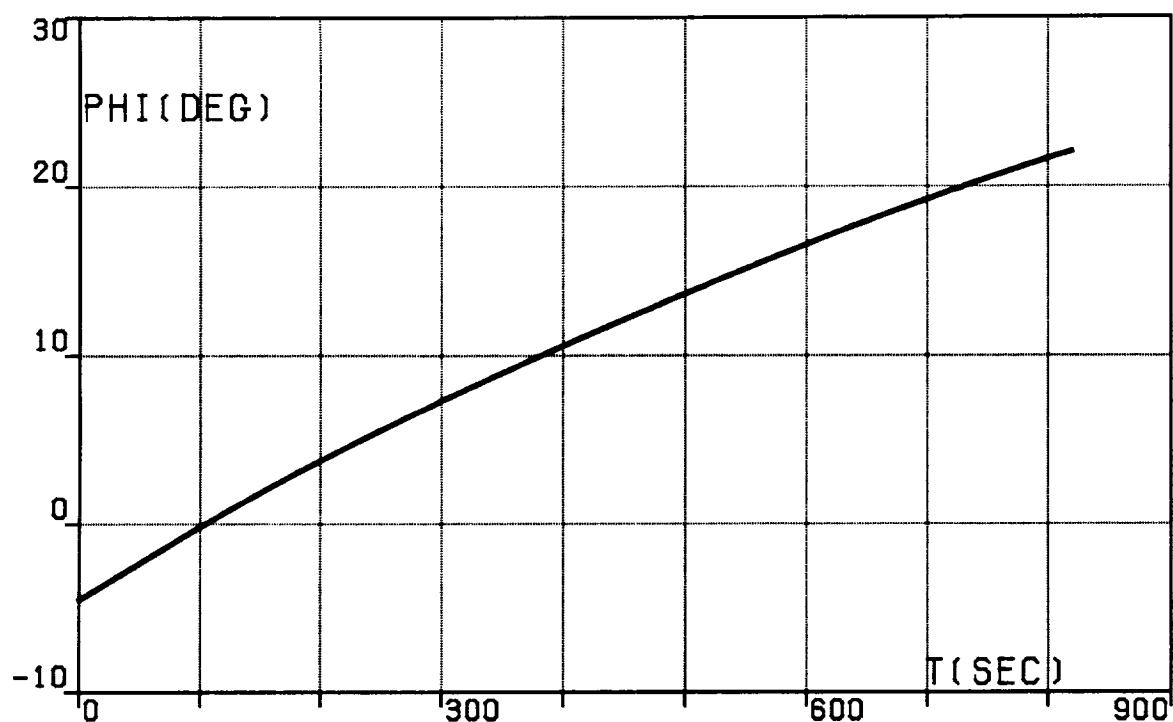


FIG.8C. TWO-SEGMENT OPTIMAL TRAJECTORY,  
TRANSFER (DA), LATITUDE.

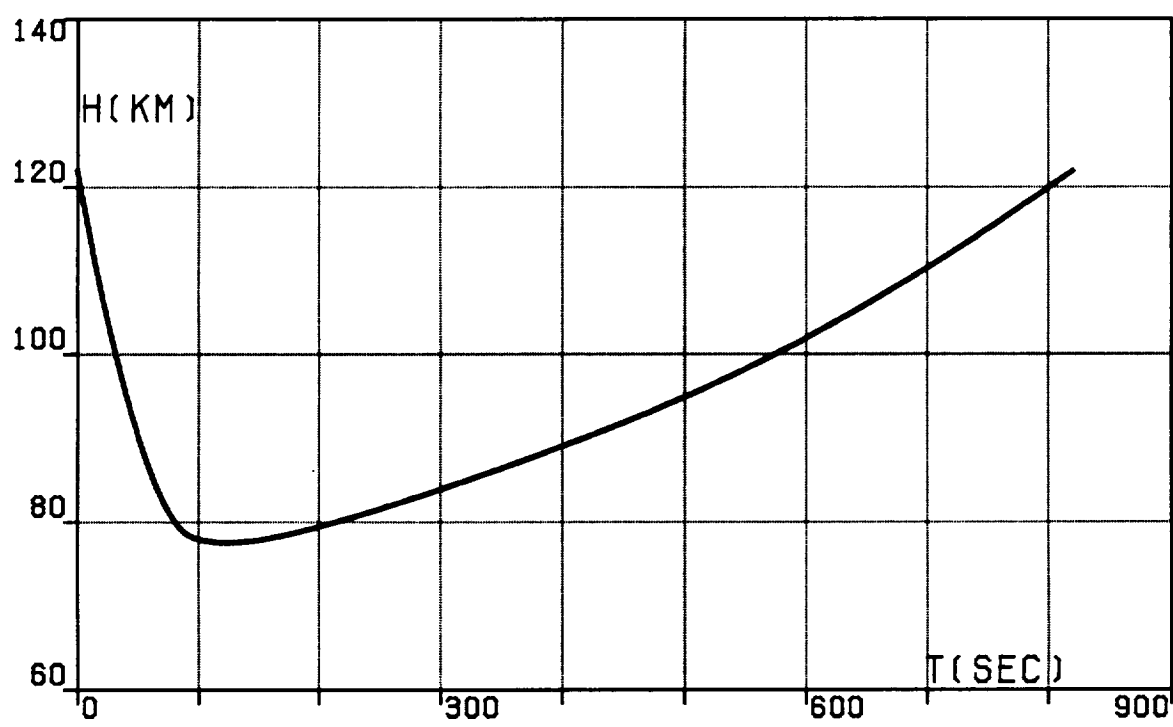


FIG.8D. TWO-SEGMENT OPTIMAL TRAJECTORY,  
TRANSFER (DA), ALTITUDE.

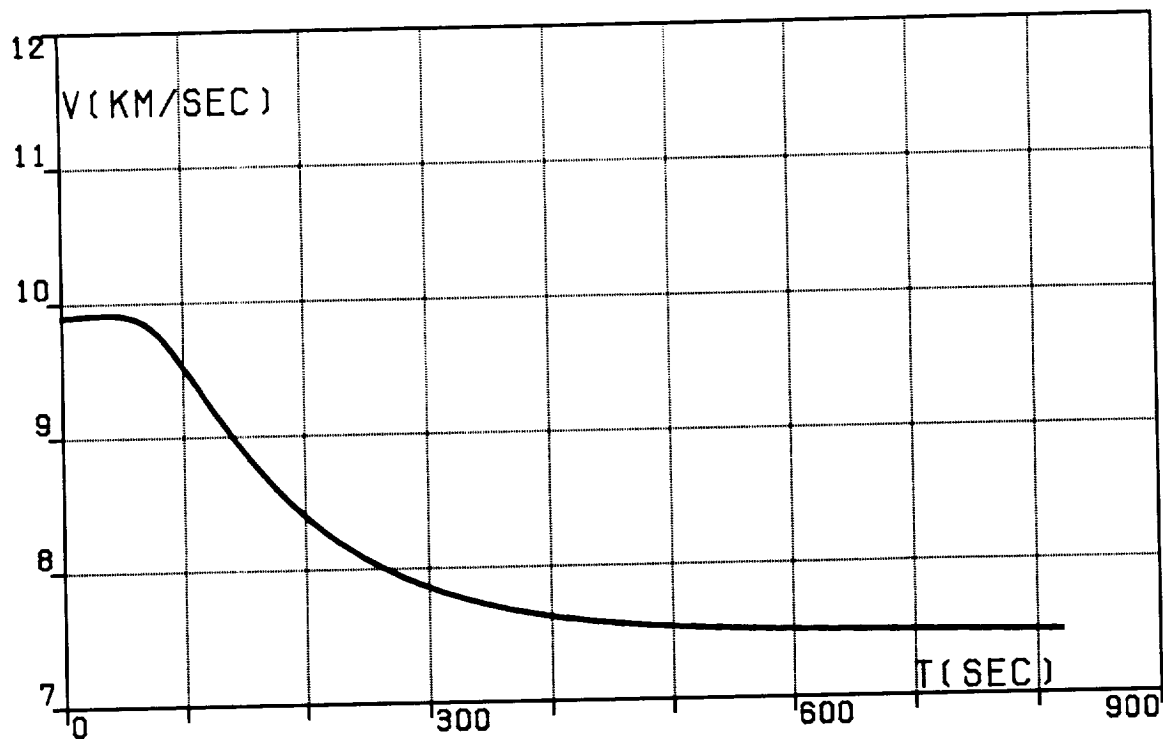


FIG.8E. TWO-SEGMENT OPTIMAL TRAJECTORY,  
TRANSFER (DA), VELOCITY, RELATIVE.

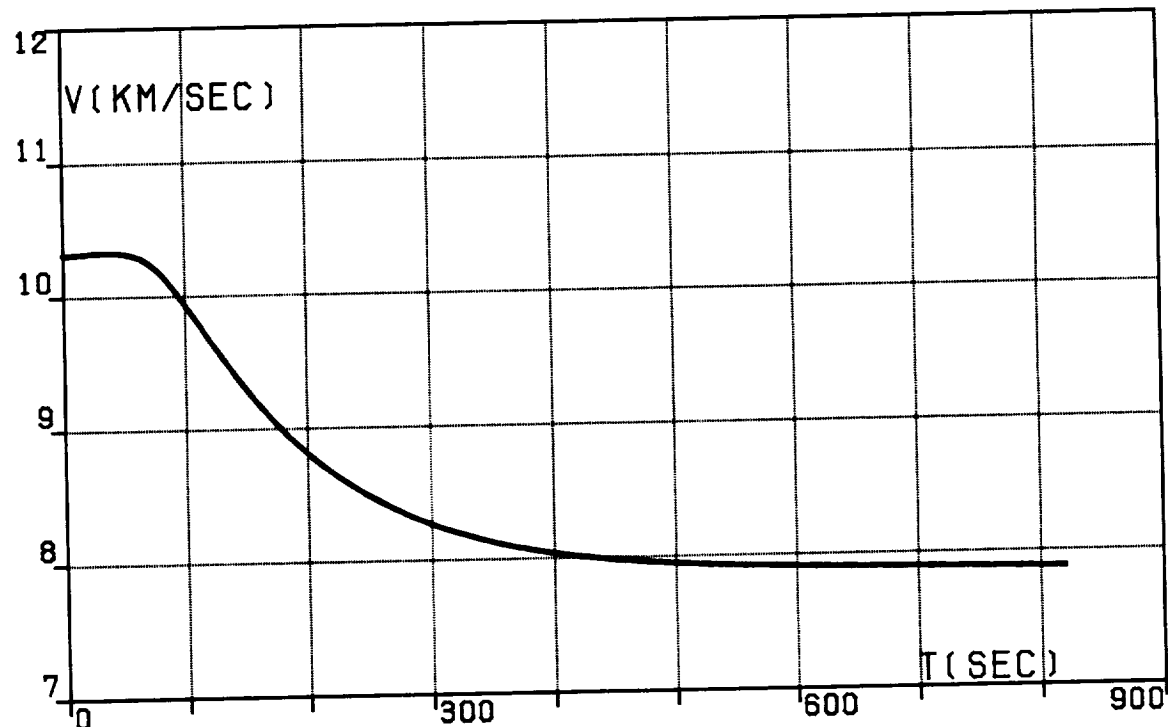


FIG.8F. TWO-SEGMENT OPTIMAL TRAJECTORY,  
TRANSFER (DA), VELOCITY, INERTIAL.

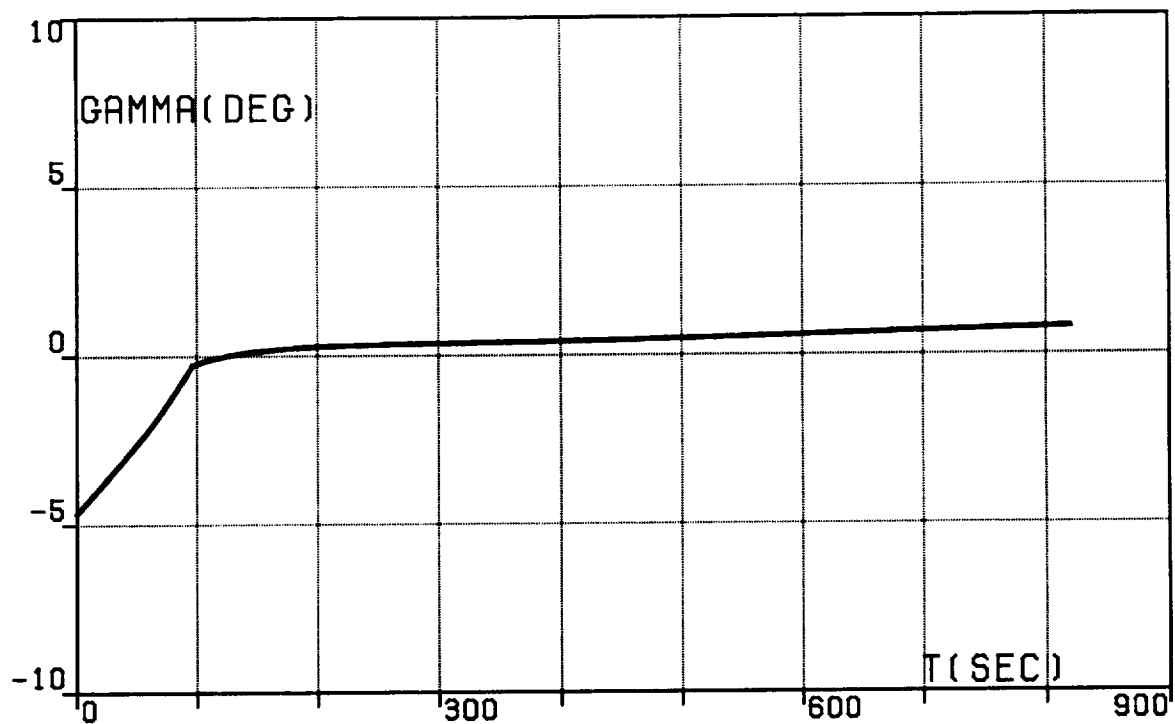


FIG.8G. TWO-SEGMENT OPTIMAL TRAJECTORY,  
TRANSFER (DA),  
PATH INCLINATION, RELATIVE.

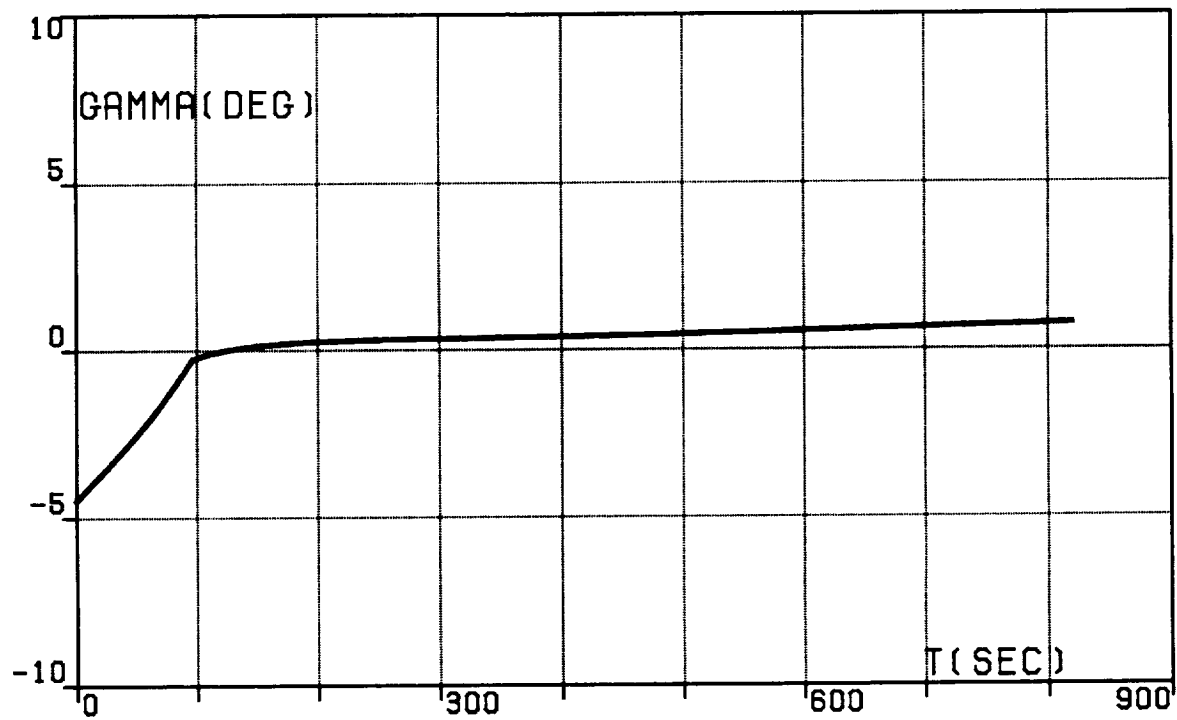


FIG.8H. TWO-SEGMENT OPTIMAL TRAJECTORY,  
TRANSFER (DA),  
PATH INCLINATION, INERTIAL.

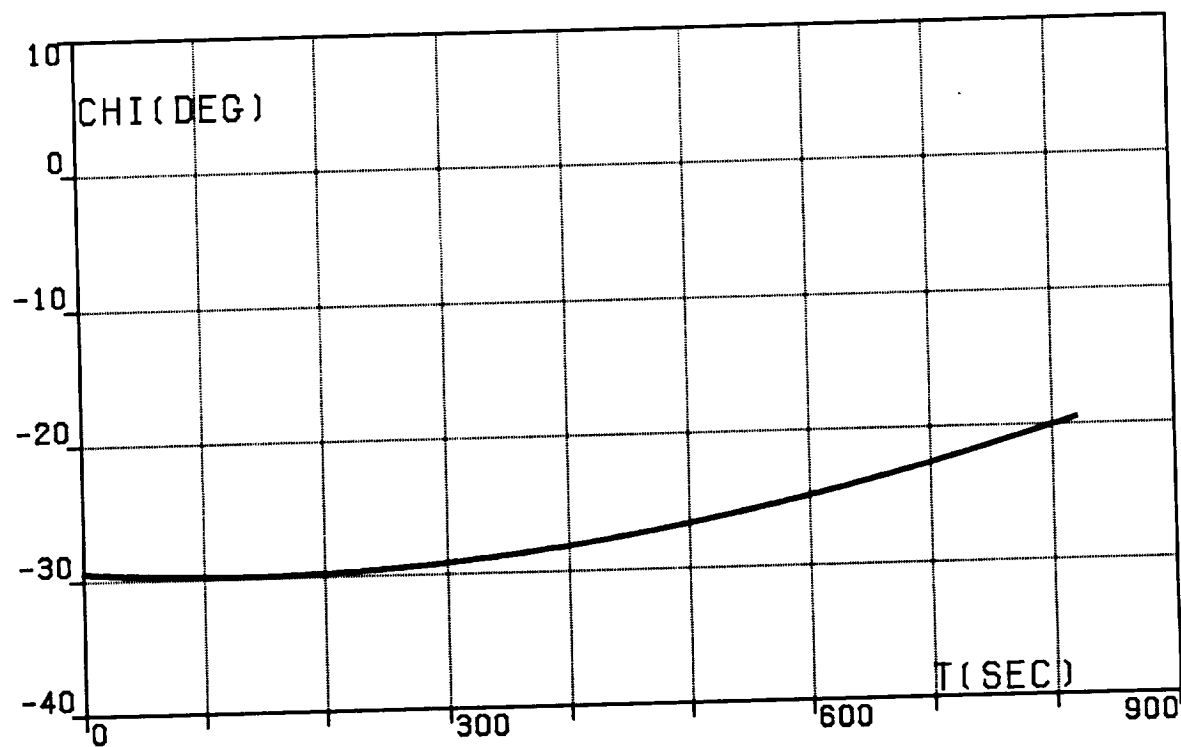


FIG.8I. TWO-SEGMENT OPTIMAL TRAJECTORY,  
TRANSFER (DA), HEADING ANGLE, RELATIVE.

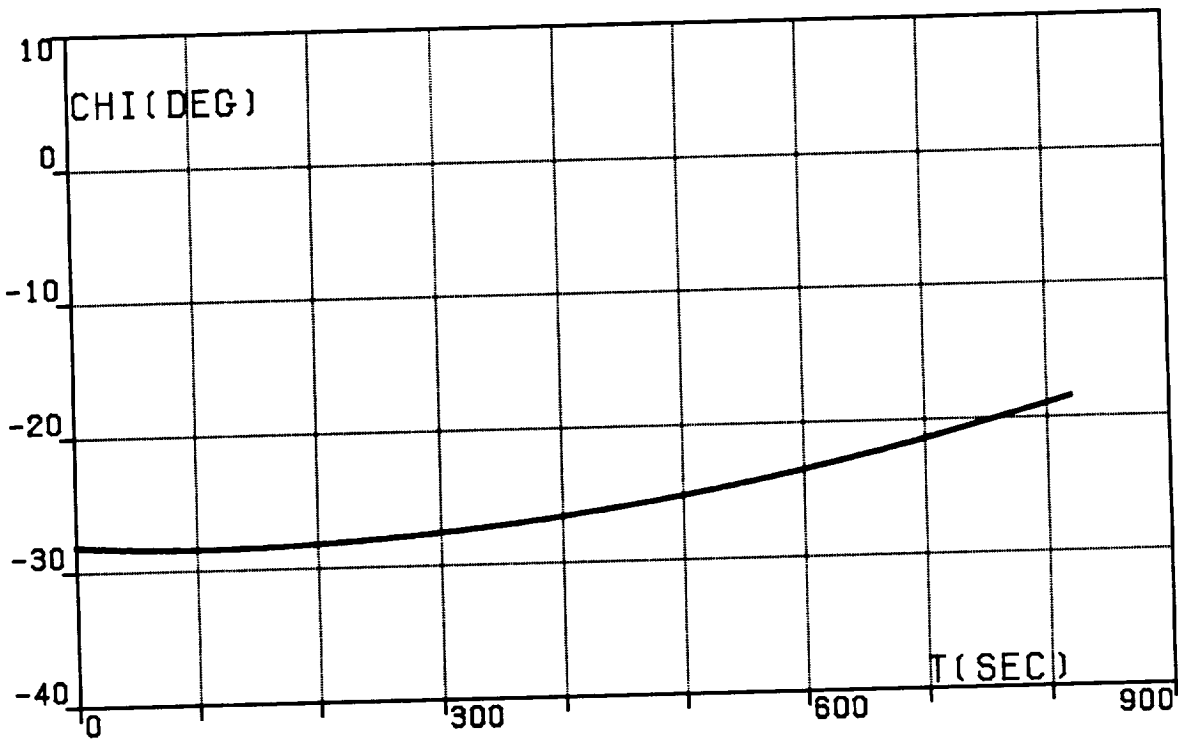


FIG.8J. TWO-SEGMENT OPTIMAL TRAJECTORY,  
TRANSFER (DA), HEADING ANGLE, INERTIAL.

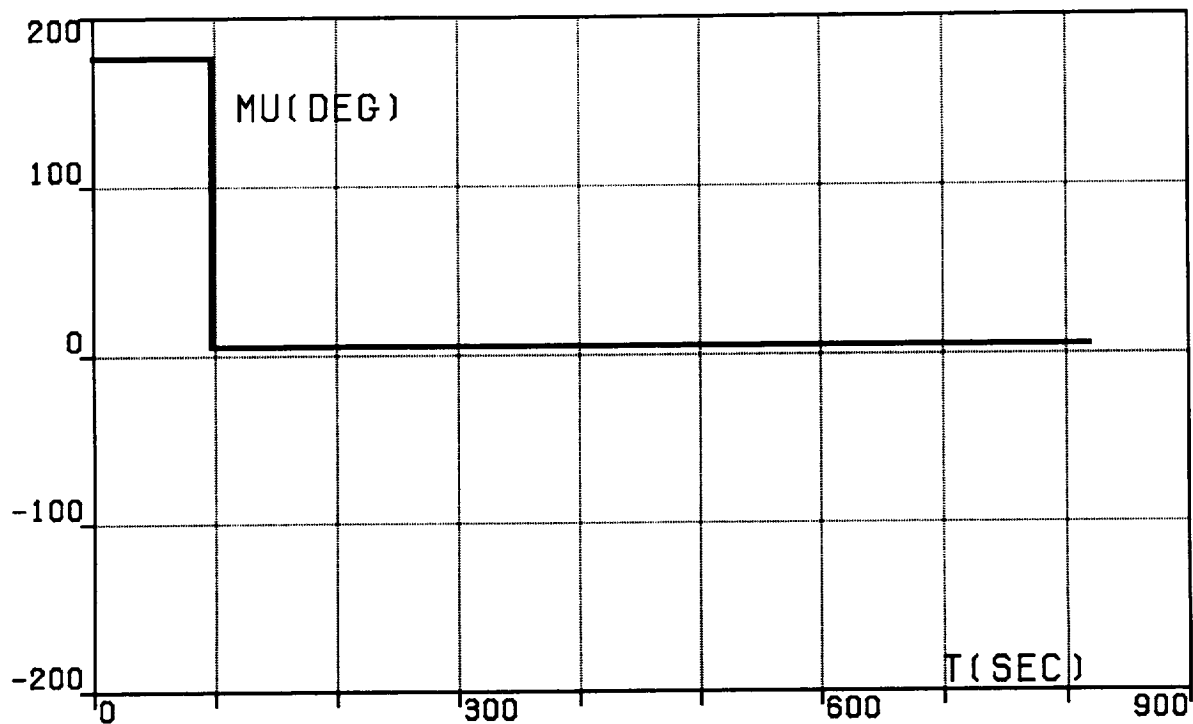


FIG.8K. TWO-SEGMENT OPTIMAL TRAJECTORY,  
TRANSFER (DA), BANK ANGLE.

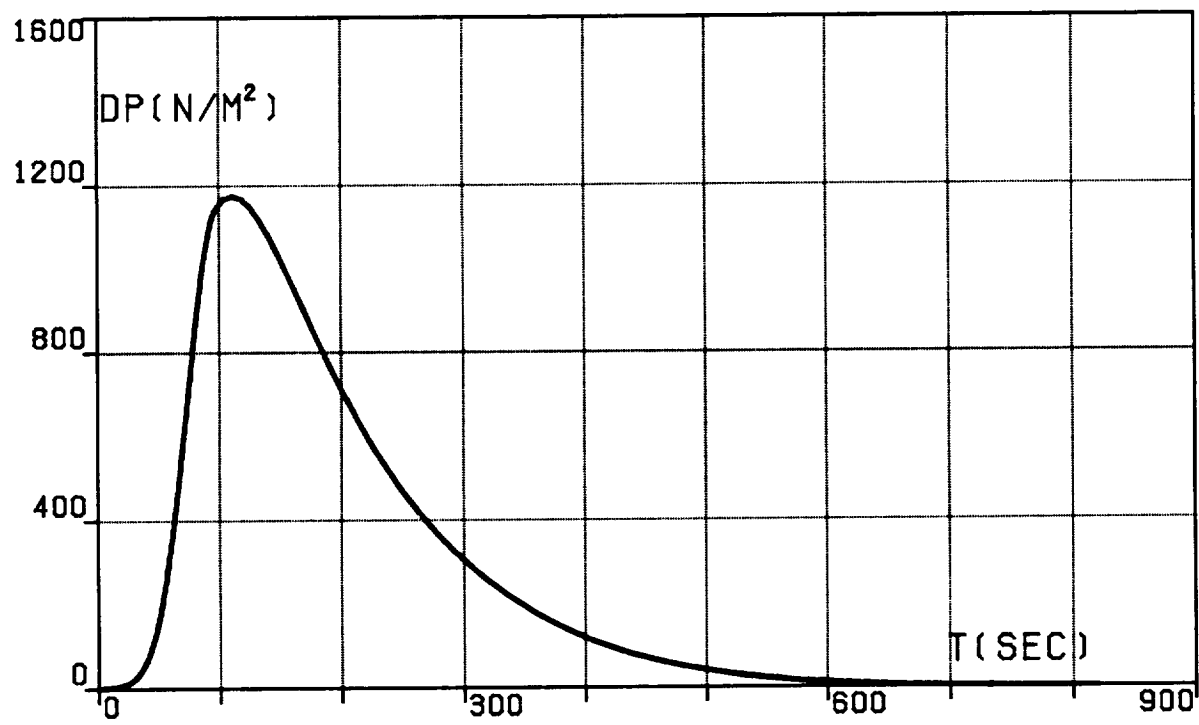


FIG.8L. TWO-SEGMENT OPTIMAL TRAJECTORY,  
TRANSFER (DA), DYNAMIC PRESSURE.

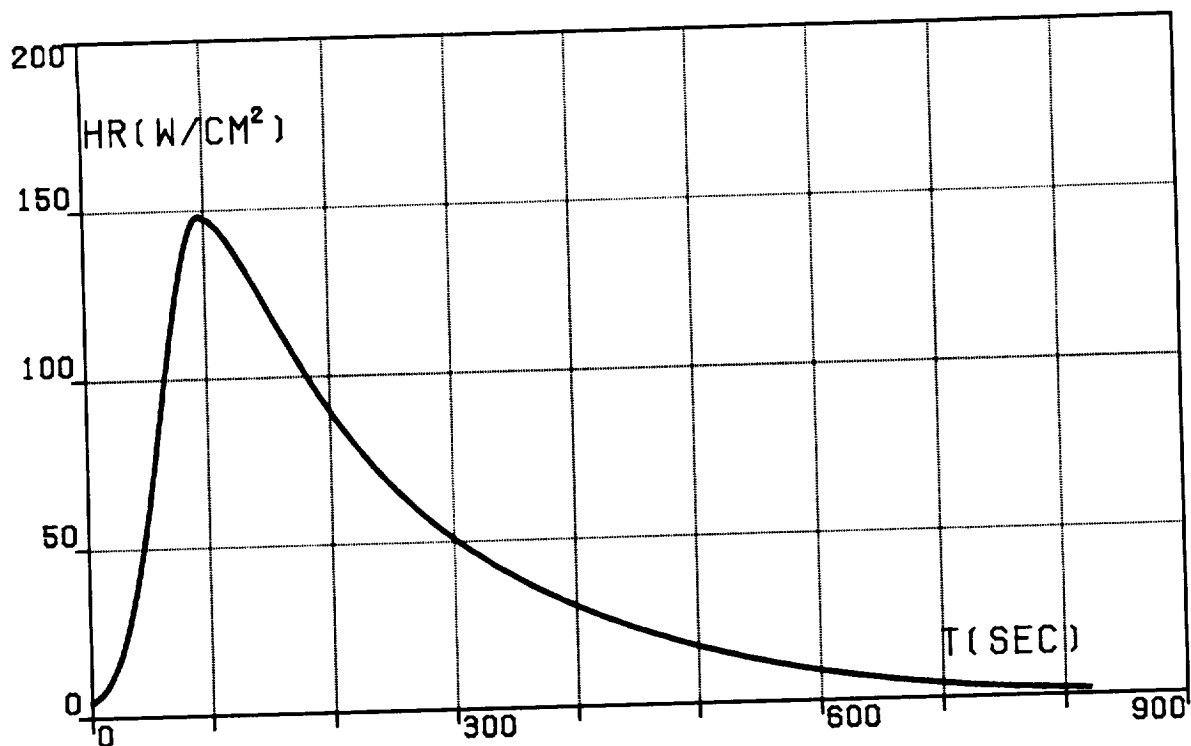


FIG.8M. TWO-SEGMENT OPTIMAL TRAJECTORY,  
TRANSFER (DA), HEATING RATE.

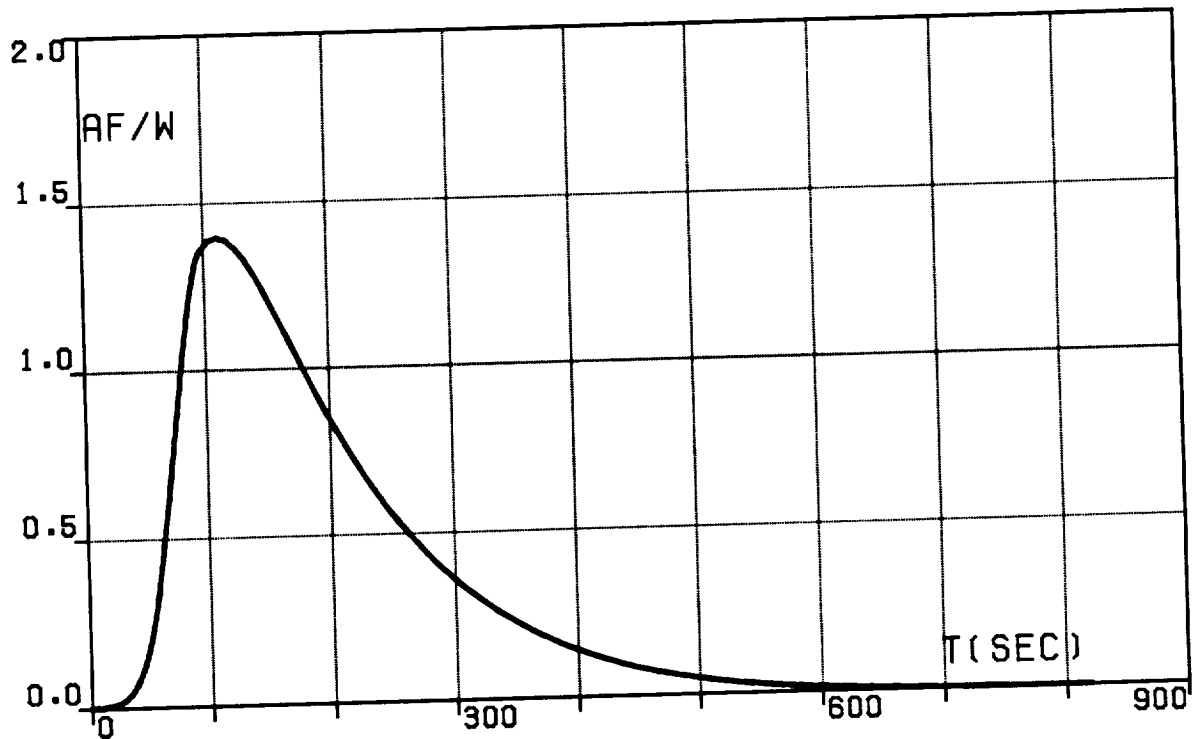


FIG.8N. TWO-SEGMENT OPTIMAL TRAJECTORY,  
TRANSFER (DA),  
AERODYNAMIC FORCE PER UNIT WEIGHT.

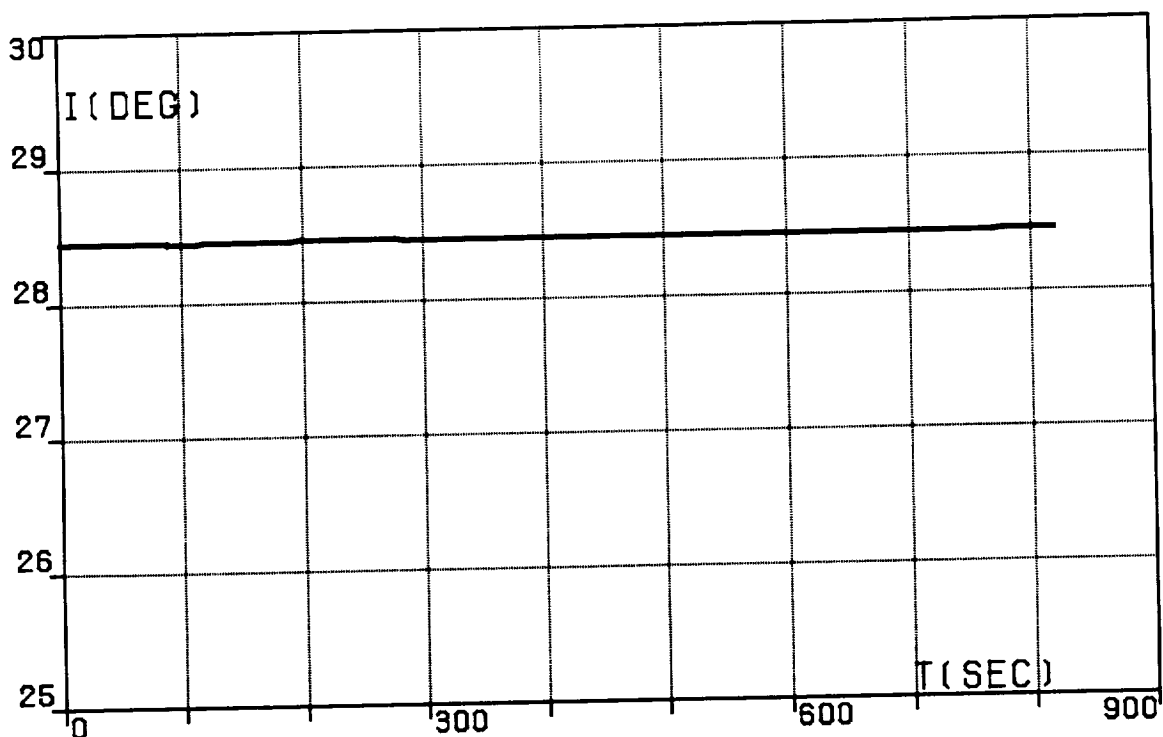


FIG.8O. TWO-SEGMENT OPTIMAL TRAJECTORY.  
TRANSFER (DA), ORBITAL INCLINATION.

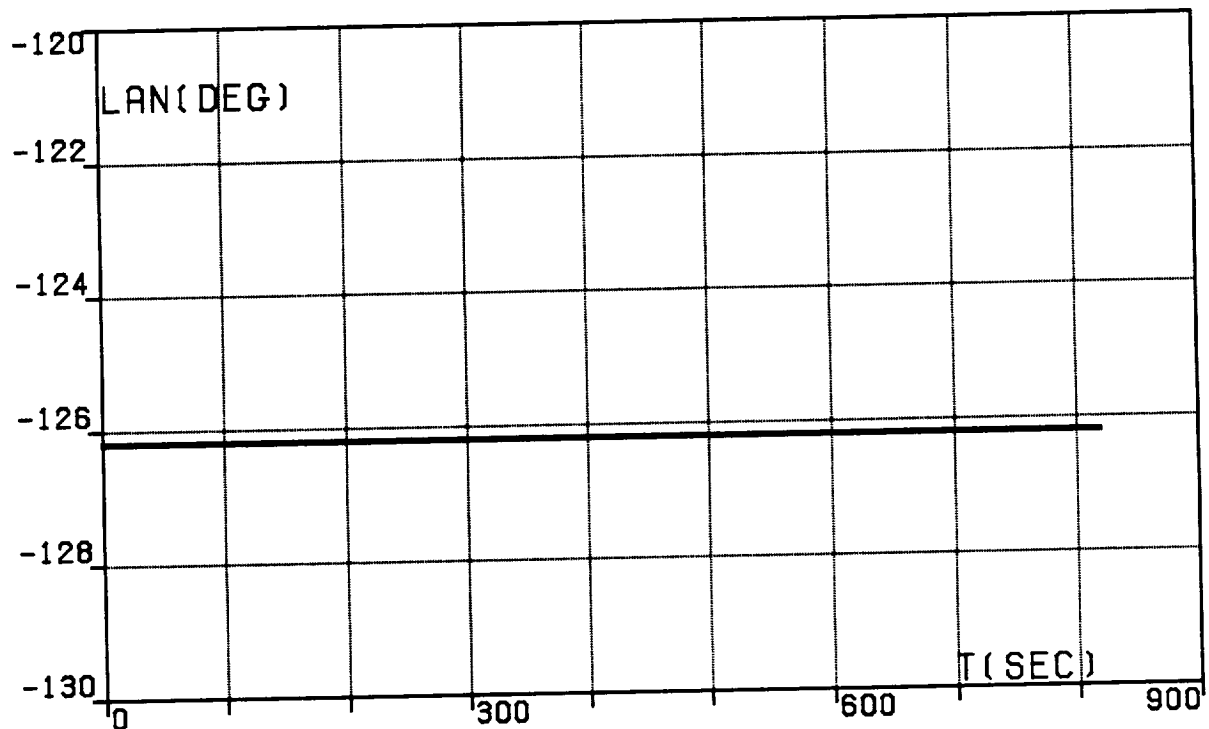


FIG.8P. TWO-SEGMENT OPTIMAL TRAJECTORY.  
TRANSFER (DA),  
LONGITUDE OF THE ASCENDING NODE.

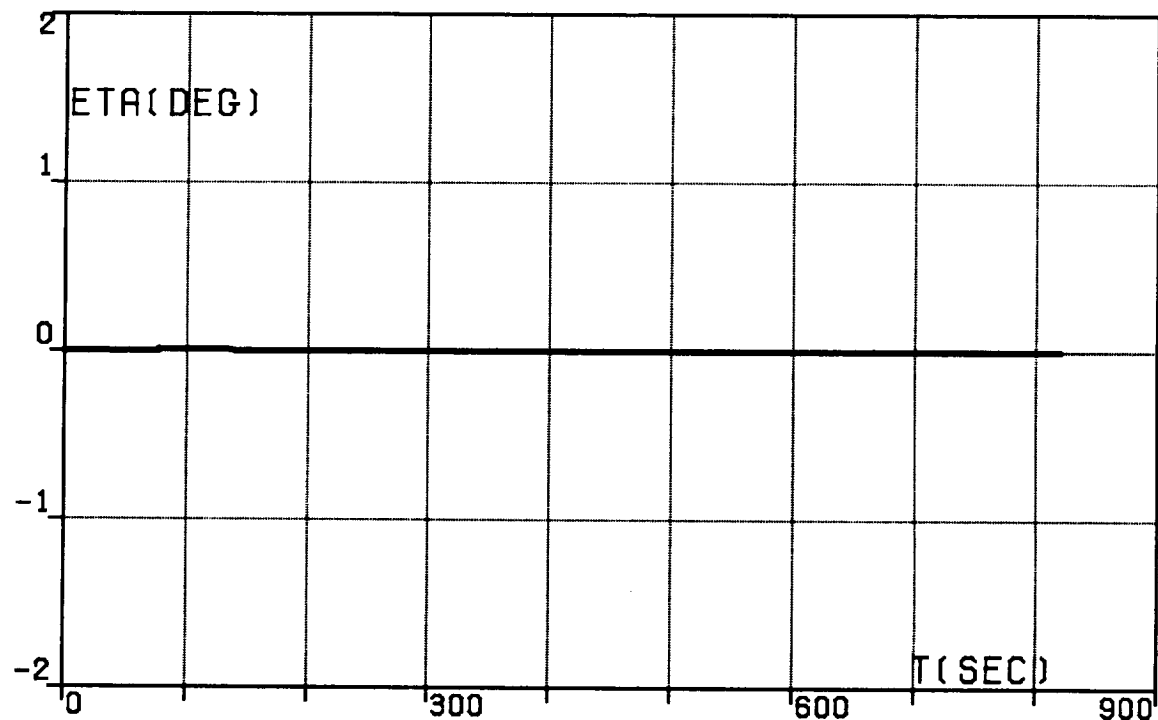


FIG. 8Q. TWO-SEGMENT OPTIMAL TRAJECTORY,  
TRANSFER (DA), WEDGE ANGLE.

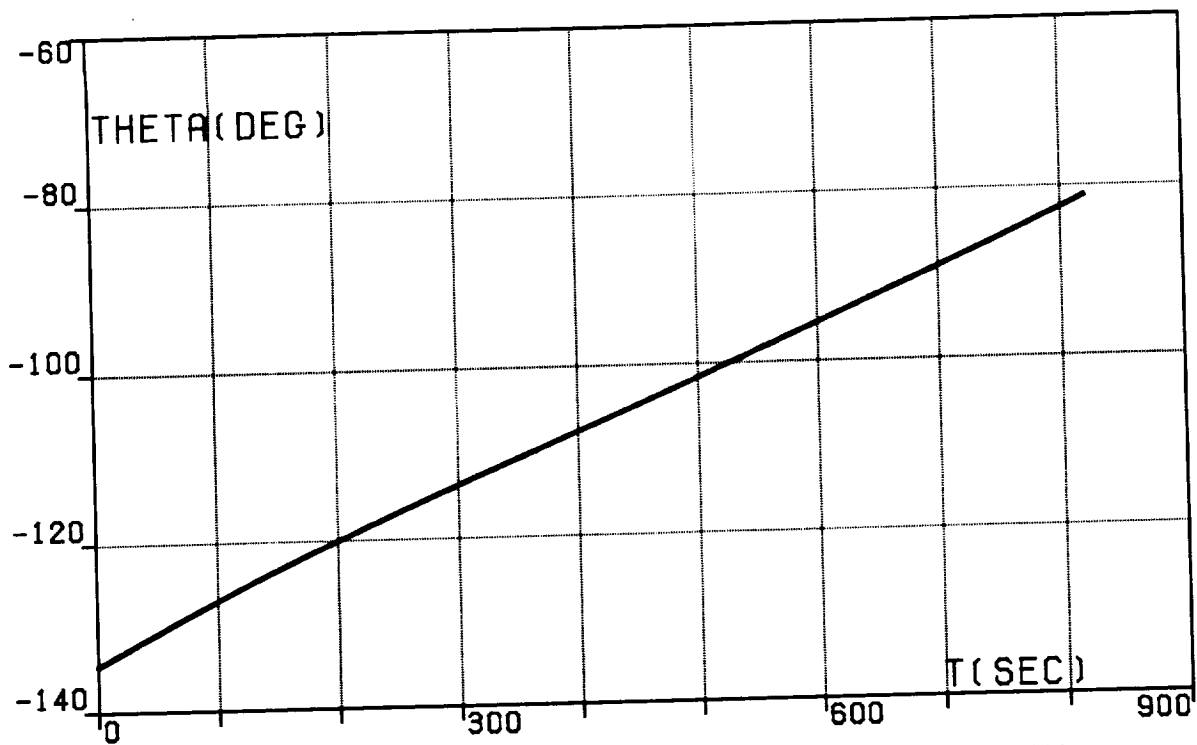


FIG.9A. THREE-SEGMENT OPTIMAL TRAJECTORY,  
TRANSFER (DA), LONGITUDE, RELATIVE.

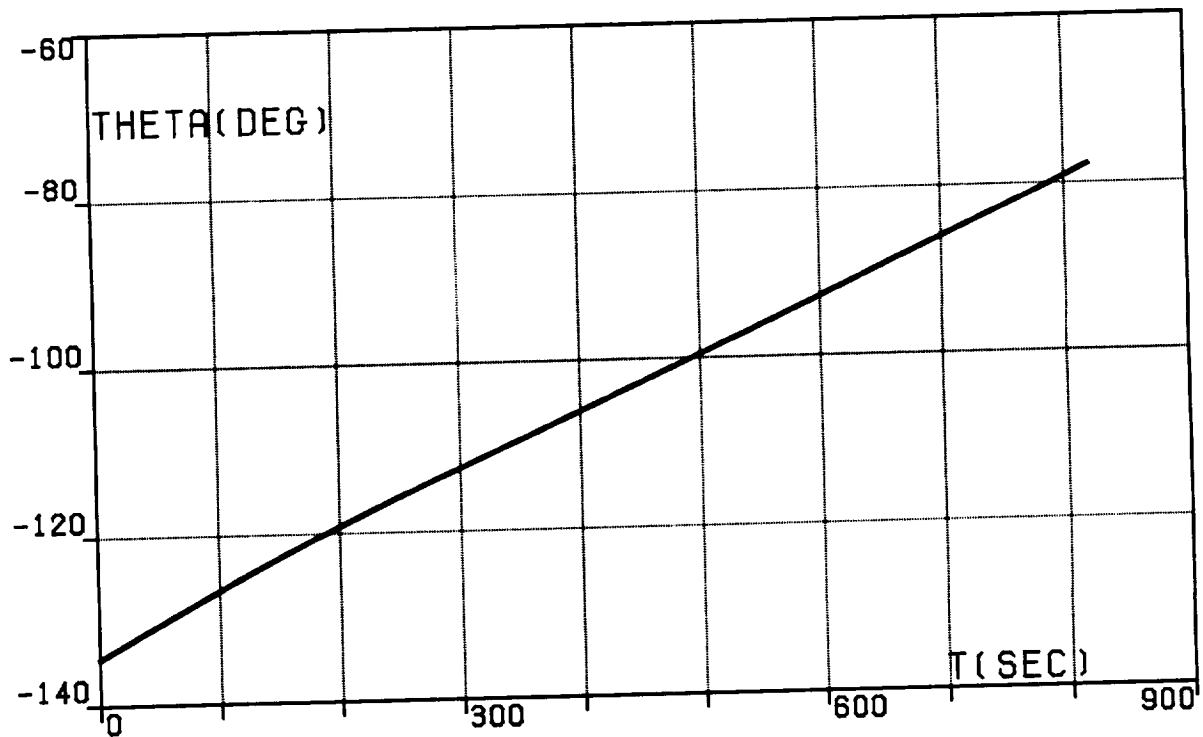


FIG.9B. THREE-SEGMENT OPTIMAL TRAJECTORY,  
TRANSFER (DA), LONGITUDE, INERTIAL.

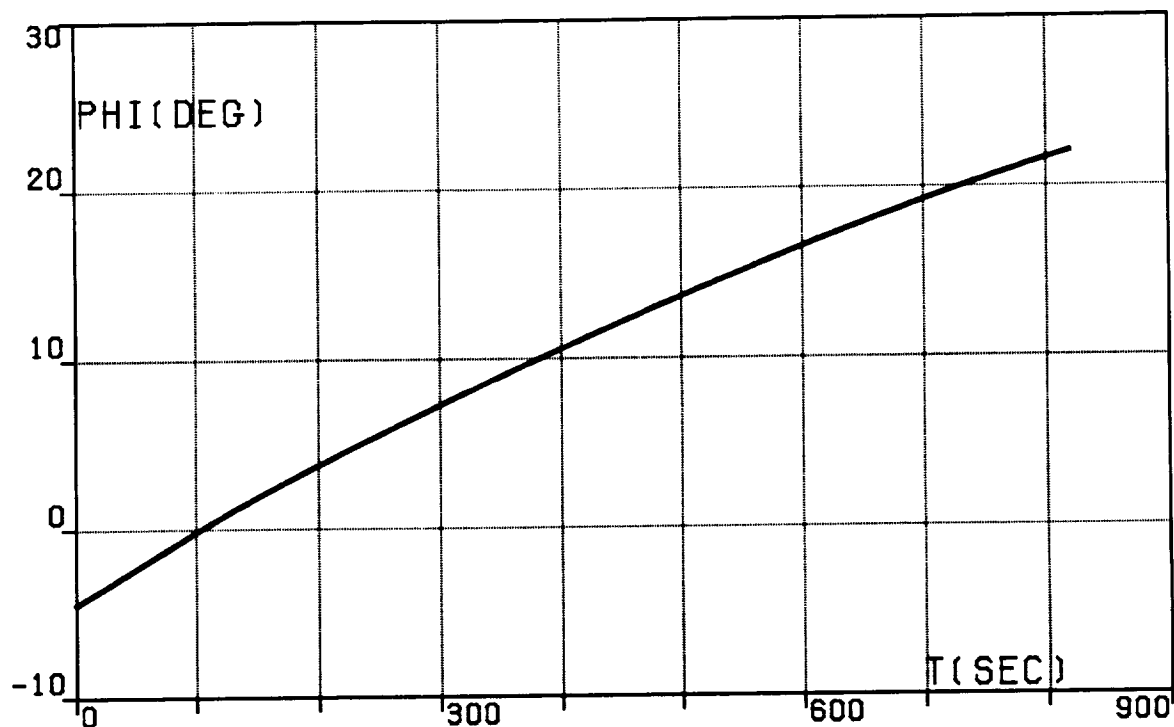


FIG.9C. THREE-SEGMENT OPTIMAL TRAJECTORY,  
TRANSFER (DA). LATITUDE.

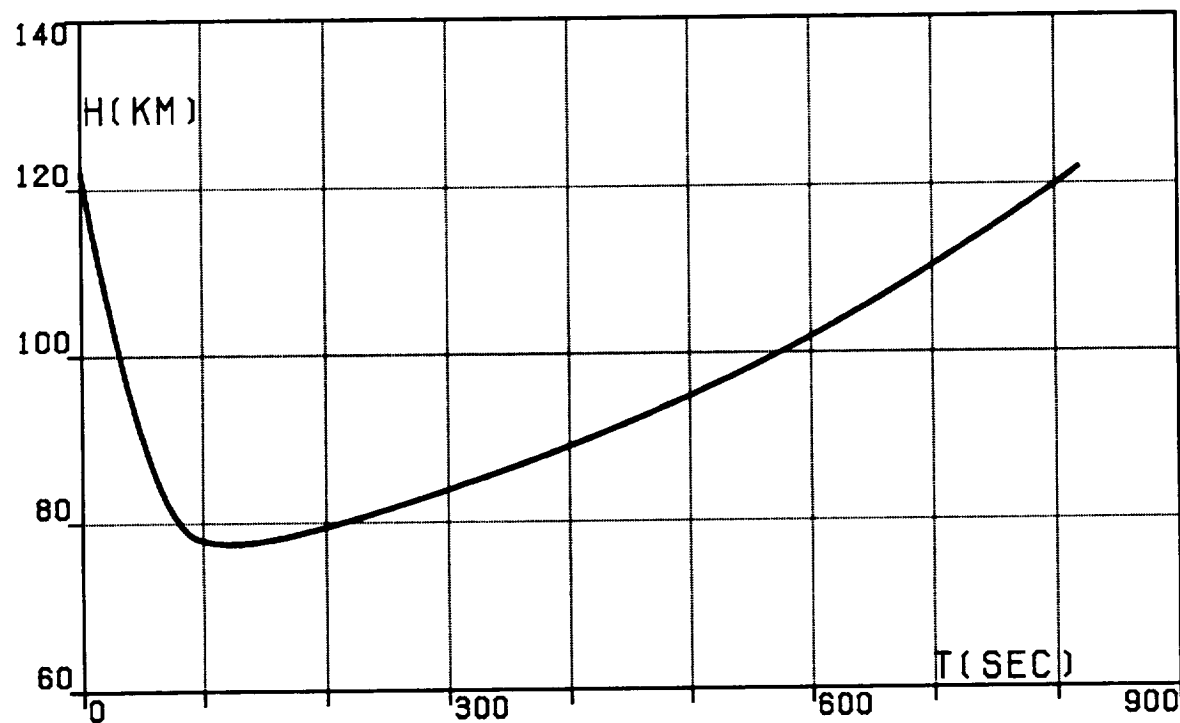


FIG.9D. THREE-SEGMENT OPTIMAL TRAJECTORY,  
TRANSFER (DA). ALTITUDE.

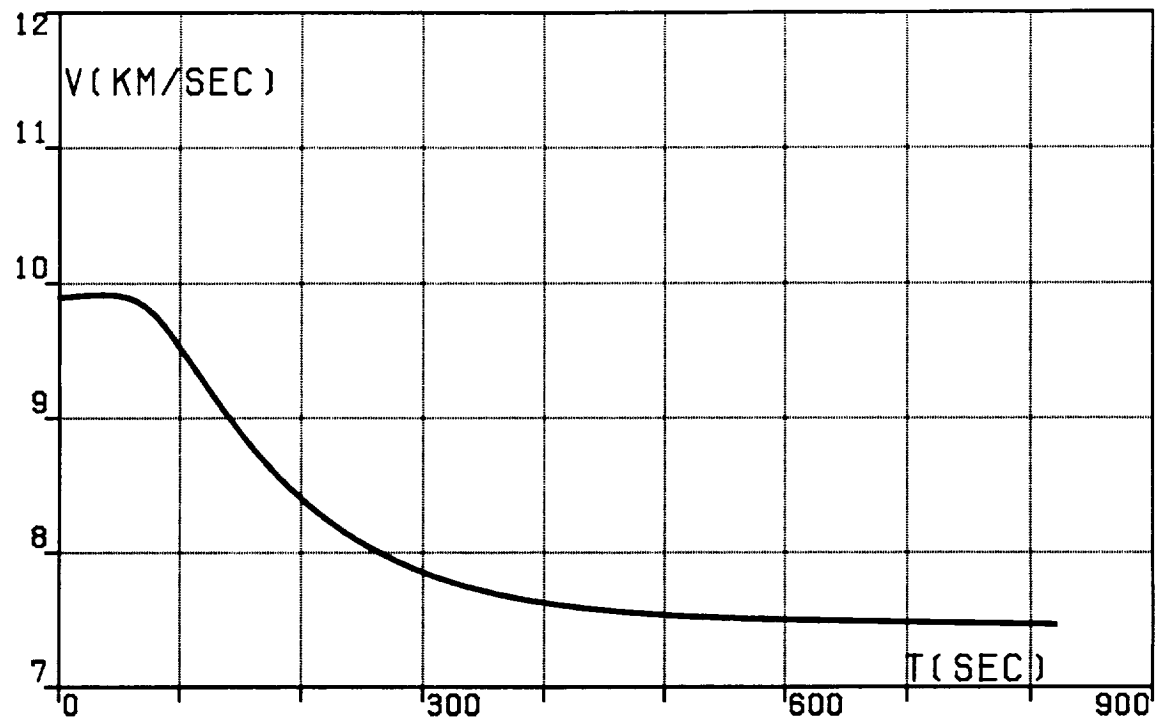


FIG.9E. THREE-SEGMENT OPTIMAL TRAJECTORY,  
TRANSFER (DA), VELOCITY, RELATIVE.

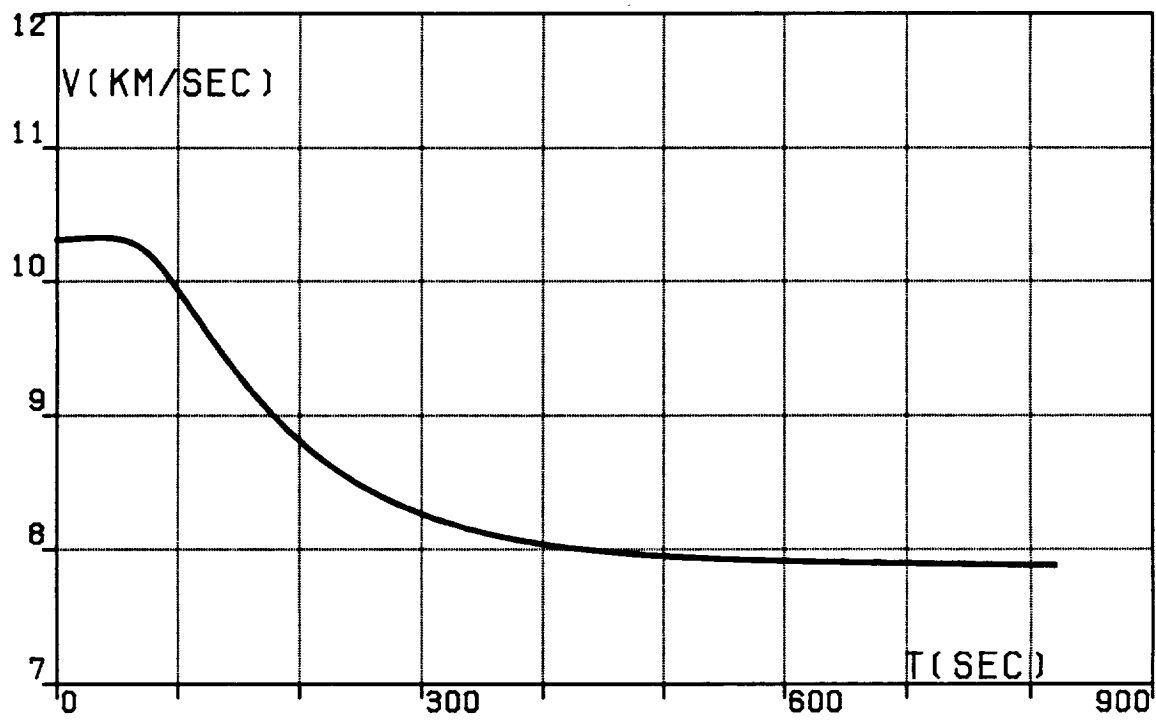


FIG.9F. THREE-SEGMENT OPTIMAL TRAJECTORY,  
TRANSFER (DA), VELOCITY, INERTIAL.

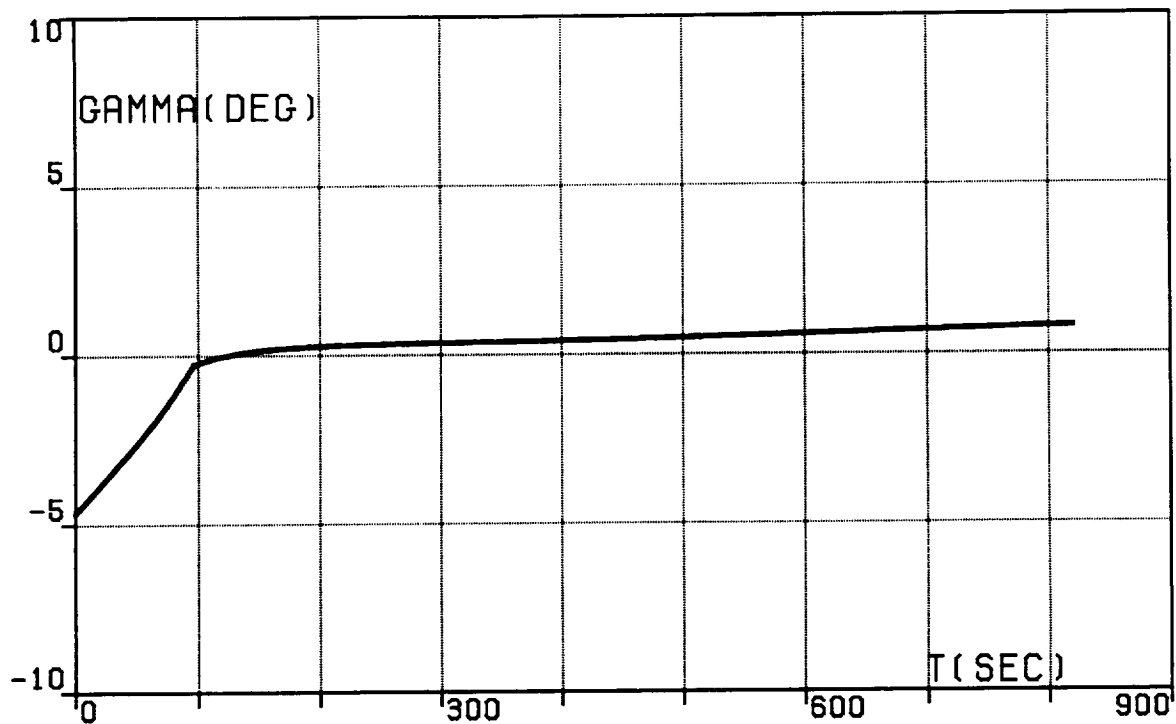


FIG.9G. THREE-SEGMENT OPTIMAL TRAJECTORY,  
TRANSFER (DA),  
PATH INCLINATION, RELATIVE.

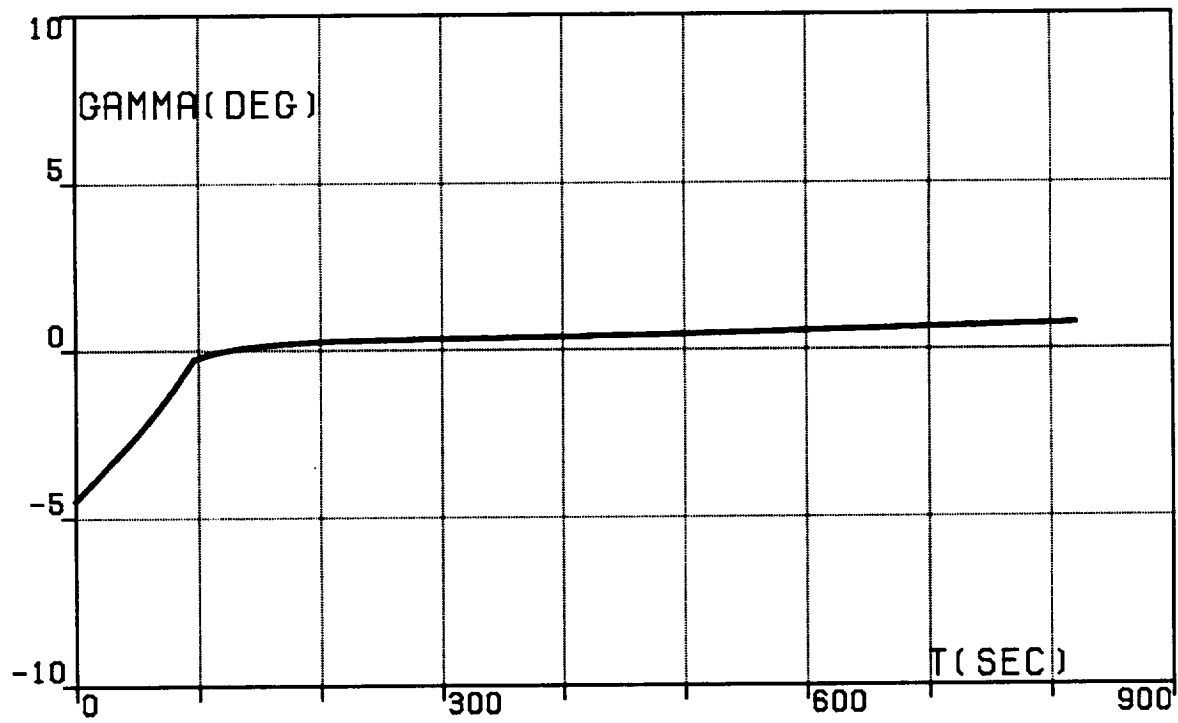


FIG.9H. THREE-SEGMENT OPTIMAL TRAJECTORY,  
TRANSFER (DA),  
PATH INCLINATION, INERTIAL.

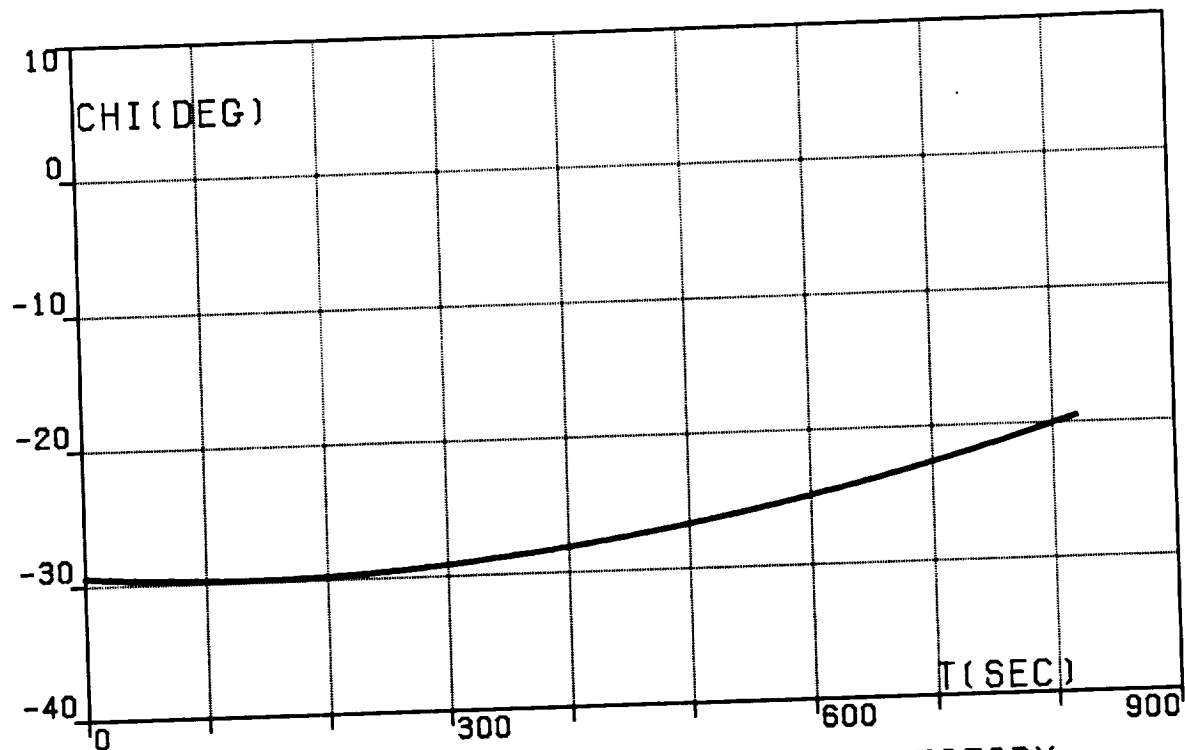


FIG.9I. THREE-SEGMENT OPTIMAL TRAJECTORY.  
TRANSFER (DA), HEADING ANGLE, RELATIVE.

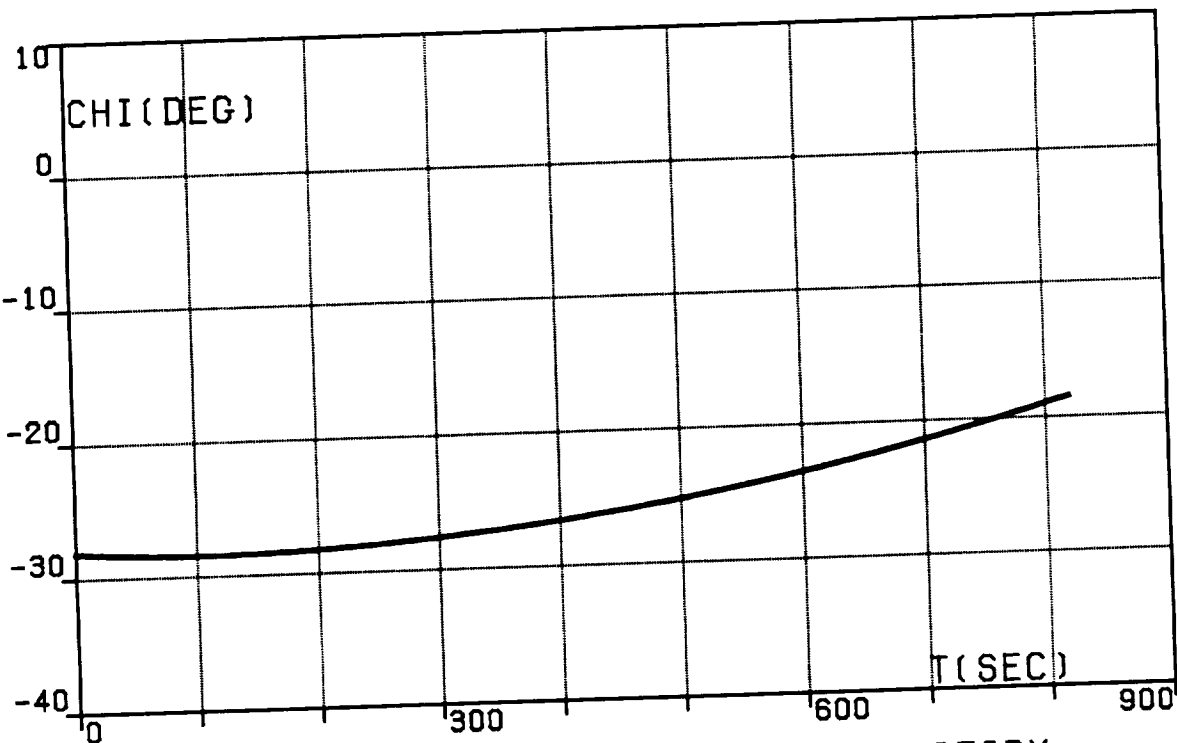


FIG.9J. THREE-SEGMENT OPTIMAL TRAJECTORY.  
TRANSFER (DA), HEADING ANGLE, INERTIAL.

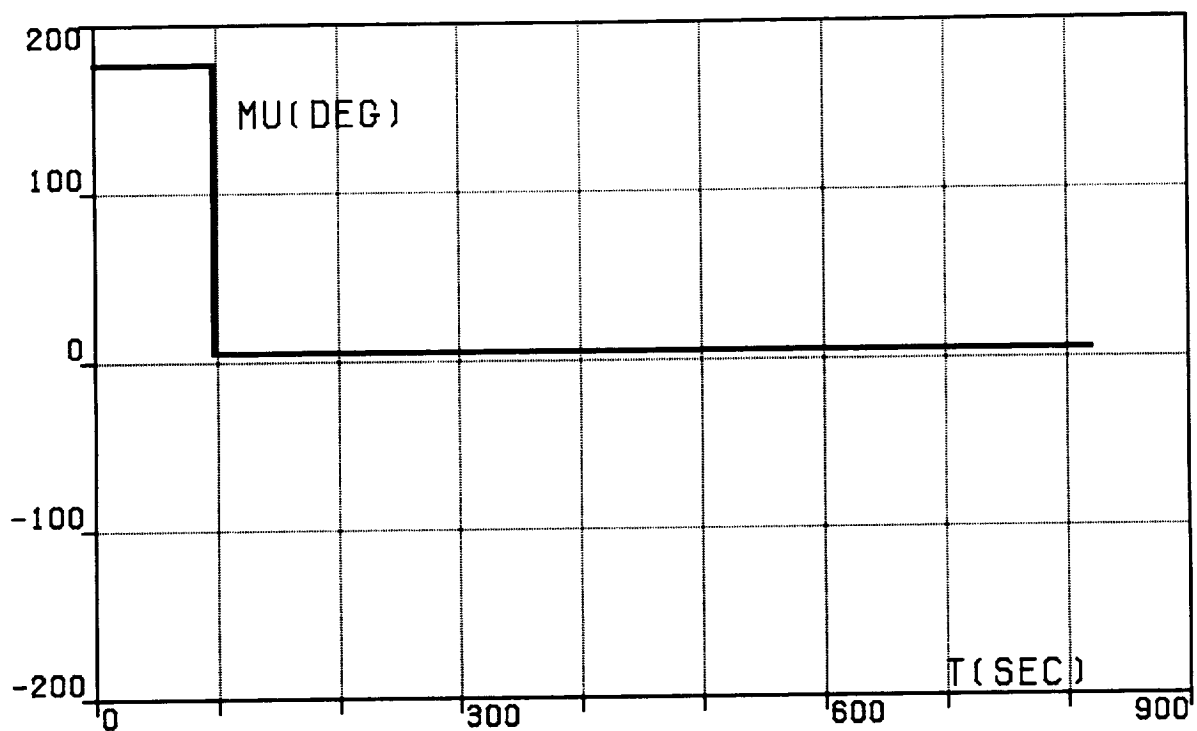


FIG.9K. THREE-SEGMENT OPTIMAL TRAJECTORY,  
TRANSFER (DA), BANK ANGLE.

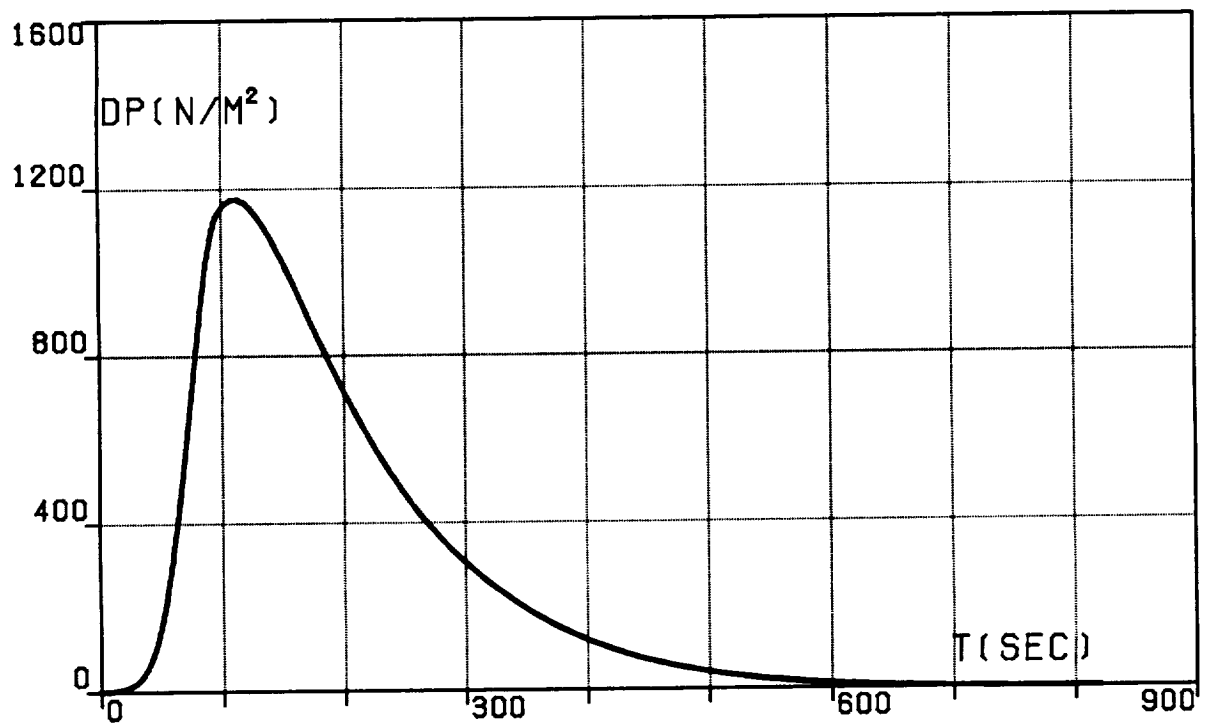


FIG.9L. THREE-SEGMENT OPTIMAL TRAJECTORY,  
TRANSFER (DA), DYNAMIC PRESSURE.

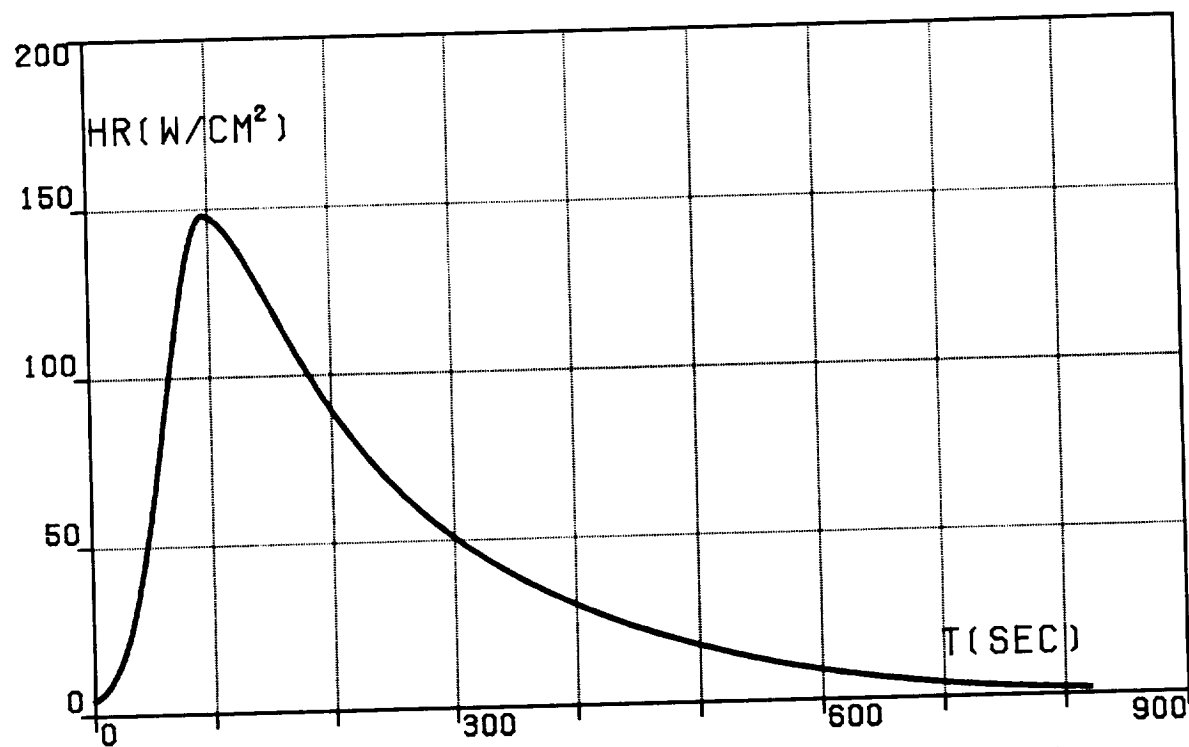


FIG.9M. THREE-SEGMENT OPTIMAL TRAJECTORY,  
TRANSFER (DA), HEATING RATE.

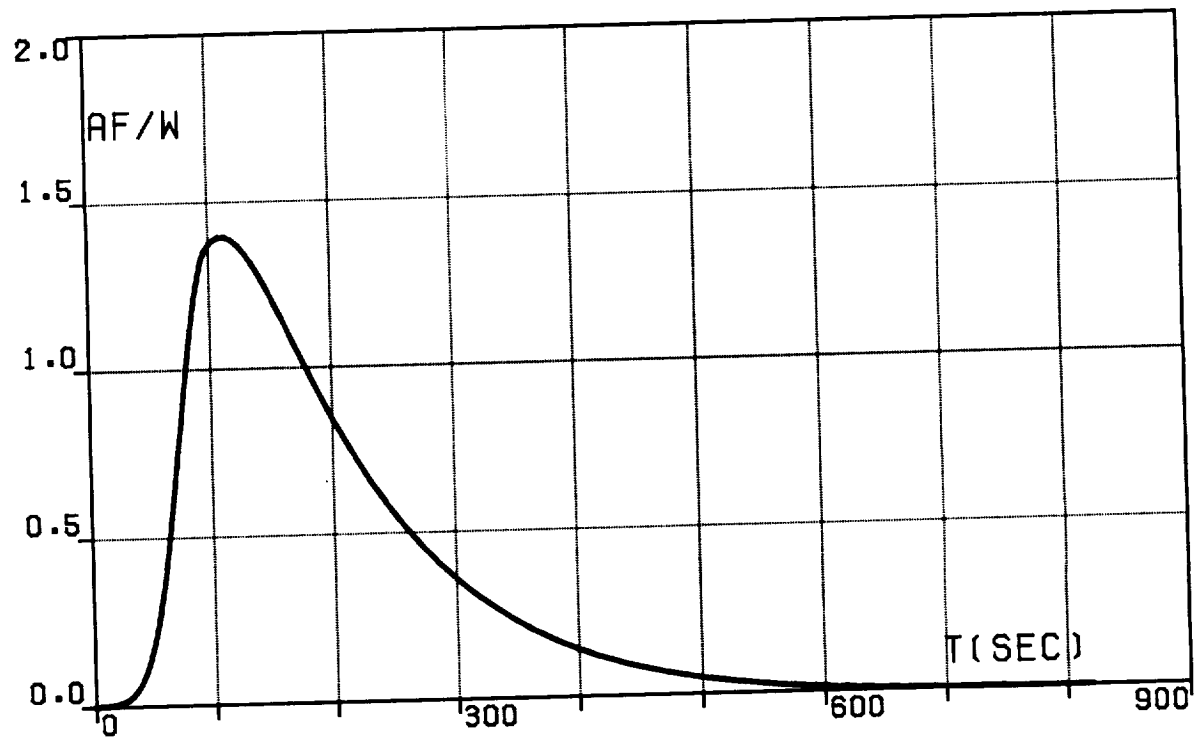


FIG.9N. THREE-SEGMENT OPTIMAL TRAJECTORY,  
TRANSFER (DA),  
AERODYNAMIC FORCE PER UNIT WEIGHT.

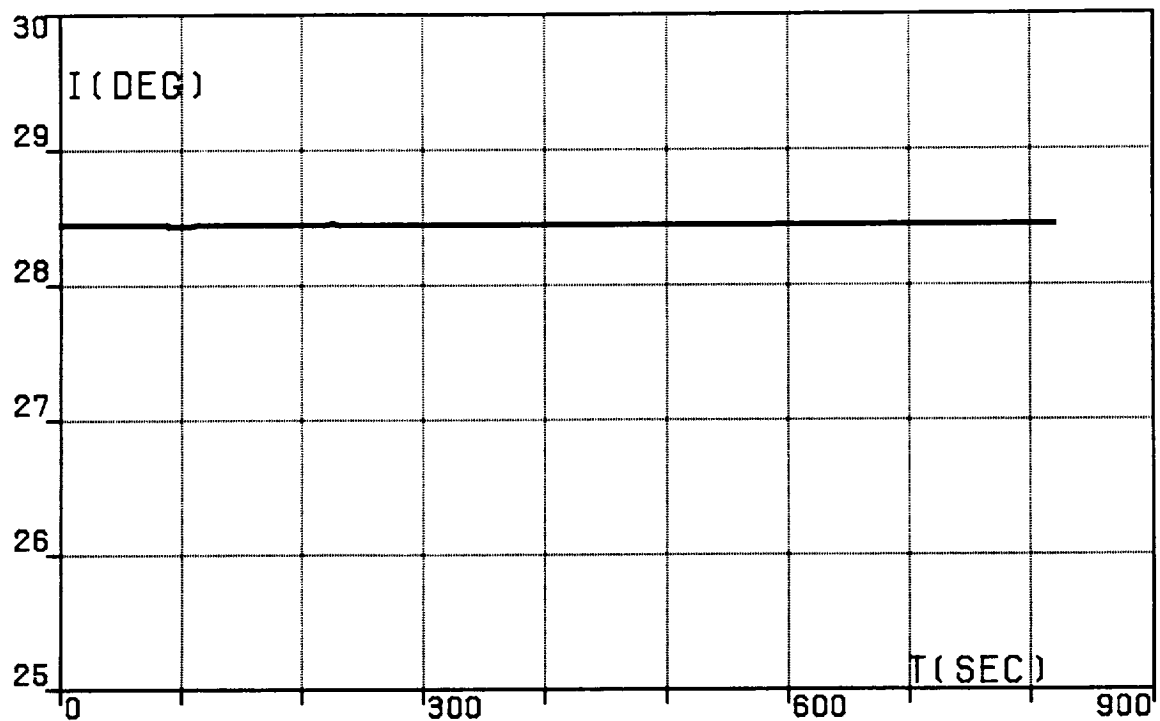


FIG.9O. THREE-SEGMENT OPTIMAL TRAJECTORY,  
TRANSFER (DA), ORBITAL INCLINATION.

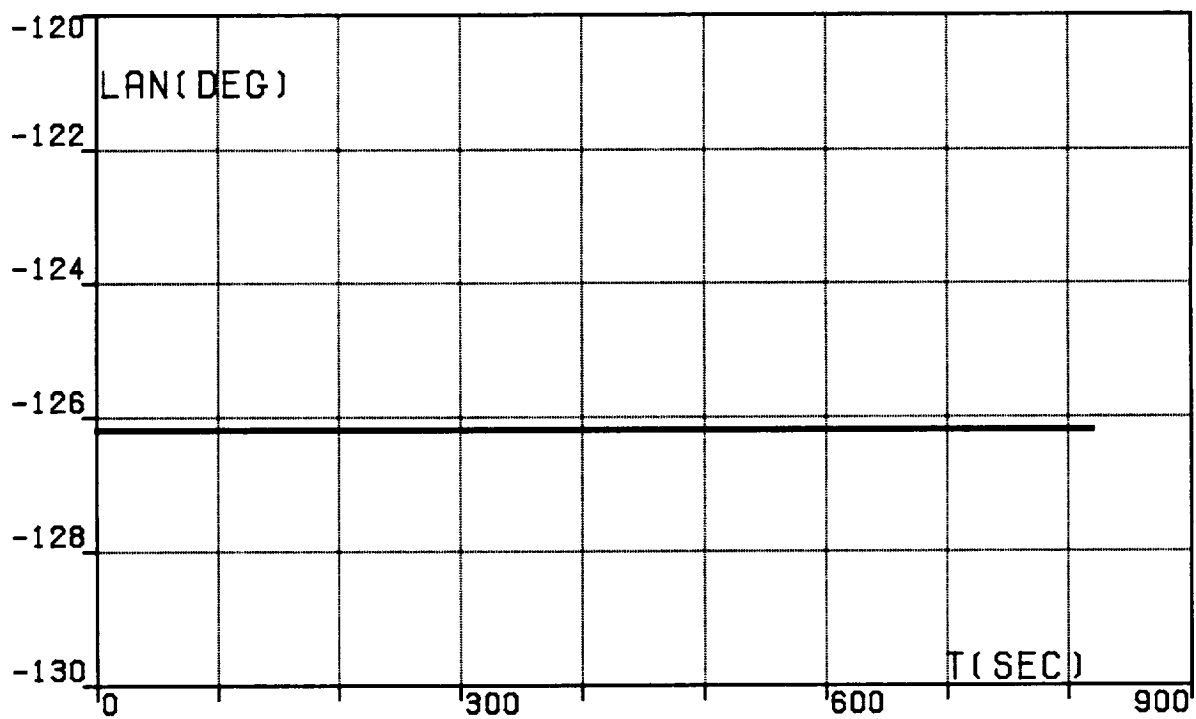


FIG.9P. THREE-SEGMENT OPTIMAL TRAJECTORY,  
TRANSFER (DA),  
LONGITUDE OF THE ASCENDING NODE.

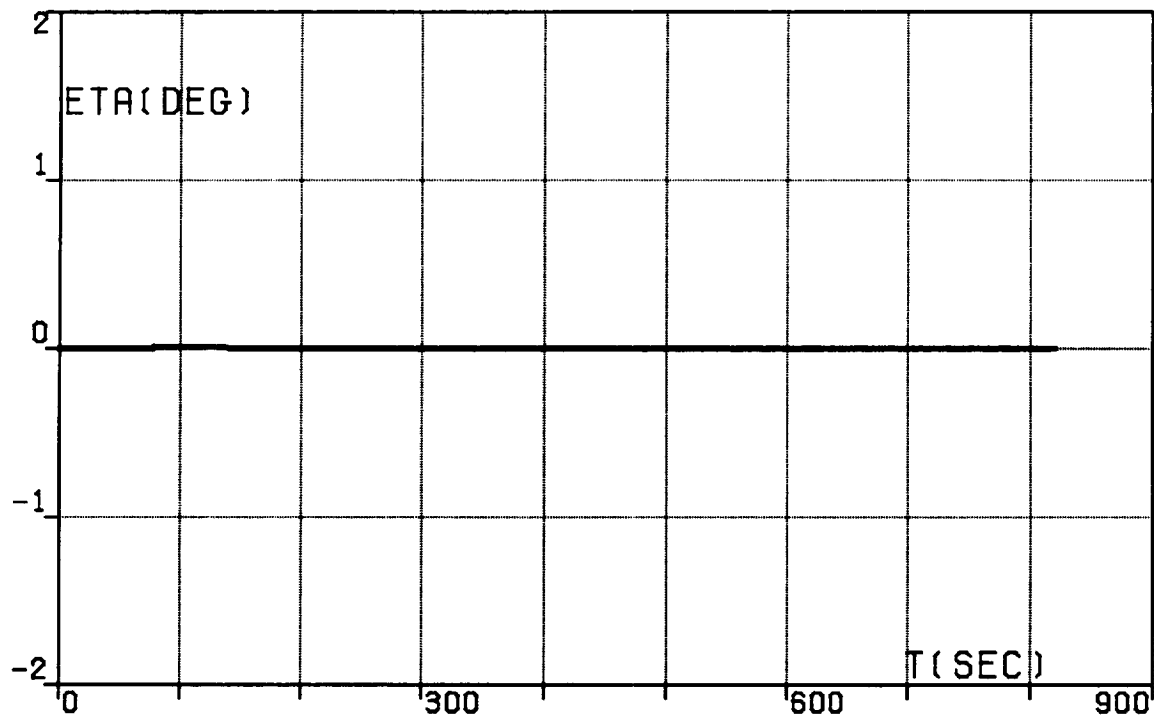


FIG.9Q. THREE-SEGMENT OPTIMAL TRAJECTORY,  
TRANSFER (DA), WEDGE ANGLE.

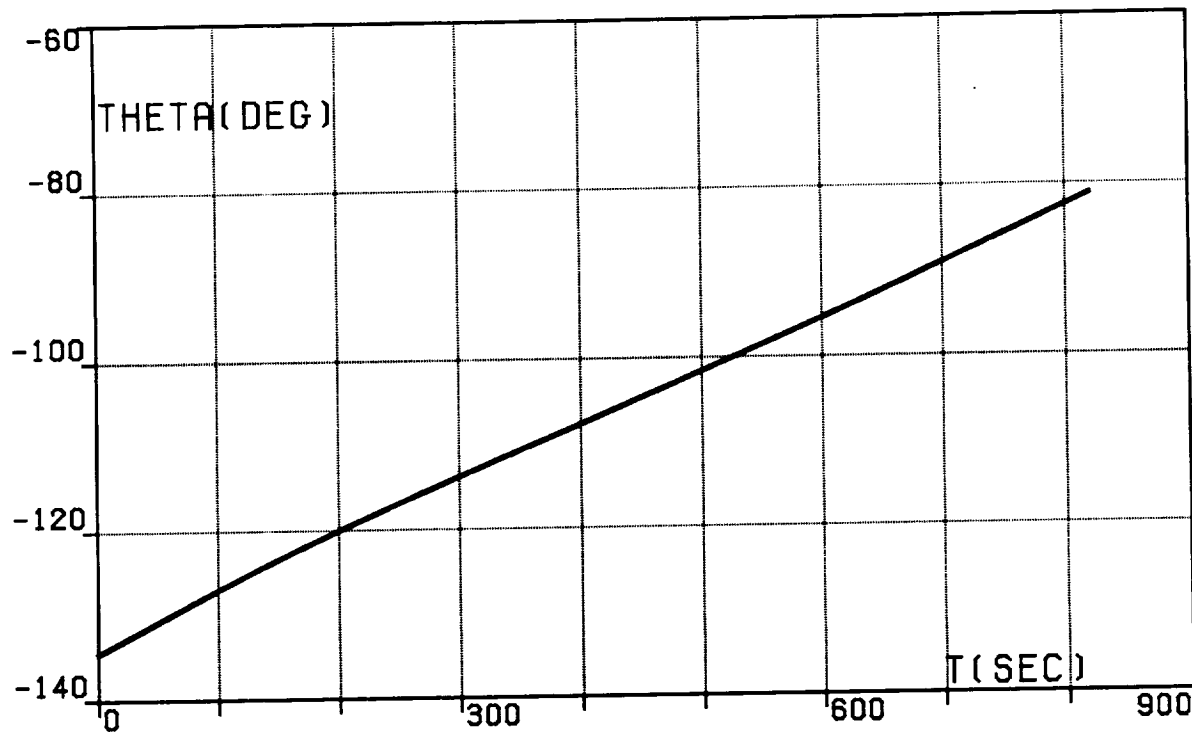


FIG.10A. FOUR-SEGMENT OPTIMAL TRAJECTORY,  
TRANSFER (DA), LONGITUDE, RELATIVE.

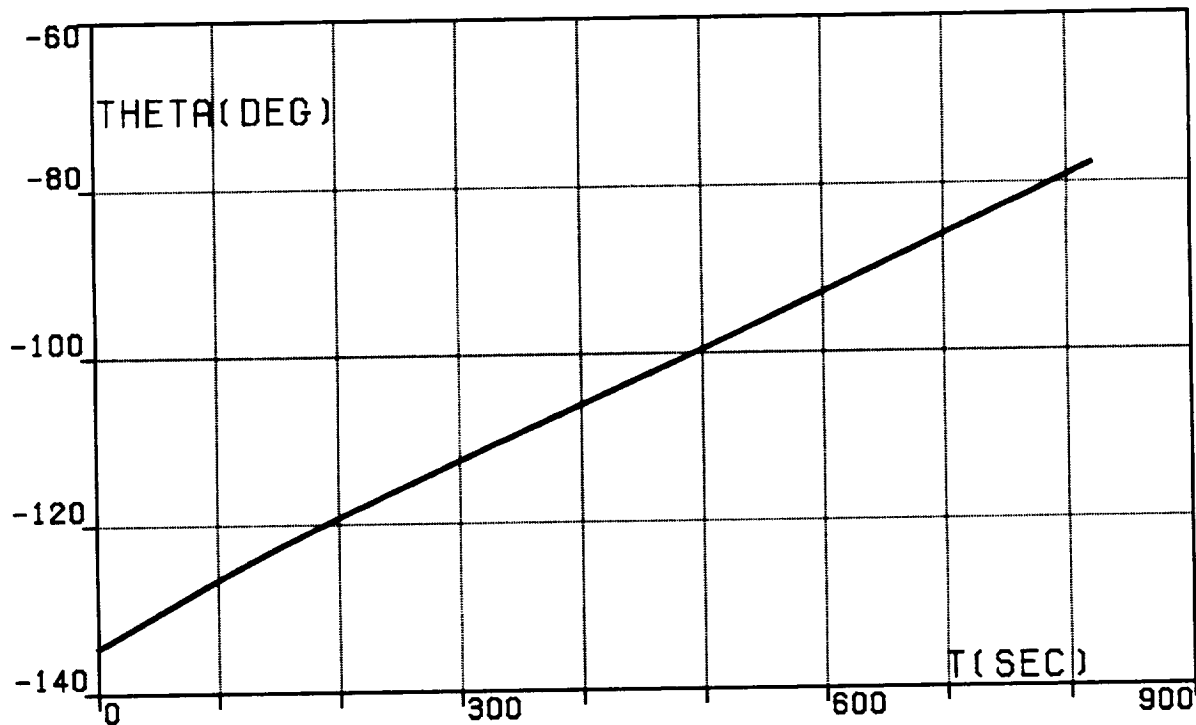


FIG.10B. FOUR-SEGMENT OPTIMAL TRAJECTORY,  
TRANSFER (DA), LONGITUDE, INERTIAL.

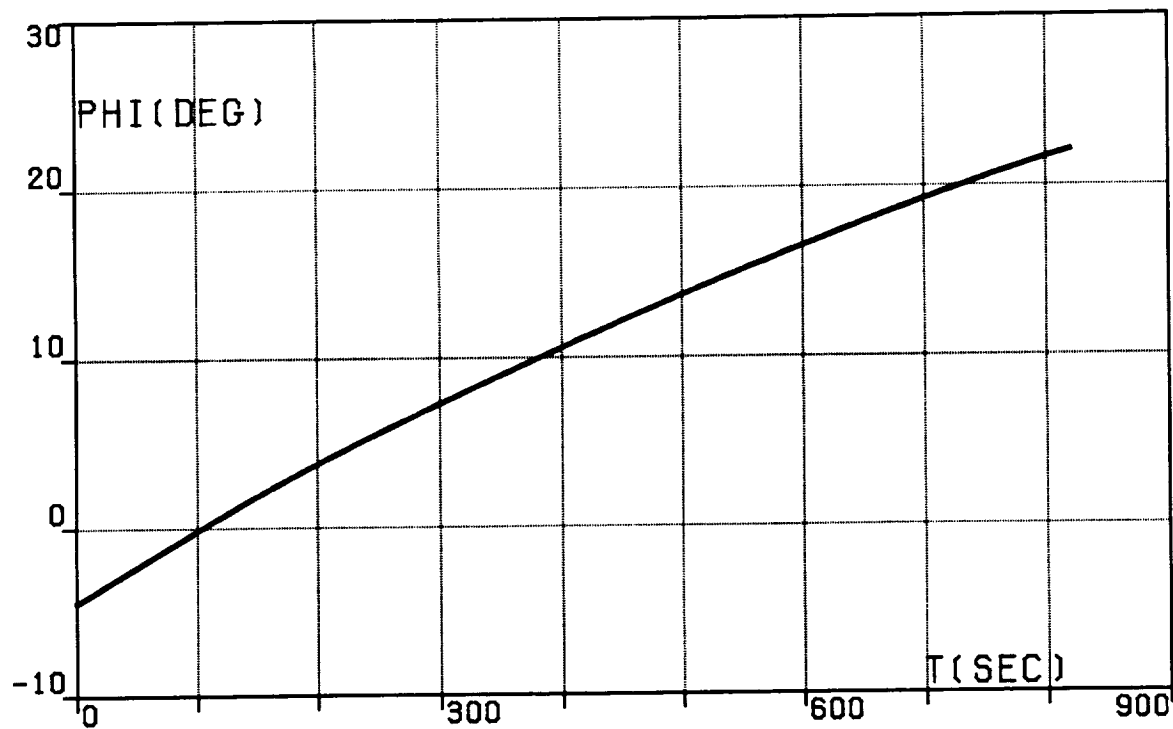


FIG.10C. FOUR-SEGMENT OPTIMAL TRAJECTORY,  
TRANSFER (DA), LATITUDE.

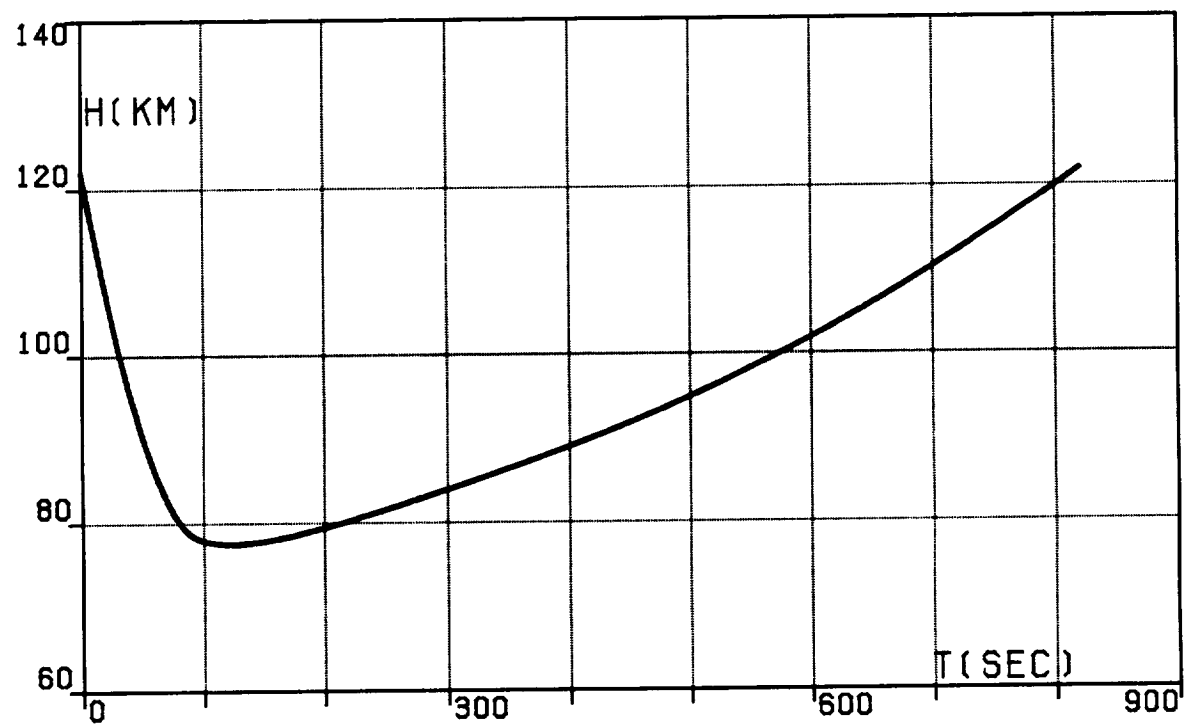


FIG.10D. FOUR-SEGMENT OPTIMAL TRAJECTORY,  
TRANSFER (DA), ALTITUDE.

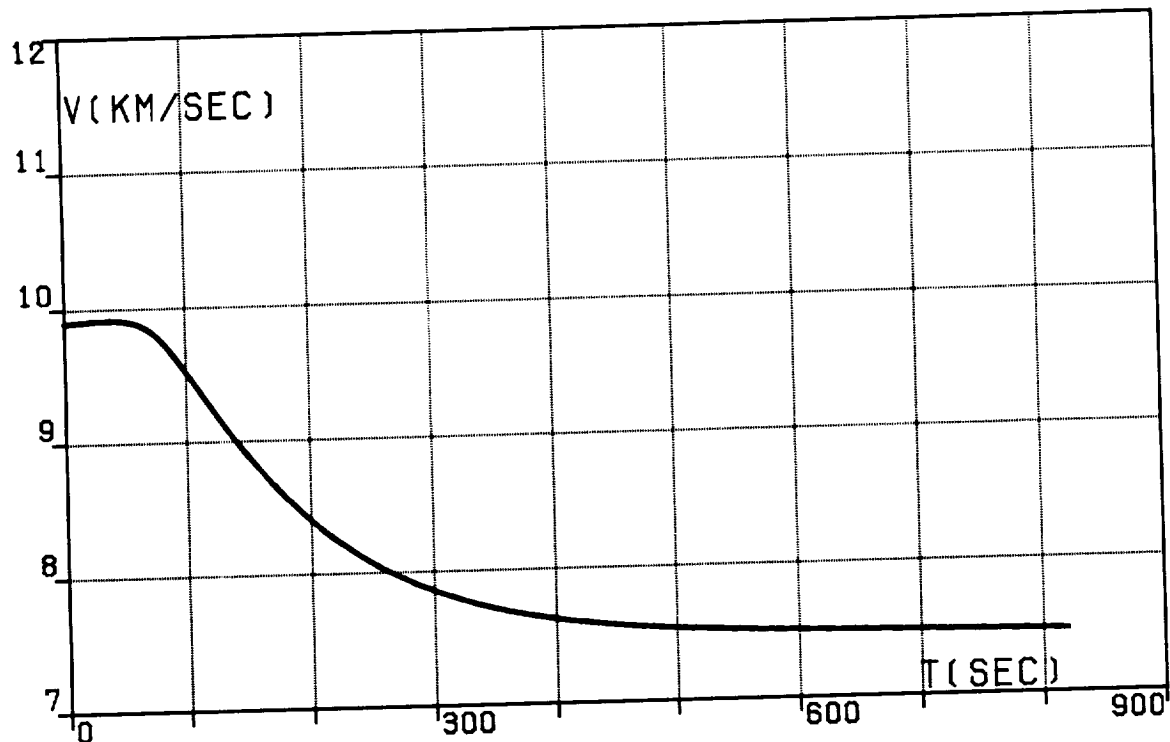


FIG.10E. FOUR-SEGMENT OPTIMAL TRAJECTORY,  
TRANSFER (DA), VELOCITY, RELATIVE.

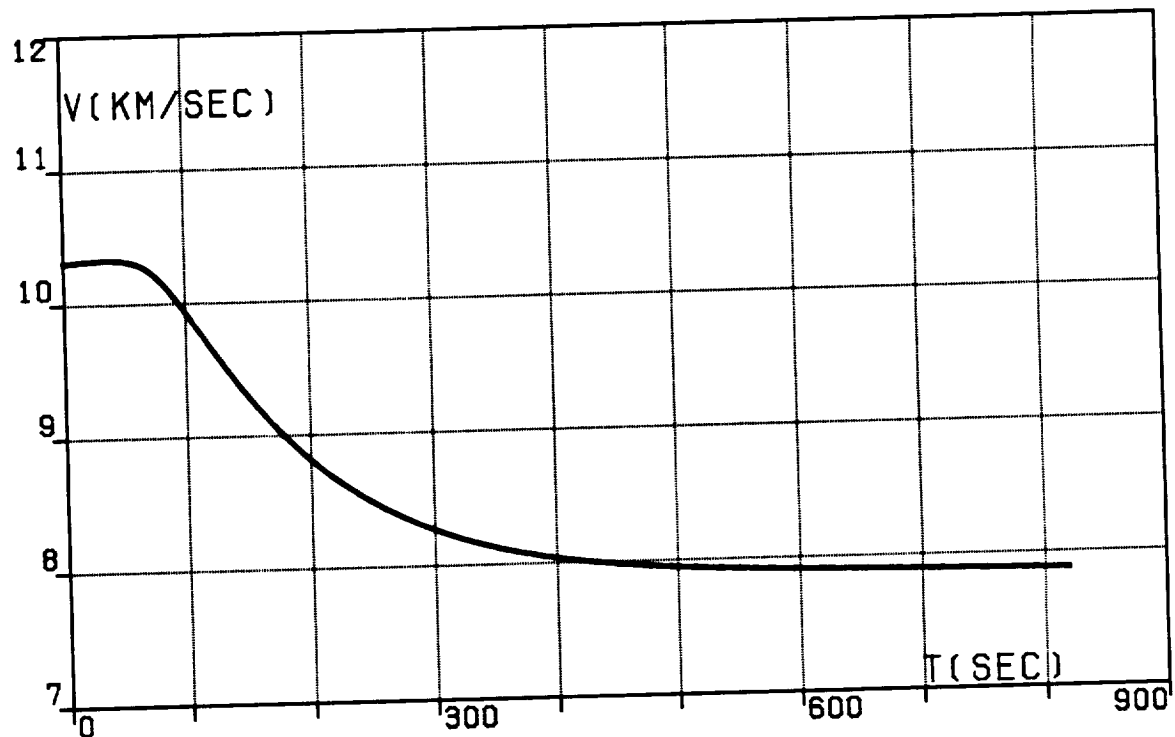


FIG.10F. FOUR-SEGMENT OPTIMAL TRAJECTORY,  
TRANSFER (DA), VELOCITY, INERTIAL.

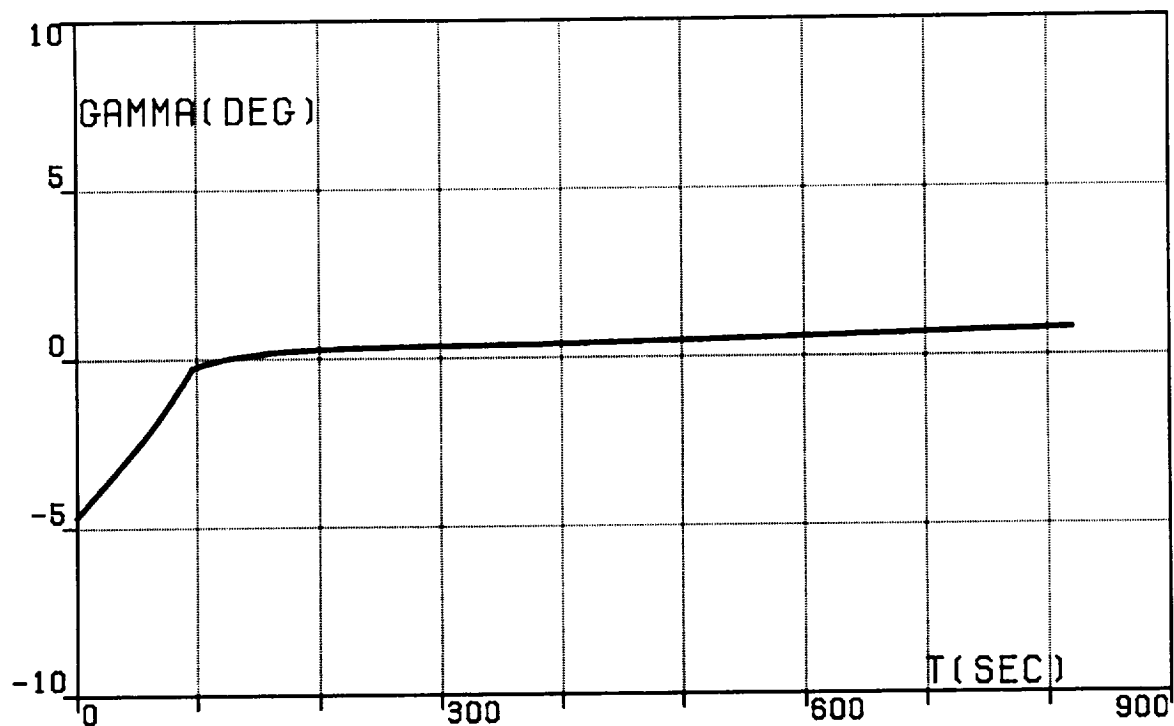


FIG.10G. FOUR-SEGMENT OPTIMAL TRAJECTORY,  
TRANSFER (DA),  
PATH INCLINATION, RELATIVE.

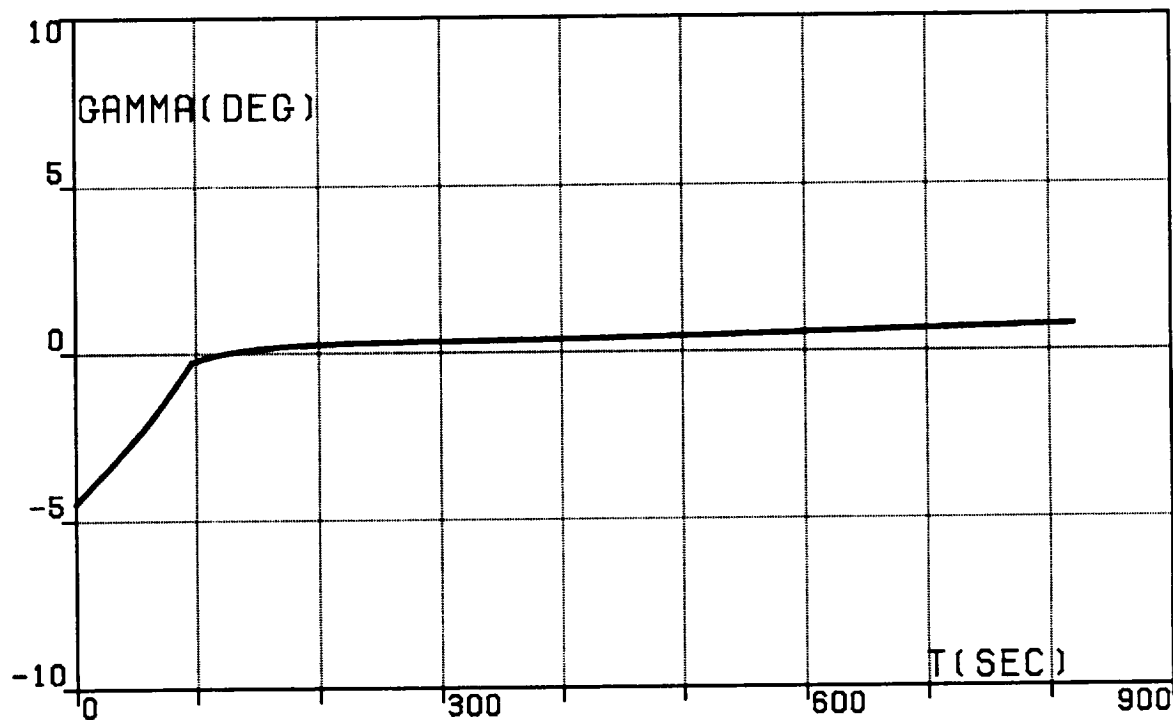


FIG.10H. FOUR-SEGMENT OPTIMAL TRAJECTORY,  
TRANSFER (DA),  
PATH INCLINATION, INERTIAL.

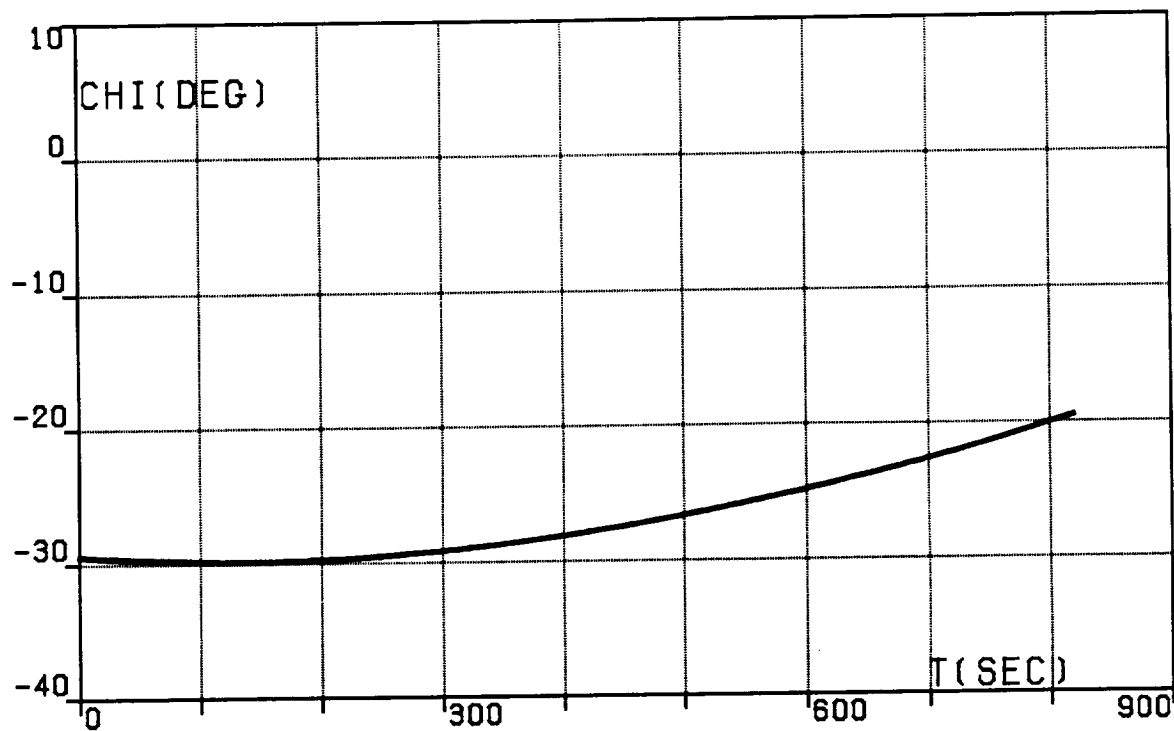


FIG.10I. FOUR-SEGMENT OPTIMAL TRAJECTORY,  
TRANSFER (DA), HEADING ANGLE, RELATIVE.

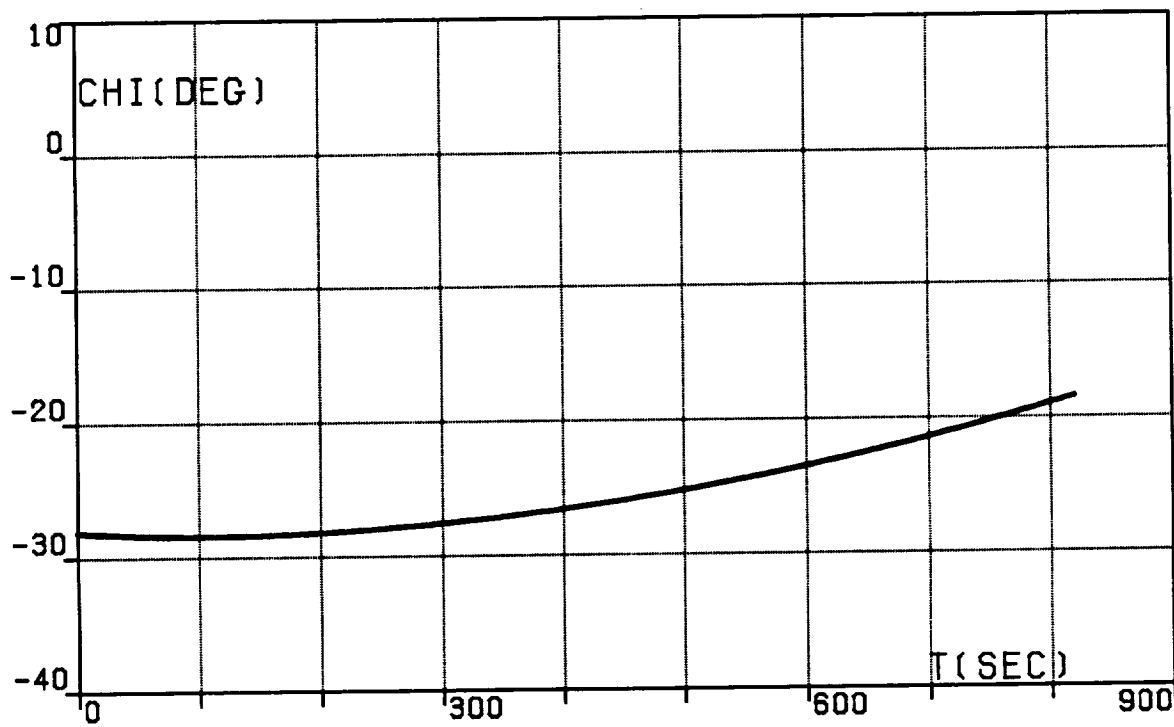


FIG.10J. FOUR-SEGMENT OPTIMAL TRAJECTORY,  
TRANSFER (DA), HEADING ANGLE, INERTIAL.

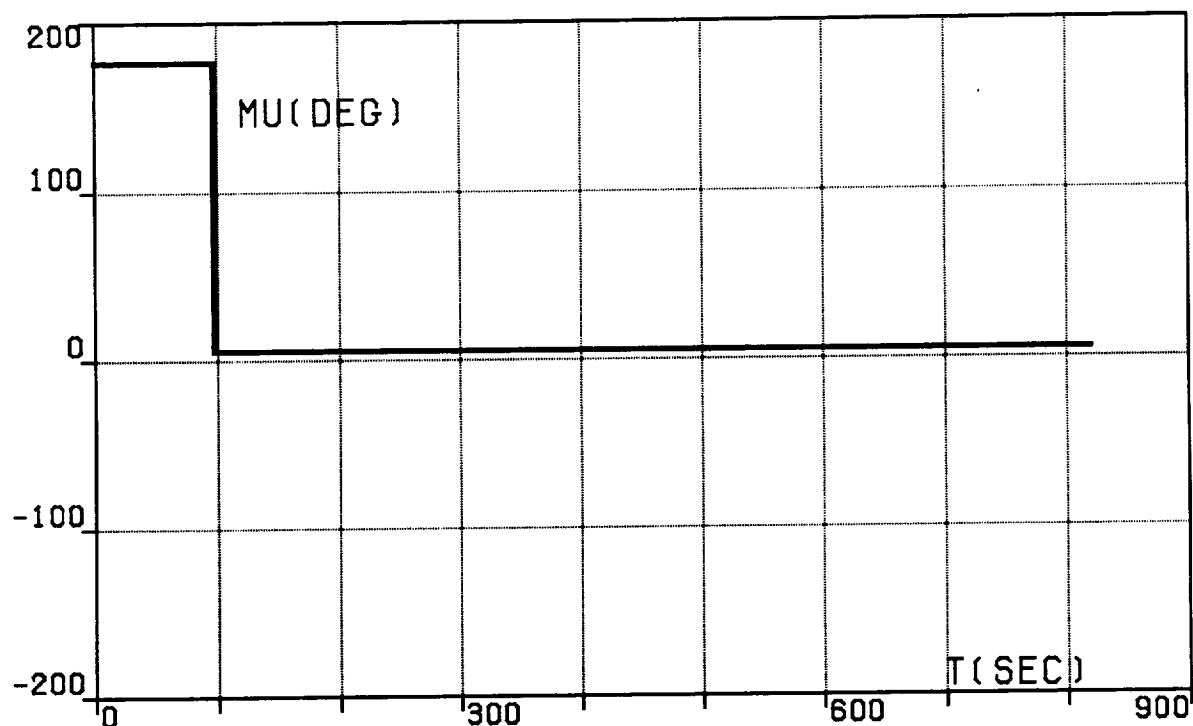


FIG.10K. FOUR-SEGMENT OPTIMAL TRAJECTORY,  
TRANSFER (DA), BANK ANGLE.

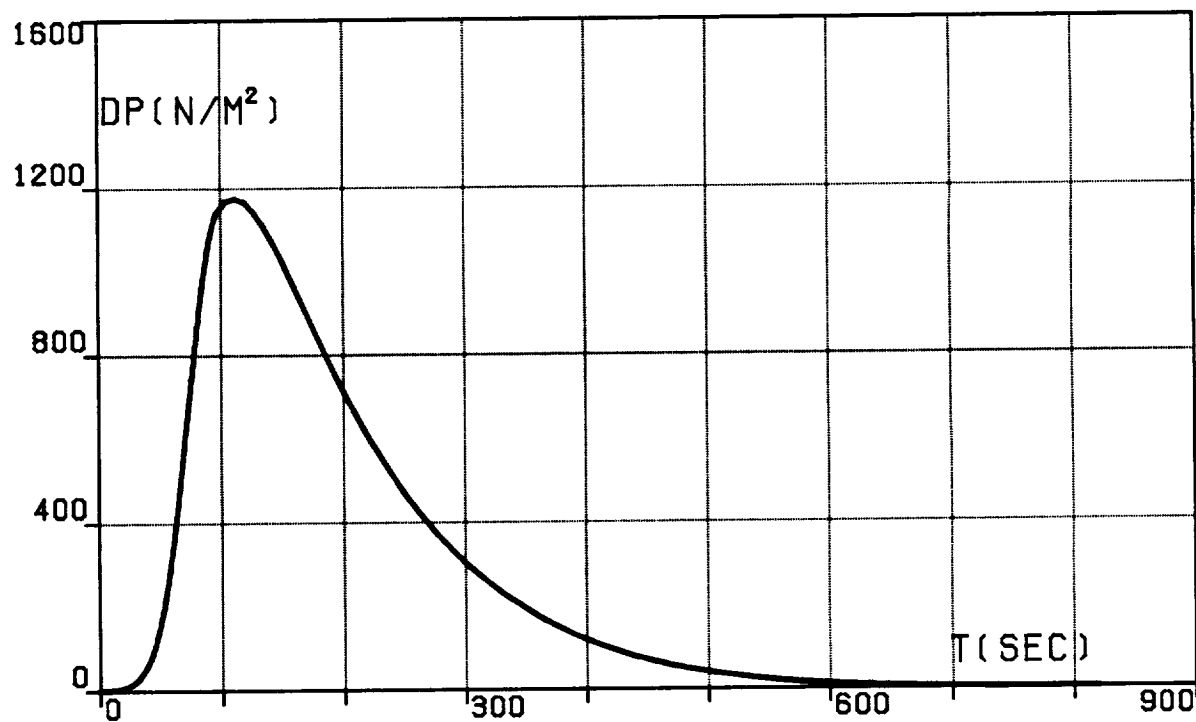


FIG.10L. FOUR-SEGMENT OPTIMAL TRAJECTORY,  
TRANSFER (DA), DYNAMIC PRESSURE.

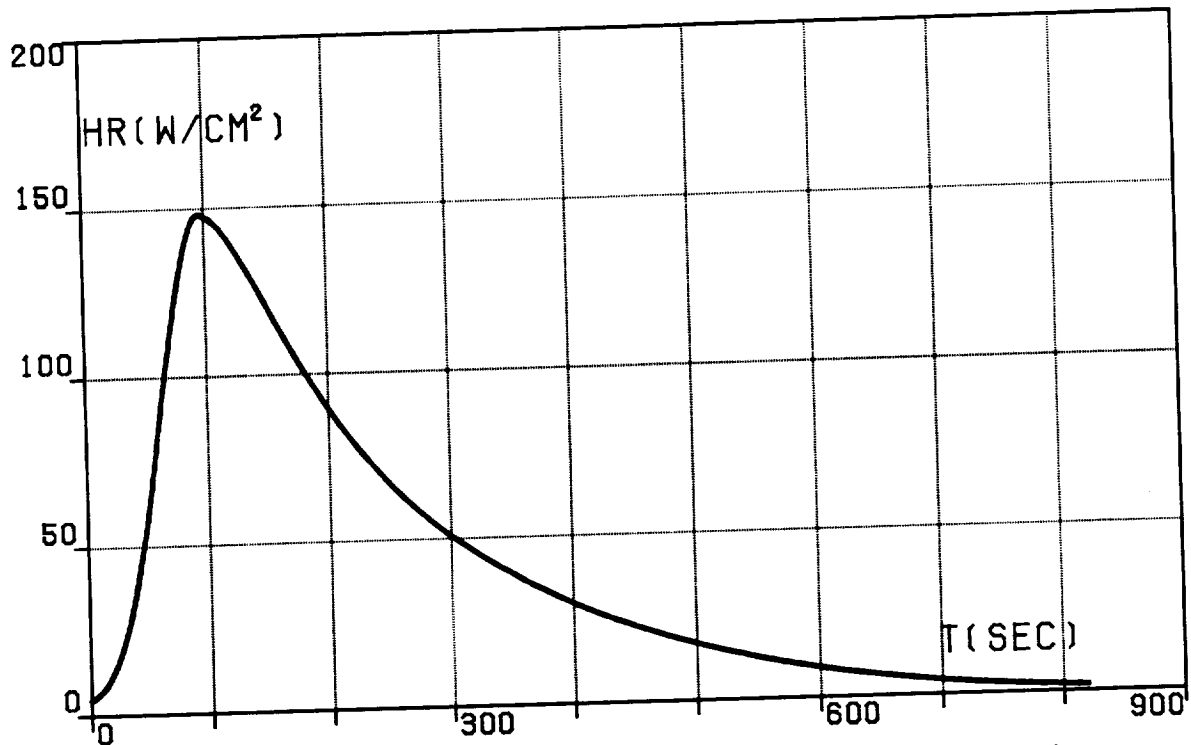


FIG.10M. FOUR-SEGMENT OPTIMAL TRAJECTORY,  
TRANSFER (DA), HEATING RATE.

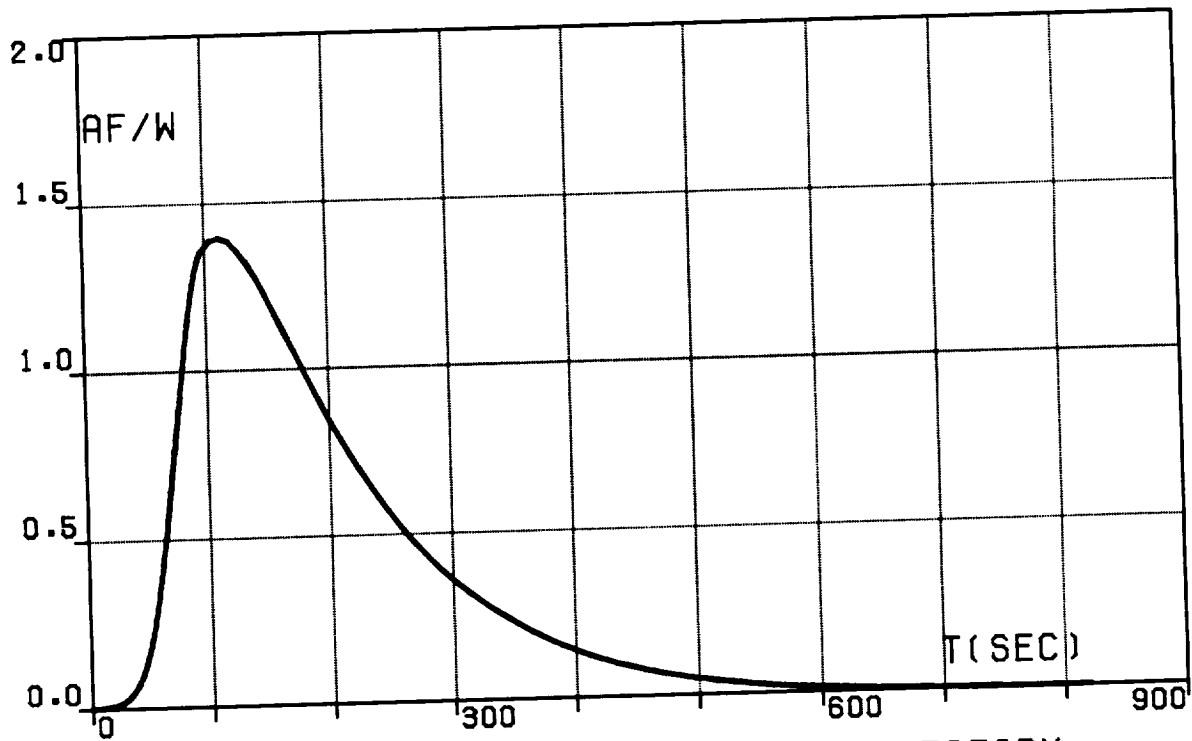


FIG.10N. FOUR-SEGMENT OPTIMAL TRAJECTORY,  
TRANSFER (DA),  
AERODYNAMIC FORCE PER UNIT WEIGHT.

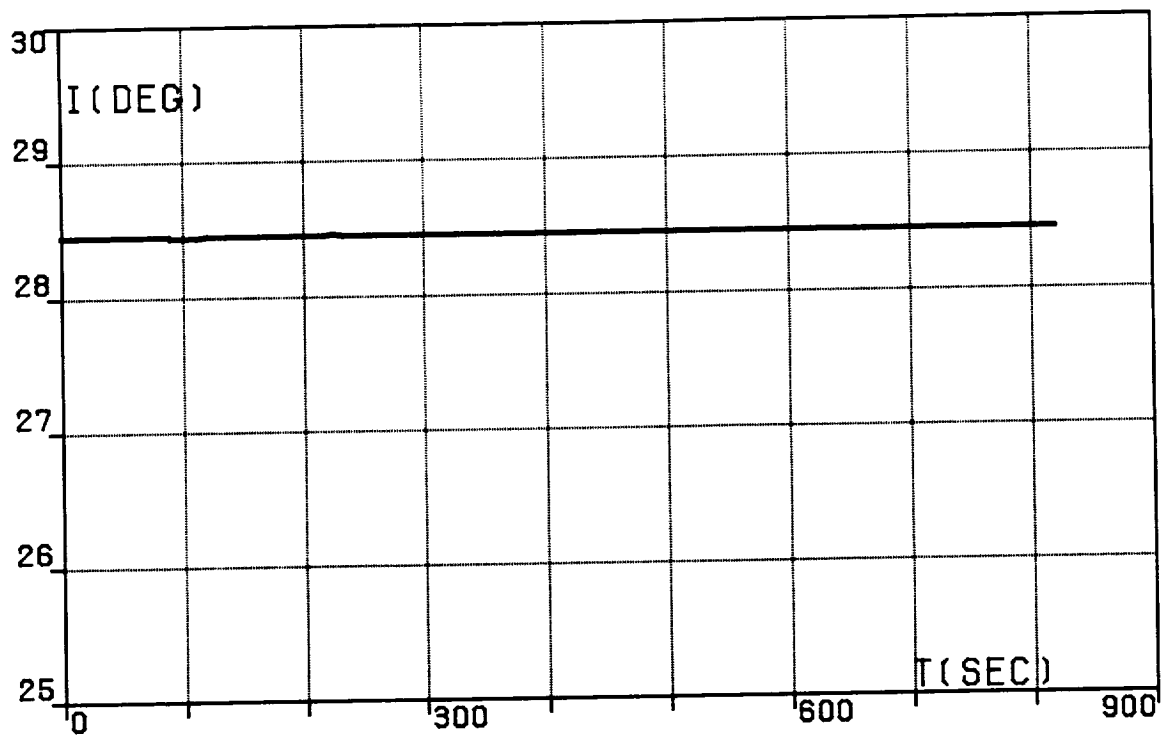


FIG.100. FOUR-SEGMENT OPTIMAL TRAJECTORY,  
TRANSFER (DA), ORBITAL INCLINATION.

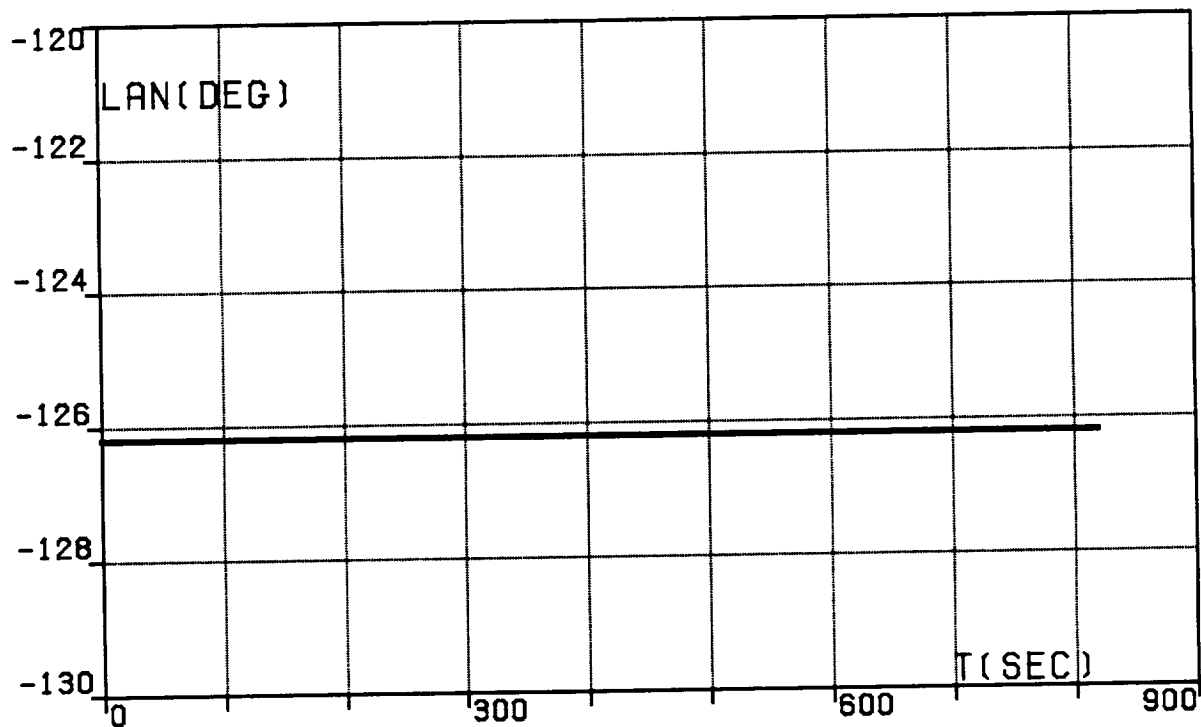


FIG.10P. FOUR-SEGMENT OPTIMAL TRAJECTORY,  
TRANSFER (DA),  
LONGITUDE OF THE ASCENDING NODE.

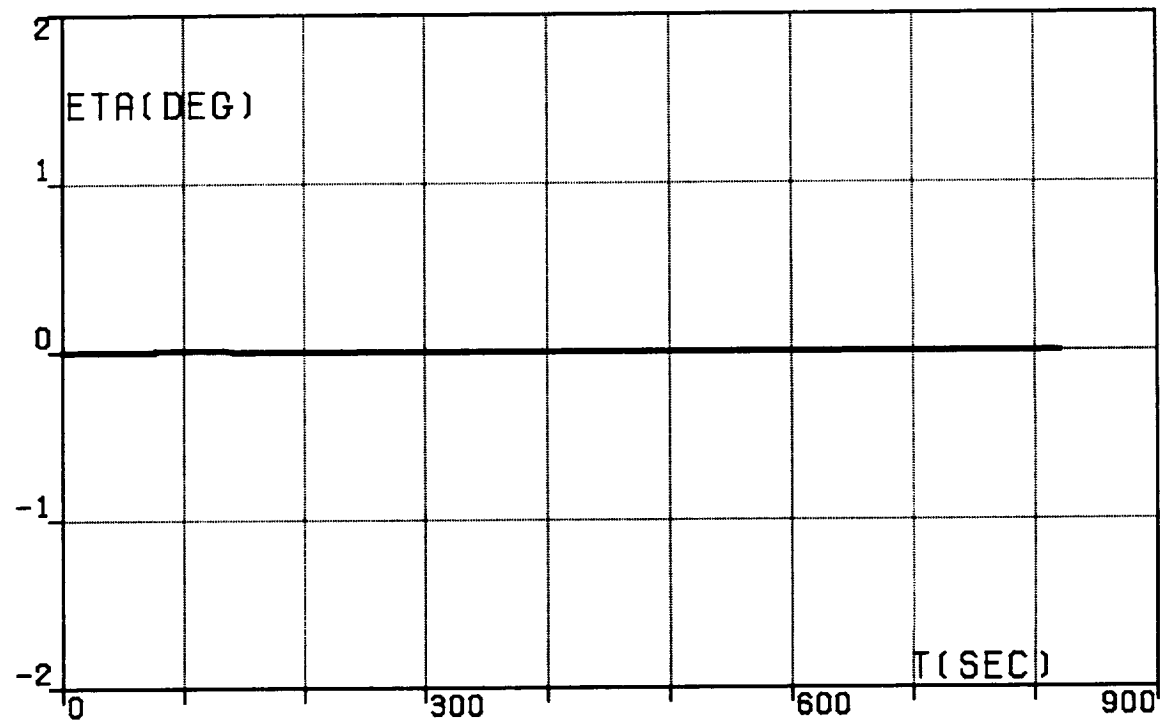


FIG.10Q. FOUR-SEGMENT OPTIMAL TRAJECTORY,  
TRANSFER (DA), WEDGE ANGLE.

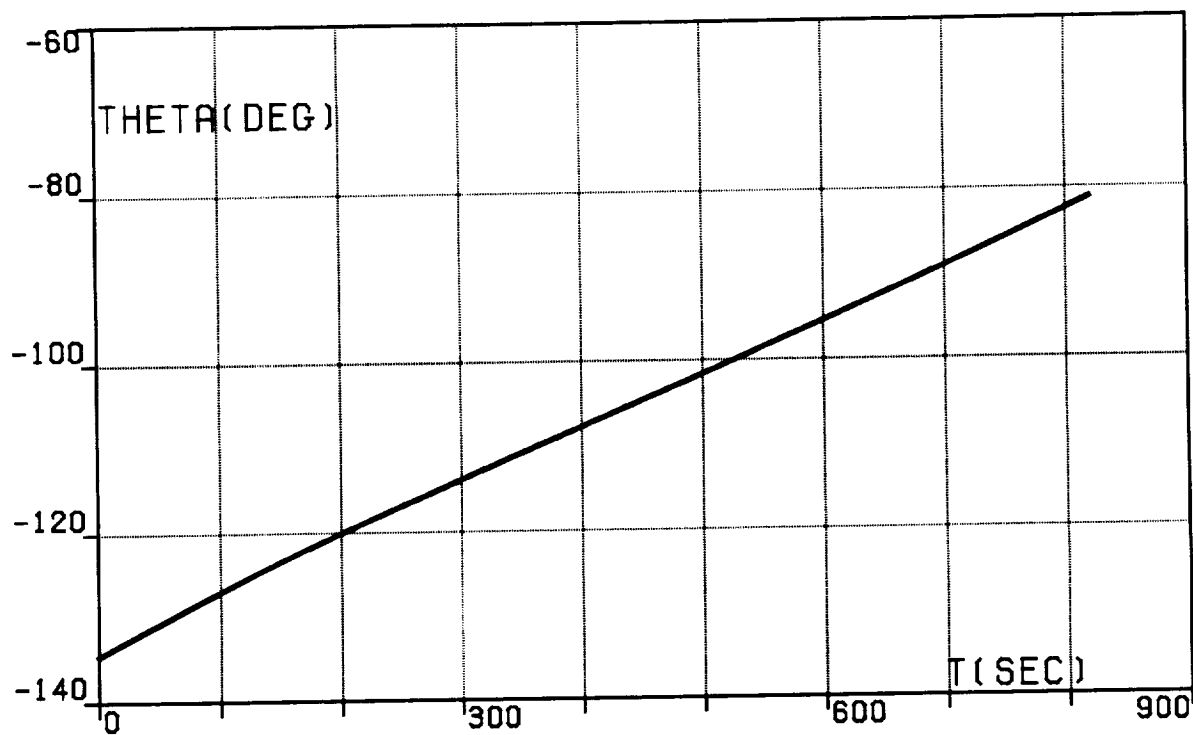


FIG.11A. FIVE-SEGMENT OPTIMAL TRAJECTORY,  
TRANSFER (DA), LONGITUDE, RELATIVE.

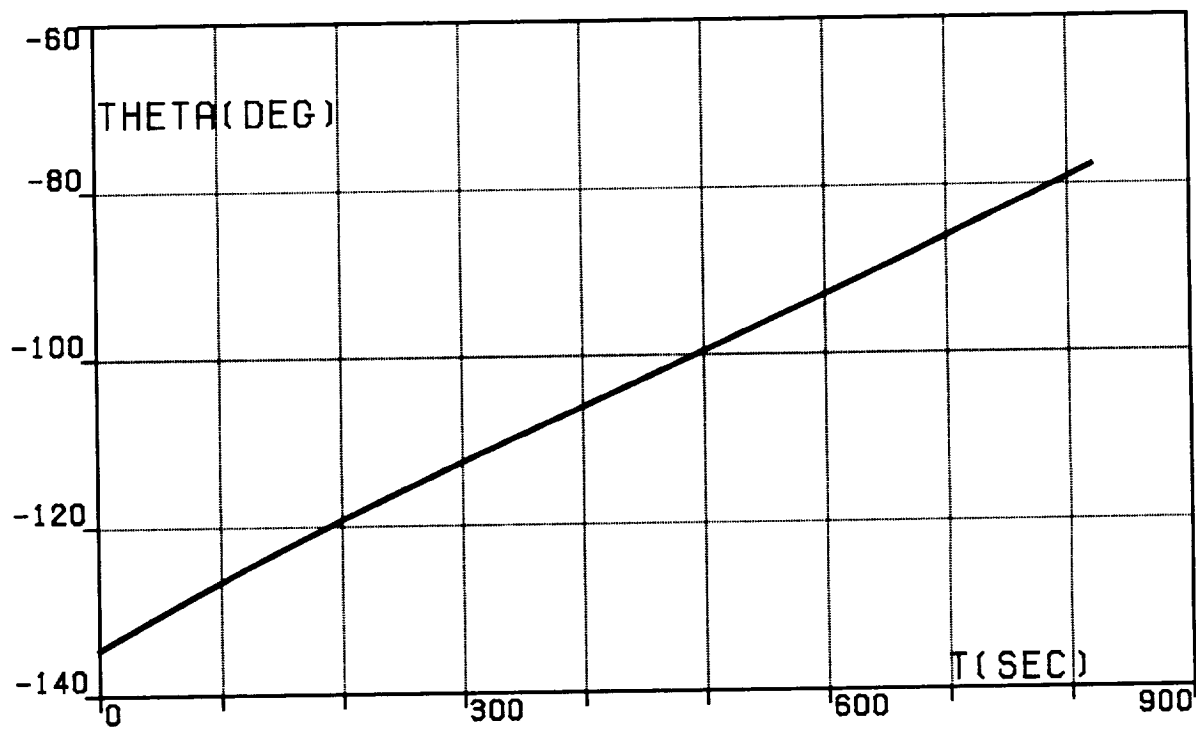


FIG.11B. FIVE-SEGMENT OPTIMAL TRAJECTORY,  
TRANSFER (DA), LONGITUDE, INERTIAL.

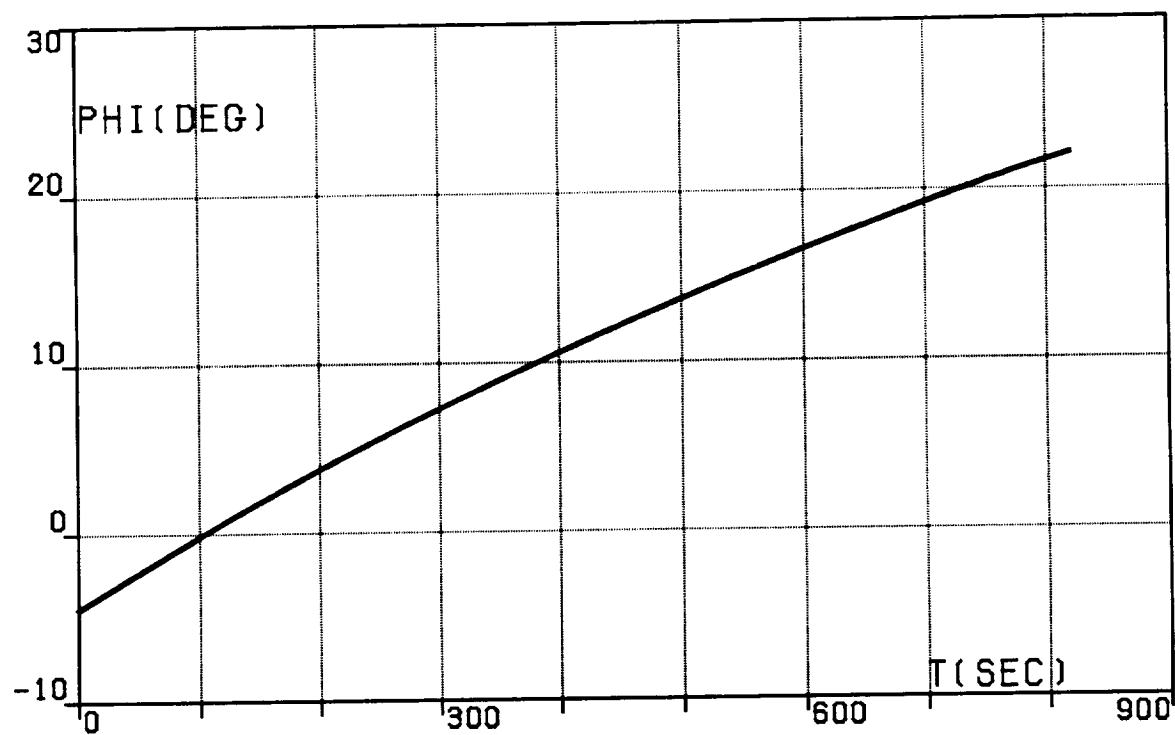


FIG.11C. FIVE-SEGMENT OPTIMAL TRAJECTORY,  
TRANSFER (DA), LATITUDE.

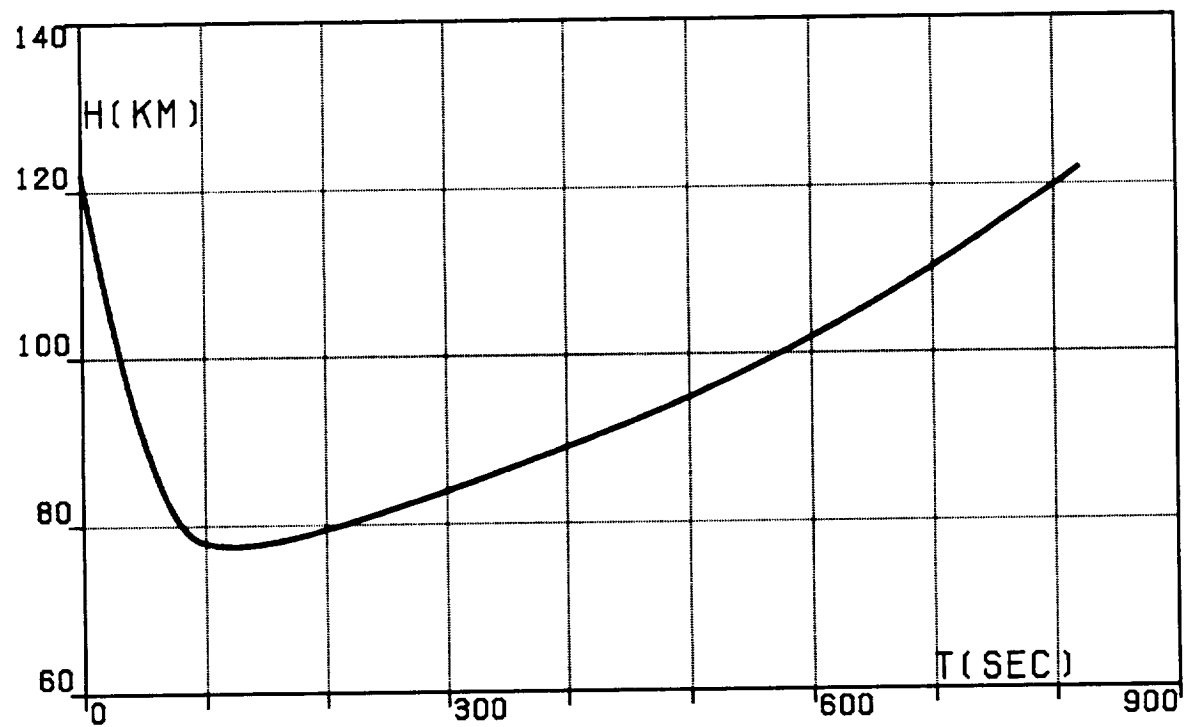


FIG.11D. FIVE-SEGMENT OPTIMAL TRAJECTORY,  
TRANSFER (DA), ALTITUDE.

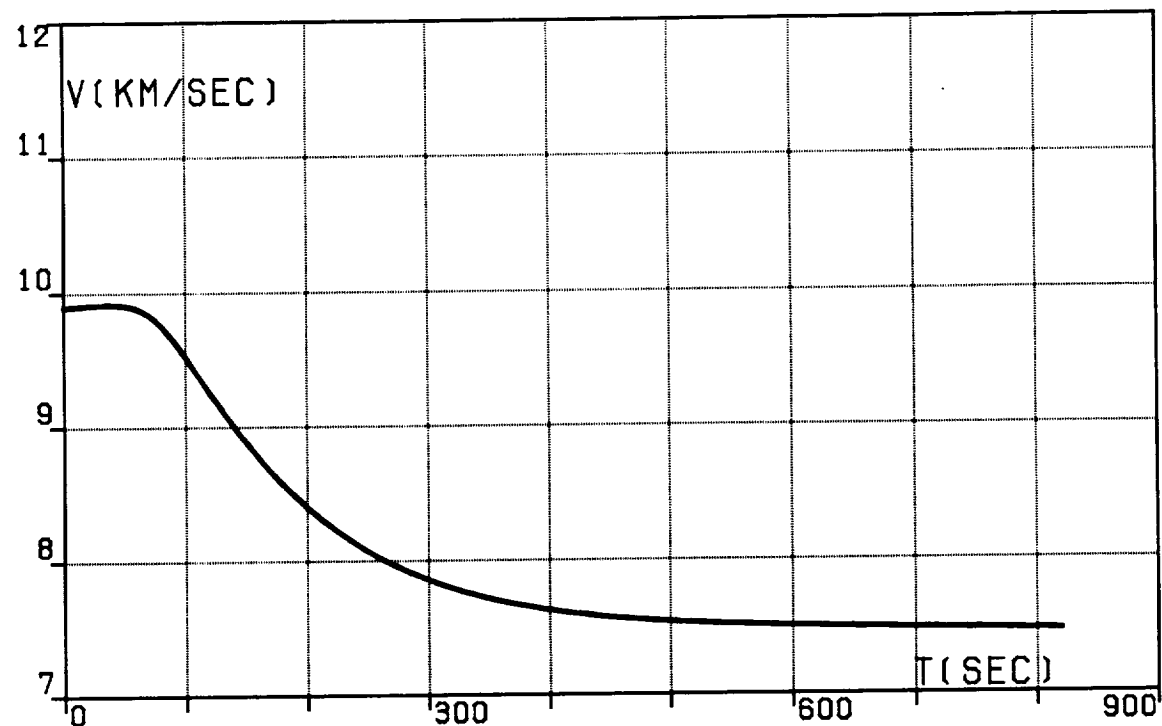


FIG.11E. FIVE-SEGMENT OPTIMAL TRAJECTORY,  
TRANSFER (DA), VELOCITY, RELATIVE.

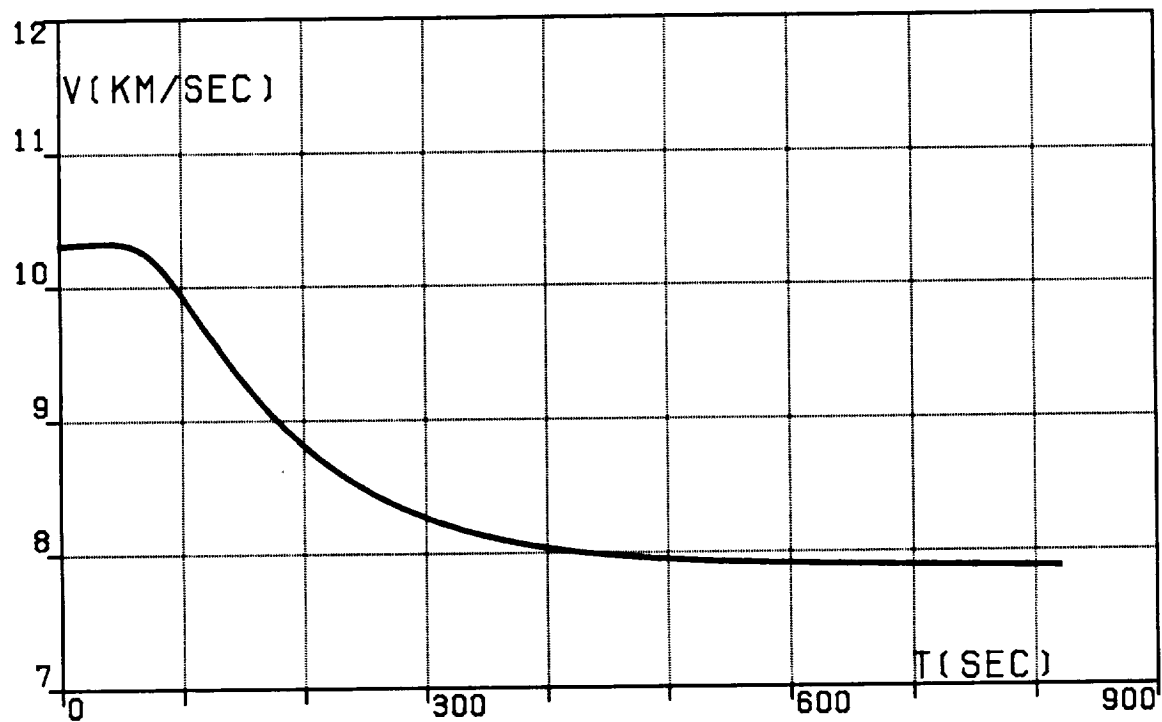


FIG.11F. FIVE-SEGMENT OPTIMAL TRAJECTORY,  
TRANSFER (DA), VELOCITY, INERTIAL.

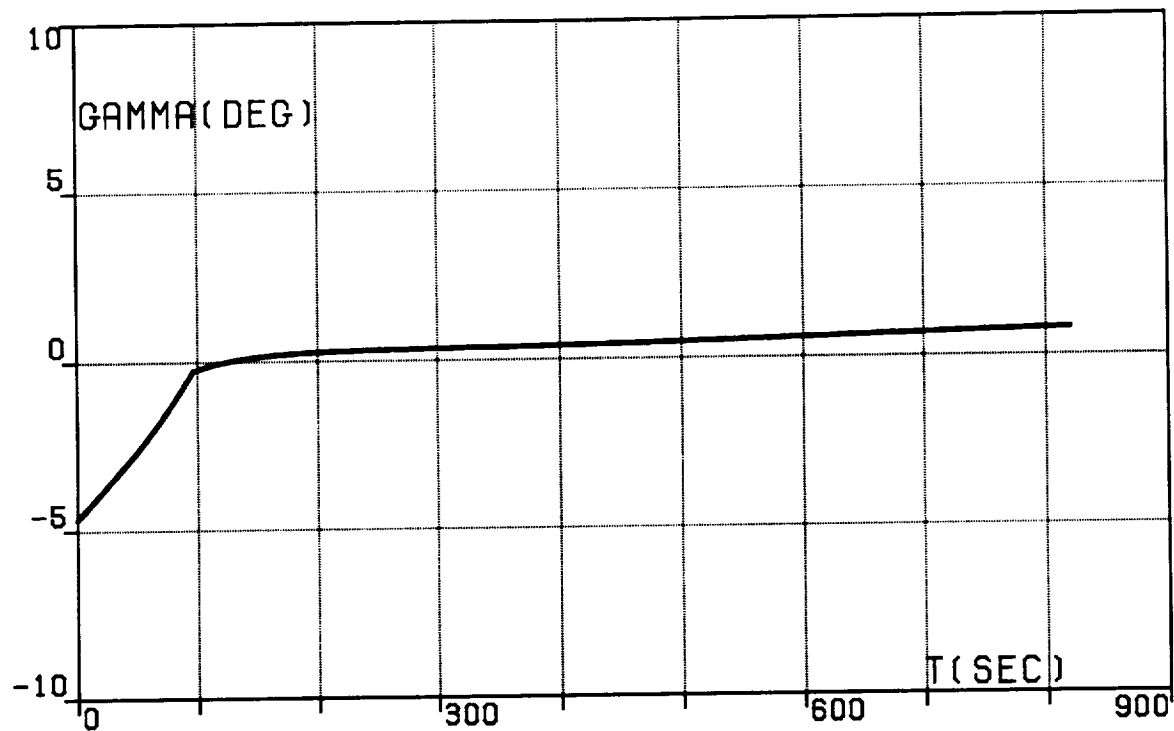


FIG.11G. FIVE-SEGMENT OPTIMAL TRAJECTORY,  
TRANSFER (DA),  
PATH INCLINATION, RELATIVE.

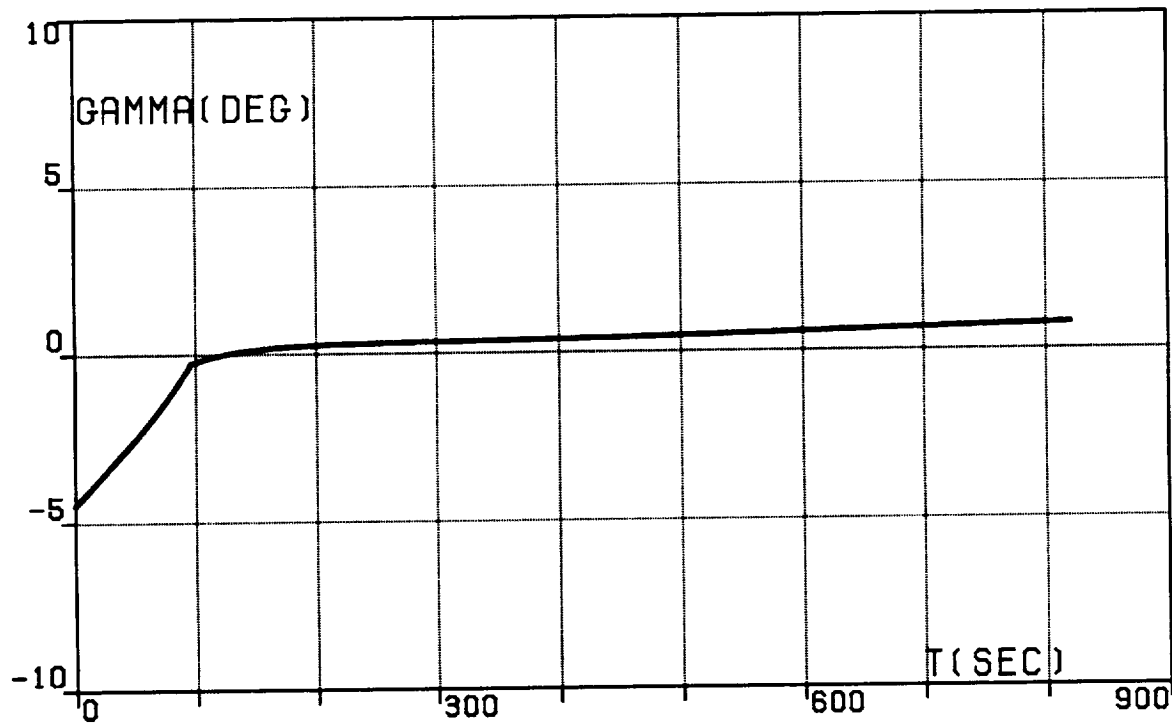


FIG.11H. FIVE-SEGMENT OPTIMAL TRAJECTORY,  
TRANSFER (DA),  
PATH INCLINATION, INERTIAL.

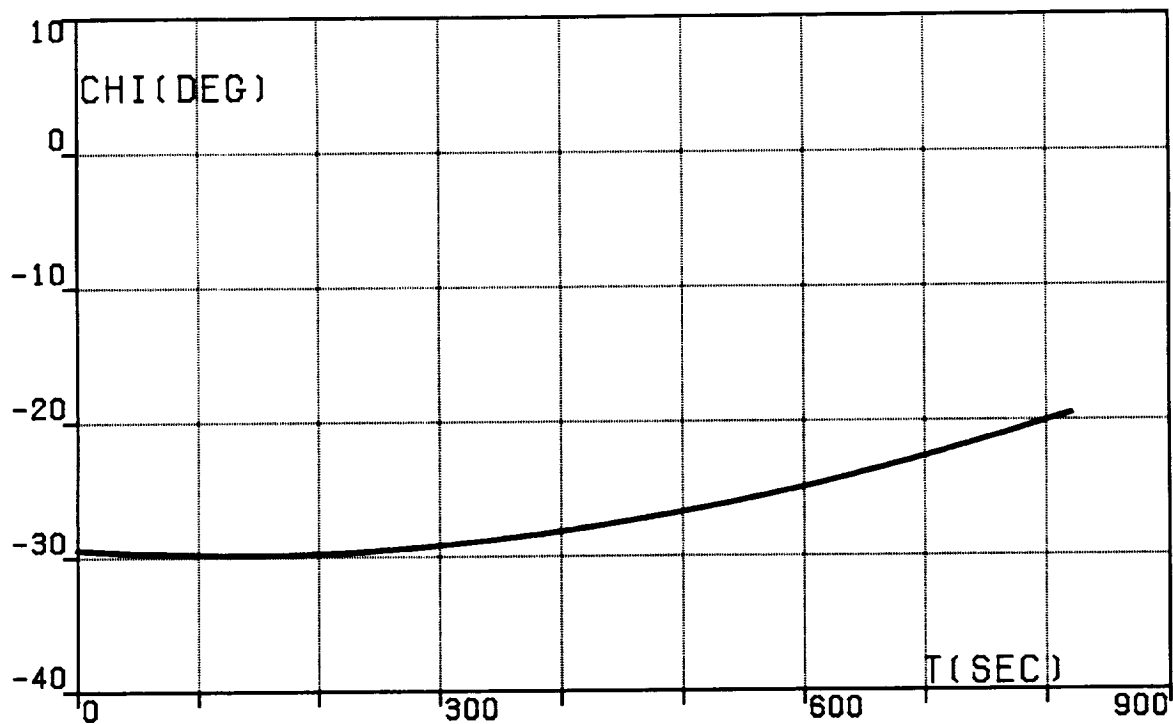


FIG.11I. FIVE-SEGMENT OPTIMAL TRAJECTORY,  
TRANSFER (DA), HEADING ANGLE, RELATIVE.

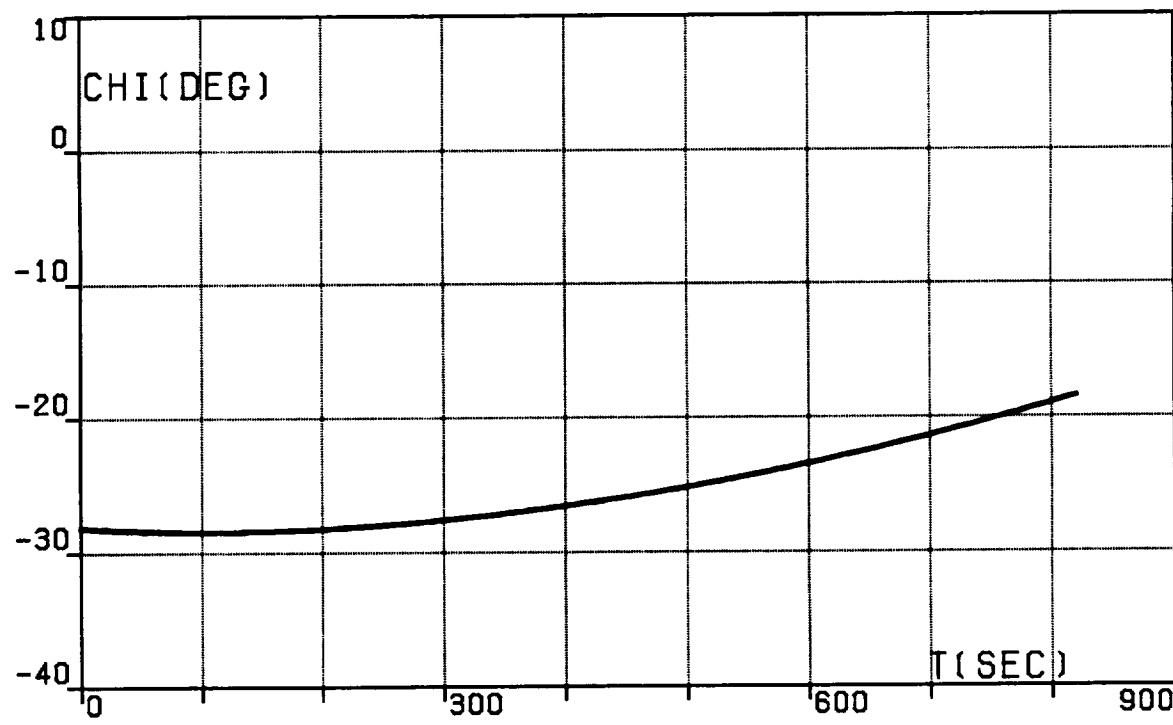


FIG.11J. FIVE-SEGMENT OPTIMAL TRAJECTORY,  
TRANSFER (DA), HEADING ANGLE, INERTIAL.

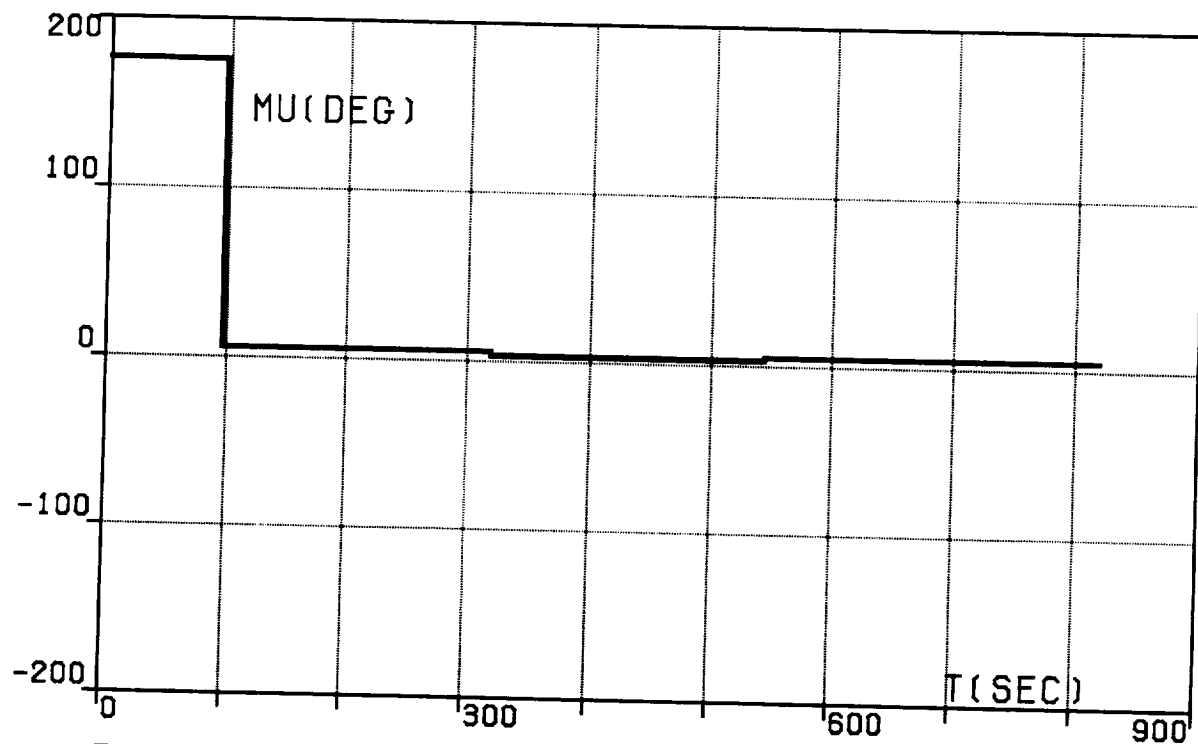


FIG.11K. FIVE-SEGMENT OPTIMAL TRAJECTORY,  
TRANSFER (DA), BANK ANGLE.

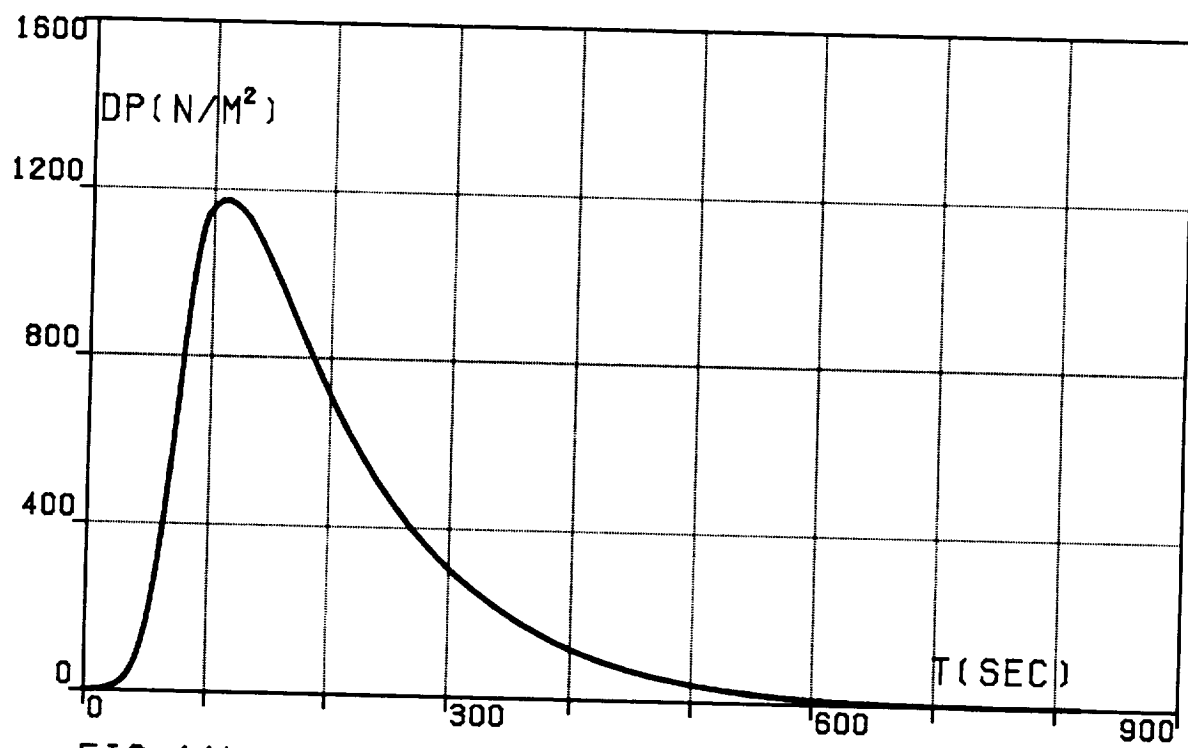


FIG.11L. FIVE-SEGMENT OPTIMAL TRAJECTORY,  
TRANSFER (DA), DYNAMIC PRESSURE.

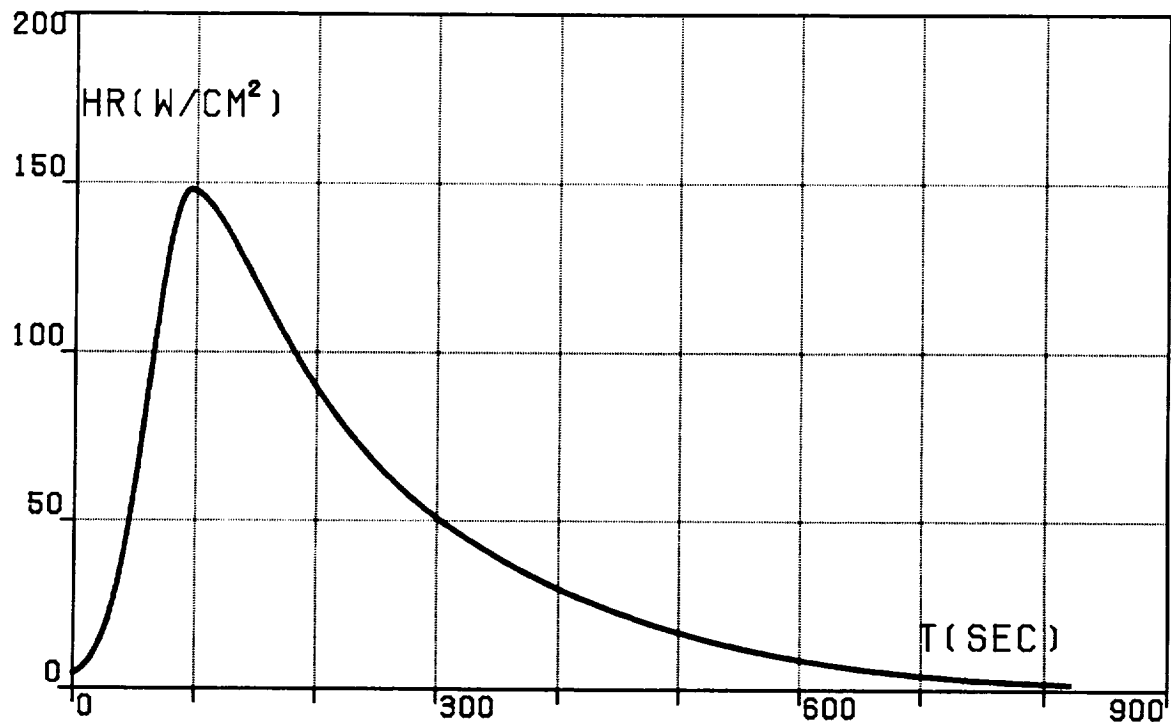


FIG.11M. FIVE-SEGMENT OPTIMAL TRAJECTORY,  
TRANSFER (DA), HEATING RATE.

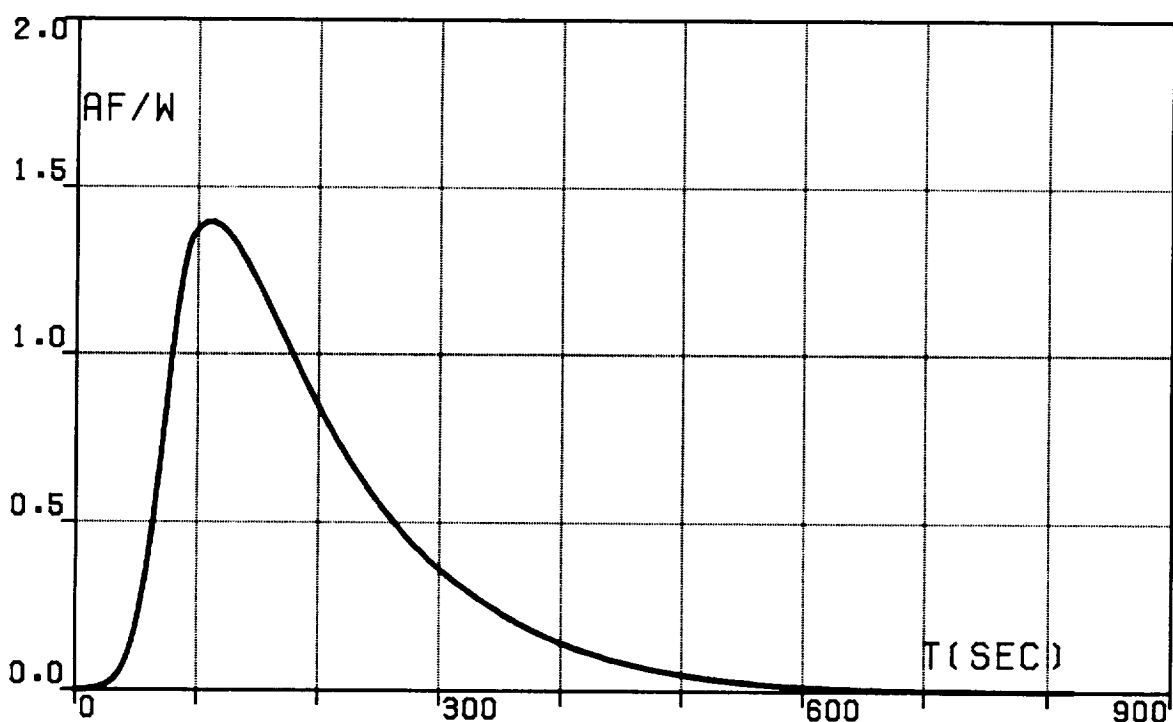


FIG.11N. FIVE-SEGMENT OPTIMAL TRAJECTORY,  
TRANSFER (DA),  
AERODYNAMIC FORCE PER UNIT WEIGHT.

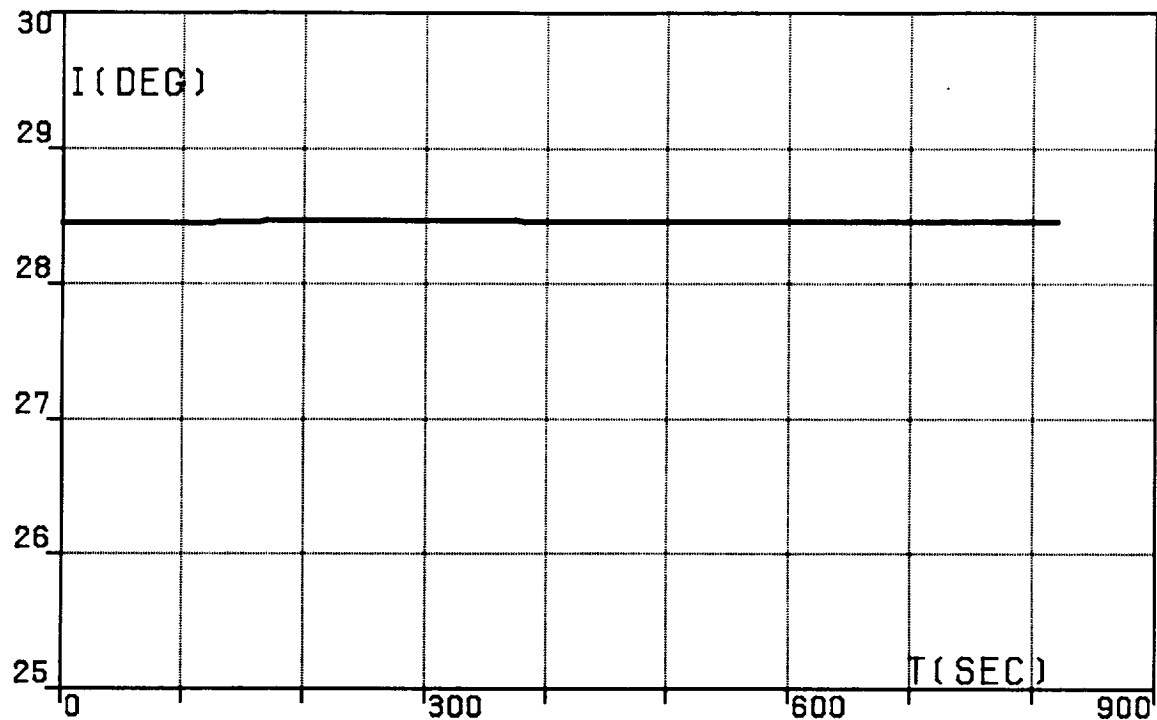


FIG.110. FIVE-SEGMENT OPTIMAL TRAJECTORY,  
TRANSFER (DA), ORBITAL INCLINATION.

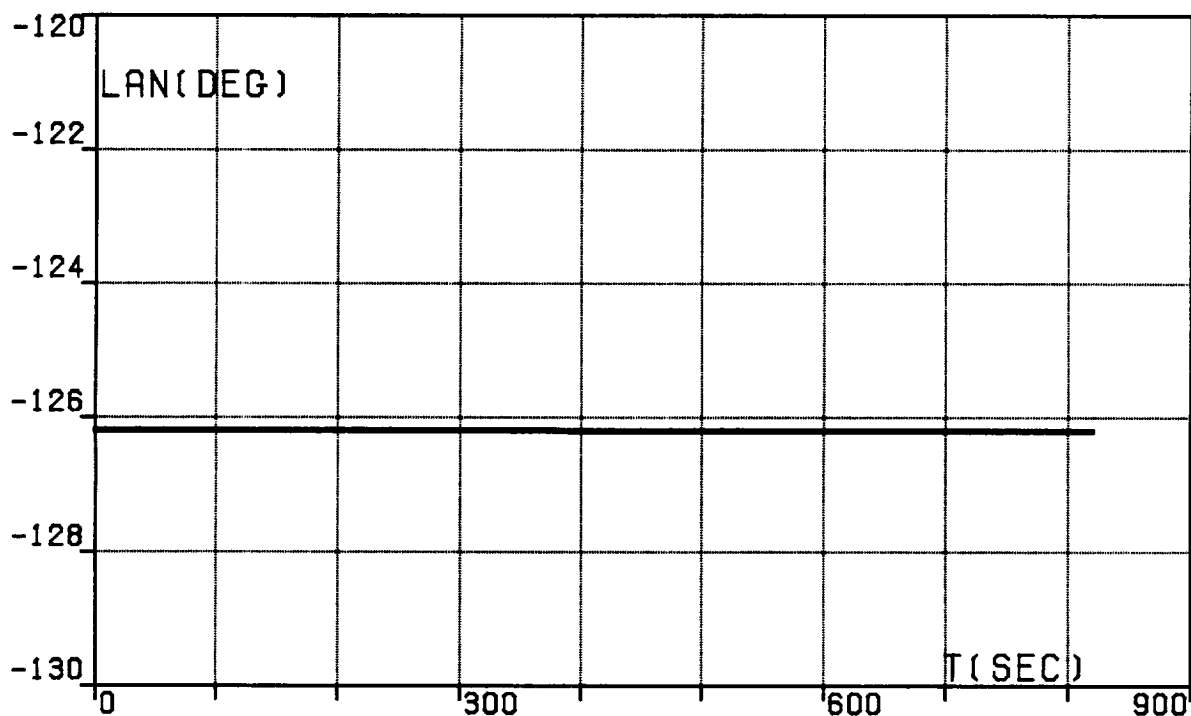


FIG.11P. FIVE-SEGMENT OPTIMAL TRAJECTORY,  
TRANSFER (DA),  
LONGITUDE OF THE ASCENDING NODE.

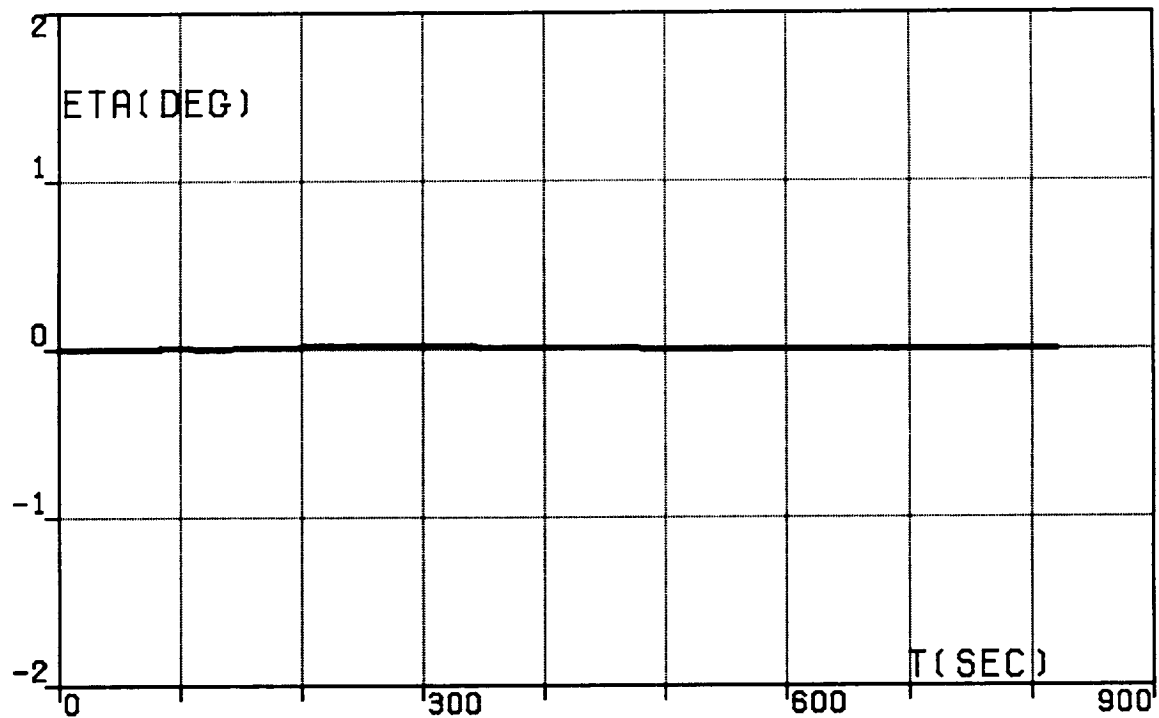


FIG.11Q. FIVE-SEGMENT OPTIMAL TRAJECTORY,  
TRANSFER (DA), WEDGE ANGLE.

